The Control of Constrained and Partially Constrained Arm Movements

by

JUSTIN WON

B.S. in Mechanical Engineering, University of California at Berkeley
(1990)

SUBMITTED IN PARTIAL FULFILLMENT
OF THE REQUIREMENTS FOR THE DEGREE OF

MASTER OF SCIENCE IN MECHANICAL ENGINEERING

at the

MASSACHUSETTS INSTITUTE OF TECHNOLOGY
February 1993

© Massachusetts Institute of Technology 1993

Signature of Author _____
Department of Mechanical Engineering
January 15, 1992

Certified by _____
Professor Neville Hogan
Thesis Supervisor

Accepted by _____
Professor Ain A. Sonin
Chairman, Departmental Committe on Graduate Studies

MASSACHUSETTS INSTITUTE
OF TECHNOLOGY

MAR 24 1993 ARCHIVES

LIBRARIES

THE CONTROL OF CONSTRAINED AND PARTIALLY CONSTRAINED HUMAN ARM MOVEMENTS

by

JUSTIN WON

Submitted to the Department of Mechanical Engineering on January 15,1992 in partial fulfillment of the requirements for the Degree of Master of Science in Mechanical Engineering

ABSTRACT

This thesis is concerned with the process by which humans control arm posture, movement, and interaction with the environment. By studying the stability properties of the human neuromuscular system while it performs simple point-to-point arm movements, this thesis will evaluate the concepts of equilibrium and virtual trajectories as a means of executing movement of the arm. Strong positional stability properties of the arm reinforce the notion that a moving attractor point dominates the behavior of the arm during movement.

To experimentally test the notion of stable trajectories in two-joint movements, a new experimental paradigm was designed. Human subjects grasped the instrumented handle of a two-link robot manipulandum and performed specified point-to-point planar arm trajectories. Computer-controlled clutches were used to subtly change the movements by constraining the trajectory to be along an arc of radius equal to the length of one link of the manipulandum. Targets points were arranged to lie along the arc so that the subject could complete the movement even when constrained. Three situations were tested: (1) unconstrained throughout the movement, (2) constrained through the entire movement, and (3) initially constrained and then released during movement.

Experimental results showed significant forces during the constraint strongly oriented so as to restore the hand to the unconstrained hand path. In addition when released from the constraint, these forces caused a strong tendency to return the hand to the unconstrained path before the end of the movement was reached. The presence of these restoring forces (even when considering the anisotropy of the end-point arm stiffness) implies that an attractor point exists between the start and target points for a significant portion of the movement. In addition, a virtual trajectory model is shown to be competent qualitatively in reproducing the experimental data. These results extend earlier single-joint results to the multi-joint case and provides further support for the theory that a single process underlies posture and movement.

Thesis Supervisor: Neville Hogan

Title: Professor of Mechanical Engineering and Brain and Cognitive Sciences

Acknowledgments

Really this thesis would have been inconceivable without Neville Hogan. In the few short years that I have worked for him, I think I have learned more about taking a disciplined look at the physical world than in my entire lifetime. His contributions to this thesis were considerable not only with his comments and suggestions but with his enthusiasm and infectious curiosity. I can only hope that someday I will be able to match that incredible idea generator which he applied as advisor for this research.

I would also like to thank Emilio Bizzi who allowed me to use the facilities within his lab and for his extremely helpful contributions when designing my experimental paradigm. In addition, I would also like to thank Sandro Mussa-Ivaldi, Simon Giszter, and Margo Cantor for their help with the hardware which allowed me to get the experiment up and running with a minimum of fuss. I would also like to thank Reza Shadmehr for being a great friend and for being there to show me the ropes of the motor control world during our many longish conversations (I think Marc still holds a grudge). With the likes of Neville, Emilio, Sandro, Simon and Reza, human movement becomes less of a mystery everyday.

Then of course there is the Newman Lab where I have spent a significant portion of my time. Pat Lord was ever helpful in many ways from computers to photography. Thanks also to: Tony for being the ideal guy to bounce a few confusing ideas off of. Sylvain and our philosophical discussions. Michael and the across the street runs. Joe and that the fact that "he's working on it". Karon and her really cool project. Johnboy and his farm implements. Denis and his good natured acceptance of the constant ribbing.

Lastly I have to thank my family for helping to make all this happen. They have never failed to support me through thick and thin. If I didn't know that I would always have their love and support, the world would be a harder place to face.

This work was supported in part by a grant from the National Institute of Health, Grant No. 40029, and in part by a fellowship from the Department of Defense and the Air Force. The research was performed in the Bizzi Laboratory in the Department of Brain and Cognitive Sciences.

To HJ, KS, CJ, and A

The ones who each constructed a little part of me...

Contents

Chapter 1 Introduction **13**

1.1 Motivation 13

1.1.1 Contact Stability 14

1.1.2 Movement Generation 15

1.2 Equilibrium Point Hypothesis 16

1.3 Objectives 18

1.4 Summary of Remaining Chapters 19

Chapter 2 Background **21**

2.1 Equilibrium Point Hypotheses 21

2.1.1 The Lambda Model 22

2.1.2 The "Alpha" Model 26

2.2 Static Impedance Measurement 32

2.2.1 Conservative Field 34

2.2.2 Control of stiffness 36

2.3 Movement Generation by Virtual Trajectories 38

2.3.1 Virtual Trajectory Derivation and Simulation 39

2.3.2 Simulation Paradigm 41

Chapter 3 The Experiments **43**

3.1 Measurement of Stiffness 43

3.1.1 The Hardware 44

3.1.2 Measurement Procedure 45

3.1.3 Data Processing 46

3.2 Reaching Experiments 47

3.2.1 The Hardware 47

3.2.2 Experimental Paradigm 49

3.2.3 Data Processing 52

3.3 The Experimental Subjects 53

3.4 "Do not intervene" Paradigm 54

Chapter 4 Task Modelling **57**
4.1 Human-Robot Model 57
4.1.1 Kinematic Analysis 58
4.1.2 Dynamic Analysis 59
4.2 Human-Robot Specifics 68
4.2.1 The Robot 68
4.2.2 The Human Arm 70

Chapter 5 Experimental Results **73**
5.1 Stiffness Measurement 73
5.1.1 Measured Forces 74
5.1.2 Stiffness Approximation 74
5.2 Movement Data 80
5.2.1 Unconstrained Reaching Movements 80
5.2.2 Fully Constrained Movement 86
5.2.3 Constrained and Released Movement 91
5.2.4 Summary of Experimental Data 94

Chapter 6 Simulation Results **99**
6.1 Model Assumptions 99
6.2 Simulation Results 101
6.2.1 Parameter Tuning 101
6.2.2 Global Generalization 106
6.2.3 Summary of Simulations 113

Chapter 7 Conclusions and Recommendations **115**
7.1 Features of Human Arm Movement 115
7.2 A Possible Model 117
7.3 Recommendations for Future Work 118
7.3.1 The static impedance field 118
7.3.2 The velocity dependent impedance 119
7.3.3 The inertia parameters 120
7.4 Final Remarks 120

Bibliography **121**

Appendix A Robot System Identification **127**
A.1 The Goal 127
A.2 The Experiment 128

A.2.1 The Apparatus 128
A.2.2 The Data Collection 129
A.2.3 Data 132
A.3 A Simple Model 133
A.4 Simulations 135
A.4.1 Simulation Results 135
A.4.2 Summary 137

Appendix B Movement Data 139
B.1 Subject A 139
B.2 Subject B 147
B.3 Subject C 155
B.4 Subject D 163
B.5 Subject E 171

Appendix C Informed Consent Document 177

Chapter 1

Introduction

Movement is something that humans treat with intimate familiarity. Unfortunately this intimacy is so complete that the entire process of planning and generating movements remains essentially a black box. A human can plan and perform intricate movements with ease and dexterity and yet be unable to explain the exact method of translating the envisioned movement into the muscle activity required to generate it. Especially confounding is the ability of the human control system to perform manipulative tasks with stability and versatility unmatched by any modern robot in both industrial and research settings. It can be argued that the modern robot has the advantage of better sensors and actuators as well as a faster processor; however in some respects, it is still outperformed by the human arm. It is frustrating to know that the most common and versatile control system in the world resides within us and yet remains essentially a mystery.

1.1 Motivation

The goal of this thesis is to shed some light on this mystery by demonstrating basic properties of the human neuromuscular control system while it performs simple point-to-point arm movements. This simple goal fits into a much larger endeavour - to show that there exists a

single mechanism by which humans can control posture, movement, and interaction without the computational burden seemingly implied by these tasks.

1.1.1 Contact Stability

Such an endeavour addresses not only a fundamental neurophysiological question, but it can also possibly contribute significantly to the field of robotics and prosthetics. As mentioned previously, the human arm outperforms robotic manipulators for tasks involving dynamic interaction by the manipulator with its environment. The modern industrial robot has been most successful in performing essentially free-motion position control tasks such as spot-welding, spray painting, or pick and place operations. Tasks which involve common manufacturing operations such as drilling, reaming, routing or grinding have been traditionally difficult to perform due to instabilities caused by the significant interaction forces between the manipulator and its workpiece [Whitney 1977; Hogan 1985; Eppinger et al. 1987; Hogan 1988]. Robots that are stable when moving in free space tend to chatter uncontrollably when attempting to control the contact force exerted on an object.

Biological manipulators, on the other hand, are extremely capable of controlling interactive tasks. Ironically these biological controllers can stably control interaction using sensors which have significantly less precision and more time-delay than those available for the modern robot. In addition, computational power of the controller does not seem to be significant for guaranteeing contact stability. For example, a spinalized frog can perform a stable wiping motion against an object in response to stimulation given at the spinal cord. This implies that stable interaction within a biological system is really dependent on the physical characteristics of the system rather than on the computational ability of the controller. Therefore understanding which characteristics are relevant and important for stable interaction as well as how the biological system uses these characteristics to its advantage should be a key in improving the versatility of robotic manipulators.

In particular, studying the human arm provides an easy extrapolation to the field of robotics since many robots in some way or another resemble the human arm and attempt to mimic its ability to manipulate objects. As a result, both robots and humans must deal with similar kinematics and dynamics due to their similarity in configuration. However the human arm is able to perform difficult interactive tasks such as the manufacturing operations mentioned previously

while robots are not. Therefore this thesis is concerned with gaining insight into the human motor control system in the hopes of verifying concepts which can remove these limitations of the modern robot.

1.1.2 Movement Generation

Besides the problems with contact instability, there are also some very basic questions of generating movements planned in one coordinate frame but actuated in a different coordinate frame. This question is very basic to robotic research where in many situations the path of the end-effector is the only concern. However, the actuators of the robot specifically control the motion of the joints which indirectly determine the position of the end-effector. The problem reduces to finding the proper map to take planned end-point motion and generate joint motion.

Experimental results have suggested that humans deal with a similar problem; there are indications that humans plan movements in some exogenous reference frame. During self-paced point-to-point reaching movements, the hand of the subject generates essentially a straight line path from start to finish with a characteristic bell-shaped tangenti velocity profile [Morasso 1981; Abend et al. 1982]. The trajectories of the shoulder and elbow for the same movement were more complex, occasionally containing reversals. Other studies have shown that there exists a correlation between the activity pattern of cells within the motor cortex and the direction of movement of the hand in an external frame [Georgopoulos et al. 1982, 1983]. If arm movements are planned by the central nervous system in an extrinsic frame, there must exist some neural process which converts a desired movement planned in the external coordinate to a set of muscle activations to perform that movement.

This transformation from planned motion to muscle activity is complicated by the redundant degrees of freedom which the arm possesses in positioning and orienting the hand. As a result, the transformation from hand coordinates to joint coordinates or inverse kinematics ceases to be an injective (or one-to-one) map. Therefore a unique solution does not exist, and the scheme for creating a given position is no longer trivial. This difficulty for posture extends to movement as well where finding the motion of the joints from a given end-point motion is computationally burdensome.

If the joint motions can be found, the calculations to produce these motions may not be trivial due to the dynamics of the system. Assuming the human arm to be a simple two-link manipulator with a grounded base for simplicity, the muscles of the arm must drive two inertias - the forearm/hand and the upper arm. Due to the coupling effect of the two inertias, the motion of the hand will be affected by the Coriolis and centripetal forces produced by moving one inertia relative to the other. It has been proposed that the CNS attempts to perform inverse dynamics to find the forces necessary to perform the desired movements [Hollerbach and Atkeson 1987]. Unfortunately, this method relies on knowing the precise inertial parameters and centers of mass for both the forearm and the upper arm. In addition, the moment arm of the muscles at any given position must also be known in order to generate the exact torque required to accelerate the limb in the appropriate direction. Most importantly, this strictly feedforward computation is not robust to any disturbances acting upon the arm during the movement. Disturbances which displace the arm slightly from its given path can produce a very different trajectory than the planned trajectory.

1.2 Equilibrium Point Hypothesis

The equilibrium point hypothesis presents a unified theory which may explain how biological systems can deal with these problems of movement execution and controlling contact. It is based on the notion that muscles have spring-like properties where an opposing force can be induced by imposing motion on the muscle.[1] When two of these spring-like muscle are placed about a joint in an agonist-antagonist configuration, the limb posture is defined by the selection of the length-tension curves for each muscle. This posture is the equilibrium configuration of the limb. Under zero external load and zero velocity and acceleration, the limb will remain in this equilibrium position. In the presence of a perturbation, the arm will move from equilibrium although a restoring force is generated resisting the induced displacement.

Movement can be generated from posture through a shift of this equilibrium point from the starting configuration to the target. The forces induced in the muscles by the moving equilib-

1. This force-motion relationship is known as a mechanical impedance which describes the force response to an imposed velocity. In most of the analysis to follow, it is tacitly assumed that the static (force-displacement) component can be decoupled from the dynamic component (force-velocity or acceleration).

rium point will generate a motion to follow the equilibrium point. During motion the limb does not have to achieve its equilibrium position, and in fact the equilibrium point during movement is not constrained to remain within the accessible workspace of the limb. As a result the concept of equilibrium is ambiguous, and therefore the terms attractor point or virtual position will be used instead of equilibrium point. The shifting of the virtual position through space to generate the desired movement will be called the virtual trajectory.

Execution of planned arm trajectories can be done through the virtual trajectory. Since movement is now effectively an extension of posture, generating the movement planned in the external frame is simply a matter of knowing the initial configuration of the limb and then calculating postures from the displacement of the hand along the planned trajectory (thus obviating the need for inverse kinematics) [Mussa-Ivaldi et al. 1988]. Inverse dynamics is similarly unnecessary. The forces generating movement are provided by the displacement from equilibrium of the limb. As a result, the limb follows the moving attractor point driven by the spring-like nature of the muscles. Due to inertial dynamics, the actual trajectory will not coincide with the planned virtual trajectory. However by modulating muscular impedance, the human can generate trajectories which approximate straight line trajectories which are acceptable for most motor tasks [Hogan 1987].

Control of contact force can also be controlled through the use of an attractor point. Simply moving the attractor point within a object will cause the limb to exert a force on that object. For the static case, the imposed force will be a function of distance from the attractor point as well as the static component of the impedance. This in itself does not guarantee contact stability for the human arm. However a recent study proved that an actively controlled manipulator (mechanical or biological) can maintain stable contact with an arbitrary passive object if and only if the mechanical impedance of the manipulator is equivalent to a passive object [Fasse 1987; Colgate and Hogan 1988].[2] Through psychophysical experiments, the static component of the human arm impedance was measured [Mussa-Ivaldi et al. 1985].[3] A major feature of these static measurements was that the human arm near equilibrium exhibited very conservative or spring-like behavior. This represents a mechanical impedance

2. An object is passive if the amount of energy that can be drawn from it is not greater than the amount stored within it.
3. These experiments will be explained in more detail in the next chapter.

indistinguishable from a mechanical spring which is consistent with the above passivity criterion. In at least the static case, this result implies that contact force can be stably controlled through movement of an attractor point.

The equilibrium point hypothesis is attractive because it can explain many of the phenomena observed in the human motor control system. It is a theory which unites posture, movement and contact under a single scheme of controlling an elementary behavior of the neuromuscular system. However, many members of the neuroscience community doubt that this hypothesis can ever be disproved [Smith et al. 1991]. Since equilibrium is intrinsic to the structure of muscles and their reflex loops, attractor points will always exist as a natural description of the muscle activation. However, the crucial point for the virtual trajectory hypothesis is that the attractor point is the variable that the human uses to simplify the computational burden of generating movement and controlling contact with the environment.

1.3 Objectives

This brings us to the objectives of this body of research. There is a large body of research evidence demonstrating that the CNS generates movements of a single limb through a moving attractor point [Bizzi et al. 1978, 1982, 1984; Cooke 1979; Kelso and Holt 1980; Lestienne et al. 1981; Polit et al. 1979]. The experiment described in this document was designed to study two-joint movements of the human arm in order to evaluate the veracity of this same hypothesis for a multi-joint case. Therefore, the main objectives are as follows:

- Examine the stability properties of the arm during movement.

  If the stiffness of the arm is very low during movement as recently shown [Bennet et al. 1992; Gomi et al. 1992], then the virtual trajectory hypothesis is certainly weakened as a means of simplifying motion. Therefore, it would be instructive to observe the natural response of a moving arm to a perturbation. If the arm has low stiffness or is possibly neutrally stable during movement, then the perturbation response should be markedly different than the response of a system generating motion through a virtual trajectory.
- Evaluate the ability of the virtual trajectory hypothesis to recreate the experimental data.

Previous work has shown that the virtual trajectory hypothesis is competent in recreating unperturbed point-to-point movements. This confirmation was attained through a forward simulation which certainly does not guarantee that it has found the unique solution to the problem. Through the experiments carried out within this thesis, additional requirements will be found about the behavior of the arm during movements. Specifically, perturbation responses will be added to our knowledge of reaching movements. The virtual trajectory model will then be tested for its capability of recreating not only the unperturbed but the perturbed movements as well?

- Evaluate the virtual trajectory model as a means to generate movements in all portions of the workspace by generalizing from a single trajectory.

  If the virtual trajectory can sufficiently capture the behavior of the perturbed movements, can a virtual trajectory for a single movement be used to accurately recreate movements in other parts of the workspace travelling in different directions? The goal is to show that the virtual trajectory represents a basic module which can generate a large class of movements.

1.4 Summary of Remaining Chapters

Chapter 2 presents a summary of previous research performed on the equilibrium hypothesis. Physiological explanations for the spring-like behavior of muscles will be presented and used to provide an explanation for the results from the single-joint experiments. In addition, research performed on the use of virtual trajectories and postural fields to generate two-joint movements will be summarized.

Chapter 3 describes the two basic experiments performed in terms of the experimental protocols as well as a description of the equipment used. Data processing techniques will also be discussed in this chapter.

Chapter 4 presents the dynamic analysis used to model the experimental task described in Chapter 3. A detailed derivation of the equations of motion for the human moving the experimental apparatus will be shown.

Chapter 5 contains the results of the postural field measuring experiment and the movement experiments. General features of the data will be discussed.

Chapter 6 will discuss the results of the analysis performed on the data. Discussion will center on the predictions of the derived virtual trajectory and its ability to recreate the experimental data.

Chapter 7 concludes the work with a final discussion and recommendations for further work.

Chapter 2

Background

The following chapter presents a historical background of the equilibrium point hypothesis and its consequences. In the first section, an overview of the original formulation of the equilibrium point hypothesis by Feldman will be presented. This first section will also introduce the so-called "alpha" model and its application in describing the deafferated monkey experiments by Bizzi et al. The second section contains a description of the static impedance measurement experiments performed by Mussa-Ivaldi et al. The final section summarizes the work performed by Flash on generating two-joint arm movements using the virtual trajectory hypothesis.

2.1 Equilibrium Point Hypotheses

The following two subsections describing the lambda and "alpha" model are presented with one caveat. The focus of this thesis is on analyzing a series of psychophysical experiments to discern if equilibrium is an appropriate control signal for the CNS. As a result, this study is only cursorily concerned with the neurophysiological mechanism through which the CNS can control equilibrium. Although this may seem negligent, the motivation for this approach stems from the logical progression of finding "What is the signal?" before even attempting to find "How is this signal executed?". Therefore, this document will not attempt to reconcile

any differences between Feldman's lambda model and the alpha model. These two bodies of research are presented simply as a means of providing evidence of the CNS using equilibrium as a possible control input. Since both postulate movement through a shift in equilibrium, the importance is placed on whether the equilibrium point is the control input to the system and not on the relative contributions of spinal reflex versus intrinsic muscle properties.

2.1.1 The Lambda Model

In 1965, Asatryan and Feldman showed experimentally that muscles coupled with their reflex loops behave much like non-linear mechanical springs. From the experimental data, Feldman postulated that of all the controllable parameters of the motoneuronal pool, only the threshold length could be independently controlled. This threshold value represents the length beyond which the muscle must be stretched to trigger the stretch reflex. Using the spring analogy, this means that the non-linear spring-like muscle can only be controlled through a modification of its equilibrium length.

The hypothesis stemmed from a series of experiments performed on the human elbow. The subject was placed in an apparatus which permitted only planar extension and flexion of the forearm. A series of trials were performed where the subject maintained a predetermined elbow angle against a bias torque. The applied torque would suddenly decrease causing the forearm to move to a new position. During this sudden unloading, the subject was told explicitly not to actively intervene with the induced movement. For each trial, the subject maintained the same initial elbow position, but the magnitude of the change in load varied from trial to trial. The experiment was then repeated several times with different combinations of initial loads and positions.

Invariant Characteristics

Data from the unloading experiments can be plotted as muscle torque against elbow angle as shown in Figure 2.1. A single curve represents data from a single set of experiments where the initial combination of bias torque and initial position remained constant; only the magnitude of the change in load varied. As a result, the solid data point on a single curve represents the load and position of the elbow before unloading. The subsequent data points along the same curve represent the data from the unloading trials in the form of the final position of the elbow after the

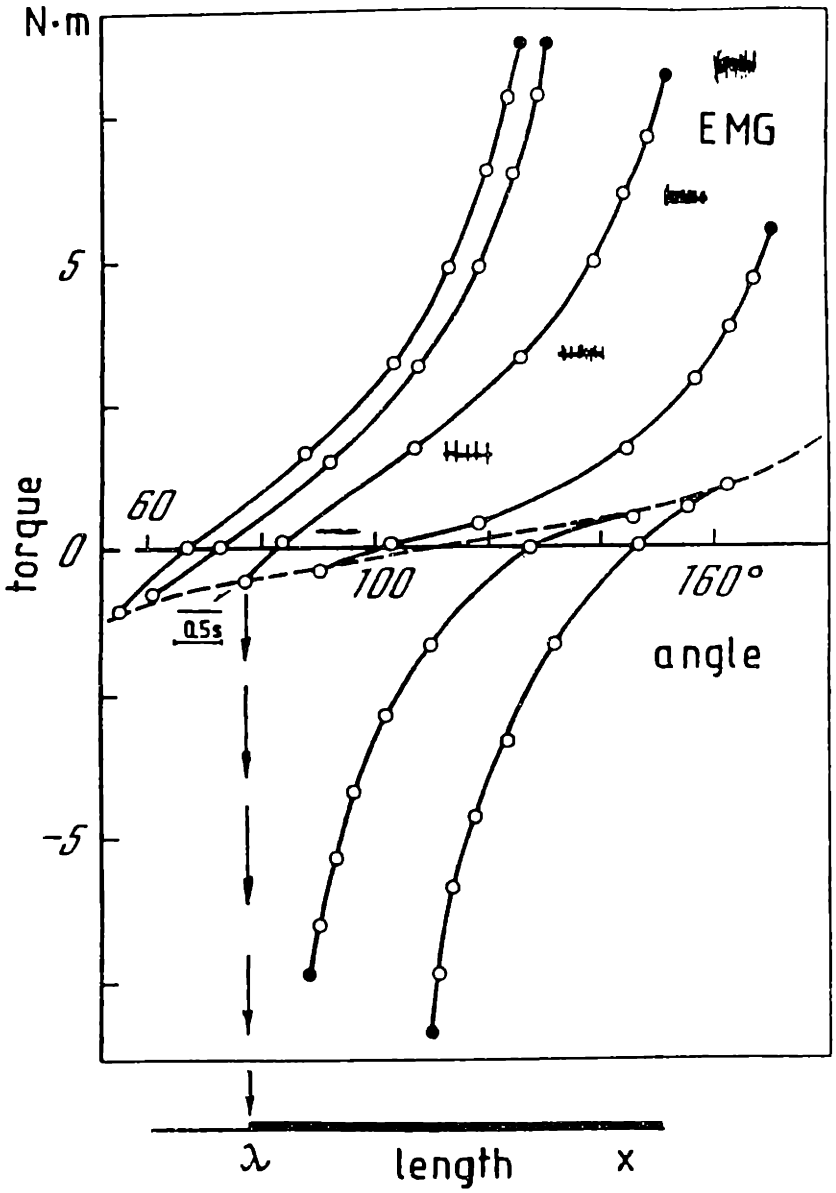

Figure 2.1: A family of invariant characteristics for the elbow. The solid circles represent the different initial combinations of muscle torque and predetermined elbow angle. The open circles represent the same combination but after the forearm has come to rest during unloading. The dashed line represents the passive muscle properties. (From Feldman 1986)

initial load had been reduced to the plotted torque. The different curves represent similar unloading experiments for different initial combinations of loads and positions.

These curves in Figure 2.1 were called invariant characteristics (IC) of the muscle for two major reasons. First of all, Asatryan and Feldman (1965) showed that space-time variations in the unloading procedure were unable to change the shape of the IC curves signifi-

cantly. Secondly and more importantly, the shape of the curves did not change significantly for different starting combinations of load and position. This is shown in Figure 2.1 where the different IC's have similar shape but branch off at different states of the relaxed muscle (dashed line). Therefore, it would seem that an IC curve can be translated to a new position but not reshaped [Asatryan and Feldman 1965].

Due to the instruction to the subject to not intervene, it was assumed that the change in firing frequency of the motoneurons during unloading was due to a spinal cord reflex. For this reason, the strong invariance of these curves to everything except initial combination of position and load led Feldman to propose that the only controllable parameter of a muscle is the threshold length λ of the stretch reflex. When λ is held constant, the static muscle force has a single-valued dependence on muscle length which is invariant across different threshold lengths. This invariant single-valued function represents essentially a non-linear spring. Tuning λ shifts this function to a different equilibrium position making equilibrium length the only controllable input.

The Lambda Model as a Motor Control Theory

Since within this hypothesis the control of muscles is accomplished through modification of the threshold length, tuning this parameter for an agonist-antagonist set of muscles defines an equilibrium point for the limb. In the absence of motion and external load, the limb will remain at this position set by the equilibrium lengths of the spring-like muscles. Changing the rest lengths of the muscles below the current lengths activates the stretch reflex and generates movement to the new equilibrium point defined by the new rest lengths [Feldman 1966].

Controlling muscle length during co-activation also provides a method of controlling the net stiffness about the joint [Feldman 1980]. Since the static force-length curves are exponential in shape, the stiffness varies with displacement from the threshold λ. Therefore by choosing appropriate muscle lengths for the agonist and antagonist muscles, the stiffness about equilibrium can be set to a desired level by placing the net equilibrium position at points along both IC's which have the appropriate local slopes as shown in Figure 2.2. Setting small threshold distances from the equilibrium position give a low stiffness due to the fact that the equilibrium position is along the flatter portion of the IC. Increasing the difference in threshold length from

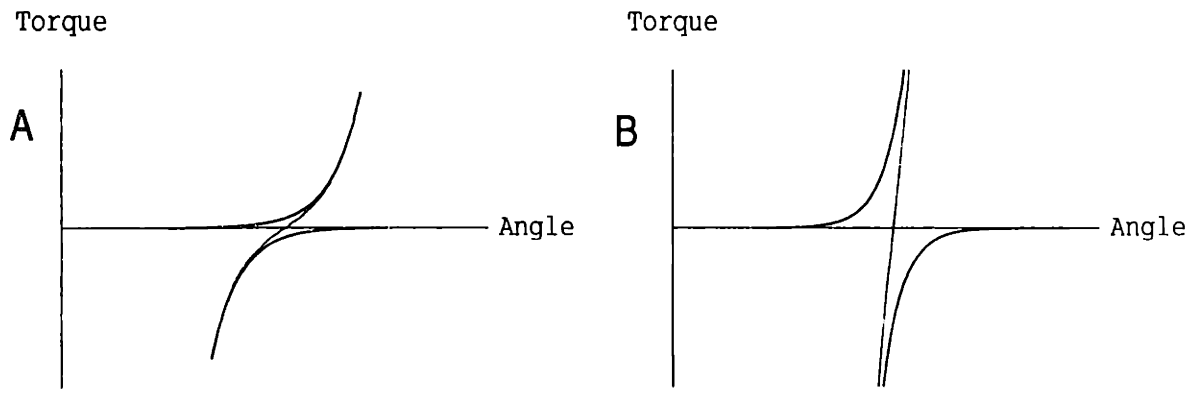

Figure 2.2: Modulating stiffness through co-contraction. Two IC curves for the extensor and flexor (black lines) and the net joint stiffness (grey line). (A) Low stiffness. (B) Higher stiffness.

equilibrium increases the stiffness as the equilibrium position falls along the steeper portion of the exponential-like IC.

Unfortunately there are some inconsistencies when using the lambda model as a means of generating movement. Within the lambda model, the major source of force generation is through the stretch reflex (the mechanical force generated by stretching of the muscle itself is assumed to be small). Yet this introduces a spinal cord feedback loop which inherently has a time delay of approximately 30 to 50 ms. Since controlling human movement is the same as controlling any dynamic system, control theory tells us that this delay severely limits the magnitude of the feedback gain of the stretch reflex during movement due to the danger of instability [McMahon 1984; Hogan et al. 1987; Hogan 1990]. Moreover the presence of a low feedback gain during movement has been experimentally verified by several researchers [Valbo 1973; Bizzi et al. 1978; Sanes 1983]. A low feedback gain during movement calls into doubt the authority of the stretch reflex to control movement.

A second inconsistency is the inability of the lambda model to explain the ability of deafferated humans and monkeys to maintain posture and perform movements. Yet they are able to perform these feats even though they are unable to generate any muscle activity through a reflex loop. This result implies that the threshold length cannot be the *sole* method of controlling equilibrium in a muscle as formulated by Feldman.

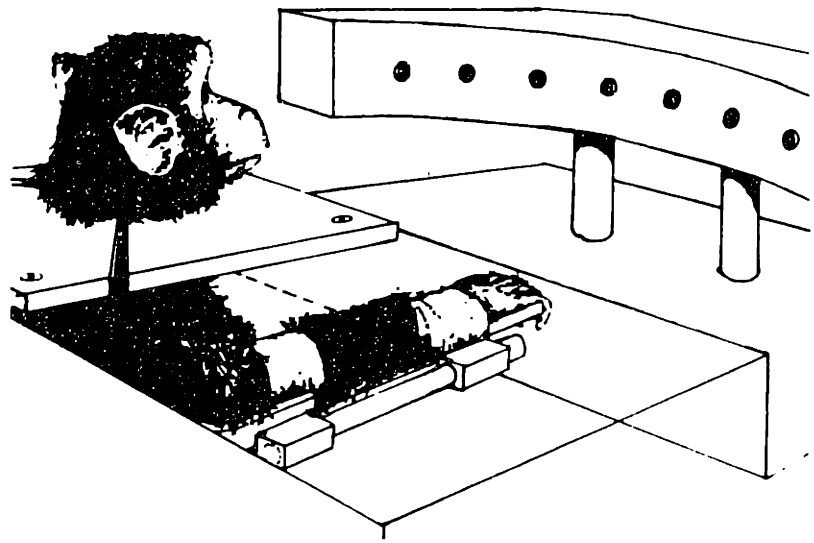

Figure 2.3: The single joint experimental apparatus for the monkey experiments. The target lights are mounted at 5° intervals. The neck cover prevents the monkey from seeing its arm. [Polit and Bizzi 1979]

2.1.2 The "Alpha" Model

The "alpha" model is an attempt to explain the phenomenon of controlling posture and movement without feedback.[1] It was shown experimentally that trained rhesus monkeys could undergo a bilateral dorsal rhizotomy (C_2-T_3) and still perform accurate single-joint pointing tasks with no afferent or visual feedback even in the presence of significant disturbances [Polit and Bizzi 1979].

The Monkey Experiments

The experimental monkeys were placed in an apparatus similar to Feldman's which allowed rotation only about the elbow in a horizontal plane. In addition, a series of target lights were placed in front of the monkey along a small arc centered about the axis of rotation of the elbow as shown in Figure 2.3. A torque motor coupled to the pivot arm of the forearm splint was used to load the arm. A cover over the arm removed visual feedback of the arm position.

The intact monkey was trained to point to whichever target light was illuminated and to stay at that position for one second. After the monkey had become sufficiently proficient at the

1. The term "Alpha Model" was introduced by the Feldman group to describe a motor control scheme performed in the absence of spinal cord reflexes. It is not a term used by the motor control group at M.I.T. It is used here to denote a section specifically devoted to the discussion of the deafferated monkey experiments and their contribution to our understanding of intact arm movements. It does not denote a motor control hypothesis. As a result in this case, it is an inappropriate but relevant term.

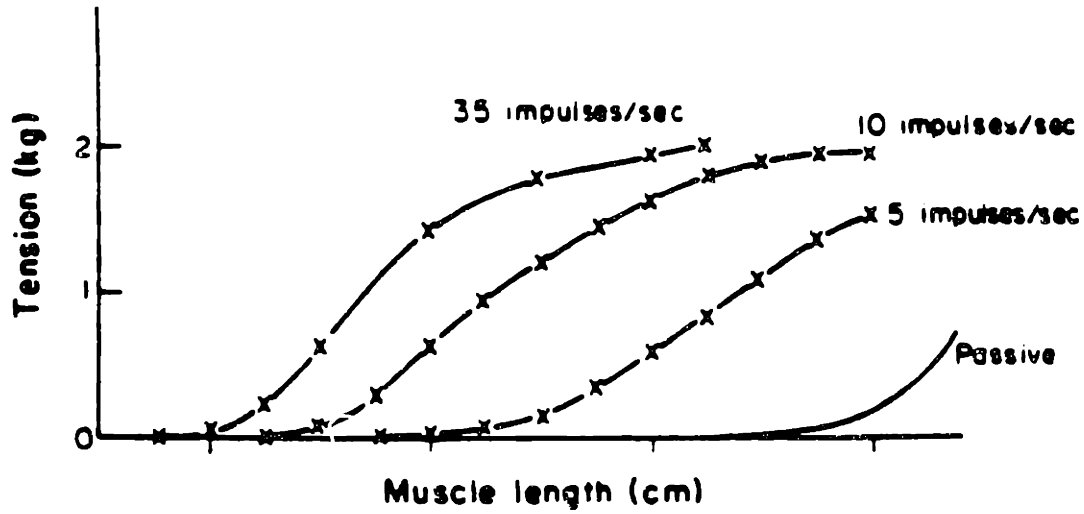

Figure 2.4: The nonlinear static behavior of the length dependence of an areflexive muscle for different activations. [Joyce et al. 1969; Hogan 1984a].

pointing task, an experiment was performed where the monkey would perform the same pointing movements. During 20 percent of the trials and before movement, the torque motor applied a random load which displaced the arm an average of 10° from its initial position. Without visual feedback, the intact monkey was able to point to the appropriate target even with the initial perturbation. These same monkeys were then deafferated, and the same experiment was repeated. These monkeys were still able to position the arm even in the presence of the disturbance with no feedback - afferent or visual. This surprising result implies that there seems to exist a central program which sets the parameter of the movements which can operate entirely feedforward if needed [Polit and Bizzi 1979].

Modulating Impedance

Polit and Bizzi postulated that this central program was executed by setting equilibrium points for both the intact and deafferated cases - the assumption being that the highly trained monkey does not use a different motor program after deafferation. In both cases, this can be done by modulating the mechanical impedance of the muscle itself [Hogan 1984a]. Unlike Feldman's control of muscle length, the alpha model postulates α-motoneuron activity modifying the inherent length and velocity dependence of the muscle. Experimental results support this claim [Rack and Westbury 1969]. In Figure 2.4, the stiffness of the muscle increases with activation for at least the smaller displacements along the length-tension

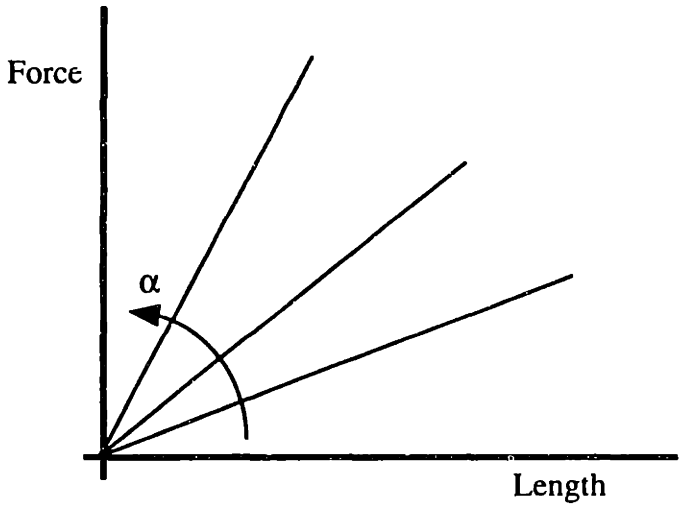

Figure 2.5: Schematic of the areflexive length-tension muscle curves. This simple model is meant only to represent variable stiffness behavior of muscles in a comprehensible manner.

curves. This same phenomenon will be represented schematically by Figure 2.5 which shows a linear spring whose stiffness increases with activation.

By placing two of these tunable springs in an agonist-antagonist configuration about a single joint (Figure 2.6a), equilibrium can be achieved through coactivation as seen in Figure 2.6b where activation results in a choice of length-tension curves for each muscle. Since the moments about the joint induced by each muscle oppose one another, the equilibrium position is the point at which the magnitude of each muscle moment is the same or as in Figure 2.6b, the point at which the two length-tension curves meet. Movement of the equilibrium point, therefore, can be achieved by a change in activation which changes the length-tension curve of the muscle as shown in Figure 2.6c.

Since both muscles are in tension about the joint, the stiffnesses of each muscle add to make the total net angular stiffness about the joint. If stiffness is a tunable parameter, net elbow impedance is trivial to modulate. Figure 2.6d shows the elbow maintaining the same equilibrium point, but by choosing appropriate activation the net stiffness can be increased.

Virtual Trajectory

The equilibrium point hypotheses (lambda or alpha) postulate movement in the form of a shift in equilibrium. This theory originally took the form of a final position controller where the CNS

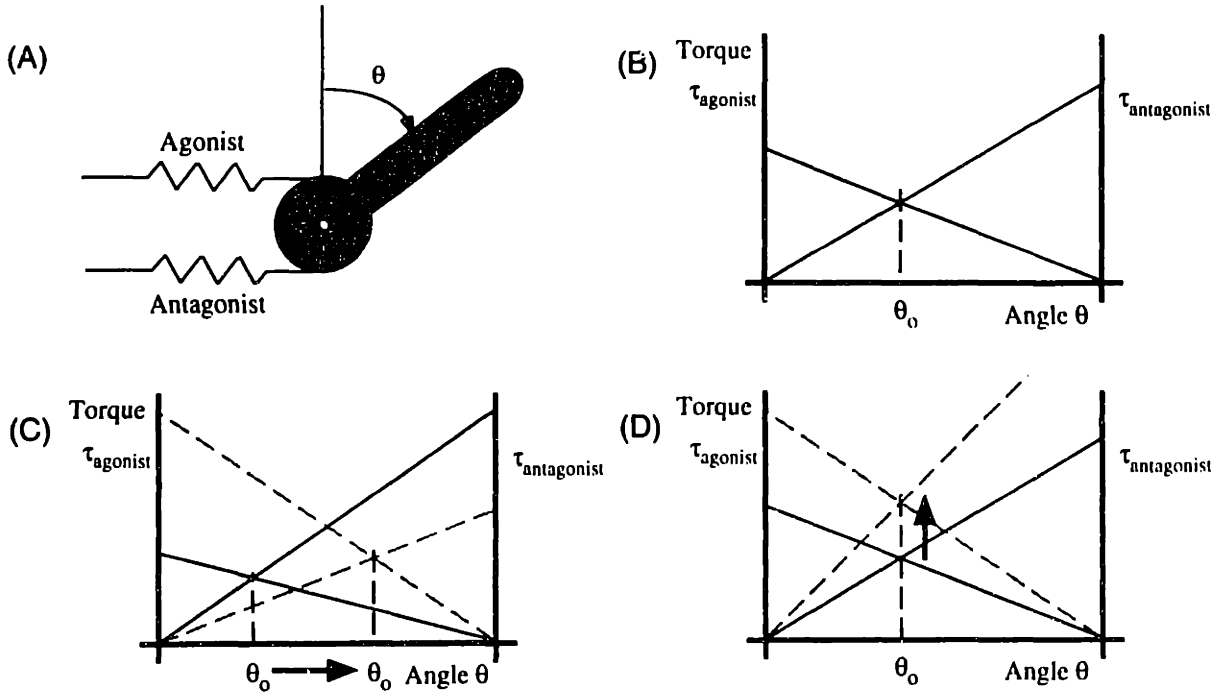

Figure 2.6: (A) Muscles with tunable stiffness about a joint. Note that forces by each muscle causes moments which subtract. However the net stiffness about the joint is the sum of the stiffness. (B) Equilibrium point defined by the intersection of the length-tension functions for the extensors and flexors. (C) Movement of the equilibrium position by a change in activation. (D) Tuning of net joint stiffness.

would define a new posture at the intended target of the movement. Under this structure, the equilibrium point would be at the target as soon as the dynamics of the muscle activation would allow. However in the early 1980s, Bizzi et al. performed further monkey experiments which revised this hypothesis.

These experiments were also single-joint pointing tasks. The monkey performed flexion and extension movement with a 60° amplitude. The first of these new experiments used a holding action at the initial position. The target would be illuminated, and the arm of the monkey would be held by the torque motor at the starting position for varying durations. Figure 2.7 displays the results of this experiment; it plots the initial accelerations upon release versus the holding time of both the intact and deafferated monkeys.

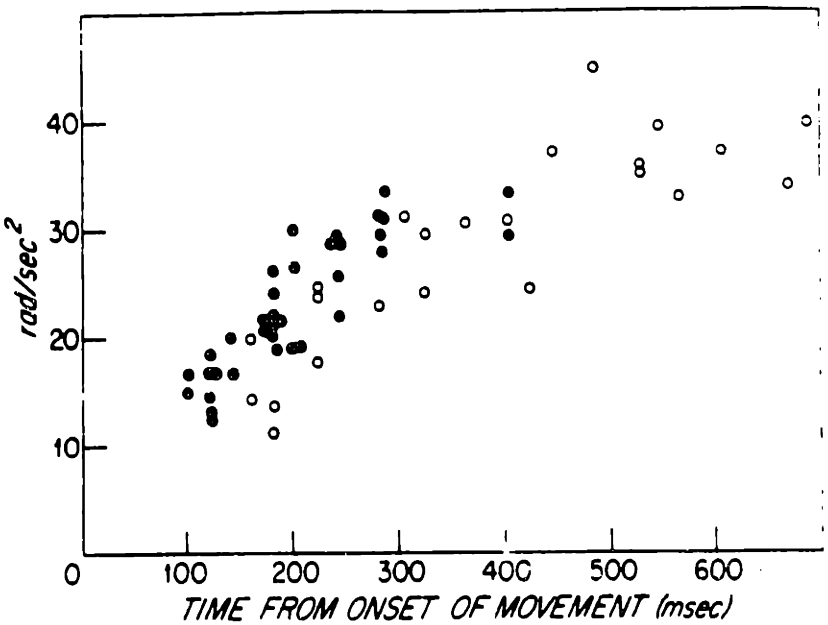

Figure 2.7: Initial acceleration upon release plotted against the duration of the holding period after the onset of movement. The solid circles represent the data from the intact animal. The open circles are for the deafferated animal. (From Bizzi et al. 1984)

The initial accelerations in Figure 2.7 steadily grow with the length of release time until it reaches a steady-state after 400 ms from the start of EMG activity. In addition, the measured torque by the elbow during the holding phase shows transient behavior up to 500 ms after the start of EMG activity. These periods of transient of behavior are much longer than the estimated 200 ms it takes the series of twitch contractions to bring about steady-state force if we assume a conservative third order linear model [Hogan 1984b]. This result showed that the attractor point must undergo a more gradual shift from start to target than initially proposed by the final position control.

This conclusion was verified by the second experiment where before the onset of movement the deafferated monkey was servoed to the target position. Sometime after measuring EMG activity in the agonist, the limb is released, and the arm is free to move. The lack of afferent and visual feedback to the monkey keeps it uninformed of these changes. As a result when the target is illuminated, the agonist muscle activates; however the arm moves back toward the initial position to some intermediate point before returning to the target as shown in Figure 2.8 [Bizzi et al. 1984].

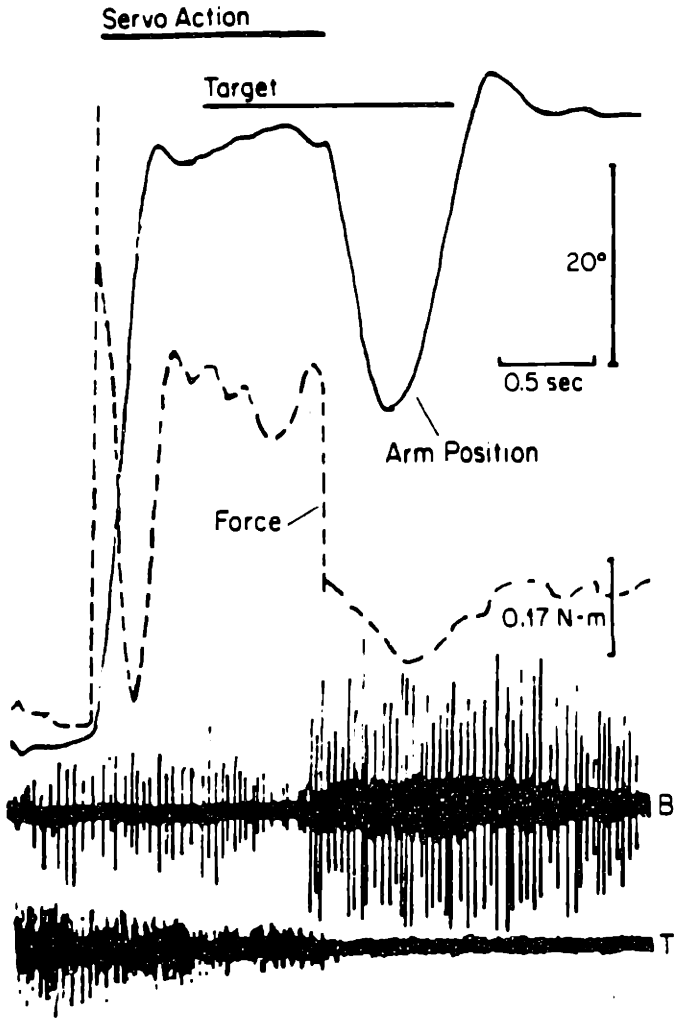

Figure 2.8: Forearm movement of the deafferated animal where the arm was taken to the final position before the onset of movement (shown by upper bar). The target was illuminated (lower bar), and the arm was held and then released. The arm returned to an intermediate position between the start and finish before moving back to the target position (solid line). The measured torque is given by the dotted line. EMGs of the biceps and triceps are also shown. (From Bizzi et al. 1984)

Again, this result can be explained by a moving virtual point which starts at the initial point and forms a trajectory to the target. This trajectory has a time constant much larger than the twitch contraction time of a muscle. It was then proposed and supported through simulations that the CNS commands a time history of shifts in the virtual position along the desired path [Hogan 1984b]. The time history was called the virtual trajectory and as discussed previously provides a computational simplifying control structure for human movement.

Summary: Alpha Model

The alpha model provides a competent explanation of how a deafferated monkey can perform pointing movements in the absence of reflex loops. The most misunderstood point of these experiments is that although *qualitatively* there were no differences between the intact and the deafferated monkeys, this is not to say that movement and posture in intacts is completely devoid of reflex activity. The qualitative similarity of the two cases imply that sensory feedback is not essential to controlling movement since the monkeys were able to apply their training as intacts to the task of moving without feedback. This hypothesis does not preclude the use of feedback to augment the ability to perform movements; it only questions its necessity in performing the fundamental motor control strategy [Bizzi et al. 1984].

Nevertheless through the modification of reflex loops (lambda model) or through the tuning of neuromuscular impedance (alpha model), there is a large body evidence that the CNS can use the equilibrium point as a control input to generate single-joint movements.

2.2 Static Impedance Measurement

The ability to quantitatively test the virtual trajectory hypothesis depends on some measure of the muscular impedance of the human arm. Since impedance relates output force to input motion, the mechanical impedance of the human limb can be measured by displacing it from a given posture and recording the evoked restoring force. This technique was used by Mussa-Ivaldi et al. (1985) in a series of psychophysical experiments to measure the steady-state force-displacement relation of an arm constrained to move in the horizontal plane only.

The subject was seated grasping the instrumented handle of a computer-controlled two-link manipulandum as shown in Figure 2.9. A sling supported the upper arm of the subject and constrained movement to a horizontal plane at shoulder level. A brace prevented movement about the wrist. The subject was told to maintain a posture under a particular visual target. Once under the target, a series of random displacements in different directions was applied to the hand by the manipulandum. The magnitude of these displacements ranged from 5 to 8 mm; the directions ranged from 0° to 325° at 45° intervals. After each perturbation, the resulting displacement and force imposed at the handle were recorded.

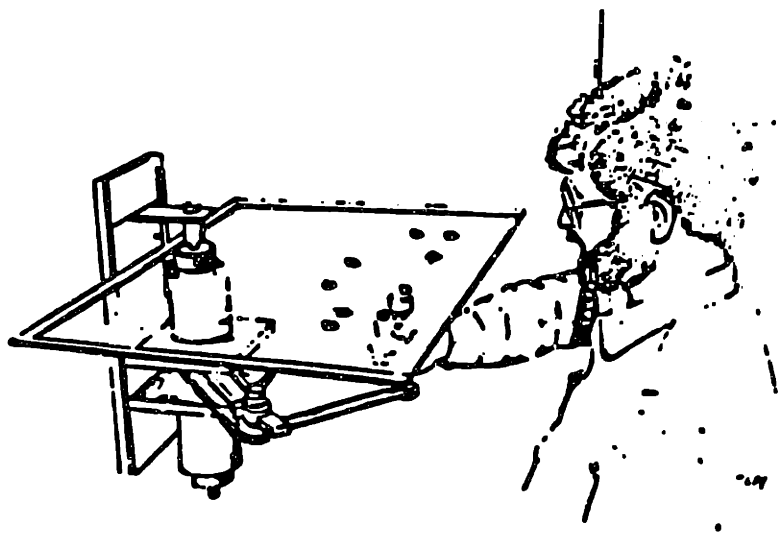

Figure 2.9: The experimental setup of the stiffness measuring experiment. The subject grasped the handle of a two-link manipulandum and maintained a posture under a target. (from Mussa-Ivaldi et al. 1985)

As shown earlier in this chapter, the force-displacement function for the muscle is fundamentally nonlinear. However for small displacements about equilibrium, we can assume that the high-order terms of the Taylor series expansion of the force-displacement function are negligible; and therefore the function will be considered as linear. Therefore the two-dimensional relationship in the x and y directions of the handle can be expressed as

$$F_x = K_{xx}dx + K_{xy}dy \tag{2.1}$$

$$F_y = K_{yx}dx + K_{yy}dy \tag{2.2}$$

where F_x and F_y are the components of the restoring force, dx and dy are the components of the imposed displacement, and K_{xx}, K_{xy}, K_{yx}, and K_{yy} are the linear stiffness terms. These two equations can be restated in the form of a stiffness matrix K.

$$\vec{F} = Kd\vec{x} \tag{2.3}$$

$$\begin{bmatrix} F_x \\ F_y \end{bmatrix} = \begin{bmatrix} K_{xx} & K_{xy} \\ K_{yx} & K_{yy} \end{bmatrix} \begin{bmatrix} dx \\ dy \end{bmatrix} \tag{2.4}$$

Note that the matrix K is not assumed to be symmetric. The terms in the stiffness matrix were estimated from the data by using a linear least squares regression [Mussa-Ivaldi et al. 1985]. Figure 2.10 shows the results of the regression fit. Figure 2.10a displays the actual

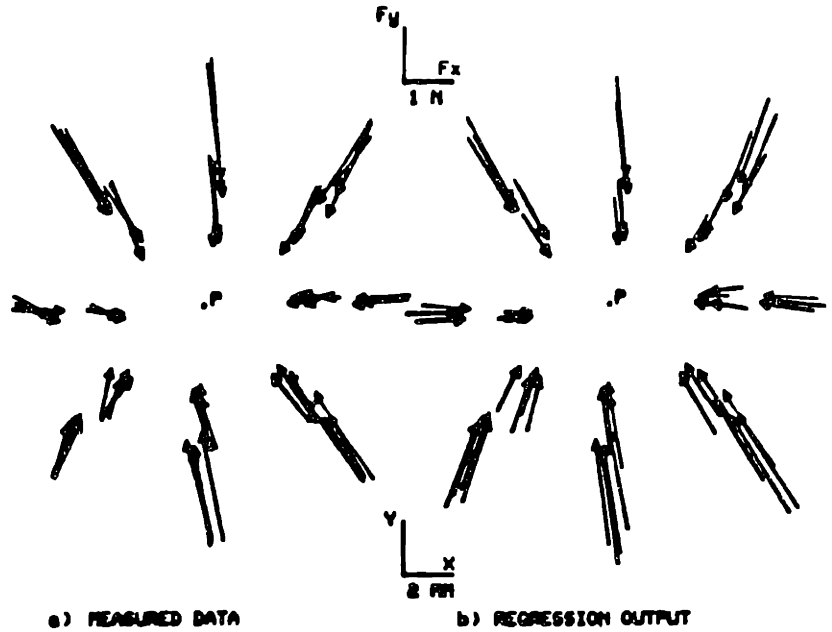

Figure 2.10: (a) Vector diagram of the restoring forces measured from a subject maintaining a posture with the hand at equilibrium point P. (b) The forces computed from the estimated stiffness.

data while Figure 2.10b shows the forces predicted by the stiffness matrix for the same displacement. The similarities of the two plots implies that the linear model is capable of providing an excellent fit of the experimental data.

2.2.1 Conservative Field

The spring-like nature of the arm's end-point impedance can be seen from the stiffness matrix K. For the neuromuscular system of the arm to be spring-like, the restoring force field defined by equation 2.4 must be integrable which is mathematically equivalent to having zero curl. In the 2x2 case, zero curl is equivalent to a symmetric stiffness matrix. To visualize the amount of curl in the system, the K matrix can be decomposed into a conservative or symmetric component (K_s) and a curl or anti-symmetric (K_a) component [Mussa-Ivaldi et al. 1985].

$$K = K_s + K_a \tag{2.5}$$

where

$$K_s = \frac{(K + K^T)}{2} \tag{2.6}$$

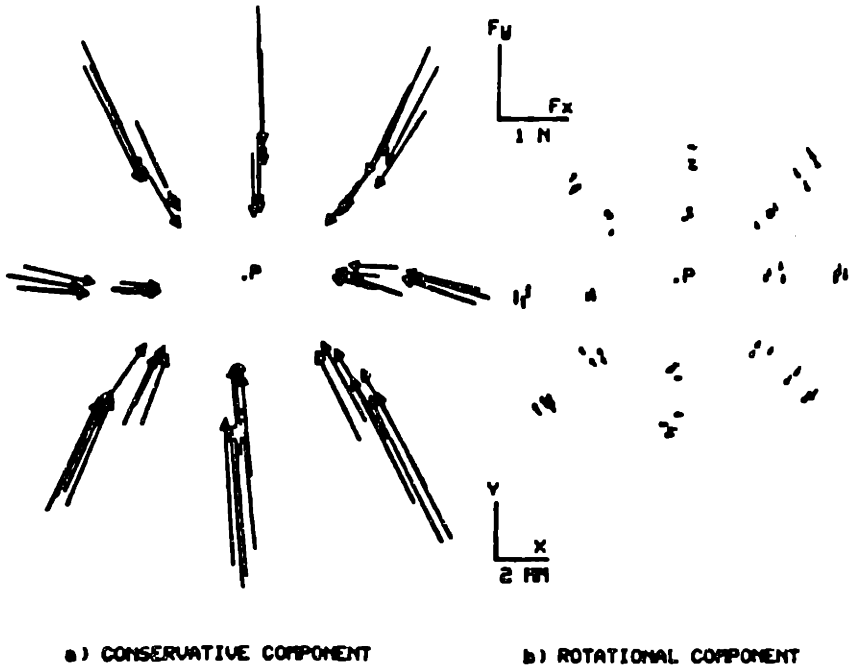

Figure 2.11: Force components calculated from the estimated stiffness. (a) The conservative or symmetric component. (b) The rotational or antisymmetric component. (from Mussa-Ivaldi et al. 1985)

$$K_a = \frac{(K - K^T)}{2} \tag{2.7}$$

Figure 2.11 displays the relative contributions of each of the components to the total force field. Figure 2.11b shows a very small rotational component when compared to the conservative component in Figure 2.11a. In fact, Mussa-Ivaldi et al. (1985) found in about half the measurements, the curl was not statistically distinguishable from zero. In every case, the curl was extremely small. This essentially zero curl in the static component of the end-point impedance implies that the behavior of the neuromuscular system in the arm is equivalent to a mechanical spring.

Such a result may seem trivial when taking into account of the spring-like nature of the muscles themselves. However, the proven existence of intra-muscular feedback pathways provides a mechanism for generating curl. Curl can be produced through unbalanced feedback where stretch in a muscle at one joint produces activation in a muscle at another joint which is larger or smaller than the activation if the second muscle was similarly stretched. The lack of curl implies that either the gain of these intra-muscular reflexes is very small or these reflexes are balanced in such a way to maintain a spring-like impedance.

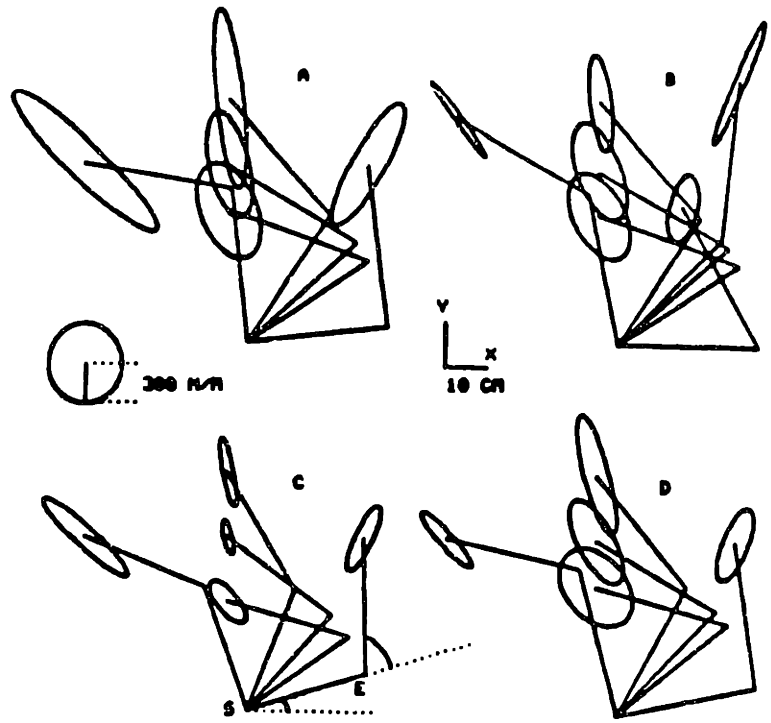

Figure 2.12: Stiffness ellipses measured from four subjects for five different postures. (from Mussa-Ivaldi et al. 1985)

As stated in Section 1.2, the spring-like nature of the end-point impedance has important benefits in terms of contact stability. The fact that an active object such as the arm is constrained to behave as a passive object guarantees contact stability with passive objects.

2.2.2 Control of stiffness

The symmetric component of the stiffness matrix can be graphically represented as an ellipse characterized by the magnitude (area of ellipse), shape (the ratio of axes), and the orientation (direction of major axis). Using this convention, Mussa-Ivaldi et al. (1985) plotted the end-point stiffnesses of the subjects in the five different configurations. Figure 2.12 shows the data from four of the subjects in the different configurations. Note the systematic change in shape and orientation as the arm moves to a new configuration. The ellipses elongate as the hand moves distally away from the shoulder. The ellipses also reorient themselves to keep the major axis pointed toward the shoulder. In addition when testing the same subject over a period of days or months, it was found that the characteristic shape and orientation of the ellipses at each posture remained remarkably invariant. The magnitude or area of the ellipse, however, varied significantly and could be controlled by the subject.

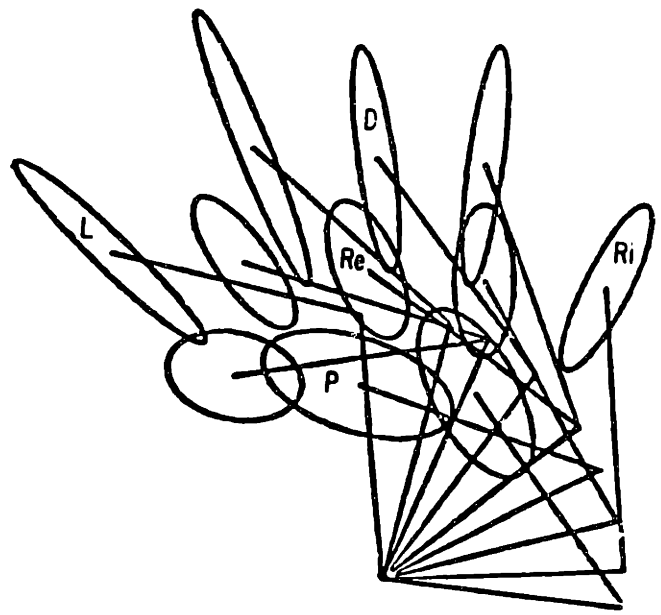

Figure 2.13: Predicted endpoint ellipses from a constant joint stiffness measured from subject A. (from Mussa-Ivaldi et al. 1985)

To explain this remarkable pattern, Mussa-Ivaldi et al. (1985) postulated that the shape and orientation of the stiffness ellipse in joint space is invariant over *all* tested postures and that the change in endpoint stiffness could be explained by the geometric transformation of the joint stiffness to the endpoint stiffness. From the endpoint stiffness measured at one posture of a subject, the joint stiffness was calculated using the Jacobian transformation. With this joint stiffness, predictions were made of the endpoint stiffness at other postures assuming a constant joint stiffness. Figure 2.13 displays the results of this simulation. Comparing this plot with the plot of subject A in Figure 2.12 shows a remarkable correspondence for all the tested postures with the exception of the most proximal position. Further analysis by Shadmehr (1991) took the five measured endpoint stiffness and plotted the corresponding ellipses in joint space as shown in Figure 2.14. The similarity in shape and orientation of the five ellipses in joint space also suggests that the joint stiffness is independent of configuration and nearly invariant over all postures.

This invariance of shape and orientation seems to extend over more than just setting posture. Further experiments by Mussa-Ivaldi et al. (1985) showed that when the subject was asked to stabilize a load applied in a constant direction the subject would evenly scale the major and minor axes of the ellipse. In other words, the area of the ellipse would increase

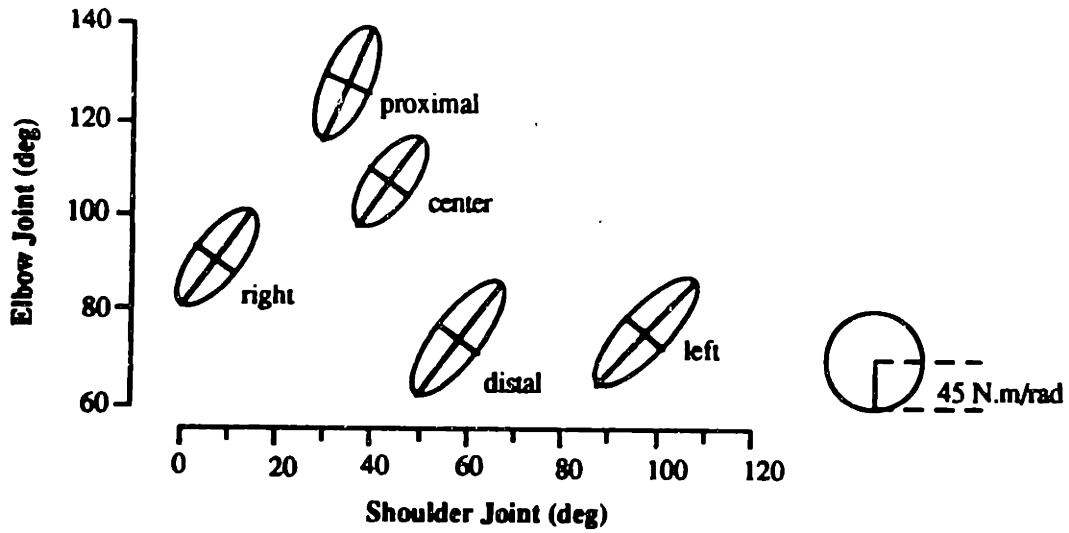

Figure 2.14: The stiffness ellipses of the five measured positions plotted in joint space. (from Shadmehr 1991)

without changing the shape or orientation. Experiments on the effect of motor learning on the postural field have also found an inherent difficulty of the CNS to modulate the shape or orientation [Personal conversation with R. Shadmehr, M.I.T.].

These results imply either a mechanical or neural constraint on the ability of the human subject to modulate an arbitrary stiffness. The human seems incapable of changing individual entries of the joint stiffness matrix; the human can only scalar multiply the entire matrix. In other words, the basic geometric shape and orientation of the ellipse is fixed except for the ability of the human to scale the size of the ellipse. Similar to the findings of the curl-free stiffness, there seems to be some type of balance or constraint on the control of the individual single- and two-joint muscles to preserve this invariance.

2.3 Movement Generation by Virtual Trajectories

From the knowledge gained about the behavior of the static component of the impedance of the human arm, is it possible to verify the notion of generating movement of the two-joint arm through a shift in an attractor point? This section will present the work of Flash (1987) which makes use of the stiffness measurement of Mussa-Ivaldi et al. (1985) to make predictions of human multi-joint arm movements.

2.3.1 Virtual Trajectory Derivation and Simulation

Flash (1987) took experimental kinematic data from various planar point-to-point two-joint arm movements and showed that a single virtual trajectory may be the foundation for generating a large class of movements. The analysis performed by Flash fell into two parts. The first analysis took a single measured movement and calculated a virtual trajectory to generate this movement using various assumptions of the size and shape of the stiffness and damping ellipses. The second analysis used this derived virtual trajectory as the driving input to a computer simulation which attempted to recreate the other experimentally recorded movements.

When backcalculating the virtual trajectory from an actual movement, Flash used a third order interpolation of joint stiffness to account for the small changes of the joint stiffness with changes in configuration of the arm. In addition, this configuration varying stiffness matrix was also multiplied by a constant scaling factor. The damping terms were assumed to be the product of the assumed stiffness with a time constant assumed to be between 0.05 s to 0.125 s. With these assumptions, Flash found that the derived virtual trajectories follow straighter point to point paths than the actual movement. This can be considered surprising since in no way is the virtual trajectory constrained to be a straight line; it simply results from choosing an appropriate set of physical parameters for the arm. In fact, these parameters cannot be chosen arbitrarily; the shape and orientation of the stiffness correspond to the experimental results of Mussa-Ivaldi et al. (1985). The shape and orientation of the velocity dependent term were chosen as sensible, conservative assumptions when faced with the unavailability of any quantification of neuromuscular damping in the two-joint arm.

After deriving a single virtual trajectory from one movement by a subject, Flash then translated, rotated and scaled the trajectory to place the endpoints on the corresponding start and targets of different measure trajectories. This "new" virtual trajectory as well as the stiffness and damping model to derive the trajectory was then used to calculate the torque inputs to the equations of motion of the computer simulation. The resulting simulated hand paths and velocity profiles were then compared to the actual measured data of the corresponding movements. Figure 2.15 displays the results of these simulation. The first movement in Figure 2.15 was used to derive the equilibrium path (labeled E) from the measured path

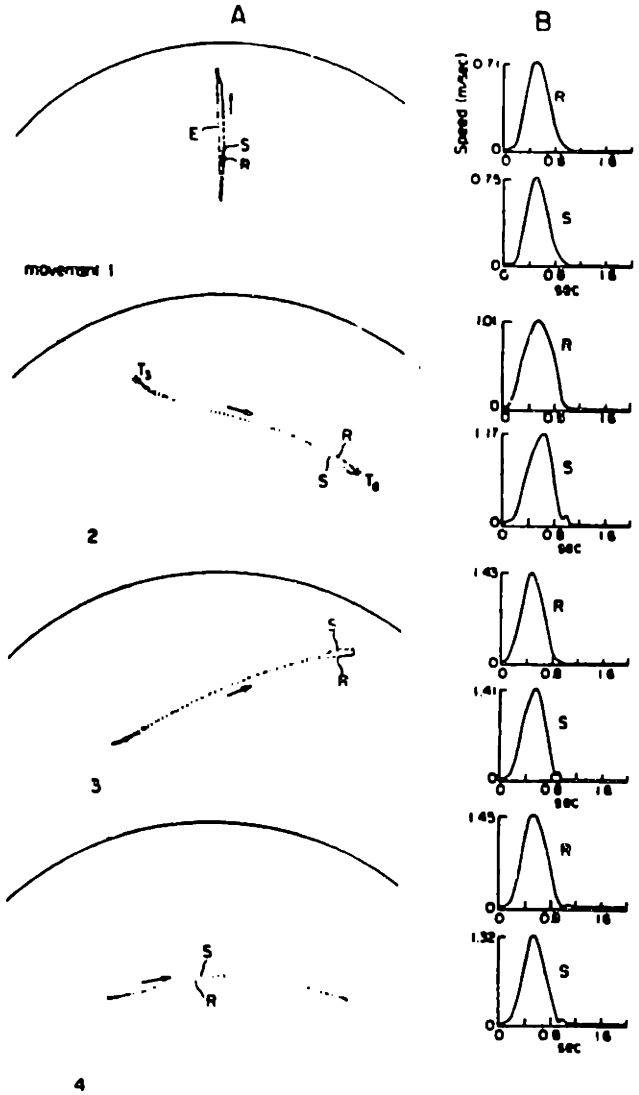

Figure 2.15: The virtual trajectory simulations. The virtual trajectory for this subject was derived from movement 1 at top. Subsequent movements (2-4) were generated by modifying this derived trajectory. R - the measured path. E - the virtual trajectory.

(labeled R). Scaling this trajectory across new start and end points resulted in the simulation results shown in the last three figures. These simulated results (labeled S) have excellent correspondence with the measured data in both the hand path and the velocity profiles.

The result that calculated virtual trajectories are essentially straight lines from start to finish implies that reaching movements may be internally represented as a virtual trajectory rendered in the coordinate frame of the hand. These virtual trajectories are easily represented in the cartesian frame of the hand but acquire complexity when shown in the joint space. The close fit

of the simulated result to the actual result suggests that new movements can be created by generalizing from a single trajectory; this single virtual trajectory can be portrayed as a basic building block for movement which can be modified (stretched, rotated, or translated) to create a wide class of movements.

2.3.2 Simulation Paradigm

There is general disagreement on the value of simulations to verify motor control hypotheses. Hasan (1991) argues that the large number of uncertain parameters in the human neuromuscular system makes any claims through simulation suspect. Others point out that a purely mechanical simulation is not very effective since it is not tied to any biological model making it nearly impossible to analyze in neurophysiological terms [Smith and Humphrey 1992]. These parties raise a valid point since the parameters used by Flash are questionable. In particular, Flash needed to increase the postural stiffness by at least a factor of three to find a straight-line virtual trajectory representation of the movement. Such large stiffness during movement has been questioned by several studies [Bennett et al. 1991; Gomi et al. 1992].

Yet one cannot ignore the ability of Flash's single derived trajectory to make predictions of many movements taking place in different portions of the workspace. The quality of fit for the generated movements was as close as the fit of the trajectory used for deriving the virtual trajectory. This quality of fit is compelling especially since inaccurate parameters can only degrade the global prediction. Such an attractive result invites further study, and it is the intention of the experiments described in the next chapter to further test the veracity of Flash's results.

Chapter 3

The Experiments

This chapter provides a detailed description of the two experiments performed within this study. The first of these experiments is a postural field measuring experiment similar to the experiments described in Section 2.2. The experimental protocol, equipment and techniques for estimating two-dimensional stiffness of the human arm will be presented within the first section of this chapter. The second section will describe the set of reaching experiments. Again the protocol, equipment, and data processing techniques will be introduced for these experiments. The chapter will conclude with an explanation and a justification of the "do not intervene" paradigm which is fundamental to these types of psychophysical experiments.

3.1 Measurement of Stiffness

The procedure used to measure the static component of the human arm impedance is nearly identical to the experiment used by Mussa-Ivaldi et al. (1985). Differences exist only in the hardware used as well as the perturbation given. However the basic strategy remains the same: provide a perturbation which induces a displacement of the arm and then relate the evoked force to the input displacement to estimate the impedance.

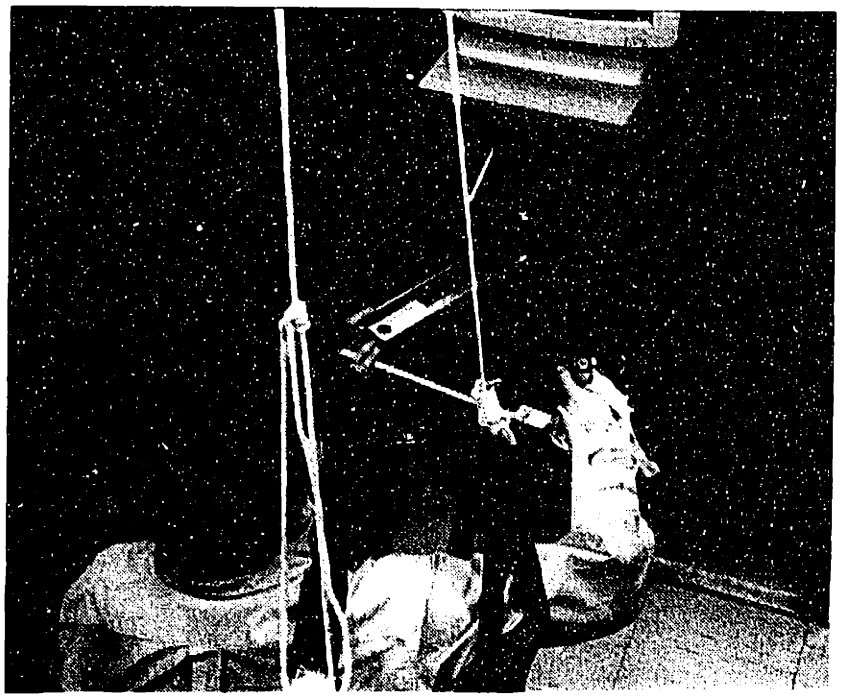

Figure 3.1: Subject grasping the larger two-link manipulandum. The arm of the subject is supported by a sling suspended from the ceiling which maintains the arm in plane with the arm of the robot. The handle grasped by the subject is instrumented with a six-axis force transducer.

3.1.1 The Hardware

The perturbations are provided by a computer controlled parallel four bar two link manipulandum as shown in Figure 3.1 [Faye 1986; Fasse 1993]. Subjects are seated in front of the manipulandum grasping the handle containing the force transducer at shoulder level. The arm of the subject is suspended with a sling so that the upper arm and forearm remain in plane with the arms of the robot. In addition, the subject wears a wrist cuff which effectively removes the degree of freedom about the wrist.

A 386 personal computer is used to sample position and force data from the robot as well as command torques to the motors at a frequency of 100 Hz. Position is measured at the joints by optical encoders (Teledyne Gurley 25/04s-NB17-IA-PPA-QAR1S) while force at the handle is measured by a six-axis Lord force transducer. Torque at the elbow and shoulder joints of the robot are applied by two low inertia D.C. torque motors (PMI JR16M4CH). Included within the torque motor is a tachometer enabling velocity feedback for controller damping purposes.

The perturbation is applied by a simple endpoint controller of the following form:

$$\vec{\tau} = J^{T}\left(K(\vec{x} - \vec{x}_o) + B\dot{\vec{x}}\right) \tag{3.1}$$

where $\vec{\tau}$ are the commanded motor torques, J is the manipulator Jacobian, $\vec{x}$ is the current endpoint position vector, $\vec{x}_o$ is the equilibrium position vector, and $\dot{\vec{x}}$ is the endpoint velocity vector. The stiffness K and the damping B used for the perturbation are as follows.

$$K = \begin{bmatrix} -0.7 & 0 \\ 0 & -0.7 \end{bmatrix} \text{N/mm} \tag{3.2}$$

$$B = \begin{bmatrix} -20 & 0 \\ 0 & -20 \end{bmatrix} \text{N/mm/s} \tag{3.3}$$

The perturbations applied are a ramp in the equilibrium position $\vec{x}_o$ from the rest posture of the subject to a 7 cm displacement in a given direction. This ramp occurs over a three second period. The arm of the subject as it goes through this gradual ramp in displacement will be assumed to be in a quasi-static state at all time points. Therefore, stiffness can be estimated directly from the force measured at the handle.

3.1.2 Measurement Procedure

Endpoint stiffness was measured at three different positions which correspond to regions of the workspace at which the three reaching movements will take place. These three locations are shown relative to the shoulder of the subject in Figure 3.2. The three reaching trajectories to be tested are also shown in Figure 3.2. Measuring at these locations provides a representative sample of the endpoint stiffness for the arm configurations used during the movements.

At each indicated position, the subject maintains a posture while a series of perturbations are applied. This series consists of twenty-four ramped displacements each taking the hand in a different direction. The ramps span the entire 360 degrees of possible directions with no two directions closer than fifteen degrees apart.

All measurements are done with the subject's eyes closed. The subject is also instructed to "hold the handle firmly, but not tightly" with the intent that the subject holds posture with a moderate amount of co-contraction but short of maximum co-contraction. During the imposed displacement, the subject is also instructed to "do not actively resist or

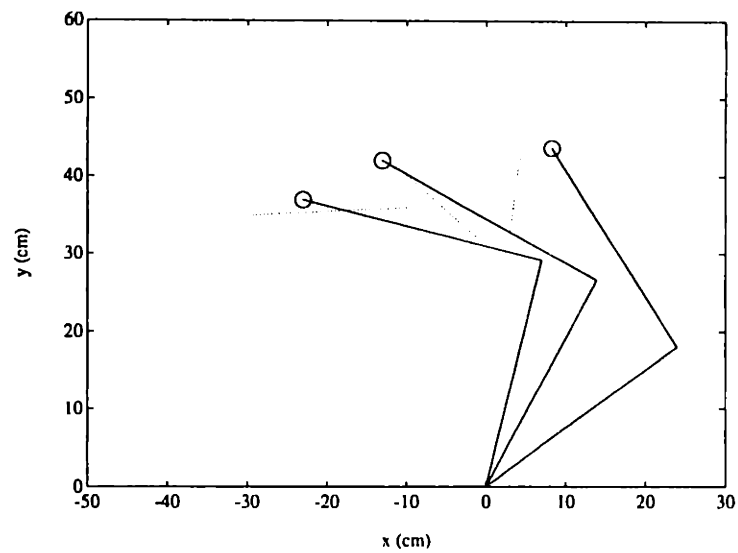

Figure 3.2: The three postures where stiffness was measured. Superimposed are the three movements to be tested.

interfere with the applied perturbations" so that the "natural" static response of the system can be measured. Initially if the resulting displacements are small (< 1 cm), then the subject is told to relax his co-contraction. If the displacements are large (> 6 cm), the subject is told to increase co-contraction. Once an acceptable displacement is achieved, the subject is instructed to maintain a constant co-contraction for the series of twenty-four displacements to be recorded.

3.1.3 Data Processing

The data collected consists of the x and y position of the hand as well as the x and y components of the force measured at the displacements. From this data set, the coefficients K_{xx}, K_{xy}, K_{yx}, and K_{yy} are found which creates the best approximation of the data by the following equations.

$$F_x = K_{xx}dx + K_{xy}dy \tag{3.4}$$

$$F_y = K_{yx}dx + K_{yy}dy \tag{3.5}$$

where dx and dy are the x and y displacements from posture and with F_x and F_y as the x and y components of measured force. The K coefficients are found by a simple linear regression on both equations.

The linear regression was performed using the statistics package within the software application, Mathematica 2.0 [Wolfram 1991]. The regression procedure attempts to find the

best linear combination of basis functions which best approximates the data. For this particular case, the procedure finds the best β_j's which minimize the residual sum of the squares, $\sum_i e_i^2$, in the following equation.

$$F_i = \beta_1 + \beta_2 dx + \beta_3 dy + e_i \tag{3.6}$$

where F_i is the ith response, dx_i and dy_i are the basis functions for the ith sample. The acceptability of the fit is judged by the size of the R^2 value and the offset coefficient β_1.

3.2 Reaching Experiments

The movement experiments consisted of the subjects making point-to-point reaching movements between two targets. In all, the subjects performed three different trajectories in different locations of the arm's workspace. Each trajectory was tested separately. As a result in each experimental trial, the subject makes repetitive back and forth movements pausing each time when the target has been reached. At particular intervals, a constraint is applied to the trajectory forcing the arm to follow a different trajectory than intended.

3.2.1 The Hardware

These experiments were performed on another manipulandum different from the one used in the stiffness measurement. Although the two are similar in design, the second manipulandum shown in Figure 3.3 is approximately half the size of the other. In addition to its smaller size, the robot used in these experiments differs from its larger counterpart in that it is equipped with two electromagnetic brakes (Dodge #FB30-10-713) placed on each motor shaft. These brakes are capable of independently locking the shoulder or elbow joints of the robot with an impedance sufficiently large that the human is incapable of causing a displacement along that degree of freedom.

Position of the joints of the robot as well as the force applied to the handle are measured and recorded by a set of three computers working in conjunction. The joint angles are measured by two conductive film potentiometers (NEI F78SC502 5 kΩ) and recorded by a DEC LSI 11/73 sampling at 100 Hz. This computer is also in charge of controlling the two magnetic brakes as well as running the targeting lights. Force at the handle is measured by a six-axis force transducer (Lord LTS-210F) which is sampled by an 8088 model computer at

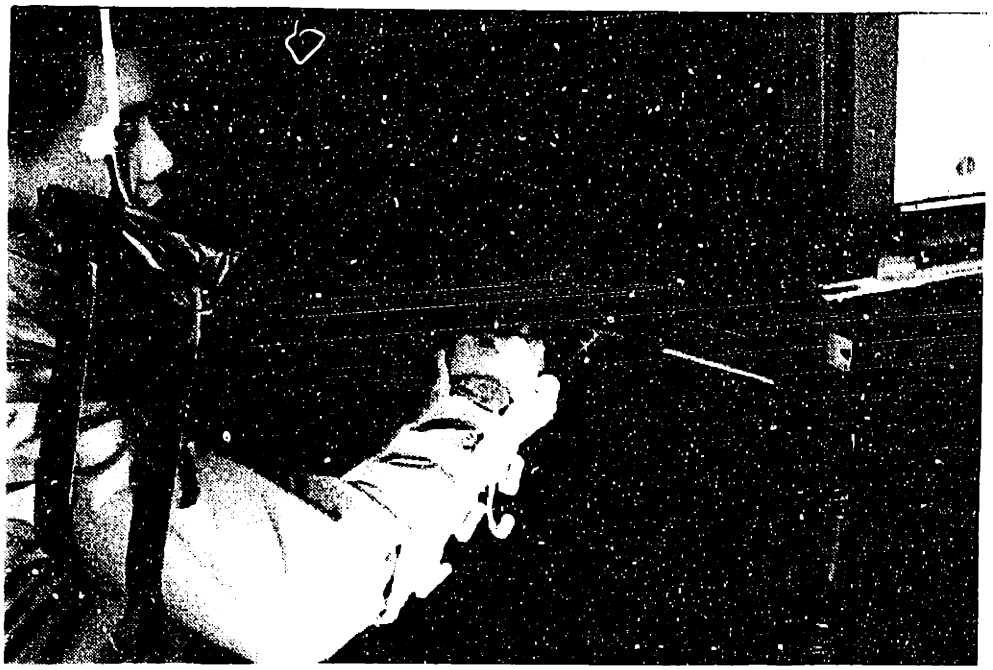

Figure 3.3: Subject grasping the smaller manipulandum. Similar to the stiffness experiment, the subject's arm is suspended by a sling to maintain the arm along a horizontal plane.

60 Hz. Coordination and synchronization of these two computers are handled by a 386 personal computer. Errors in synchronizing the commencement of sampling of the two computers is below the 0.017 s period of sampling for the 8088.

The electromagnetic brakes apply torque to the motor shafts through friction between two flat mating surfaces. Figure 3.4 presents the details of one of the two brakes. Current into the electric coil of the brake generates an electric field which brings the rotatable upper clutch plate into contact with the fixed plate at the base. The friction torque applied to the shaft is proportional to the amount of downward force applied by the induced magnetic field. The downward force of the magnetic field is opposed by three leaf springs which also assist in plate separation after the brake releases.

For this experiment, friction torque is not explicitly controlled; rather the intent is to apply maximum resistive torque and the minimum resistive torque. As a result when the brake is used, a voltage of 90 Volts is applied with zero voltage applied otherwise. A conservative estimate for maximum friction torque is approximately 200 in-lbs. A more exact estimate is unnecessary as long as the rated torque can withstand any force applied by the human at the handle.

Figure 3.4: Detail of the electromagnetic friction brake. The upper plate rotates with the motor shaft while the brake housing is bolted to ground. A generated magnetic field in the brake pulls the upper plate into contact with the lower plate causing a resistive torque due to friction.

The clutch release time or the time required for the brake to go from maximum friction to minimum friction has been measured to be between 70 to 75 ms. This was measured by locking both joints of the robots with the brakes. A 300 gm weight tied to the handle applies a gravitational force through a pulley. While sampling position and force, one of the brakes of the robot is released. This procedure is repeated for the other brakes. Both brakes showed similar estimates in release time which was measured by examining the velocity of the released joint as well as the force measured at the handle.

3.2.2 Experimental Paradigm

Similar to the stiffness measuring experiment, the subject is seated in front of the manipulandum grasping the handle at the end-effector of the robot. The arm is supported by a sling, and the wrist is constrained by the wrist cuff as shown in Figure 3.3. A pair of light emitting diodes (LED's) are suspended over the workspace of the robot to serve as targets for the

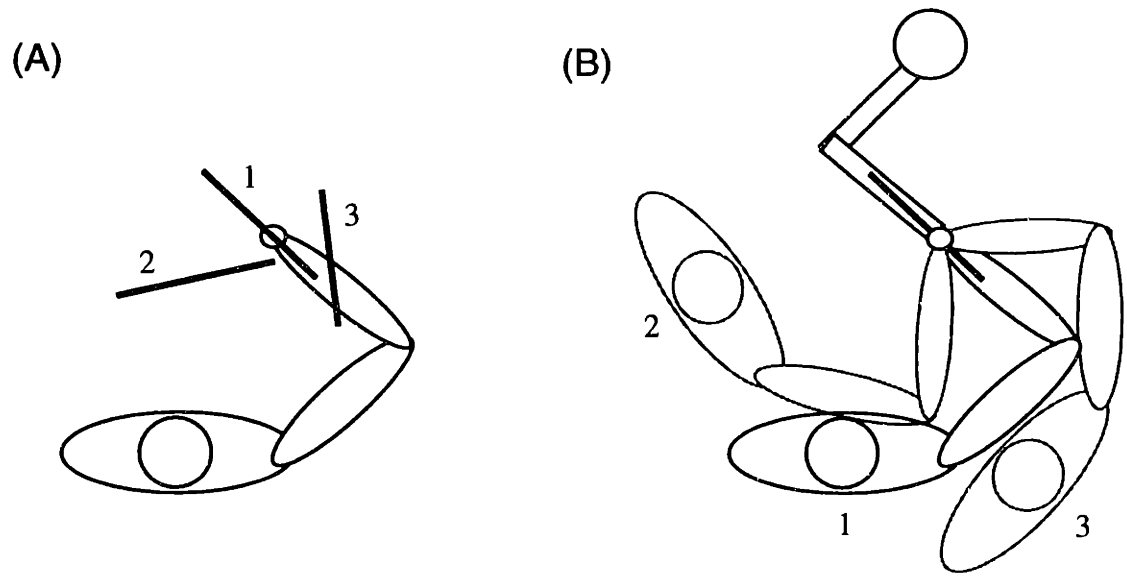

Figure 3.5: (A) The three trajectories shown relative to the shoulder of the subject. (B) The position and orientation of the subject relative to the robot to create the three trajectories.

point to point movements to be performed. These target lights are approximately 18 cm apart from each other.

Three different trajectories were tested as shown in Figure 3.5A. These three trajectories were performed using the same two target lights. To generate the different configurations, the chair of the subject was translated and rotated relative to the targets as shown in Figure 3.5B. As a result, the start and end points remain the same in the reference frame of the robot while the human perceives a different trajectory to be performed. This technique has the advantage that the inertia tensor of the robot remains invariant for all three trajectories relative to the targets and the hand path. Therefore differences in the trajectories will be due to a change on the human side rather than on the robot side.

For each of the trajectories, the subject starts with the handle under the illuminated target light. The subject is prompted to make a movement when the LED at the current position has been extinguished and the other LED at the target position has been illuminated. The subject is instructed to make a "move to the target as if reaching for some object at that point." The subject is also instructed to "attempt to ignore any abnormalities during the movement and perform the movements normally." Once at the target, the subject is instructed to stop and wait until the other

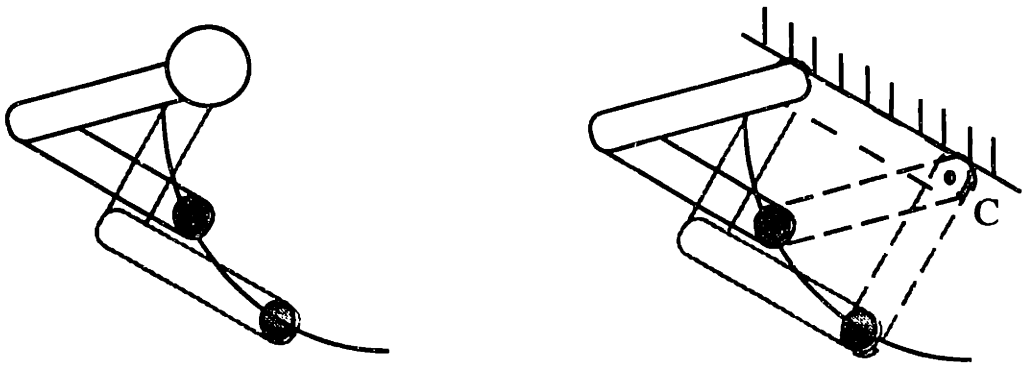

Figure 3.6: The imaginary parallelogram four-bar linkage when the robot is locked at the elbow. The dashed links are the imaginary linkages. C is the center of the circular path imposed by the constraint.

LED has been illuminated. As a result, through the course of a single trial, the subject makes several movements back and forth between the two points.

At pre-planned intervals, perturbations are applied to the subject through one of the magnetic brakes. These perturbations take two forms. The first type locks the brake associated with the elbow joint of the robot from the very start of the movement to the end. Locking the elbow removes a degree of freedom from the robot sot that the handle can no longer traverse a straight path. Instead its path is constrained to lie on a circle whose radius is equal to length of the robot's inner link (23.2 cm). The center of this constraint circle is determined by the locked elbow angle while the position along the circle is determined by the shoulder angle of the robot. The constraint is applied in such a way that both the start and target positions lie upon the circular path. As a result, the movement task can still be completed even in the presence of the constraint.

The best method to visualize the nature of this constraint is through the imaginary four-bar linkage shown in Figure 3.6. Since the elbow angle is locked relative to the base frame and not relative to the inner link, the forearm of the robot maintains a constant orientation relative to the absolute frame. Therefore the locked system can be viewed as the parallelogram linkage shown in Figure 3.6. In Figure 3.6, the position of the center of the circular constraint is defined by the elbow angle of the robot, and the position along the constraint is defined by the shoulder angle.

The second type of constraint locks the elbow joint at the beginning of the movement similar to the first case. However during movement, the constraint is released, and the arm is free to move in both degrees of freedom. The release is triggered by position and is consistently released when the hand has moved 5 cm away from the start measured along the straight line between the start and target.

During an experimental trial, these two types of constraints are applied only after at least three unperturbed movements have been performed by the subject. The number of unperturbed movements before the next constraint case are consistently varied from a minimum of three to a maximum of ten movements. These variations are intended to suppress any anticipation by the subject of a perturbed trial. To prevent the subject from receiving cues from the sound or tactile vibration of the brake engaging, the brake is toggled on and off before each of the unperturbed trials.

For a single trajectory, twenty constrained cases and twenty constrained and released cases were tested. Ten of each case were applied when the subject moved from target one to target two, and the other ten when the subject moved in the other direction from target two to target one. In addition to the constraint cases, twenty-four (twelve in each direction) of the unconstrained point to point movements were sampled and recorded by the computer. The other unconstrained movements were not recorded. This same pattern of applied constraints and unperturbed movements was presented to the subject for the three different trajectories (chair positions). However the movements for each trajectory number over two hundred so that it is unlikely that the subject can use past knowledge of a previous trial to predict constraints in the new trajectory.

3.2.3 Data Processing

Numerical Differentiation

The data from the movement experiments consists of the time history of the robot joint angles and the applied force at the handle during each movement. Since the robot is equipped solely with potentiometers, numerical differentiation of the position data is necessary to estimate joint velocities and accelerations. Previous work has shown that optimal smoothing algorithms were superior in performance to Butterworth filtering and numerically differentiating data [Murphy 1990]. The algorithm used for this work is based on the work by Dohrman, Busby and Trujillo

[Dohrmann 1986; Dohrmann et al. 1988]. This algorithm uses a state space formulation of the smoothing and differentiating problem using a series of cubic splines. Busby and Trujillo (1985) used dynamic programming to minimize the squared error given a smoothing parameter. However within the Dohrmann algorithm, the smoothing parameter is optimally chosen using the method of Generalized Cross Validation. Murphy (1990) demonstrated the ability of this technique to accurately smooth and estimate the first and second derivatives of noisy kinematic data.

From the estimates of joint velocities and accelerations given by this algorithm, endpoint values can be found by simply transforming through the manipulator jacobian J.

$$\vec{v} = J\vec{\omega} \tag{3.7}$$

$$\vec{a} = J\dot{\vec{\omega}} + \dot{J}\vec{\omega} \tag{3.8}$$

where $\vec{v}$ and $\vec{a}$ are the endpoint velocity and acceleration vectors and $\vec{\omega}$ is the joint angular velocity vector.

Trial Filtering

Incomplete data for the trajectories was filtered out of the main group before processing. Such data resulted from premature termination of sampling by the computers. Therefore, any movement which was sampled for less than 250 ms was removed from the final group of data to be processed. Only thirteen of the over seven hundred movements recorded were deleted in this way. The remaining data was then assumed to contain complete trajectory information and was thereupon sent through the processing procedure.

3.3 The Experimental Subjects

Five male right-handed subjects were used in this experiment. The five subjects were between 21 and 30 years of age with an average age of 24 years. None of the subjects had a history of any neurophysiological disorder or physical disability in their right arm.

Four of the five subjects completed the full experiments. Subject E was the only exception. Subject E did not perform the third trajectory shown in Figure 3.5.

3.4 "Do not intervene" Paradigm

Most problematic for the type of psychophysical experiments performed for this study is their reliance on the assumption that the subject completes the specified task in the perturbed trial in the same manner as the unperturbed trial. Perturbations are applied to make the measurements; however often the subject responds to the disturbance by making sudden changes to system. In such a case, measurements record the behavior of a system with a different neural state. To ensure proper measurements, the applied perturbations either have to be sufficiently subtle that it goes unnoticed by the subject or measurements must be taken before the human can implement a response.

Unfortunately, neither choice is available for the stiffness estimate experiments. The subject is told to hold a posture but to suppress any cognitive input to the system when displaced. By nature, the perturbation is not subtle and is relatively slow in order to maintain assumptions of a quasi-static displacement. In such a case, the experimenter must rely on the subject to not intervene voluntarily with the applied displacement. However both Mussa-Ivaldi et al. (1984) and Shadmehr et al. (1992) found that consistent results could be achieved with such a paradigm.

For the purposes of the set of stiffness experiments performed here, verification of the "do not intervene" paradigm will be accomplished by first checking the raw experimental data for sudden discontinuities in the measured variables which could indicate a sudden change in the system parameters due to a voluntary response. Assuming that the human voluntary response introduces a degree of randomness or inconsistency, examining the repeatability of the experimental data from trial to trial and from subject to subject provides an additional verification method.

For the movement experiments, the perturbations were designed so that they would be as subtle as possible. Much care was taken to make the application of the constraint appear unpredictable to the subject. In addition, the constraint causes a relatively small maximum deflection of approximately 3 cm from the unconstrained trajectory. However, one cannot say that the subject completes the movement in total ignorance of a change in the system. Therefore, a series of experiments were performed to quantify the ability of the human subject to detect and react to the constraint.

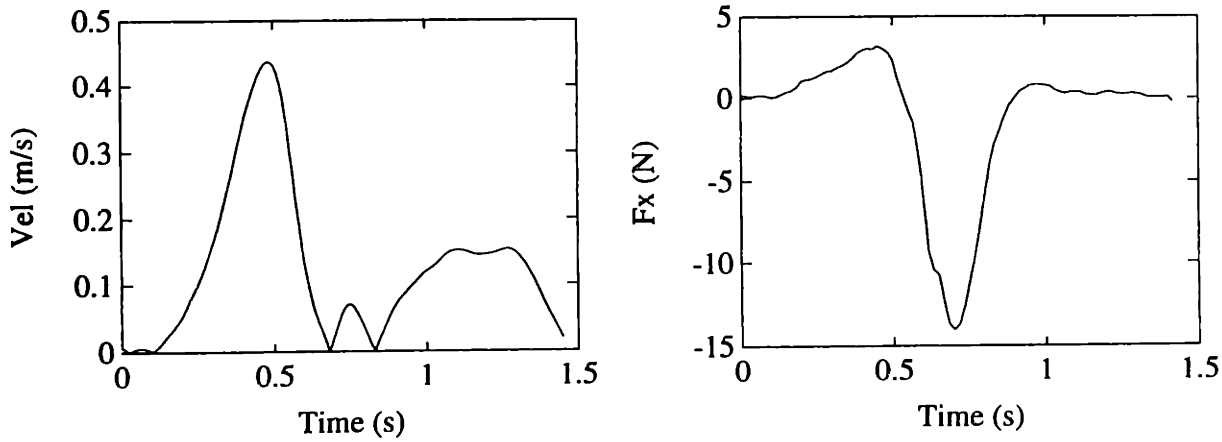

Figure 3.7: Velocity profile and force component in the x-direction for the "do not intervene" test for Subject A. Voluntary response to perturbation occurs when the velocity decreases and the force direction switches.

The subject was placed in the configuration for trajectory 1. After making a series of unconstrained movements, the constraint was applied for the entire duration of a movement. Instead of being asked to ignore changes to system, the subject was instructed to make a sudden purposeful change in his present activity. Specifically, the subject was asked to stop the movement and reverse the direction of the force he was applying to the handle. Force was chosen as the state to be changed because it has the most relevance for this constrained motion [Mansfield 1992]. A sample of the results found from this test is shown in Figure 3.7.

Consistently subjects were unable to make measurable voluntary changes within the first 500 msec of the movements. This time is much longer than the 200 to 300 msec found by other researchers [Jeannerod 1991]. However, the test performed here differs by measuring response time to a perturbation designed to be as subtle as possible. Therefore data taken up to 500 msec will be considered an accurate observations of the original intended motor program. Data after this time must be considered with caution since it must be assumed that the subject was able to "voluntarily" avoid intervening to allow this data to be useful.

Chapter 4

Task Modelling

The goal of this chapter is to model the experimental task of the human moving the small manipulandum through both unconstrained and constrained movements. Section 4.1 provides a detailed analysis of the experiment as a purely mechanical dynamic system. Assuming the human arm grasping the handle of the robot to be a two degree of freedom system of four rigid links, the two equations of motion describing the system is derived using Kane's method.

4.1 Human-Robot Model

The experimental system will be considered to be a simple five-bar rigid body linkage with the forearms and upper arms of the robot and the human representing the four moving linkages. Since the shoulder of the human is assumed to be fixed relative to the base of the robot, the fifth link represents the ground link joining the shoulder of the human and the base of the robot. Figure 4.1a displays the robot-human system as the five-bar linkage as well as the convention for defining joint angles.

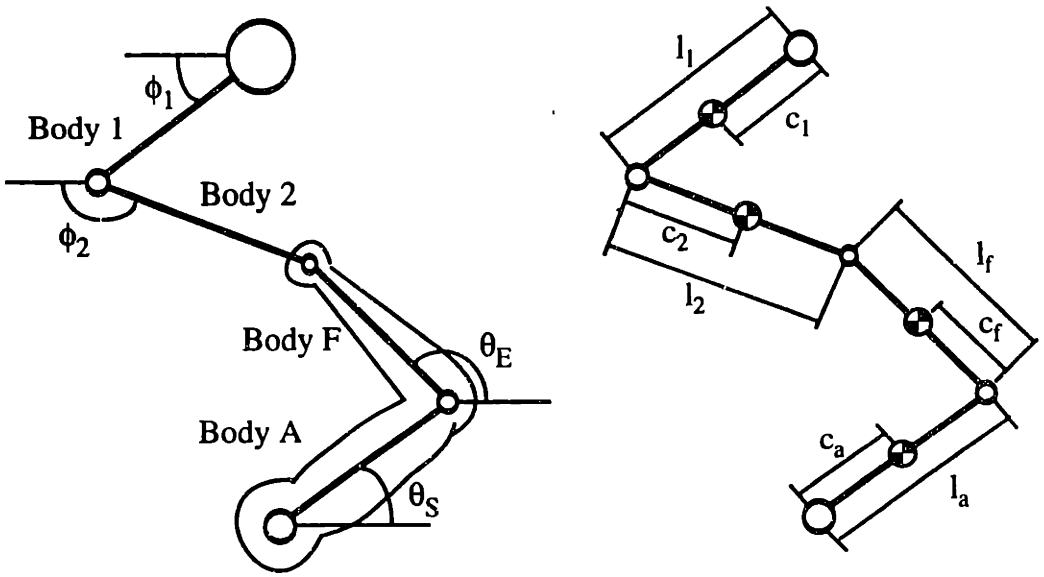

Figure 4.1: The five-bar linkage model. Figure on left defines the joint angles and labels of the rigid bodies. Figure on right defines the dimensioning convention where l are total link lengths and c are distance to centers of masses.

4.1.1 Kinematic Analysis

The system shown in Figure 4.1 has two degrees of freedom. Since the experimental data measures the joint angles of the robot, these angles are chosen as the two generalized coordinates for the dynamic analysis. Therefore in order to generate equations of motion, the velocities and accelerations of the human forearm and upper arm must be expressed in terms of the robot motion. These relationships can be derived by realizing the dependence of these joint angles on the configuration of the linkage. These functions can be found from the following constraint equations which are based on the fact that the robot axes and the human shoulder are a fixed distance apart. Without loss of generality, it is also assumed that the displacement of the shoulder from the robot is aligned along the vertical axis only (i.e. no x displacement).

$$l_a \cos\theta_S + l_f \cos\theta_E + l_1 \cos\varphi_1 + l_2 \cos\varphi_2 = 0 \tag{4.1}$$

$$l_a \sin\theta_S + l_f \sin\theta_E + l_1 \sin\varphi_1 + l_2 \cos\varphi_2 = D \tag{4.2}$$

where the l's signify the link lengths and where θ and φ represent the joint angles of the human arm and the robot as shown in Figure 4.1. D is the distance which separates the shoulder of the human arm from the robot motor axes.

The joint velocities of the shoulder and elbow as a function of the generalized speeds, $\dot{\varphi}_1$ and $\dot{\varphi}_2$, can be found by differentiating equations 4.1 and 4.2.

$$\begin{bmatrix} \dot{\theta}_S \\ \dot{\theta}_E \end{bmatrix} = J^{-1} \begin{bmatrix} l_1 \sin\varphi_1 & l_2 \sin\varphi_2 \\ -l_1 \cos\varphi_1 & -l_2 \cos\varphi_2 \end{bmatrix} \begin{bmatrix} \dot{\varphi}_1 \\ \dot{\varphi}_2 \end{bmatrix} \tag{4.3}$$

where J is the Jacobian for the human arm defined by the following equation:

$$J = \begin{bmatrix} -l_a \sin\theta_S & -l_f \sin\theta_E \\ l_a \cos\theta_S & l_f \cos\theta_E \end{bmatrix} \tag{4.4}$$

For notational simplification, the Jacobian is combined with the other matrix representing equation 4.3 with a new matrix with entries A_{XX}:

$$\begin{bmatrix} \dot{\theta}_S \\ \dot{\theta}_E \end{bmatrix} = \begin{bmatrix} A_{11} & A_{12} \\ A_{21} & A_{22} \end{bmatrix} \begin{bmatrix} \dot{\varphi}_1 \\ \dot{\varphi}_2 \end{bmatrix} \tag{4.5}$$

The accelerations of the shoulder and elbow can be derived by twice differentiating equations 4.1 and 4.2.

$$\begin{bmatrix} \ddot{\theta}_S \\ \ddot{\theta}_E \end{bmatrix} = \begin{bmatrix} A_{11} & A_{12} \\ A_{21} & A_{22} \end{bmatrix} \begin{bmatrix} \ddot{\varphi}_1 \\ \ddot{\varphi}_2 \end{bmatrix} + J^{-1} \left(\begin{bmatrix} l_1 \cos\varphi_1 & l_2 \cos\varphi_2 \\ l_1 \sin\varphi_1 & l_2 \sin\varphi_2 \end{bmatrix} \begin{bmatrix} \dot{\varphi}_1^2 \\ \dot{\varphi}_2^2 \end{bmatrix} + \begin{bmatrix} l_a \cos\theta_S & l_f \cos\theta_E \\ l_a \sin\theta_S & l_f \sin\theta_E \end{bmatrix} \begin{bmatrix} \dot{\theta}_S^2 \\ \dot{\theta}_E^2 \end{bmatrix} \right) \tag{4.6}$$

where J is once again the Jacobian of equation 4.4. Once again, a notational simplification is introduced. Equation 4.6 will be expressed as the following:

$$\begin{bmatrix} \ddot{\theta}_S \\ \ddot{\theta}_E \end{bmatrix} = \begin{bmatrix} A_{11} & A_{12} \\ A_{21} & A_{22} \end{bmatrix} \begin{bmatrix} \ddot{\varphi}_1 \\ \ddot{\varphi}_2 \end{bmatrix} + \begin{bmatrix} F_1(\theta, \varphi, \dot{\theta}, \dot{\varphi}) \\ F_2(\theta, \varphi, \dot{\theta}, \dot{\varphi}) \end{bmatrix} \tag{4.7}$$

Using simple kinematic principles, all motion by any of the rigid bodies can be expressed as functions of the motion of the joint angles of the manipulandum. With these equations in hand, dynamic equations for each of the generalized coordinates may be derived.

4.1.2 Dynamic Analysis

There are numerous methods to derive the equations of motion for this dynamic system. The two most common tools for analyzing dynamics, Newton-Euler and Lagrange, involve sig-

nificant computational complexity. Newton-Euler requires the ability to solve 12 equations simultaneously. Lagrange equations become difficult when taking derivatives of the position and velocity functions defining the shoulder and elbow movement relative to the robot joint motion. Kane's formulation on the other hand offers a computationally simple procedure to calculate equations of motion for multiple body systems. The subsection begins with an overview of this method.

Kane's Formalism

In Kane's formalism [Kane 1983; Kane and Levinson 1985; Storch and Gates 1989], general translational and rotational equations of motion are generated for each rigid body in terms of the generalized coordinates chosen for the system by summing the inertial and active forces. These forces are derived without regard to constraints on motion. The equations assume that the body moves in free space. In addition, partial velocity vectors are generated which define the admissible motion of each body in the directions of the generalized coordinates. These partial velocities are then dot product multiplied with the set of forces to obtain the admissible forces.

Mathematically speaking, we can think of the total possible motion of a rigid body as a vector space **V** defined by all the unconstrained degrees of freedom. The degrees of freedom under the constraint must, by definition of **V**, be a subspace of **V** whose basis is formed by the partial velocity vectors. If we imagine this subspace of admissible motions as a hypersurface within the general motion vector space **V**, we then take the dot product projection onto this surface to find the admissible motion from the general motion.

For example, examine the simple system shown in Figure 4.2. It is clear that this is a one degree of freedom system with the angle θ as an acceptable generalized coordinate. Note that an independent reference frame $\hat{x}$-$\hat{y}$-$\hat{z}$ has been defined for the body J which is rotated from the inertial reference frame $\hat{n}_1$-$\hat{n}_2$-$\hat{n}_3$ by the angle θ. From the generalized coordinate, the generalized speed is defined as follows:

$$u_1 = \dot{\theta}\hat{n}_3 \tag{4.8}$$

which is simply the time derivative of the generalized coordinate θ in vector form. Using the reference frame defined for the rigid body J, it is a simple matter to define the velocities and accelerations of J. As a matter of convention, the rigid body which the velocity or acceleration describes will be denoted by a superscript. For example, ω^J denotes the angular velocity of body

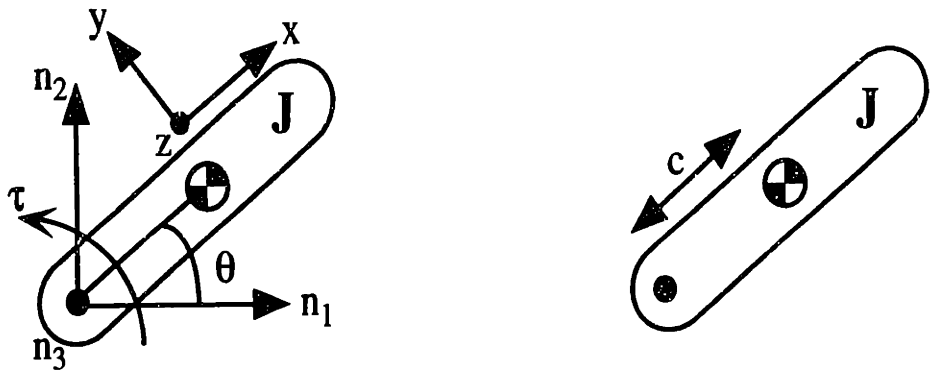

Figure 4.2: Simple system with torque τ applied to a rotational inertia J. Note that both reference frames follow the right-hand rule which implies that $\hat{n}_3$ and $\hat{z}$ are defined out of the page.

J. The asterisk in the superscript for the translational velocity and acceleration denotes that this is given for the center of mass.

$$\omega^J = \dot{\theta}\hat{z} \tag{4.9}$$

$$v^{J*} = c\dot{\theta}\hat{y} \tag{4.10}$$

$$\alpha^J = \ddot{\theta}\hat{z} \tag{4.11}$$

$$a^{J*} = c\ddot{\theta}\hat{y} - c\dot{\theta}\hat{x} \tag{4.12}$$

where c is the distance to the center of mass as shown in Figure 4.2. Given equation 4.11 and equation 4.12, the inertial torque and force can be derived. The asterisks in the superscripts indicate that these are the inertia generated force and torque; the subscripted J indicates that the force and torque act on body J.

$$T_J^* = -J\alpha^J = -J\ddot{\theta}\hat{z} \tag{4.13}$$

$$F_J^* = -ma^{J*} = -m\left(c\ddot{\theta}\hat{y} - c\dot{\theta}^2\hat{x}\right) \tag{4.14}$$

The only active or applied force is the torque τ which gives the following vector quantities for generalized active force and torque.

$$T_J = \tau\hat{n}_3 \tag{4.15}$$

$$F_J = 0 \tag{4.16}$$

We note that the forces and torques of equations 4.13 through 4.16 were generated without regards to the only admissible motion of this system which is a rotation about $\hat{z}$. Equation 4.14 specifically contains a component $\hat{x}$ which represents a force in the non-admissible motion subspace. To define the admissible motion subspace, partial velocity vectors are found by the following equation.

$$\dot{q}_j^i = \frac{\partial \dot{q}^i}{\partial u_j} \tag{4.17}$$

where $\dot{q}_j^i$ is the jth partial velocity of the ith body, $\dot{q}^i$ is the velocity (angular or translational) of the ith body (equation 4.9 or 4.10), and u_j is the jth generalized speed (equation 4.8). Therefore, the two partial velocity vectors for the rigid body J are

$$\omega_1^J = \frac{\partial \omega^J}{\partial u_1} = \hat{z} = \hat{n}_3 \tag{4.18}$$

$$v_1^{J*} = \frac{\partial v^{J*}}{\partial u_1} = c\hat{y} \tag{4.19}$$

Note that the partial angular velocity vector denotes the only rotational admissible direction while the partial translational velocity vector denotes the only translational admissible direction. Together these two vectors span the admissible movement space.

To find the equations of motion, it is simply a matter of projecting the generalized forces and torques onto the admissible space.

$$\omega_1^J \cdot T_J^* = -J\ddot{\theta} \tag{4.20}$$

$$\omega_1^J \cdot T_J = \tau \tag{4.21}$$

$$v_1^{J*} \cdot F_J^* = -mc^2\ddot{\theta} \tag{4.22}$$

Under D'Alembert's principle adding the inertia force and torque projections to the active force and torque projections defines the equation of motion.

$$\omega_1^J \cdot T_J + \omega_1^J \cdot T_J^* + v_1^{J*} \cdot F_J^* = 0 \tag{4.23}$$

Using D'Alembert's principle in equation 4.23, the expected equation of motion is found for this system.

$$-(J + mc^2)\ddot{\theta} + \tau = 0 \tag{4.24}$$

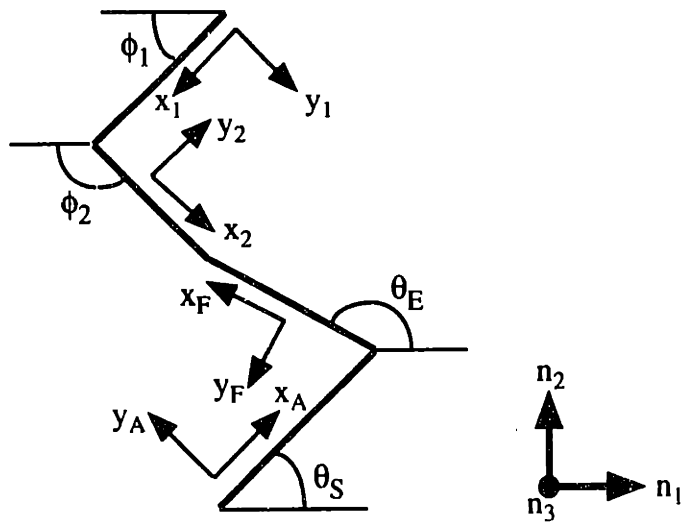

Figure 4.3: The coordinate frames for the five bar linkage. The inertial reference frame is n_1-n_2-n_3 with n_3 out of the page. The robot linkages are denoted by the numbers 1 and 2 with the human forearm denoted by the letter F and the upper arm denoted by the letter A.

From this contrived example, it is difficult to realize the advantages which Kane's method provides when analyzing systems. However when systems become quite complex and the motions of rigid bodies become nontrivial, Kane's method excels in its ability to define motion in arbitrary reference frames which can help trivialize the motion. In a given problem, several different reference frames can be chosen arbitrarily because the final step in the procedure is always a projection onto the same subspace of admissible motion. In other words, the vector space V of general motion can be formed with any basis (reference frame) since the subspace of admissible motion will have a fixed basis. This fixed basis allows consistent projections from different vector spaces onto the subspace.

The Five-bar Linkage

To derive the equations of motion for a five-bar linkage, coordinate frames are established for each of the rigid bodies as shown in Figure 4.3. Using these frames, the translational velocities and accelerations of the rigid body are derived in terms of the joint angles and the coordinate frame of the body. The inertial reference frame is denoted by the unit vectors $\hat{n}_1$, $\hat{n}_2$, and $\hat{n}_3$ while the body frames are denoted by $\hat{x}_i$, $\hat{y}_i$, and $\hat{z}_i$ where i denotes the body (i = 1, 2, F, A). The length l is the length of the entire link, and c is the distance from the reference joint to the center of mass.

- **Robot Upper Arm (Rigid Body 1)**

$$\omega^1 = \dot{\varphi}_1 \hat{n}_3 \tag{4.25}$$

$$\alpha^1 = \ddot{\varphi}_1 \hat{n}_3 \tag{4.26}$$

$$v^1 = c_1 \dot{\varphi}_1 \hat{y}_1 \tag{4.27}$$

$$a^1 = c_1 \ddot{\varphi}_1 \hat{y}_1 - c_1 \dot{\varphi}_1^2 \hat{x}_1 \tag{4.28}$$

- **Robot Forearm (Rigid Body 2)**

$$\omega^2 = \dot{\varphi}_2 \hat{n}_3 \tag{4.29}$$

$$\alpha^2 = \ddot{\varphi}_2 \hat{n}_3 \tag{4.30}$$

$$v^2 = l_1 \dot{\varphi}_1 \hat{y}_1 + c_2 \dot{\varphi}_2 \hat{y}_2 \tag{4.31}$$

$$a^2 = l_1 \ddot{\varphi}_1 \hat{y}_1 - l_1 \dot{\varphi}_1^2 \hat{x}_1 + c_2 \ddot{\varphi}_2 \hat{y}_2 - c_2 \dot{\varphi}_2^2 \hat{x}_2 \tag{4.32}$$

- **Human Upper Arm (Rigid Body A)**

$$\omega^A = (A_{11} \dot{\varphi}_1 + A_{12} \dot{\varphi}_2) \hat{n}_3 \tag{4.33}$$

$$\alpha^A = (A_{11} \ddot{\varphi}_1 + A_{12} \ddot{\varphi}_2 + F_1(\theta, \varphi, \dot{\theta}, \dot{\varphi})) \hat{n}_3 \tag{4.34}$$

$$v^A = c_a (A_{11} \dot{\varphi}_1 + A_{12} \dot{\varphi}_2) \hat{y}_A \tag{4.35}$$

$$a^A = c_a (A_{11} \ddot{\varphi}_1 + A_{12} \ddot{\varphi}_2 + F_1(\theta, \varphi, \dot{\theta}, \dot{\varphi})) \hat{y}_A - c_a (A_{11} \dot{\varphi}_1 + A_{12} \dot{\varphi}_2)^2 \hat{x}_A \tag{4.36}$$

- **Human Forearm (Rigid Body F)**

$$\omega^F = (A_{21} \dot{\varphi}_1 + A_{22} \dot{\varphi}_2) \hat{n}_3 \tag{4.37}$$

$$\alpha^F = (A_{21} \ddot{\varphi}_1 + A_{22} \ddot{\varphi}_2 + F_2(\theta, \varphi, \dot{\theta}, \dot{\varphi})) \hat{n}_3 \tag{4.38}$$

$$v^F = l_a (A_{11} \dot{\varphi}_1 + A_{12} \dot{\varphi}_2) \hat{y}_A + c_f (A_{21} \dot{\varphi}_1 + A_{22} \dot{\varphi}_2) \hat{y}_F \tag{4.39}$$

$$\begin{aligned} a^F = {} & l_a (A_{11} \ddot{\varphi}_1 + A_{12} \ddot{\varphi}_2 + F_1(\theta, \varphi, \dot{\theta}, \dot{\varphi})) \hat{y}_F - l_a (A_{11} \dot{\varphi}_1 + A_{12} \dot{\varphi}_2)^2 \hat{x}_A + \\ & c_f (A_{21} \ddot{\varphi}_1 + A_{22} \ddot{\varphi}_2 + F_2(\theta, \varphi, \dot{\theta}, \dot{\varphi})) \hat{y}_F - c_f (A_{21} \dot{\varphi}_1 + A_{22} \dot{\varphi}_2)^2 \hat{x}_F \end{aligned} \tag{4.40}$$

The partial velocities can now be found from the angular and translational velocities. The partial velocity is by definition the partial derivative with respect to the generalized speed as shown:

$$v^n = v_m^n \dot{q}_m \tag{4.41}$$

where v_m^n is the partial velocity of body n with respect to generalized speed m.

- **Partial Velocities for $\dot{\varphi}_1$**

$$\omega_1^1 = \hat{n}_3 \tag{4.42}$$

$$\omega_1^2 = 0 \tag{4.43}$$

$$\omega_1^A = A_{11}\hat{n}_3 \tag{4.44}$$

$$\omega_1^F = A_{21}\hat{n}_3 \tag{4.45}$$

$$v_1^1 = c_1\hat{y}_1 \tag{4.46}$$

$$v_1^2 = l_1\hat{y}_1 \tag{4.47}$$

$$v_1^A = c_a A_{11}\hat{y}_F \tag{4.48}$$

$$v_1^F = l_a A_{11}\hat{y}_F + c_f A_{21}\hat{y}_A \tag{4.49}$$

- **Partial Velocities for $\dot{\varphi}_2$**

$$\omega_2^1 = 0 \tag{4.50}$$

$$\omega_2^2 = \hat{n}_3 \tag{4.51}$$

$$\omega_2^A = A_{12}\hat{n}_3 \tag{4.52}$$

$$\omega_2^F = A_{22}\hat{n}_3 \tag{4.53}$$

$$v_2^1 = 0 \tag{4.54}$$

$$v_2^2 = c_2\hat{y}_2 \tag{4.55}$$

$$v_2^A = c_a A_{12}\hat{y}_F \tag{4.56}$$

$$v_2^F = l_a A_{12}\hat{y}_F + c_f A_{22}\hat{y}_A \tag{4.57}$$

The inertial forces and torques are the product of the mass or inertia with the negative acceleration. Equations 4.58 and 4.59 define the inertial forces and torques for a rigid body n.

$$F_n^* = -m_n a^n \tag{4.58}$$

$$T_n^* = -I_n \alpha^n \tag{4.59}$$

The active torques are the torques applied by friction and damping at the robot joints and by muscles at the human shoulder and elbow. The torque at the elbow joint of the robot is unusual due to the fact that it is directly connected to both the base and the inner link of the

robot. Therefore the torque at the elbow has an torque relative to the base, τ_{2A}, and a torque relative to the inner link, τ_{2R}.

$$T_1 = (\tau_1 - \tau_{2R})\,\hat{n}_3 \tag{4.60}$$

$$T_2 = (\tau_{2R} + \tau_{2A})\,\hat{n}_3 \tag{4.61}$$

$$T_F = \tau_E \hat{n}_3 \tag{4.62}$$

$$T_A = (\tau_S - \tau_E)\,\hat{n}_3 \tag{4.63}$$

Finally, the equations of motion can be calculated by taking the sum of the inertial forces and torques and the active torques dotted with their respective partial velocity.

$$\sum_n v_i^n \cdot F_n^* + \sum_n \omega_i^n \cdot T_n^* + \sum_n \omega_i^n \cdot T_n = 0 \tag{4.64}$$

where n denotes the rigid body (n = 1, 2, A, F) and i denotes the generalized speed (i = 1, 2).

Using D'Alembert's principle with Kane's projection method, the following equations of motion can be found.

$$\begin{bmatrix} K_1 & K_2 \\ K_4 & K_5 \end{bmatrix} \begin{bmatrix} \ddot{\varphi}_1 \\ \ddot{\varphi}_2 \end{bmatrix} + \begin{bmatrix} K_3 \\ K_6 \end{bmatrix} = \begin{bmatrix} 0 \\ 0 \end{bmatrix} \tag{4.65}$$

where

$$K_1 = -(H_{11} + G_{11}A_{11}^2 + G_{22}A_{21}^2 + 2G_{12}A_{11}A_{21}\cos\theta_E) \tag{4.66}$$

$$\begin{aligned} K_2 = {} & -H_{12}\cos(\varphi_2 - \varphi_1) - G_{11}A_{11}A_{12} - G_{22}A_{21}A_{22} \\ & -G_{12}(A_{11}A_{22} + A_{21}A_{12})\cos\theta_E \end{aligned} \tag{4.67}$$

$$\begin{aligned} K_3 = {} & H_{12}\dot{\varphi}_2^2 \sin(\varphi_2 - \varphi_1) - G_{11}A_{11}F_1 - G_{22}A_{21}F_2 \\ & -G_{12}[A_{21}(A_{11}\dot{\varphi}_1 + A_{12}\dot{\varphi}_2)^2 - A_{11}(A_{21}\dot{\varphi}_1 + A_{22}\dot{\varphi}_2)^2]\sin\theta_E \\ & -G_{12}(A_{11}F_2 + A_{21}F_1)\cos\theta_E + \tau_1 - \tau_{2R} + A_{21}\tau_E + A_{11}(\tau_S - \tau_E) \end{aligned} \tag{4.68}$$

$$K_4 = K_2 \tag{4.69}$$

$$K_5 = -(H_{22} + G_{11}A_{12}^2 + G_{22}A_{22}^2 + 2G_{12}A_{12}A_{22}\cos\theta_E) \tag{4.70}$$

$$\begin{aligned} K_6 = {} & H_{12}\dot{\varphi}_1^2 \sin(\varphi_1 - \varphi_2) - G_{11}A_{12}F_1 - G_{22}A_{22}F_2 \\ & -G_{12}[A_{22}(A_{11}\dot{\varphi}_1 + A_{12}\dot{\varphi}_2)^2 - A_{12}(A_{21}\dot{\varphi}_1 + A_{22}\dot{\varphi}_2)^2]\sin\theta_E \\ & -G_{12}(A_{12}F_2 + A_{22}F_1)\cos\theta_E + \tau_{2R} + \tau_{2A} + A_{22}\tau_E + A_{12}(\tau_S - \tau_E) \end{aligned} \tag{4.71}$$

H_{XX} and G_{XX} are the entries in the inertia-like tensor for the manipulandum and the human arm respectively.

$$H = \begin{bmatrix} I_1 + m_1 c_1^2 + m_2 l_1^2 & m_2 l_1 c_2 \\ m_2 l_1 c_2 & I_2 + m_2 c_2^2 \end{bmatrix} \tag{4.72}$$

$$G = \begin{bmatrix} I_a + m_a c_a^2 + m_f l_a^2 & m_f l_a c_f \\ m_f l_a c_f & I_f + m_f c_f^2 \end{bmatrix} \tag{4.73}$$

Four-bar linkage

When the elbow joint is locked, a degree of freedom is taken away which transforms the system into essentially a four-bar linkage. The robot can be modelled as a single virtual link centered at a virtual center of rotation as described in Chapter 3. The equations of motion in equation 4.65 can still be used if the velocity and acceleration of ϕ_2 are set to zero. However it is numerically simpler to use an equation of motion derived for the four-bar case. The four-bar linkage modelled is shown in Figure 4.4. The shoulder and elbow velocities and accelerations can be related to the crank velocity by simple kinematics.

$$\begin{bmatrix} \dot{\theta}_S \\ \dot{\theta}_E \end{bmatrix} = J^{-1} \begin{bmatrix} l_c \sin\theta_C \\ -l_c \cos\theta_C \end{bmatrix} \dot{\theta}_C = \begin{bmatrix} f_1 \\ f_2 \end{bmatrix} \dot{\theta}_C \tag{4.74}$$

$$\begin{bmatrix} \ddot{\theta}_S \\ \ddot{\theta}_E \end{bmatrix} = \begin{bmatrix} f_1 \\ f_2 \end{bmatrix} \ddot{\theta}_C + J^{-1} \begin{bmatrix} l_c \cos\theta_C + l_a \cos(\theta_S) f_1^2 + l_f \cos(\theta_E) f_2^2 \\ l_c \sin\theta_C + l_a \sin(\theta_S) f_1^2 + l_f \sin(\theta_E) f_2^2 \end{bmatrix} \dot{\theta}_C^2 = \begin{bmatrix} f_1 \\ f_2 \end{bmatrix} \ddot{\theta}_C + \begin{bmatrix} f_3 \\ f_4 \end{bmatrix} \dot{\theta}_C^2 \tag{4.75}$$

where J is the Jacobian of equation 4.4.

Kane's method can be easily applied to find the following equation of motion.

$$A_1 \ddot{\theta}_C + A_2 \dot{\theta}_C^2 + A_3 = 0 \tag{4.76}$$

where

$$A_1 = -H_{11} - G_{22} f_2^2 - 2G_{12} f_1 f_2 \cos(\theta_E - \theta_S) - G_{11} f_1^2 \tag{4.77}$$

$$A_2 = -G_{11} f_1 f_3 - G_{22} f_2 f_4 - G_{12}(f_2 f_3 + f_1 f_4) \cos(\theta_E - \theta_S) - G_{12}(f_1^2 - f_2^2) \sin(\theta_E - \theta_S) \tag{4.78}$$

$$A_3 = (f_2 - f_1)\tau_E + f_1 \tau_S + \tau_C \tag{4.79}$$

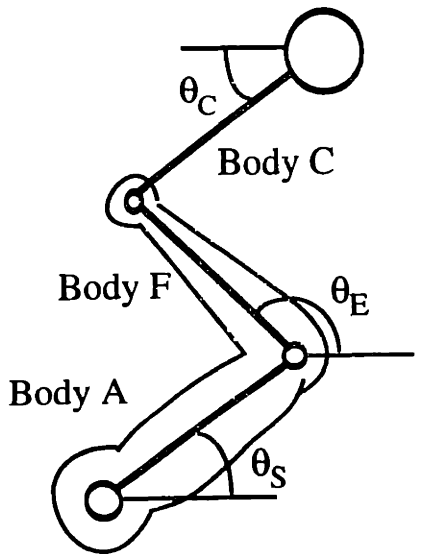

Figure 4.4: The four bar linkage with θ_c as the crank angle. The two-link robot has been reduced to the single body labeled C.

4.2 Human-Robot Specifics

Given a set of dynamic equations, the accuracy of any simulation will depend on the accuracy of the chosen physical parameters. In the case of the robot, finding these parameters is relatively easy. For the human, many assumptions will have to be made with the goal being to attain a "reasonable" model of the human arm.

4.2.1 The Robot

Inertia Parameters

As shown in Figure 4.1, the robot is assumed to consist of two rigid links. Using springs, a simple harmonic oscillator was set up using the links of the robot in various configurations (cf. Appendix A). From this setup, a system identification was performed on the robot in order to quantify the inertia parameters. With this method, the following inertia tensor for the robot was found.

$$H = \begin{bmatrix} 0.027 & 0.01\cos(\phi_2 - \phi_1) \\ 0.01\cos(\phi_2 - \phi_1) & 0.0096 \end{bmatrix} \text{ kg m}^2 \tag{4.80}$$

Friction and Stiction

The only other major dynamic effect besides inertia is the presence of coulomb friction and stiction. The coulomb friction at a joint will be modeled simply as the product of a constant torque with the sign function of velocity as given by the following equation.

$$\tau = -\tau_{Fric} \operatorname{sgn} \dot{\varphi} \tag{4.81}$$

where

$$\operatorname{sgn} \dot{\varphi} = \begin{cases} 1 \text{ if } \dot{\varphi} > 0 \\ 0 \text{ if } \dot{\varphi} = 0 \\ -1 \text{ if } \dot{\varphi} < 0 \end{cases} \tag{4.82}$$

so that the torque due to friction always opposes the motion.

The more difficult phenomenon to model is stiction. The model when velocity is sufficiently small must remove the degree of freedom associated with the sticking joint. The method used within this work is the stiction model proposed by Karnopp (1985) which has the advantage of having constant causality easing the difficulty in numerical simulations. In Karnopp's model, a region of small velocity is defined to model the condition for sticking because the digital simulations will very rarely if ever compute an exact value of zero for the velocity. Therefore if $-DV < V < DV$, the simulation will assume sticking occurs.

When sticking occurs, the friction torque at the joint is calculated to balance all other torques on the joint so that the net acceleration of that joint is zero. Therefore when the simulation numerically integrates the states, the velocity of that joint will remain constant at a absolute value less than DV. Note that this model does not explicitly zero the value of velocity during stiction which would necessitate resetting the numerical integrator with a new set of initial conditions. Rather it considers a small finite velocity as acceptable during sticking under the assumption that such an error does not affect the gross behavior of the system thereby simplifying the numerical integration. The joint can break free of stiction if the calculated friction torque exceeds a set value. After breakaway, the model switches to coulomb friction until the velocity becomes once again smaller than DV.

4.2.2 The Human Arm

Since the goal of this thesis is to evaluate whether virtual trajectories can be considered appropriate signals to the CNS, the human arm model used for the simulations are based upon this method of control. Therefore, a set of impedance parameters are assumed along with a virtual trajectory to generate the movement.

Inertia Parameters

Inertia of the human arm is calculated using equations derived from cadaver studies by Dempster [Miller and Nelson 1973; Plagenhoef 1971]. The following lists the mass, center of gravity and radius of gyration, k, about the CG for the upper arm, forearm, and hand based on total body weight and lengths of the segments.

- Upper Arm

$$m_a = 0.028\text{xWeight} \tag{4.83}$$

$$c_a = 0.436 l_a \tag{4.84}$$

$$k_a = 0.322 l_a \tag{4.85}$$

- Forearm

$$m_{f2} = 0.016\text{xWeight} \tag{4.86}$$

$$c_{f2} = 0.430\,(l_f - c_h) \tag{4.87}$$

$$k_{f2} = 0.303\,(l_f - c_h) \tag{4.88}$$

- Hand

$$m_h = 0.006\text{xWeight} \tag{4.89}$$

The length l_f was represented in the model as the length from the elbow to the point where the hand grasps the handle. In the calculation of the forearm parameters, c_h, the length from the wrist to the center of the fist, was subtracted from l_f to find the true forearm length. In addition, the mass, CG, and inertia parameters of the forearm in the model incorporate the hand as part of the same link. Therefore to find m_f, c_f, and I_f, the hand and the forearm must be combined to find the parameters of the total body. Using the following equations, these parameters are found. The hand as a fist is assumed to be a point mass centered at a distance l_f from the elbow.

$$m_f = m_{f2} + m_h \tag{4.90}$$

$$c_f = \frac{m_{f2}c_{f2} + m_h l_f}{m_{f2} + m_h} \tag{4.91}$$

$$I_f = I_{f2} + m_h l_f^2 \tag{4.92}$$

Impedance Parameters

The stiffness parameters are taken from the postural field measurement experiment. Under the assumption that the human is capable of only scaling joint stiffness, the measured joint stiffness matrix will be multiplied by a scalar which will be assumed to be constant throughout the movement.

$$K_{J,scaled} = \alpha K_J \tag{4.93}$$

The stiffness matrix K_J will be taken from experimental measurements while the scaling factor α will be a tunable parameter. The damping matrix is assumed to be aligned with the stiffness matrix and will also have a scaling constant which will be tuned during simulations.

$$B_{J,scaled} = \rho B_J \tag{4.94}$$

where ρ is the scaling factor and B_J is the joint viscosity matrix which is chosen to have similar shape and orientation as the joint stiffness matrix. Note that these are the same modelling assumptions made by Flash (1987) in her planar movement simulation.

Chapter 5

Experimental Results

This chapter will present the experimental data for the five subjects. The results of the postural force field measurement will be presented in the first section. The measured forces about equilibrium as well as the best linear approximation of the field will be the central point of the first section. The remainder of this chapter will concentrate on the movement data where simple quantification of various features of the data will be given as a means of showing the strong stability properties of the arm during movement.

5.1 Stiffness Measurement

As stated in Chapter 3, three stiffness measurements were made for each subject. Each of these measurements were spread about the region defined by the three trajectories to be tested in the movement experiments. These experimentally measured stiffnesses were consistent across each trial and each subject. In addition, the qualitative features of the field's curl, size, shape, and orientation described by Mussa-Ivaldi et al. (1984) were prevalent in all of the measurements. Since the task simulations of the reaching experiment were limited to recreating the data of one subject, only the data from this subject (Subject C) will be presented in this section. However because the data is so consistent with the findings of Mussa-Ivaldi et al. (1985), the data for the other four subjects hold no surprises.

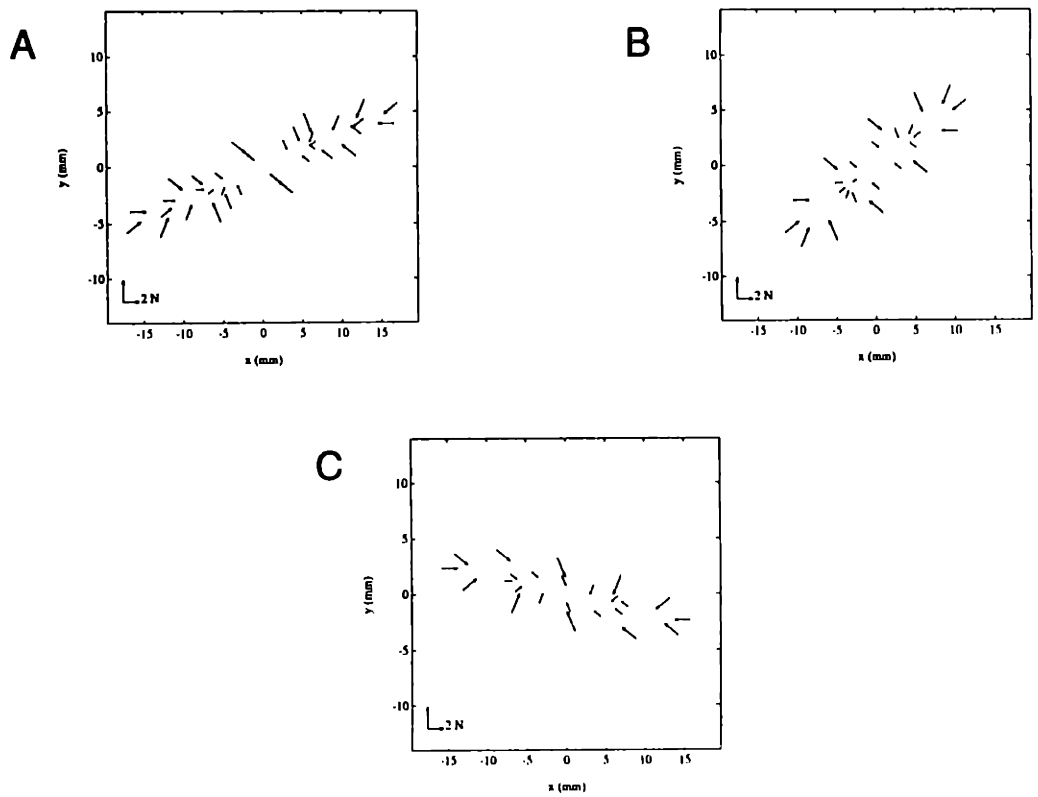

Figure 5.1: The measure restoring forces about equilibrium at the three positions. (A) Posture 1 (B) Posture 2 (C) Posture 3

5.1.1 Measured Forces

The forces about posture were measured at three different locations in the workspace of the arm. In order to preserve the linearity assumption, all displacements which exceeded 3 cm were filtered out of the data. The maximum evoked forces within this filtered data set ranged from 2 to 3 N. The forces and displacements about equilibrium for the three postures for Subject C are shown in Figure 5.1. These plots represent half second time intervals during a displacement in a particular direction. This was done to further demonstrate the anisotropy of the measured field.

5.1.2 Stiffness Approximation

A linear stiffness matrix was fit for the set of forces and displacements at each posture through a linear regression. The three endpoint stiffness for Subject C are given in Table 5.1. The matrices in column 1 represent the best linear approximation of the measured data. Using these matrices, forces at each of the displacements shown in Figure 5.1 were calculated and compared to the

Table 5.1: Fitted Endpoint Stiffnesses for Subject D in N/m

	Endpoint Stiffness	**Conservative Component**	**Non-Conservative Component**
Position 1	$\begin{bmatrix} -160.7 & 175.9 \\ 129.7 & -550.8 \end{bmatrix}$, $R^2 = 0.891$	$\begin{bmatrix} -160.7 & 152.8 \\ 152.8 & -550.8 \end{bmatrix}$	$\begin{bmatrix} 0 & 23.1 \\ -23.1 & 0 \end{bmatrix}$
Position 2	$\begin{bmatrix} -247 & 184.7 \\ 115.6 & -380.6 \end{bmatrix}$, $R^2 = 0.902$	$\begin{bmatrix} -247 & 150.2 \\ 150.2 & -380.6 \end{bmatrix}$	$\begin{bmatrix} 0 & 34.6 \\ -34.6 & 0 \end{bmatrix}$
Position 3	$\begin{bmatrix} -133.6 & -44.1 \\ -96.3 & -645.5 \end{bmatrix}$, $R^2 = 0.857$	$\begin{bmatrix} -133.6 & -70.2 \\ -70.2 & -645.5 \end{bmatrix}$	$\begin{bmatrix} 0 & 26.1 \\ -29.1 & 0 \end{bmatrix}$

actual data as shown in Figure 5.2. Note that the linear fit provides an accurate approximation of the experimental data for the displacements measured.

In addition to the fitted stiffness, Table 5.1 also presents the conservative and non-conservative components of the stiffness matrix as given by the following equations:

$$K_{cons} = \frac{(K + K^T)}{2} \tag{5.1}$$

$$K_{non} = \frac{(K - K^T)}{2} \tag{5.2}$$

where K_{cons} and K_{non} are the conservative and non-conservative matrices in columns 2 and 3 of Table 5.1. K is the fitted matrix of the first column. To compare the curl to the conservative component, these two components were plotted separately at the measured positions in Figure 5.3. Note that the non-conservative component of each force vector has a much smaller (< 10%) relative contribution to the total force than the conservative component. This "spring-like" nature of the human arm means that stable control of interaction with arbitrary passive environments through the use of an attractor point is guaranteed due to the passive nature of the arm [Colgate and Hogan 1988].

The symmetric (conservative) approximation is best visualized through the stiffness ellipses developed by Mussa-Ivaldi et al. (1985). The major and minor axes of the stiffness

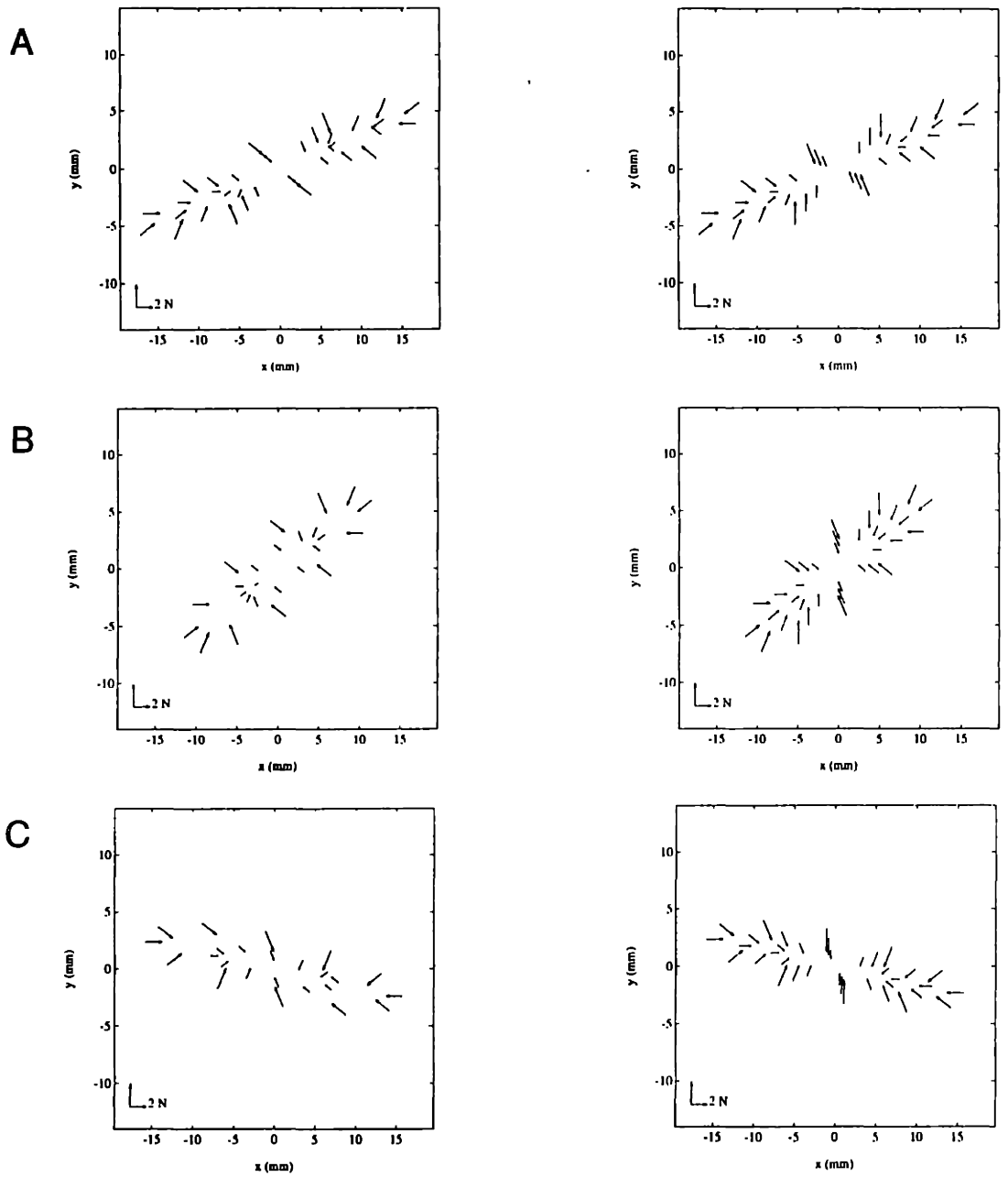

Figure 5.2: Comparison of the actual data (left column) to the fitted solution (right column) for the three positions. (A) Position 1. (B) Position 2. (C) Position 3.

ellipse are defined by the eigenvalues and eigenvectors of the symmetric matrix. The eigenvalues represent the lengths of the major and minor axes while the directions of the corresponding eigenvectors denote the orientation of the ellipse. Using this convention, the three stiffness ellipses defined by column 2 of Table 5.1 are plotted at their measured positions. Note that these

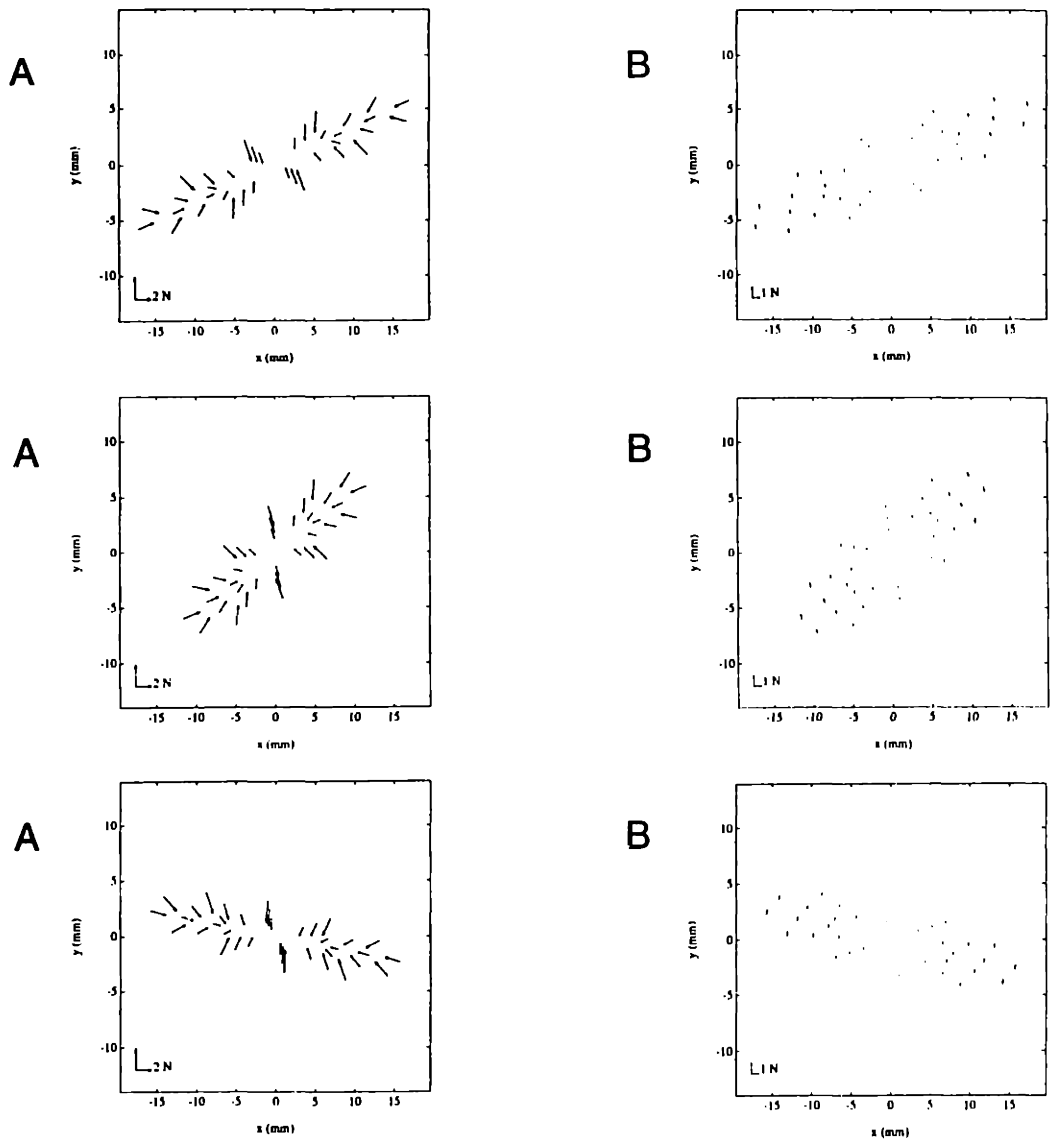

Figure 5.3: Linear approximation for the three positions. (A) Conservative component (B) Non-conservative component.

ellipse show variability in their shapes and orientations from position to position. However the direction of the major axes is almost aligned with the shoulder of the subject in every case as demonstrated by Mussa-Ivaldi et al.

Due to this wide variability over the workspace, a single endpoint ellipse is incapable of providing a global approximation of the human arm in different configurations. However, Mussa-Ivaldi et al. showed that a simple transformation to joint space provides a means by

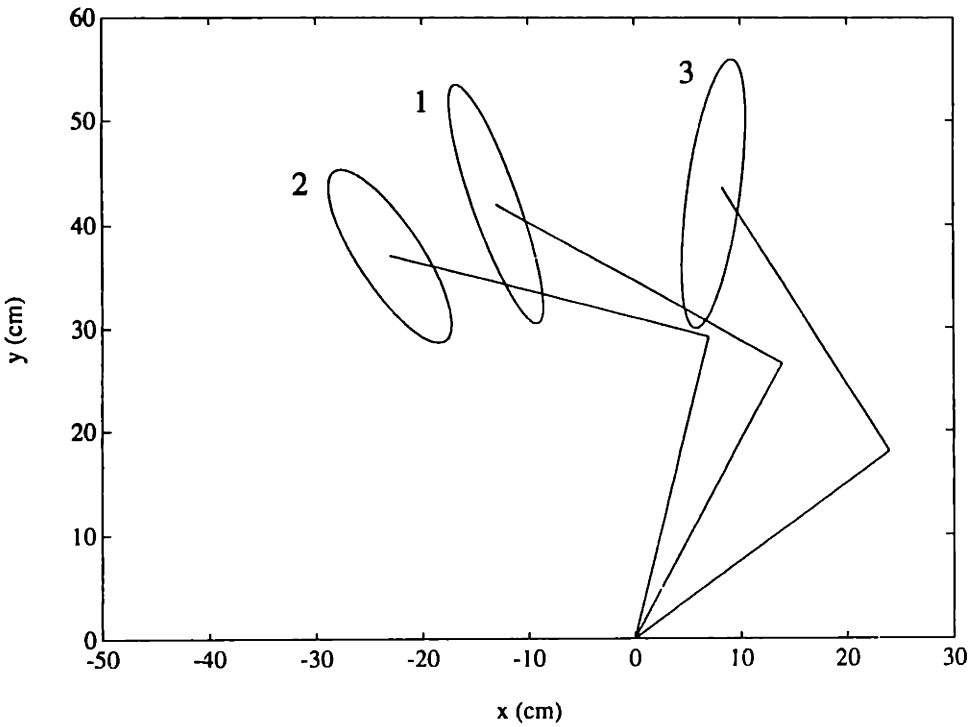

Figure 5.4: Endpoint stiffness for Subject D at three locations.

Table 5.2: Joint Stiffnesses for Subject D in N-m/rad.

	Joint Stiffness	**Eigensolution**
Position 1	$\begin{bmatrix} -21.1 & -7.44 \\ -11.7 & -31.5 \end{bmatrix}$	ratio = 0.41 angle = 59 deg
Position 2	$\begin{bmatrix} -28.9 & -11.4 \\ -17.9 & -29.5 \end{bmatrix}$	ratio = 0.33 angle = 46 deg
Position 3	$\begin{bmatrix} -25.5 & -8.78 \\ -13.6 & -32.2 \end{bmatrix}$	ratio = 0.42 angle = 54 deg

which a single stiffness can generalize over much but not all of the workspace. The endpoint stiffness K_x can be mapped to a joint stiffness K_θ by the following Jacobian transformation.

$$K_\theta = J^T K_x J \tag{5.3}$$

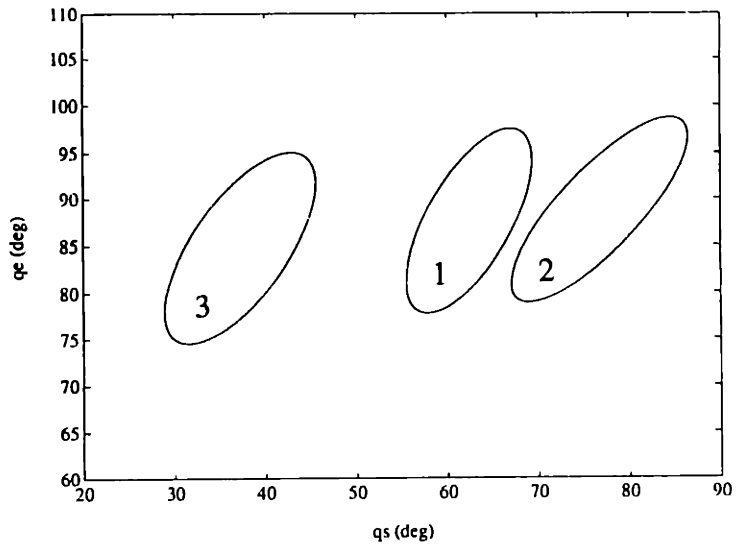

Figure 5.5: The three joint space stiffness ellipses.

where J represents the Jacobian of the human arm. This transformation was performed on the symmetric stiffness of Table 5.1. Column 2 of Table 5.2 provides information about the shape and orientation of the equivalent ellipse for each joint stiffness. The ratio represents the relative size of the major and minor axes which denotes the shape of ellipse. The direction is the angle between the major axis and horizontal. Although not perfect, the relative shape and orientation between positions do show an impressive consistency. To further demonstrate this phenomenon, the three joint stiffness have been plotted in joint space in Figure 5.5.

Mussa-Ivaldi et al. were able to simulate the configuration dependent endpoint stiffness ellipses from a single joint stiffness matrix. Qualitatively the generalization was good; yet the constant joint stiffness underestimates the large variations of endpoint stiffness with configuration especially in the proximal regions. However the movement experiment is confined to a only a small portion of the total workspace where a single constant joint stiffness should be a sufficient approximation. In addition, movements are a minimum of 25 cm away from the shoulder so that errors in endpoint stiffness at proximal locations will be assumed to be negligible. Therefore the stiffness for position 1 will be used as the model for the

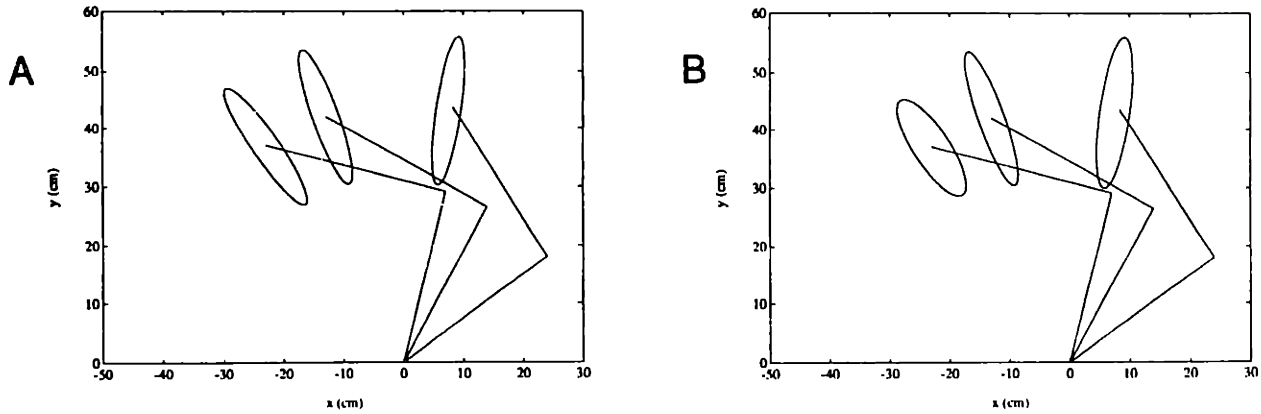

Figure 5.6: Comparison of predicted stiffness and actual stiffness. (A) Constant joint space model. (B) Actual measured endpoint stiffness.

human stiffness. A comparison of the predicted endpoint stiffness from our constant joint stiffness model to the actual data is shown in Figure 5.6.

5.2 Movement Data

For each of the three trajectories, there are a total of six different types of trials. The movement can be unconstrained throughout the motion, constrained throughout the movement, and constrained then released during the movement. Each of these cases were implemented on trajectories moving from point a to point b and on trajectories from point b to point a for a total of six different cases. Presented in this section will be a sampling of characteristic data from each type of trajectory from the various subjects.

5.2.1 Unconstrained Reaching Movements

Hand Paths

The point to point planar arm movements can be considered to be the most "conventional" motor control experiment of the three constraint cases - conventional because there is a large body of research with which to compare these results. This provides a means of calibrating the experiment. Since this set of experiments is based on the assumption that the subject is using a typical motor program, the unconstrained movements allow a comparison with other experiments by other researchers in order to check that the subject is making a "normal" movement. In addition, the unconstrained movements represent the datum or reference for the two constrained

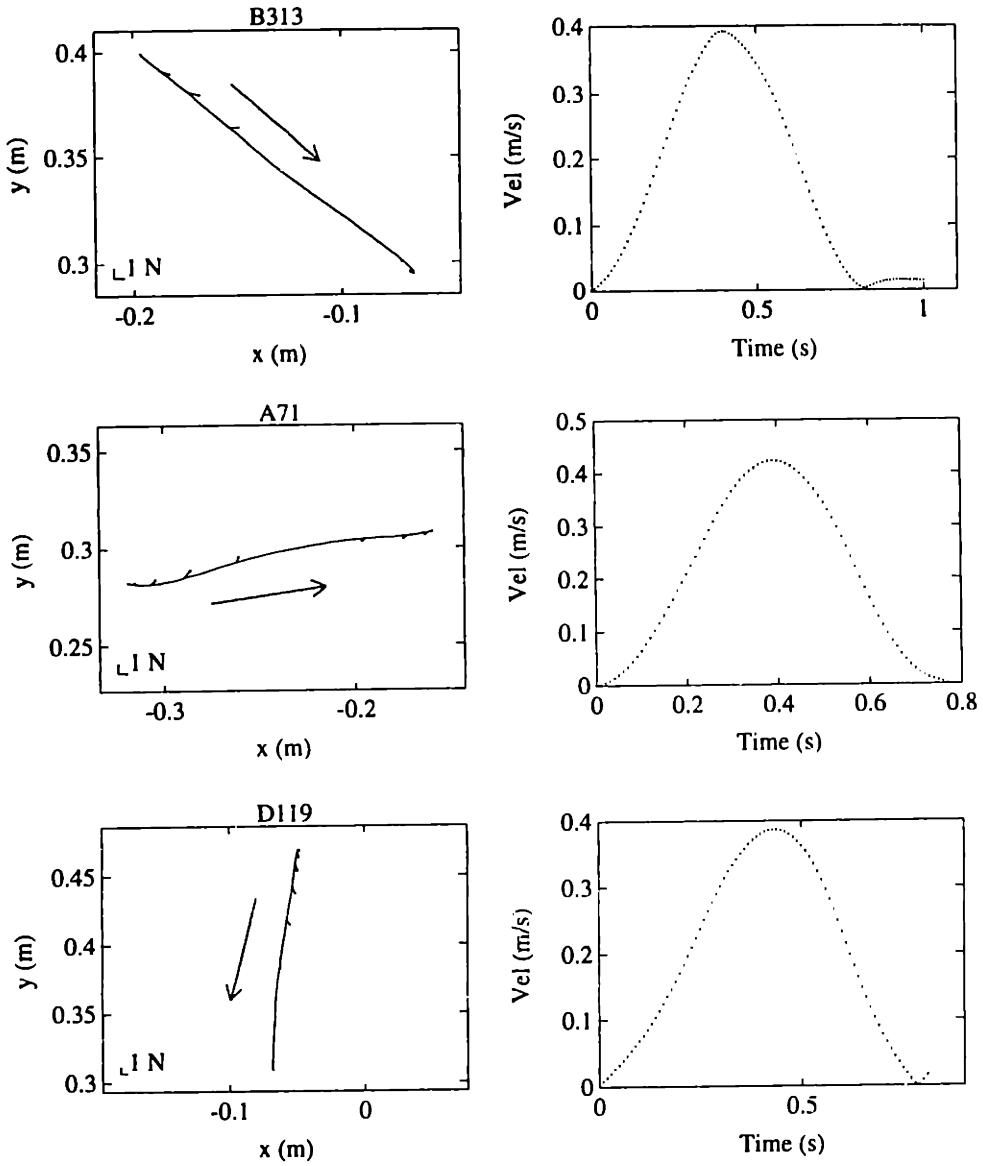

Figure 5.7: Up to down or left to right trajectories for the three sets of starting and ending points. The path of the hand is given on the plots to the left while corresponding tangential velocities profile are given to the right. Plot titles contain letter designation of subjects as well as the trial number.

movements. Assuming that the constraints are sufficiently surreptitious, the unconstrained movement can be assumed to be an example of the intended movement if no constraint perturbs the trajectory.

Figure 5.7 and Figure 5.8 display typical unconstrained movements by the five subjects for all three trajectories tested. Figure 5.7 contains the up to down directions for trajec-

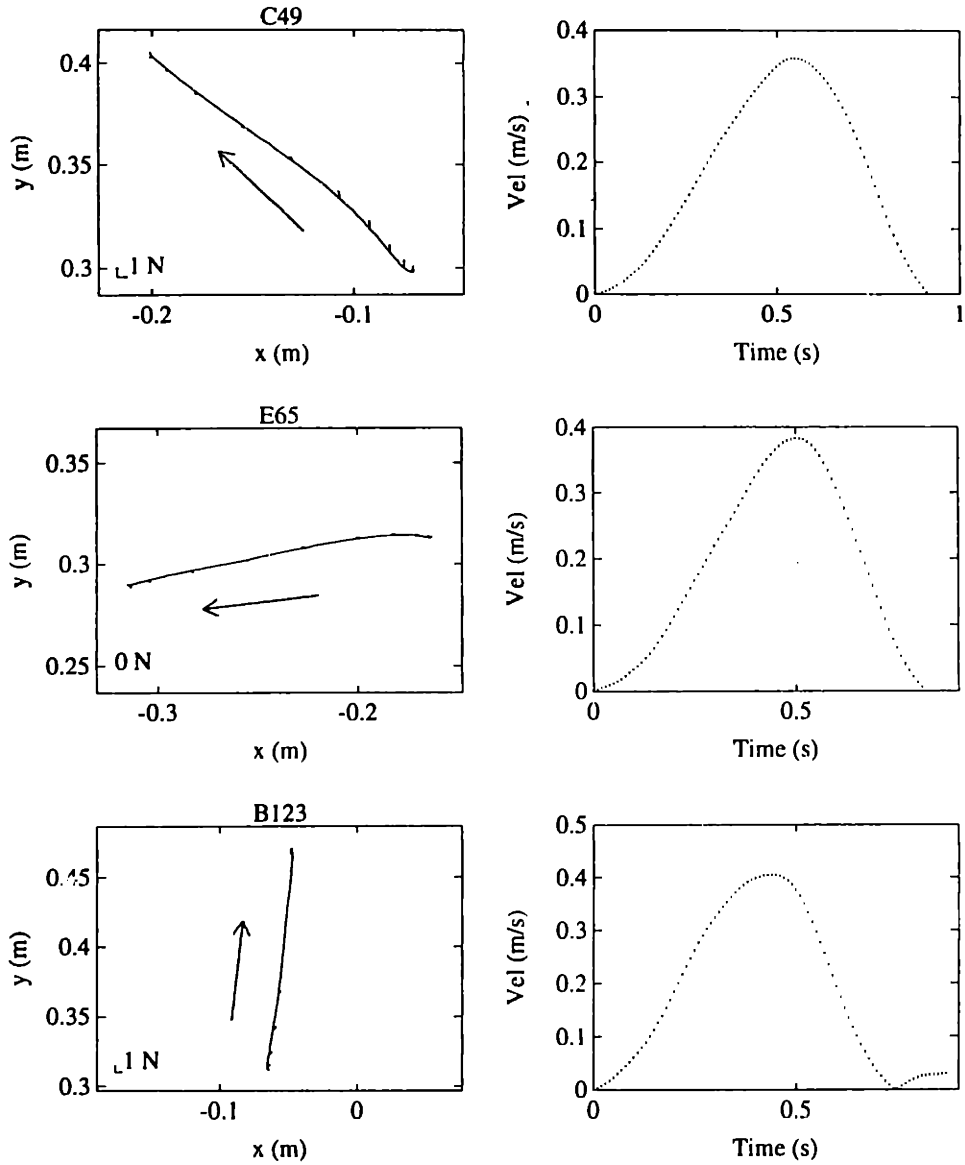

Figure 5.8: Down to up or right to left trajectories for the three sets of starting and ending points. Again the path of the hand is given on the plots to the left while corresponding tangential velocities profile are given to the right. Plot titles contain letter designation of subjects as well as the trial number.

tories one and three, and the left to right direction for the second trajectory. Figure 5.8 contains the trajectories in the opposite direction of those in Figure 5.7.

The first typical feature of all the data is the shape of the hand path. Although not explicitly instructed, subjects consistently made direct movements from start to finish. Direct, in this

Table 5.3: Duration of Unconstrained Movement

	Trajectory 1		Trajectory 2		Trajectory 3	
	Time (s)	St. Dev.	Time (s)	St. Dev.	Time (s)	St. Dev.
Subject A	0.826	0.057	0.700	0.044	0.680	0.054
Subject B	0.731	0.044	0.699	0.054	0.718	0.060
Subject C	0.780	0.053	0.698	0.053	0.731	0.046
Subject D	0.726	0.049	0.722	0.050	0.733	0.052
Subject E	0.753	0.063	0.733	0.058	NA	NA

Total	
Time (s)	St. Dev.
0.7311	0.066

case, means a qualitatively but not perfectly straight path. Indeed, most of the trajectories upon first glance do look like essentially straight lines. Closer inspection shows definite curved components to the shape of the hand path, but the overall shape can be qualitatively described as straight. This result corresponds closely to observations first made by Morasso (1981) who found an invariance and simplicity in the shape of the hand paths in the external space with variability and complexity in the joint space of the arm. In simpler words, the subjects all consistently made near-straight point to point hand movements for all the two point trajectories tested which is consistent with the results in Figures 5.7 and 5.8.

Movement Duration

Besides the straightness of the path, another invariance is the duration of movement. This invariance is represented by the little or no deviation in total time of movement between each trial, between each trajectory, and between subjects as shown in Table 5.3. Granted that all three movements have identical distances from start to finish. However these three trajectories are rotated by a minimum of 45 degrees from each other and occur in different parts of the workspace. It is not fundamentally obvious that the duration times for all three trajectories should be nearly identical. The simplicity of the task may encourage the similarities between trials and between subjects; however the simplicity does not take away from the fact that this seems to be a basic motor behavior. The consistency of the movement duration

for all three movements could imply that a single motor strategy or action unit is being applied in all cases. This single unit can be generalized to create any trajectory through a simple translation and rotation in the hand frame thus giving trajectories which are kinematically nearly identical with differences caused only by dynamics and configuration dependent effects.

Minimum Jerk?

Morasso also observed that these point to point straight paths have a tangential velocity profile which is characteristically bell-shaped. Based on the smoothness and gracefulness of human movement, Hogan (1984b) postulated a model of human movement based on minimizing jerk as a means of obtaining an adequate description of human movement. This description predicts a symmetric bell-shaped velocity profile which closely matches the experimental data from two joint unconstrained movements. This profile can be described by the following fifth order polynomial [Flash and Hogan 1985].

$$v(t) = \Delta x\,(60\tau^3 - 30\tau^4 - 30\tau^2)\,/\,t_f \tag{5.4}$$

where Δx is the length of the trajectory, t_f is the total time, and τ is time normalized by the total time of movement.

The data from this experiment also showed a bell-shaped pattern somewhat consistently. All velocity profiles are single-peaked for the gross motion of the arm.[1] Differences of the actual data from the minimum jerk profile occur mainly in the unsymmetrical nature of the actual velocity profiles. However similar to the findings of Flash and Hogan (1985), these differences are small and the mathematical model still adequately describes the nature of the data.

To further test this notion, velocity profiles for a single subject making a single type of trajectory were aligned at their peaks and averaged at each time step to find the composite velocity profile as shown in Figure 5.9. Figure 5.10 displays the average velocity profiles for the three trajectories. These profiles were found from the data of Subject B as the subject moved from target one to target two in each case. Super imposed on these mean profiles is a minimum jerk profile based on equation 5.4.

1. Additional peaks appear at the end of the movement as the subject adjusts for the target location. This is not considered as part of the gross motion motor program which takes the arm from start to near the target.

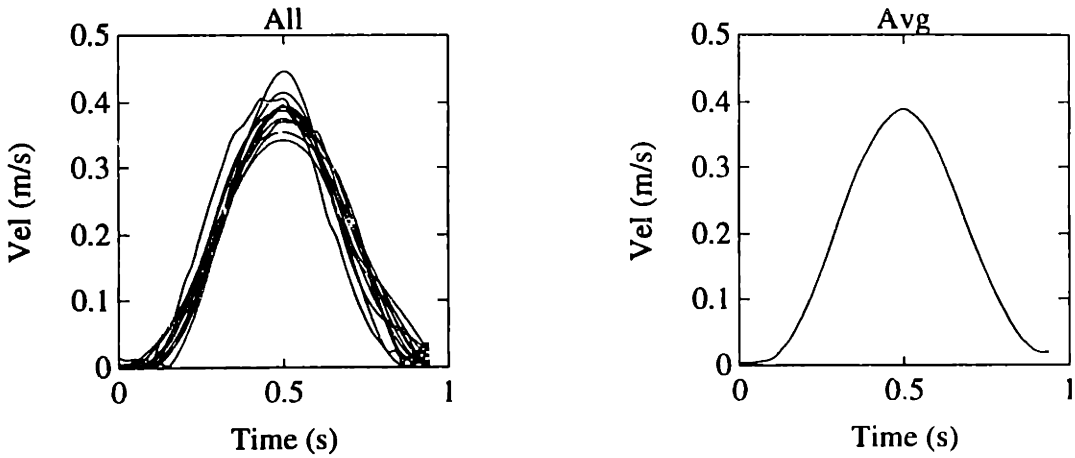

Figure 5.9: The left figure shows all of the velocity profiles by one subject performing one movement. The velocity peaks are aligned and the average is taken to find the profile on the right.

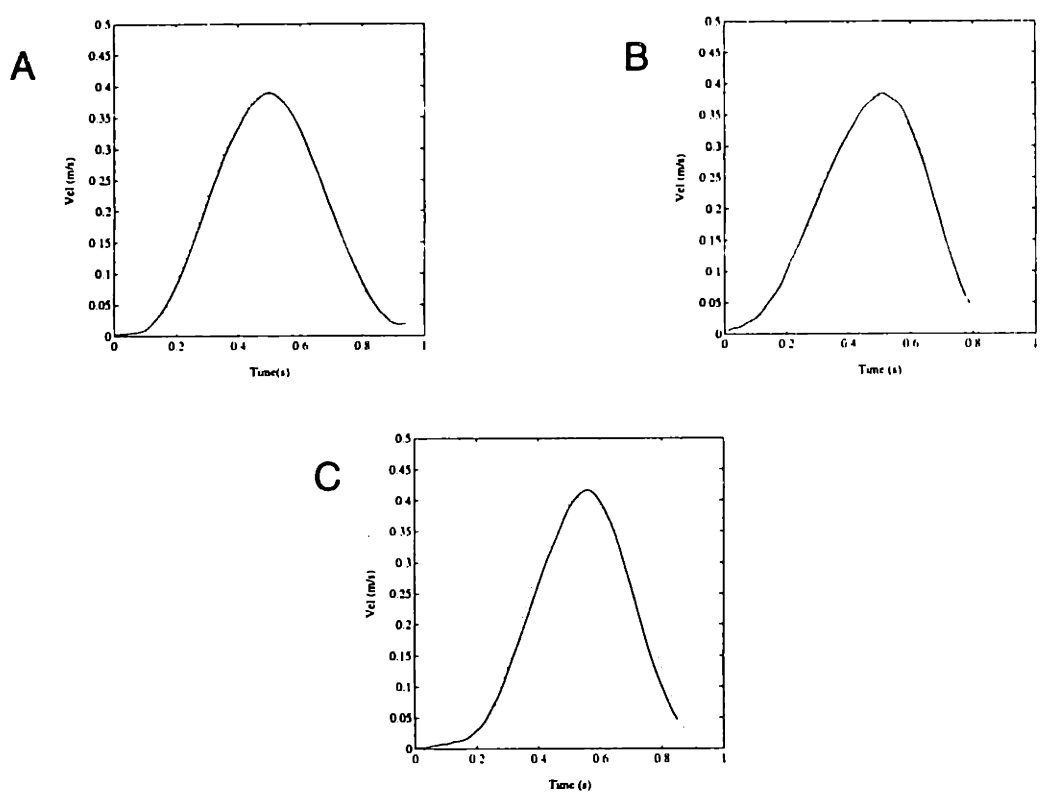

Figure 5.10: Comparison of Min Jerk (dotted line) and averaged data (solid) for Subject B. (A) The profile for the diagonal left to right movement. (B) The profile for the horizontal left to right movement. (C) The profile for the vertical up to down movement.

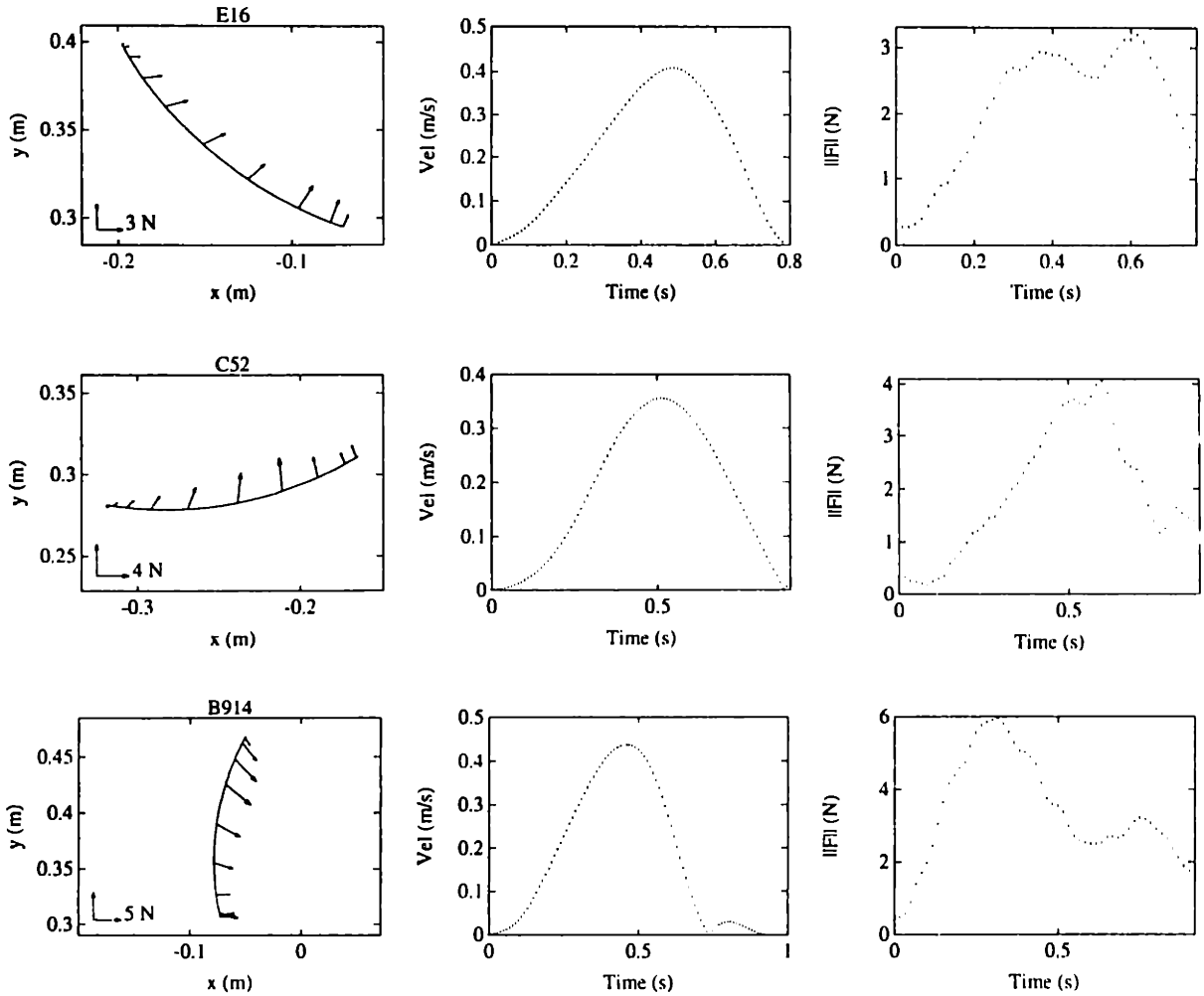

Figure 5.11: Up to down or left to right trajectories for the three sets of starting and ending points. The path of the hand is given on the plots to the left while corresponding tangential velocities profiles are in the middle with total force magnitude on the right. Plot titles contain letter designation of subjects as well as the trial number.

5.2.2 Fully Constrained Movement

The constraint applied by the magnetic brake forces the nominally straight hand path along a circular constraint with radius equal to the length of the inner linkage of the robot. Figure 5.11 and Figure 5.12 show typical data for this type of trajectory. In nearly all of the data, the circular constraint evokes forces from the arm to the handle which are strongly oriented inward towards the center of the circular constraint. Note that in some of the force magnitude plots of Figures 5.11 and 5.12, the forces show a change from a decreasing force to an increasing force after 500 ms of movement. This is possible evidence that the subject does intervene in response to this

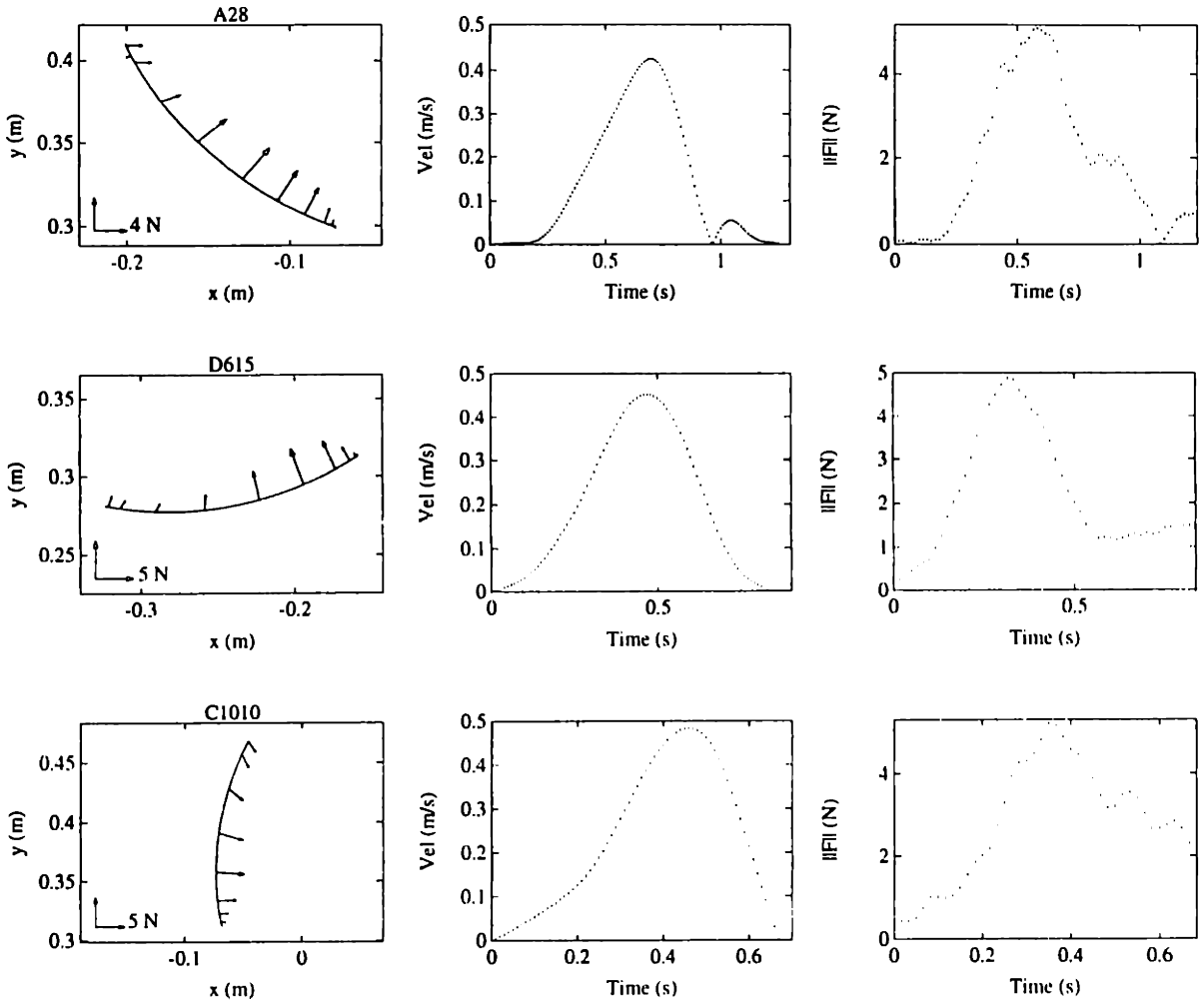

Figure 5.12: Down to up or right to left trajectories for the three sets of starting and ending points. The path of the hand is given on the plots to the left while corresponding tangential velocities profiles are in the middle with total force magnitude on the right. Plot titles contain letter designation of subjects as well as the trial number.

constraint, and therefore it would be advisable to limit analysis to the first 500 ms of data as argued in the Chapter 3.

Stability

Our first conclusion may seem trivially obvious; however it does imply an unavoidable requirement for the behavior of the human arm. Throughout the experiment, every subject was able to stably interact with the constraint. In every case, the trajectory could be com-

pleted smoothly and with efficiency of motion. From this result, one can conclude that instability is not an issue for this contact task. Moreover since the constraint is applied at random intervals, it can be assumed that the underlying motor program has not changed from the unconstrained case to the fully constrained case which implies that this stability property is inherent to human movements.

Given these assumptions and observations, it is known from previous research that the necessary condition for stable interaction with arbitrary passive environments is that the human must be equivalent to a passive system at the point of interaction. In addition, the constraint applied represents one of the "worst case" passive environments, that of a very stiff spring. Therefore the behavior about equilibrium (whether it is the control signal or not) defined by the net activity of the muscle is at least locally constrained to be passive which reinforces the fact that the spring-like single and multi-joint muscles behave in a conservative manner about equilibrium. Since the subject is capable of stably interacting with the sudden unexpected applied constraint, this passive behavior must occur not only during control of contact but during the planar free movement as well.

Unfortunately, the planar free movements represents another form of a constraint; the arm is free to move in only two degrees of freedom. Therefore, a strong statement about passive arm impedance can not really be made about truly free arm movement (unrestricted movement in all degrees of freedom) from the experimental data. Nonetheless, the planar result still makes a compelling argument for the importance of impedance and attractor points for human motor activities.

Force Magnitude

As mentioned previously, the applied constraint evokes forces from the human arm which *increase as the difference between the constrained path and the unconstrained path increases.* These evoked forces represent a positional dependence of the interface force which is only natural if the arm truly has spring-like properties. However it has come into question whether this positional dependence has sufficient influence over the system to make control of the attractor point a viable simplification in movement control [Bennett et al. 1992; Katayama and Kawato 1992]

Table 5.4: Maximum Magnitude of Evoked Forces

	Trajectory 1		Trajectory 2		Trajectory 3	
	Force (N)	St. Dev.	Force (N)	St. Dev.	Force (N)	St. Dev.
Subject A	4.3119	0.8293	4.0459	1.0753	5.0031	0.8677
Subject B	3.3746	0.7163	4.6249	0.7662	4.3518	1.4186
Subject C	3.0103	0.4362	4.3982	0.9189	4.8175	0.8068
Subject D	4.0544	0.7375	4.6380	1.1156	4.5958	0.8249
Subject E	3.5902	0.5981	3.6042	0.8925	NA	NA

Overall Max Force	
Force (N)	St. Dev.
4.1675	1.0524

Table 5.4 presents the average maximum force magnitude present for the first 500 ms of movement. As argued previously, the data of the first 500 ms of movement will assumed to be free of any intervention by the subject. The maximum force magnitude for each constrained trajectory was found and then averaged with the maximum magnitudes found in the other trials of the same trajectory and the same subject. The maximum force magnitude is similar across all three trajectories and all five subjects. The overall maximum force ranges from 3 to 5 N. This now raises the question of whether the magnitudes of these evoked forces can be considered significant relative to the dynamics of the system.

Consider the unconstrained and constrained cases. The perturbation of the constraint is quite subtle causing a maximum deflection of 3 cm from a line connecting the start and end points. As a rough estimate of the stiffness evoked by the perturbation, we can take the force measured during the constraint and subtract the force at the equivalent position in time measured for the unconstrained case. Assuming similar dynamics between the two cases due to the small size of the perturbation, subtracting the unconstrained force is roughly equivalent to subtracting dynamic forces as well as finding differences in muscle generated forces. Given that measured unconstrained forces never exceed 1 N, we find that the estimated force difference can range from 2 to 4 N. Since maximum force occurs at the maximum displace-

ment of 3 cm, an order of magnitude estimate for the stiffness at the endpoint is around 60 to 130 N/m which is in the same order of magnitude of the postural stiffnesses of Mussa-Ivaldi et al. However, note that this estimate was made based on very large assumptions of the dynamics of the system as well as assuming no damping within the system. These results cannot be considered conclusive by any means.

However, a more conclusive result can be found by looking at just the relative magnitudes of the forces involved. The forces measured during the unconstrained case had an upper bound of 1 N. These forces are due not only to muscle forces but also to the inertial dynamics of the four links. By constraining the movement and thereby deflecting the arm by 3 cm at the top of the arc, the forces found at the handle can be increased at least threefold. These displacement induced forces which are greater than two to three times the forces due to inertia should be significant enough to have a marked effect on the dynamics of an unconstrained system as will be shown in Section 5.2.3.

Force Direction

Independent of the magnitude of the forces, the evoked forces do have strong directional characteristics. To show this, the dot product between the measured force vector and the radial vector (the displacement vector between the present position and the center of the circular constraint) at each time step of the sampled force was calculated and normalized by the lengths of the two vectors. This product is then averaged over the entire movement. This product is simply the cosine of the angle between the two vectors. Geometrically speaking, it is the length of the projection that the unit measured force vector makes onto the radial direction as shown in Figure 5.13. Therefore a projection measure near one implies that the forces point radially inward; zero implies forces point tangentially along the constrained path; projections less than zero imply forces which point outward away from the center of the constraint. Table 5.5 displays this quantitative measure of the direction of the forces for the first 500 ms of movement.

The results of the projection analysis show a definite inward orientation for the direction of the force vectors. The total pooled projection average is 0.822 which translates into an angle of 28 degrees relative to the radial direction. Assuming inertial dynamics make relatively small changes in the direction of the evoked force vector (< 45 degree rotation), this projection measure implies that the location of the attractor point must reside somewhere within the circular

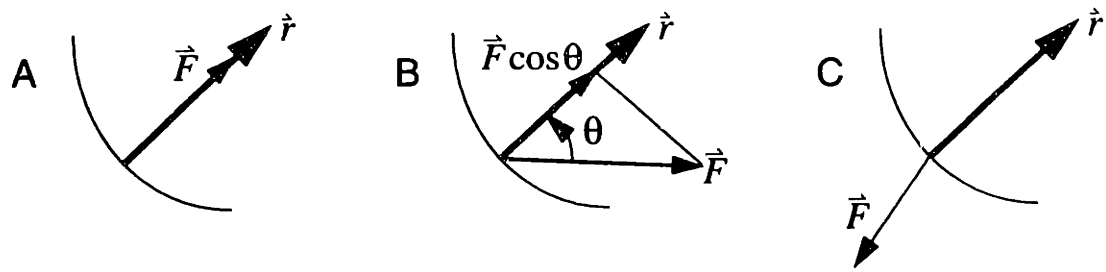

Figure 5.13: The dot product relationship. (A) When proj=1, the projection is the entire vector. (B) When proj = $\cos\theta$, the projection is a portion of the total vector. (C) When proj < 0, the force vector is pointing outward away from the interior of the circle.

Table 5.5: Average projection of forces onto radial direction by trajectory and subject

	Trajectory 1		Trajectory 2		Trajectory 3	
	Proj	**St. Dev.**	**Proj**	**St. Dev.**	**Proj**	**St. Dev.**
Subject A	0.8773	0.3393	0.7677	0.5404	0.8976	0.2050
Subject B	0.8652	0.3363	0.9233	0.2082	0.8472	0.2623
Subject C	0.9423	0.1033	0.8676	0.2925	0.8944	0.1998
Subject D	0.9350	0.0761	0.8970	0.2217	0.9167	0.1244
Subject E	0.9213	0.1225	0.8173	0.3986	NA	NA

Overall Proj Avg	
Proj	**St. Dev.**
0.8822	0.2856

path of the constraint. Note that this analysis is derived completely from the experimental data itself. No assumptions or models were necessary to perform these calculations. Therefore, we have the strong result that the neuromuscular system keeps the attractor within the circle defined by the constraint.

5.2.3 Constrained and Released Movement

In the previous section, it was shown that the magnitude of the evoked forces seemed to be more significant than predicted by Bennett et al. and Gomi et al. However due to the nature

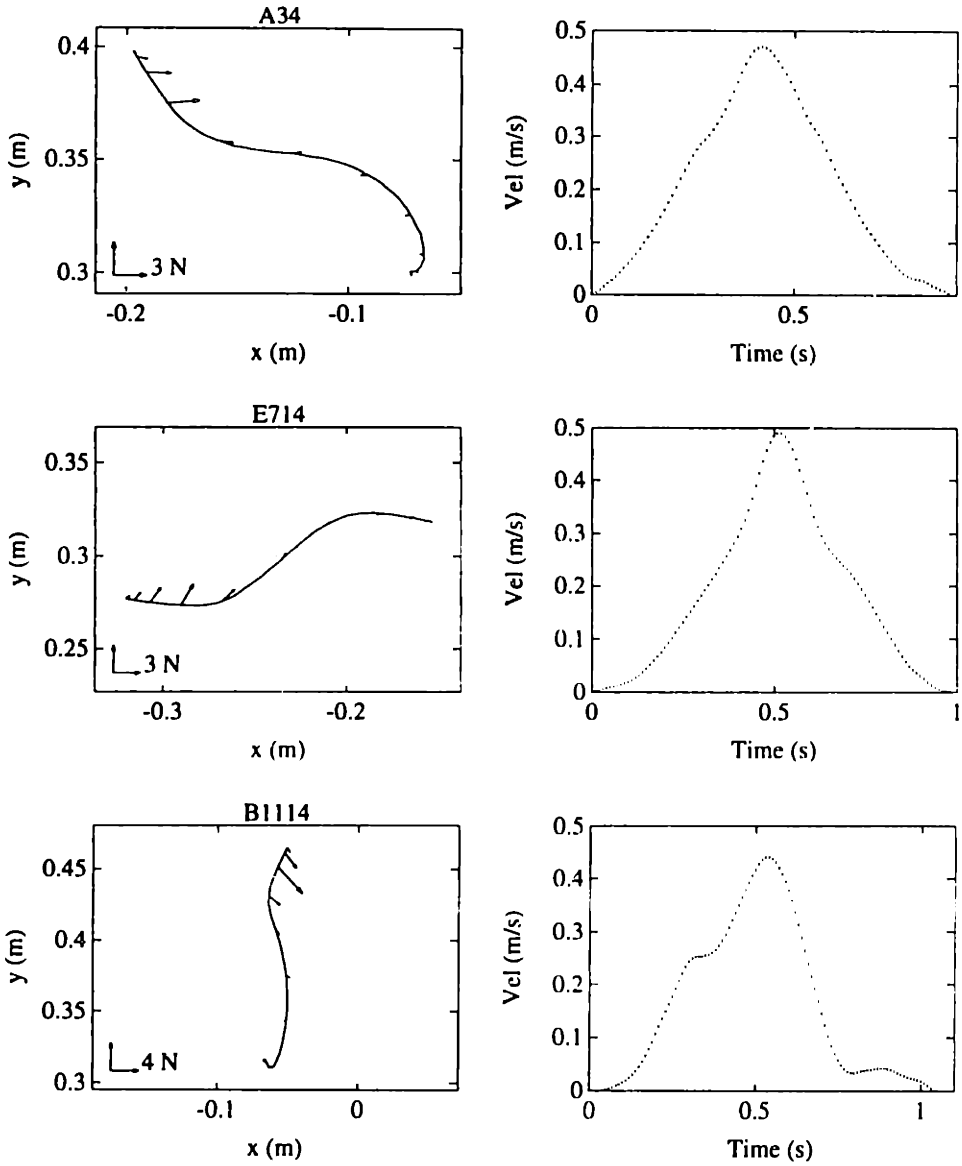

Figure 5.14: Up to down or left to right trajectories for the three sets of starting and ending points. The path of the hand is given on the plots to the left while corresponding tangential velocities profiles are on the right. Plot titles contain letter designation of subjects as well as the trial number.

of the problem, estimates of stiffness can only be roughly approximated, and it remains to be shown that the forces evoked by the constraint deflection can significantly affect the motion of the system. Figure 5.14 and Figure 5.15 present representative data for the constrained and released trials. Note that release occurs well within the 500 ms voluntary response time tested in Chapter 3.

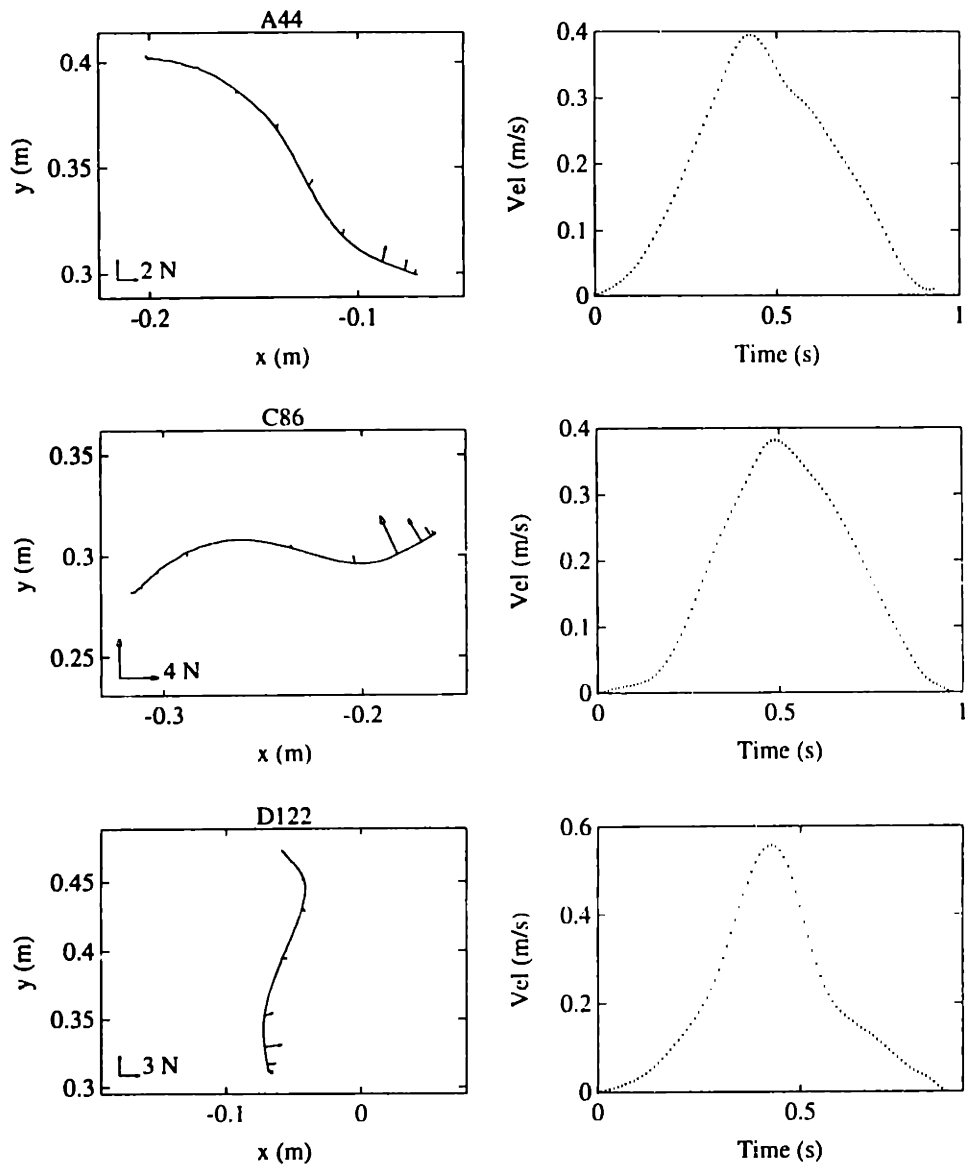

Figure 5.15: Down to up or right to left trajectories for the three sets of starting and ending points. The path of the hand is given on the plots to the left while corresponding tangential velocities profiles are on the right. Plot titles contain letter designation of subjects as well as the trial number.

Almost all of the data show a marked inward return of hand after release from the constraint. Once again, inward is defined as pointing into the circle towards the center. Table 5.6 summarizes the shape of the responses after release in terms of positive and negative area. Figure 5.16 shows what is meant by positive and negative area. These area measures are used to quantify the amount of inward return performed by the arm. Positive area represents the area residing between the hand path and the circle defined by the constraint passing

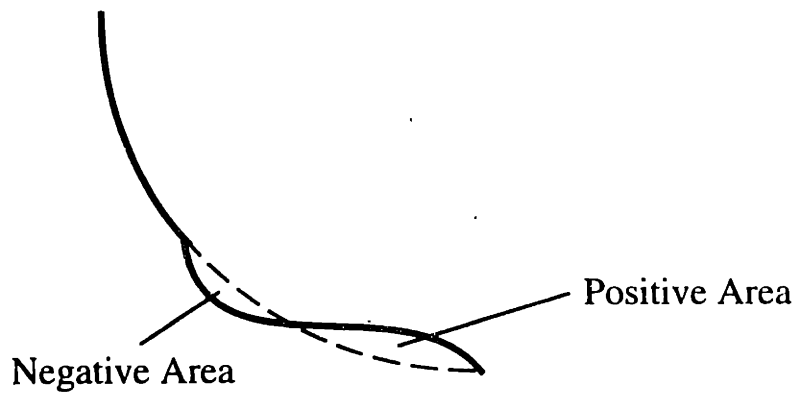

Figure 5.16: Definition of Positive and Negative Area. Negative area represents the area between portions of the hand path outside of the circular constraint and circle defining the constraint. Positive area is the area between portions of the hand path inside of the circular constraint and the circle defining the constraint.

through the starting and ending paths. The area between the two curves is counted as positive area only if the hand path is inside the circle. Otherwise the area is a negative area. The units of these areas are unimportant since these measures of positive and negative areas will be compared between one another and not used as an absolute measure.

The data presented in Table 5.6 show a very strong tendency for the hand path to head inward after release. The positive area for a given trajectory are at least 80 times larger than the corresponding negative area. The negative areas are in general so small that it is difficult to separate them from inaccuracies of the area calculating algorithm. Nonetheless, the data unquestionably shows that the forces evoked by the constraint are strong enough to cause the hand to make a significant return towards the unconstrained path.

5.2.4 Summary of Experimental Data

The three sets of experimental data combine to make a very strong case for the significance of an attractor point during human movement. The unconstrained point to point movements demonstrated that the movements studied were consistent with previous experimental studies on planar reaching movements, and as a result the movements performed within this experimental paradigm could be deemed as typical arm movements. The applied constraint increased the magnitude of the forces measured at the handle doubling or tripling the force measured during unconstrained movements. This implied that a small perturbation in position was sufficient to

Table 5.6: Positive and Negative Areas for the Constrained and Released Trajectories

	Trajectory 1			
	A pos	**St. Dev.**	**A neg**	**St. Dev.**
Subject A	2.3317	0.9107	0.0275	0.0852
Subject B	1.7801	0.4657	0.0089	0.0148
Subject C	1.8727	0.3963	0.0214	0.0344
Subject D	2.0250	0.5822	0.0109	0.0272
Subject E	1.8437	0.7247	0.0076	0.0133

	Trajectory 2			
	A pos	**St. Dev.**	**A neg**	**St. Dev.**
Subject A	1.7297	0.4327	0.0120	0.0157
Subject B	2.1432	0.6377	0.0103	0.0151
Subject C	1.8919	0.6579	0.0228	0.0351
Subject D	2.0027	0.4845	0.0042	0.0072
Subject E	1.9693	0.4577	0.0031	0.0096

	Trajectory 3			
	A pos	**St. Dev.**	**A neg**	**St. Dev.**
Subject A	1.6455	0.6586	0.0101	0.0177
Subject B	1.4392	0.6628	0.0139	0.0311
Subject C	1.6403	0.5049	0.0062	0.0132
Subject D	1.4087	0.3909	0.0083	0.0159
Subject E	NA	NA	NA	NA

Total Positive Area		Total Negative Area	
A pos	**St. Dev.**	**A neg**	**St. Dev.**
1.8379	0.6365	0.0120	0.0315

generate large forces relative to the inertial forces. In addition, these evoked forces were shown to have a strong tendency to point inward along the constraint. Making assumptions of the inertia and damping of the system, this bounds the possible location of the attractor point to be within the circular path or beyond but not outside of the path. Finally, the constrained and released experiments demonstrated the inherent stability of the trajectory. After

release of the constraint, the evoked forces are unquestionably significant enough to cause a deflection in the hand path inwards towards the line connecting the start and end points. These results provide strong evidence that the force-position relationship of the human arm cannot be ignored when studying human movement. Moreover, these results were taken from the experimental data itself. No model was implicit in interpreting these results. Therefore a satisfactory model of the human motor control system for reaching movements must be able to predict these very basic results.

In 1992, Katayama and Kawato generalized from Bennett's dynamic elbow stiffness experiment to derive virtual trajectories for two joint movements with low stiffnesses. As seen in Figure 5.17, the virtual trajectories for straight-line movements are necessarily complex to account for dynamics. Due to the complex nature of these trajectories, it is doubtful that these motor plans could recreate the two most basic experimental findings: 1) consistent inward pointing forces in response to a small positional perturbation for all trajectories and 2) consistent inward returns upon release for all trajectories. Even if a low stiffness trajectory does exist which can satisfy these two findings, it is doubtful that this would be a global result for different trajectories due to the great variability in Katayama and Kawato's derived trajectories.

In the following chapter, a more consistent model will be proposed which is better equipped to reproduce the experimental findings of this chapter.

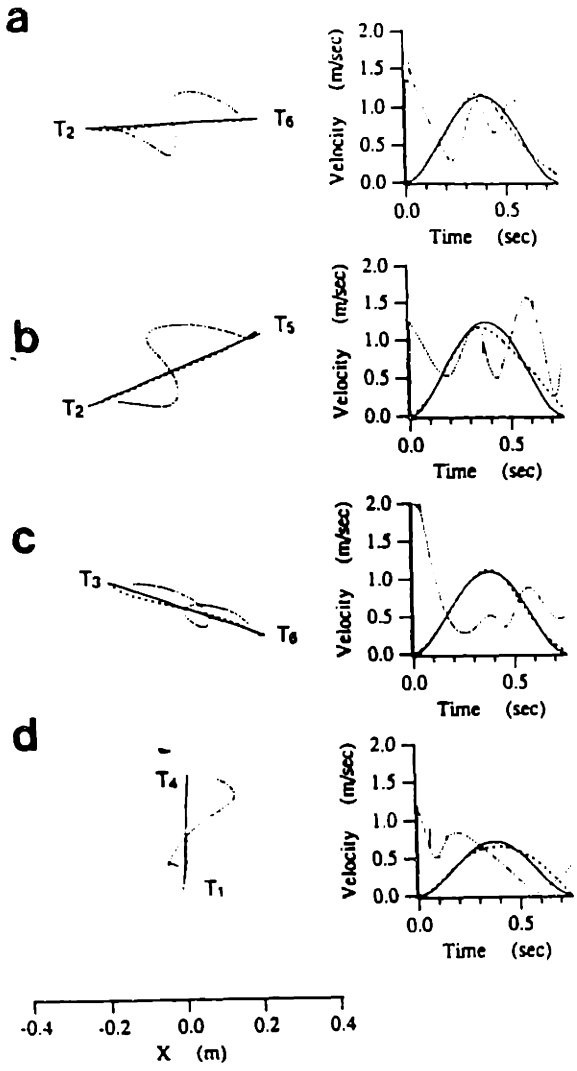

Figure 5.17: Virtual trajectories and tangential speed profiles for movements with low stiffness. [Katayama and Kawato 1992]

Chapter 6

Simulation Results

This chapter will present the major findings of the attempt to recreate the experimental data using a simple linear time invariant impedance model of the human arm. The first portion of this chapter will review the major assumptions made for the models presented. The major portion of this chapter will be devoted, of course, to the simulation results. However as the results are presented, constant attention will be paid to the validity of the assumptions given in the first section. In short, the goal of this chapter is to utilize the success and failings of our naive simple model to evaluate the common assumptions used for modeling human movement. The final section will summarize the major results.

6.1 Model Assumptions

The following simulations relied on four major assumptions. Each have been used previously by Flash to recreate unconstrained point to point hand movements [Flash 1987]. The value of the experimental results presented in the previous chapter is that they represent a more rigorous tests than the model Flash used to recreate the unconstrained movements. The model must now not only kinematically fit the unconstrained data, but it must also have the same dynamic response to the perturbation of the constraint - specifically the force evoked by the constraint and the response of the arm after release from the constraint.

Assumption #1. Linear Impedance

The human arm will be assumed to have linear stiffness and damping about an equilibrium position and velocity respectively as given by the following equation for joint torques.

$$\begin{bmatrix} \tau_S \\ \tau_E \end{bmatrix} = \alpha K \begin{bmatrix} \theta_S - \theta_{So} \\ \theta_E - \theta_{Eo} \end{bmatrix} + \rho B \begin{bmatrix} \dot{\theta}_S - \dot{\theta}_{So} \\ \dot{\theta}_E - \dot{\theta}_{Eo} \end{bmatrix} \tag{6.1}$$

where K and B are the stiffness and damping matrices presented in Chapter 4. The equilibrium trajectory is given by the joint angles and velocities subscripted by the "o". As stated previously, the joint space stiffness and damping matrices are assumed to have the same eigenvectors over the entire workspace so that changes can only be applied by scaling factors α and ρ. Note that the form of the damping is different than that used by Flash. Damping for the following simulations are in terms of a velocity relative to the virtual velocity as opposed to the absolute velocity used by Flash.

Assumption #2. Time Invariant Parameters

In addition to the invariance of shape and orientation of the stiffness and damping ellipses in joint space, the model will also assume that the scaling of the matrices is constant during the entire movement. Therefore, the joint impedance will remain time invariant although the endpoint or cartesian impedance will continue to vary with arm configuration.

Assumption #3. Minimum Jerk Virtual Trajectory

The input to the system will be a virtual trajectory which is a straight line in cartesian space from the initial position to the final position. The form of this trajectory will be have a minimum jerk velocity profile taking the equilibrium point from the start to the finish. The minimum jerk displacement and velocity functions are given by the following equations and are shown in Figure 6.1.

$$x(t) = x_o + (x_o - x_f)\,(15\tau^4 - 6\tau^5 - 10\tau^3) \tag{6.2}$$

$$v(t) = (x_o - x_f)\,(60\tau^3 - 30\tau^4 - 30\tau^2)\,/\,t_f \tag{6.3}$$

where $\tau = \frac{t}{t_f}$.

Assumption #4. Identical Motor Program across Constraint Cases

The simulations are performed under the assumption that the constraint are sufficiently benign that the subject does not use different motor strategies for the unconstrained, constrained, and constrained

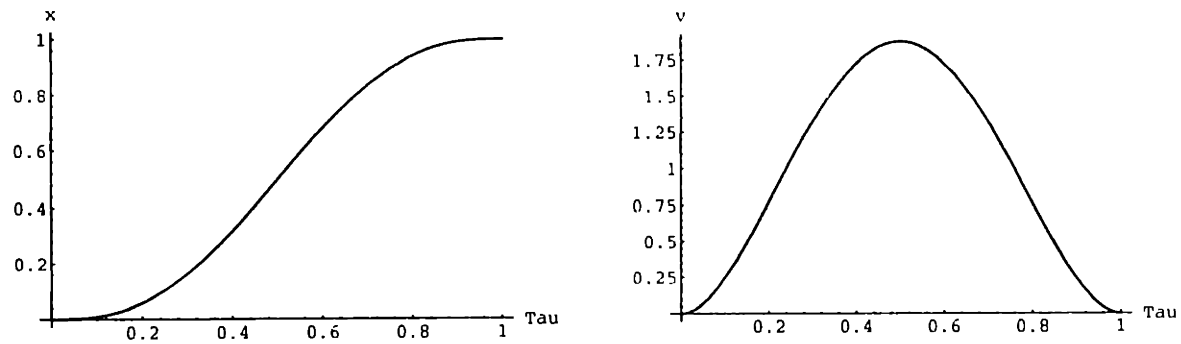

Figure 6.1: The minimum jerk displacement and velocity profiles for a unit displacement in a unit time.

and released cases. Essentially all of these cases for a single trajectory can be described by a single intent or motor program.

Assumption #5. Global Model Invariance across Trajectories

The final assumption states that all trajectories in the workspace can be generalized from a single motor program by simply translating and scaling the virtual trajectory for this motor program. The first set of simulations will explore how well a single set of impedance parameters and a minimum jerk virtual trajectory can create all six possible trajectories.

6.2 Simulation Results

This section contains a summary of the results of the simulated movements. The first subsection explains the method of choosing the appropriate scaling factors for the stiffness and damping. The next subsection explores the global ability of the model to generalize from a single motor program (parameters and virtual path) and recreate the entire set of measured movements. All of the simulations were performed using stiffness data and movement data from Subject C.

6.2.1 Parameter Tuning

Unconstrained and Constrained and Released Fitting

The choice of scaling factors for the stiffness and the damping matrices was performed by simultaneously attempting to match simulated trajectories to the measured trajectories of both the unconstrained and constrained and released movements. This technique resulted

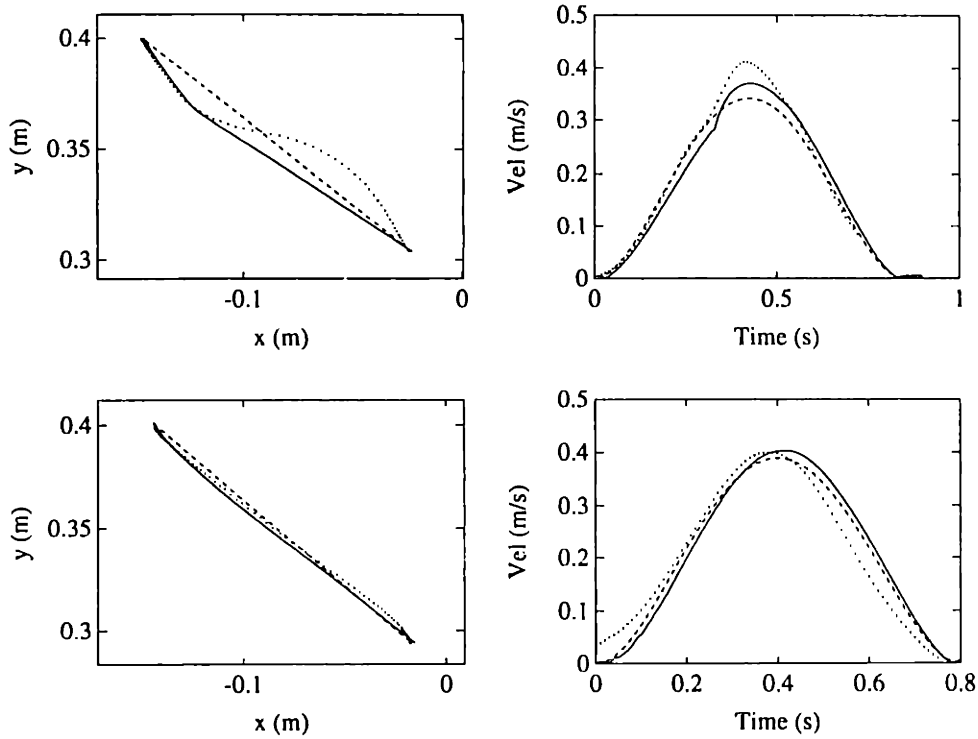

Figure 6.2: Simulation result of large damping. Solid lines are the simulated results; dashed lines are the min jerk virtual trajectory; dotted lines are a typical example of the experimental data. Note that the simulated velocity profile in the unconstrained case closely follows the minimum jerk input and that the hand path is an excellent fit. However, the constrained and released path does not show good agreement.

from an interesting but not surprising finding. Essentially what occurs is that the unconstrained trajectory fit improves as the damping scale is increased. In the extreme case of high damping, the arm simply acts as a velocity controlled system and follows an essentially straight hand path which is very close to the measured path. However such high damping hinders the rapid inward return shown by the constrained and released data. Figure 6.2 displays such a case. This result suggests that the human is not attempting a type of velocity control.

Raising the stiffness should be expected to rectify this problem. However larger stiffness with relatively large damping cannot recreate the amount of inward return shown in the experimental data. The data presented in the previous chapter seemed to indicate a significant overshoot across the equilibrium path. In other words, the hand did not simply return to the straight line but went beyond it before finishing the movement. Decreasing the damping to increase the

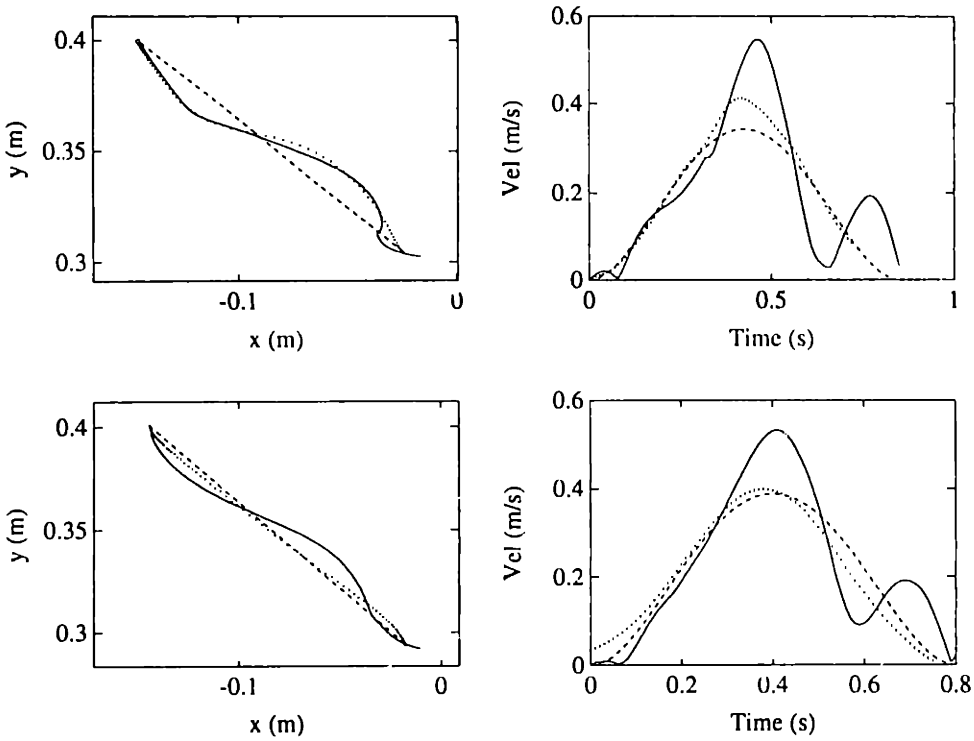

Figure 6.3: Higher stiffness but lower damping causes a much larger inward return. However, the simulated unconstrained path is still more curved than the actual path.

inward return also causes problems. A reduction in the damping affects the unconstrained case causing the simulated trajectory to be less straight due to inertia forces as shown in Figure 6.3.[1] As a result, fitting the constrained and released case without regard to the unconstrained case can result in a curved unconstrained trajectory.

In essence, one cannot always fit a single case with one set parameters and guarantee its ability to recreate the other cases. Getting an acceptable kinematic fit in the unconstrained domain as done by Flash does not necessarily reflect the accuracy of those parameters. The prime difficulty of balancing a near straight unconstrained path with the overshoot of the release case lies in the fact that it is impossible to achieve the large overshoot while maintaining a nominally straight path. This is the first failing of our linear model.

1. This is similar to the results of the one joint simulations by Hogan (1984b) of the deafferated monkey performing the Bizzi experiment described in Section 2.1.2.

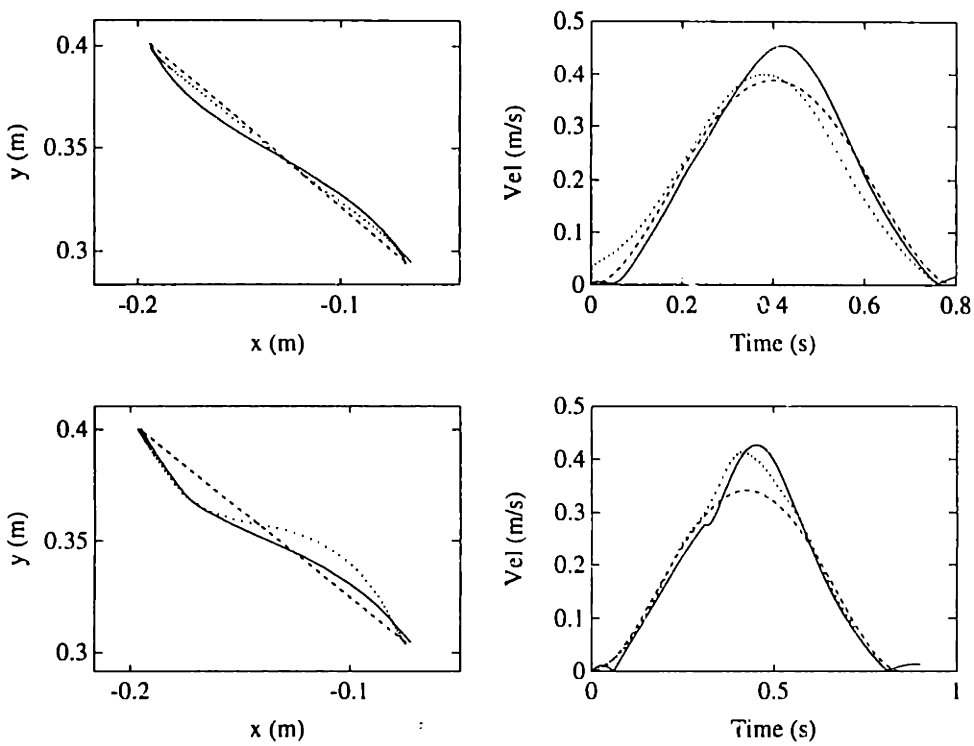

Figure 6.4: Best simulated correspondence of both cases. Note that the simulated unconstrained path is more curved than the actual data and the overshoot in the released case is less than the actual data. The stiffness is twice postural stiffness and a time constant τ equal to 0.05 seconds. Solid lines - simulation; Dashed lines - virtual trajectory; Dotted lines - typical measured data.

However this failing is not catastrophic by any means. The linear virtual trajectory model consistently recreates a very important qualitative experimental result - the inward return of the hand after release. However quantitative results such as the straightness of the path and the amount of overshoot are not as easily recreated. Figure 6.4 shows the best correspondence for the two cases. The scaling factors for these simulations are:

$$\alpha = 2.0\text{X postural stiffness} \tag{6.4}$$

$$\rho = 0.1\text{X postural stiffness} \tag{6.5}$$

or expressed as the time constant $\tau = B/K$

$$\tau = 0.05 \text{ sec} \tag{6.6}$$

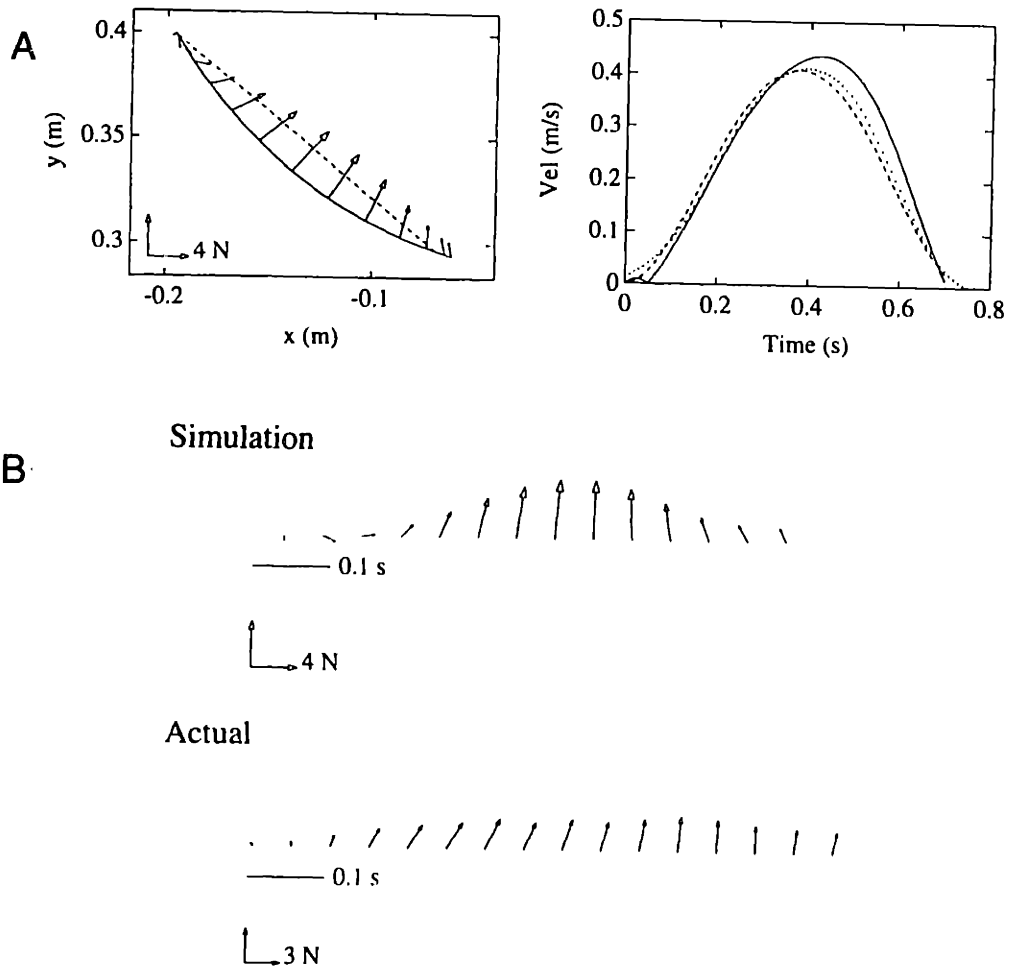

Figure 6.5: The fully constrained simulation. (A) The simulated trajectory with force vectors and the velocity profile. (B) Comparison of the force direction and magnitude for the simulated (top) and the actual (bottom). The y axis is radial force with the x axis as both time and tangential force.

Fully Constrained Simulation

Figure 6.5 completes the simulation set showing the fully constrained simulation for this set of parameters. The directions of the forces in plot B show a qualitative agreement between the simulated and the actual data. Both data sets have strong radial components at the mid-point of the movement. Strong differences in force direction occur at the beginning of the movement where the simulated force are highly non-radial. In later simulations, differences in force direction will be found both at the beginning and end of movements. It can be postulated that the non-radial forces occur as result of the small distances from the equilibrium path at the beginning and end of the movement allowing forces due to inertia to dominate.

Although the force directions show better correlation at the center of the movement, force magnitudes at this location do not quantitively agree. The simulation predicts higher force magnitudes than actually seen experimentally. Assuming that the experimental data accurately reflects the natural movement of the arm i.e. the subject did not intervene, it can be postulated that the differences in force directions and magnitudes can be due to a non-linear stiffness or a time-varying stiffness parameters or both.

If the stiffness of the arm is non-linear in such a way that high apparent stiffness is seen for small displacements while for large displacements the stiffness decreases, then it is possible that these discrepancies could be explained. High stiffness for small displacements would increase the radial component at the beginning and end of the movements. At the midpoint, the forces would be smaller due to the smaller apparent stiffness.

It is also possible that the stiffness varies as the movement progresses. If the stiffness decreases during the first half of the movement, the forces would decrease at the middle of the movement. And if as the movement nears termination the stiffness increases to stabilize the target position, the forces would maintain their magnitude. Such a time varying stiffness would also be capable of recreating the data.

6.2.2 Global Generalization

Using the parameters given in equations 6.4 and 6.5, simulations were performed for the movements performed in the experiment. The results of these simulations will be presented by trajectory type: unconstrained, constrained, and constrained and released.

Unconstrained

Figures 6.6 and 6.7 compare the simulated results with experimental results for the unconstrained movement. In general, the unconstrained kinematic fits were the most successful case to be reproduced. The simulated trajectories were less straight than those measured during the experiments. However for the most part, deviations away from the straight path agreed with the experimental data in terms of the direction of deviation; the magnitude of the deviations were, in general, larger in the simulations. This implies an agreement in the type of effect that inertia forces have on the system but a disagreement in the degree to which they affect it.

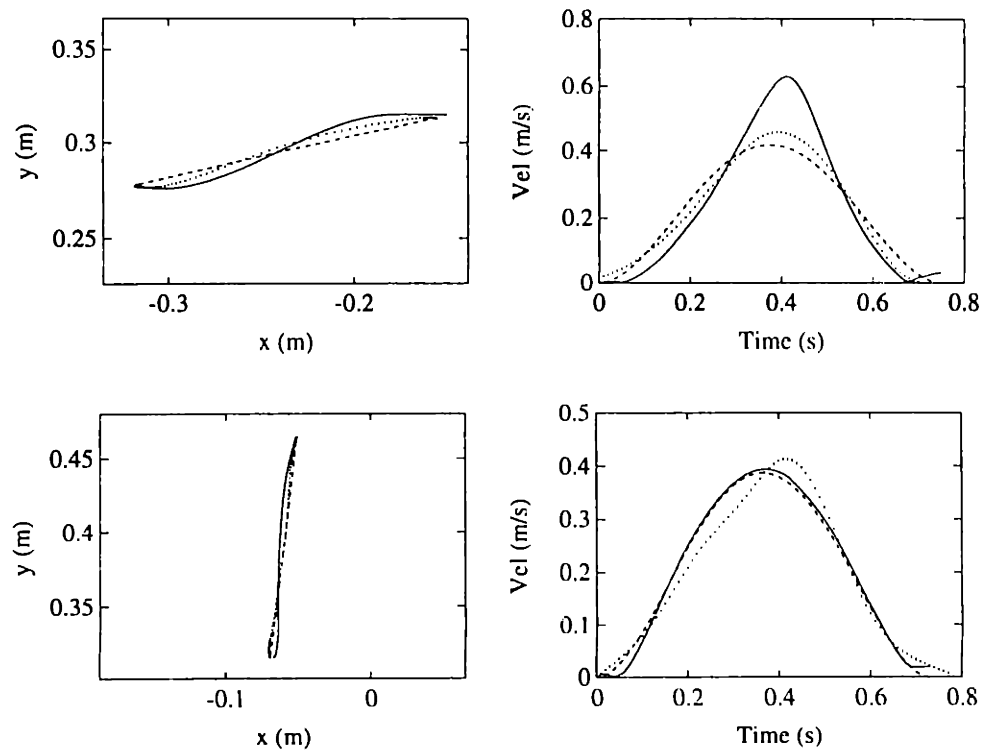

Figure 6.6: Up to down and left to right simulated unconstrained trajectories. Solid lines - Simulation; Dashed lines - Virtual Trajectory; Dotted lines - Experimental data.

The velocity profiles qualitatively showed some similarities. The simulations had similar single peaked bell-shaped patterns. The simulated velocities were more symmetrical than the measured data even for trajectories with large deviations from the straight-line path. Predictably the trajectories with larger deviations had peak velocities much higher than the measured velocities than simulated trajectories which deviated less.

The results of these simulations confirm Flash's results that a single set of parameters and a scaled virtual trajectory is capable of generalizing to movements in different directions with satisfactory qualitative agreement. However as shown in the previous subsection, these agreements do not necessarily imply a satisfactory fit for the other two cases. It remains to be seen in the next two subsections whether Flash's results can be extended.

Fully Constrained

Figures 6.8 and 6.9 display the simulation results for the fully constrained trajectories. The results of these simulations were mixed. In general, the virtual trajectory model was success-

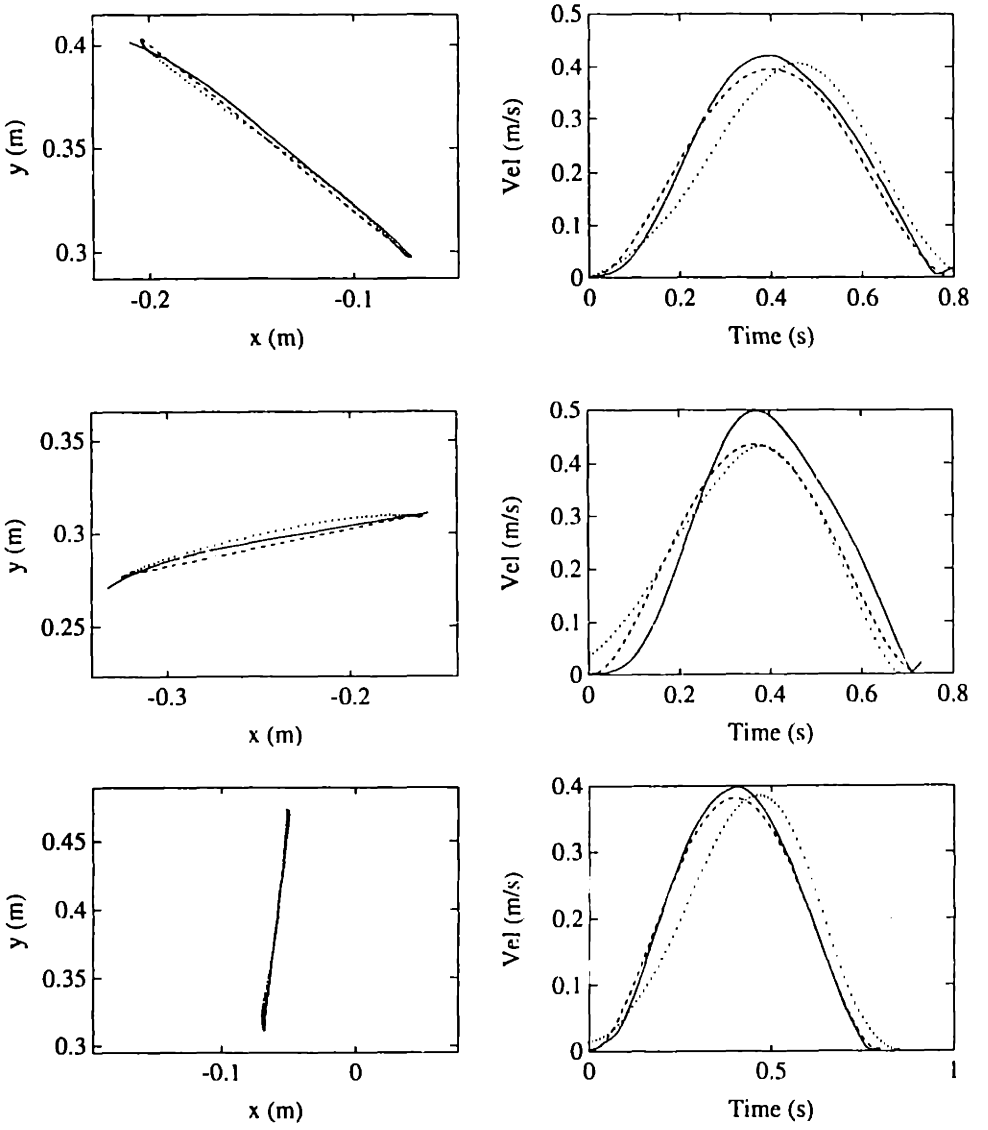

Figure 6.7: Down to up and right to left simulated unconstrained trajectories. Solid lines - Simulation; Dashed lines - Virtual Trajectory; Dotted lines - Experimental data.

fully able to produce radially inward directed forces in every case. However as before, these radially inward forces were consistent mainly through the first three-quarters of the simulation. In the diagonal case and in the horizontal case, the forces produced at towards the end of the trajectory were consistently pointing outwards away from the constraint which is inconsistent with the experimental data. Assuming the equilibrium point is always inside the constrained path, these outward forces must be due to the forces of inertia acting on the system.

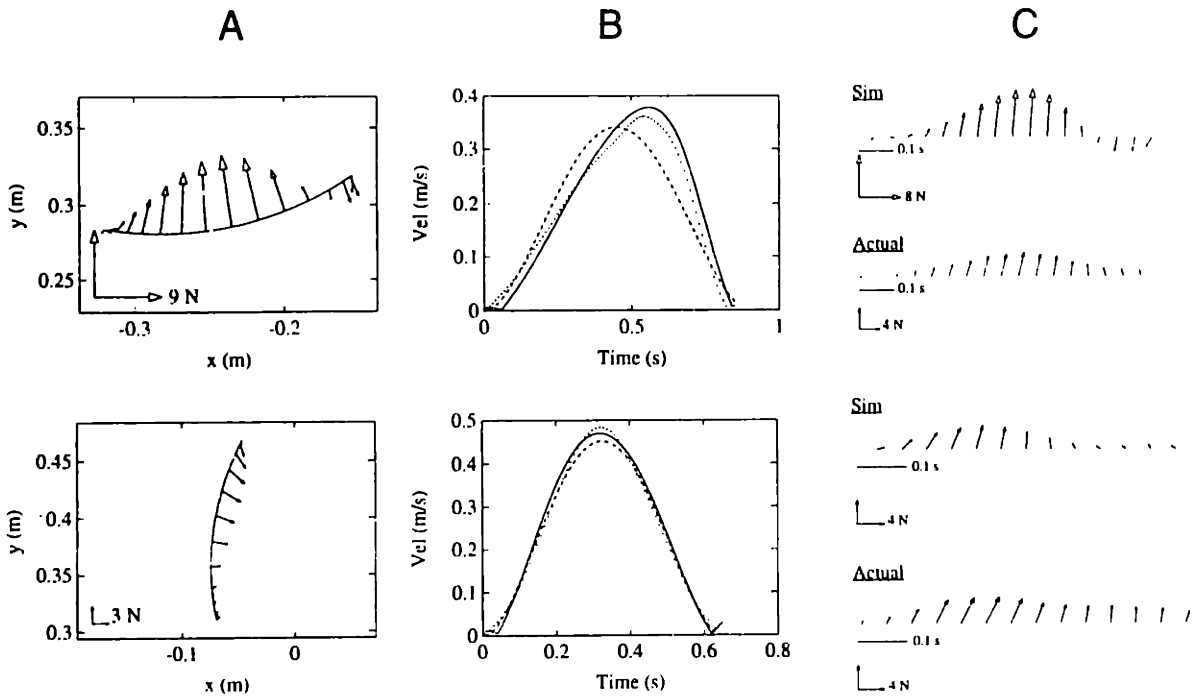

Figure 6.8: (A) and (B): Up to down and left to right for the fully constrained trajectories and their velocities. Solid lines - Simulation; Dashed lines - Virtual Trajectory; Dotted lines - Experimental data. (C): Comparison force directions and magnitudes. y-axis is the radial component while the x-axis is time as well as the tangential component.

In addition, the maximum evoked force found at the largest displacement from the straight line was consistently predicted to be much larger than those found during the experiments. In some cases, the simulated forces could be as much as twice as large than that actually measured.

These inconsistencies are the same as the ones shown earlier in Section 6.2.1. Again the same explanation applied to the constrained simulation in Section 6.2.1 may also be applied here. Assuming that the virtual trajectory remains near the straight path throughout the movement, the experimental results imply either a non-linear static impedance or a time-varying impedance. Also since the major inconsistencies occur late in the movement, it is possible that Assumption #4 is incorrect and that the subject is changing the motor program due to the presence of the constraint. This experimental case is very susceptible to such an argument since the perturbation is applied over the duration of the entire movement.

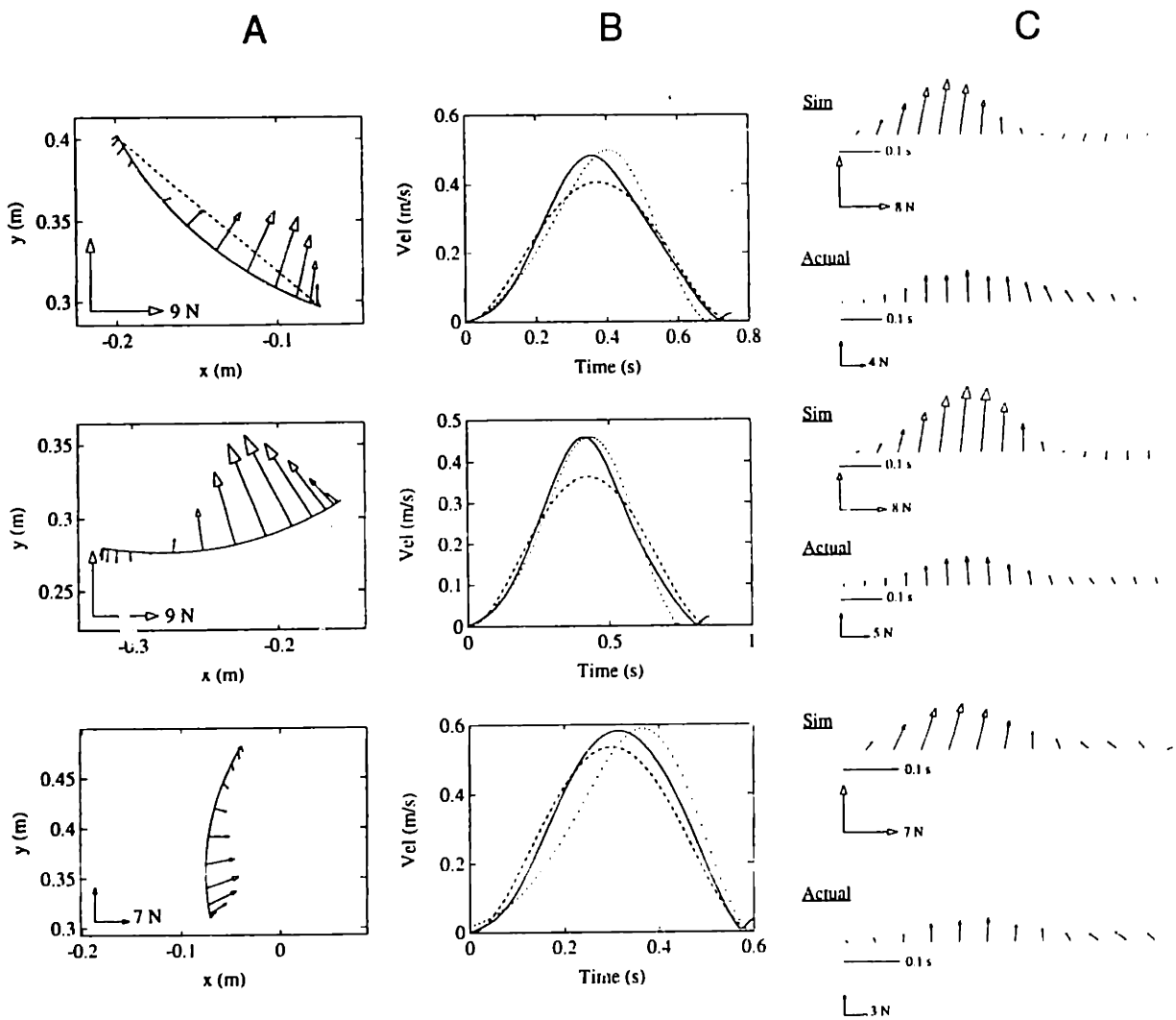

Figure 6.9: (A) and (B): Down to up and right to left for the fully constrained trajectories and their velocities. Solid lines - Simulation; Dashed lines - Virtual Trajectory; Dotted lines - Experimental data. (C): Comparison force directions and magnitudes. y-axis is the radial component while the x-axis is time as well as the tangential component.

As shown in Chapter 3, the subject seems to be incapable of intervening for the first 500 ms of the movement. For the majority of the movements, 500 ms is enough time for the subject to reach the midpoint of the movement. After this point, no assumptions can be made about the behavior of the subject in response to the constraint. Therefore no strong statements can be made about the reliability of the results beyond the first 500 ms.

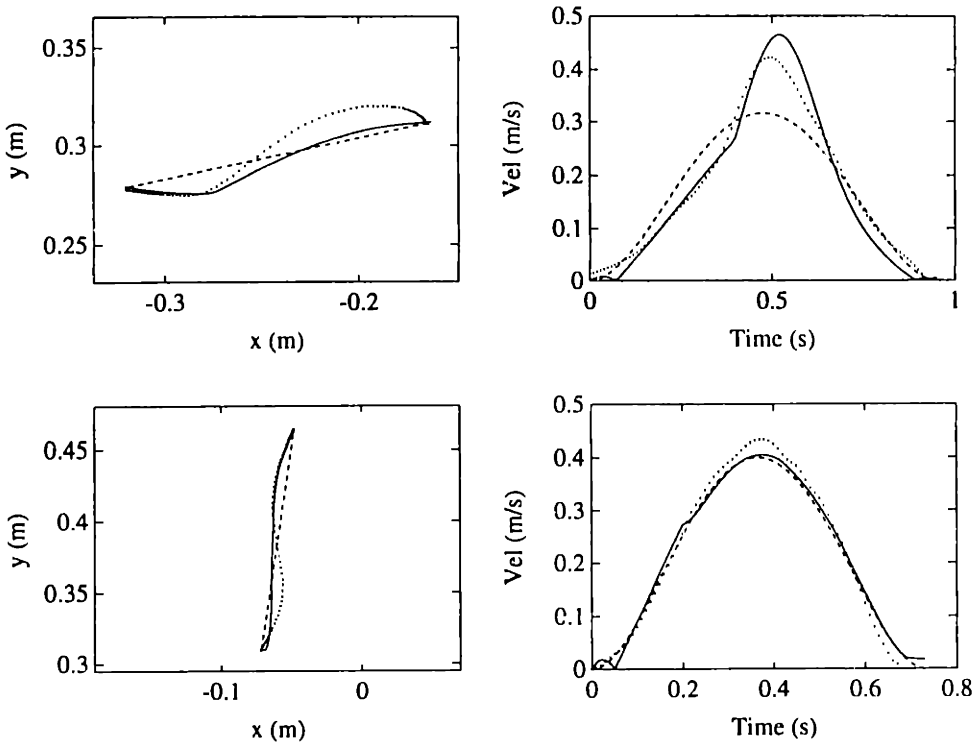

Figure 6.10: Up to down and left to right for the constrain and release trajectories and their velocities. Solid lines - Simulation; Dashed lines - Virtual Trajectory; Dotted lines - Experimental data.

Constrained and Released

Figures 6.10 and 6.8 show the simulations for the final experimental case, the constrained and released case. All of these trajectories simulated produced the same qualitative result of an inward return after release from the constraint. With the virtual trajectory model, each simulation displayed a definite desire to move inward towards the straight path after release. However similar to the case presented in Section 6.2.1, the simulated overshoot past the straight path was much smaller than the overshoot seen in the majority of the experimental data (Appendix B).

Larger overshoots are possible if the damping of the system decreases along the trajectory. This must be especially true if stiffness effects decrease as the trajectory reaches the release point as indicated by the fully constrained experiment. However, decreasing damping creates problems for the unconstrained simulation to remain close to the experimental data. The damping is necessary to decrease the amplitude of the deviations from a straight

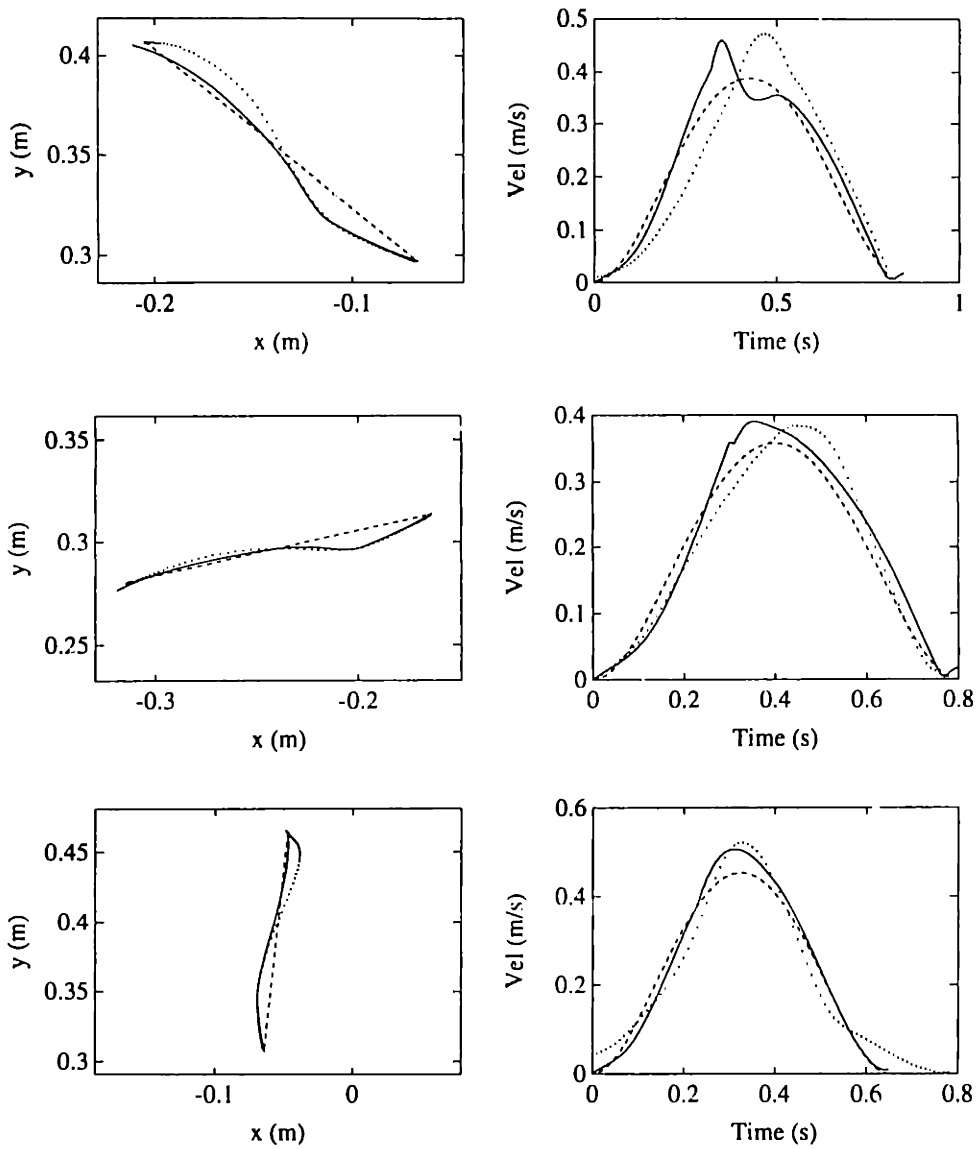

Figure 6.11: Down to up and right to left for the constrain and release trajectories and their velocities. Solid lines - Simulation; Dashed lines - Virtual Trajectory; Dotted lines - Experimental

path. Therefore, one can postulate that the damping assumption made within this model is insufficient to truly capture the data.

Arguably the assumption of the shape of the damping ellipse is very questionable. Constraining the shape and orientation to match the stiffness was done mainly as a result of not having a reliable measurement of the true damping characteristic of the arm. The linearity assumption is similarly suspect. In fact, there is strong experimental evidence that a single joint

during movement displays damping forces which have a non-linear relationship with velocity [Wu et al. 1990].

6.2.3 Summary of Simulations

Although some serious inconsistencies were found between the model results and the actual data, one cannot overlook the fact that the model was still able to capture the three main characteristics presented in the previous chapter. These characteristics were presented in the previous chapter as set of requirements which a model must satisfy in order to be considered adequate. The virtual trajectory model did display near straight unconstrained hand paths with single peaked velocity profiles; it did display inward pointing forces for the majority of the constrained movement; and it did display a marked tendency to make an inward return after release from the constraint. This was all accomplished with what can be called a "naive" model which was chosen for simplicity and out of ignorance of the true details of the system. Inconsistencies aside, the virtual trajectory model cannot be discounted as invalid based on the experiments performed within this thesis.

Chapter 7

Conclusions and Recommendations

The goal of this work was to examine the basic properties of the human arm as it performs basic reaching movements. In the past, several researchers have done complete studies on these types of movements. However due to the nature of their experimental paradigms, the analyses performed were mainly relegated to focus on the kinematic features of the data. Although Flash later performed a series of dynamic simulations, her work centered mainly of fitting the kinematic features of the data.

Within this thesis, the kinematic study of human arm movement was extended to observe not only natural planar movements but also patterns in the response to perturbations during trajectory. From the patterns observed, an additional set of conditions, above and beyond the kinematic features, were found which classify the natural behavior of the arm during movement.

7.1 Features of Human Arm Movement

The experimental results make a very strong statement about the nature of arm movements. Their strengths lie in the fact that all of the subjects essentially had essentially indistinguishable results. The inter-subject and the intra-subject consistency was so strong that the pat-

terns observed in the data were readily apparent from the raw data. These patterns define a type of litmus test by which any model of human reaching movements must pass.

1. Reaching movements have characteristically straight hand paths with a single peaked tangential velocity profile for the hand. These movements are competently described by a minimum jerk trajectory and velocity.

   The unconstrained movements reconfirmed the results of previous researchers. Hand paths during reaching are very close to straight lines from start to target with some minor but not insignificant amounts of curvature. The tangential velocity profiles were characteristically single-peaked which had excellent qualitative comparisons to a minimum jerk velocity profile. In addition, all movements exhibited similar durations in movement time for all three trajectories tested.

2. Constraining the movement evokes significant inward pointing forces. In addition, the subject is capable of stably controlling the arm even with the sudden addition of the constraint.

   The major feature of the constrained movements were the evoked forces at the handle of the robot. These forces also consistently pointed inward towards the center of the constraint throughout the entire movement. The magnitude of the forces were also significant with forces reaching a maximum of 4 to 5 Newtons as compared to the maximum of 1 Newton found during the unconstrained trajectories. By removing a degree of freedom and thereby causing a displacement away from the unconstrained path, the forces can be increased four or fivefold which implies a strong positional dependence of the behavior of the arm.

3. Constraining and releasing the arm during movements results in a consistent inward return of the arm. Moreover, the sudden release does not inhibit the ability of the subject to complete the task.

   After release of the arm, the hand always moves inward toward the straight line path between the start and target points. This release behavior is characterized by a consistent tendency to overshoot the straight path by a magnitude equal to the displacement at the release point. Even in the presence of the sudden release, the human is still able to continuously move the trajectory to the finish point where the subject is still able to accurately place his/her hand at the target.

These results are extensions which supplement what is known about human reaching. By adding these additional clues, the set of possible motor control paradigms is decreased as the models are constrained to satisfy not only the simple kinematic requirements but also a deeper system behavior requirement as well. These results surely exclude many of the possible models

which are currently popular such as inverse dynamics or the final equilibrium point hypothesis.

7.2 A Possible Model

With these requirements, the natural question arises of whether there actually exists a simple paradigm which could be considered acceptable. The second portion of this thesis was devoted to testing a possible candidate. The virtual trajectory hypothesis was used in a numerical simulation in an attempt to recreate the experimental data of all three cases using a single motor plan and a single set of parameters.

The results of the simulation were mixed. Difficulties arose in attempting to tune the linear parameter of the arm's impedance so that the simulated trajectories could closely match typical experimental data for the unconstrained, constrained, and constrained and released cases. The amount of overshoot across the straight path after release from the constraint was a typical problem. Decreasing the damping to increase the overshoot would degrade the fit of the unconstrained simulation which would show increased curvature. Increasing stiffness causes the constrained simulation result to show much higher forces than those measured experimentally.

Qualitatively however, the simulations overall were encouraging even when considering the problems described. The simulations were consistent in their abilities to satisfy all three of the characteristics described in the previous section; the simulations only differed in the degree of agreement in the specifics (amount of overshoot, magnitude of forces, etc.). Major features such as the inward return and inward pointing forces naturally occur within the framework of this model. As a result, the concept of a moving attractor point used to control and simplify movements could be considered as one of the more obvious choices in terms of naturally being able to show such behavior.

7.3 Recommendations for Future Work

7.3.1 The static impedance field

The inability of the simulations to better fit the experimental data calls for improvements to the linear time-invariant model of the arm's impedance. It is quite possible that assumption of linear stiffness is inadequate for the range of displacements from equilibrium taking place during movement. In fact, other studies have shown apparent nonlinearities and asymmetries in the endpoint stiffness of the arm [McIntyre 1990; Shadmehr et al. 1992]. In addition, Shadmehr et al (1992) showed marked decreases in stiffness as the hand is displaced from 1 cm to 4 cm. In certain directions, a change of almost 200 N/m can occur.

A better model of the force field about equilibrium can be formulated using the technique of functional approximating the vector field with a series of basis functions [Mussa-Ivaldi et al. 1991; Shadmehr et al. 1992]. If we assume that the static impedance vector field is conservative and therefore integrable, then by using a linear combination of a set of predefined fields called basis fields an approximation vector field can be fitted to the experimental data. The basis fields used for this approximation is based on the potential function defined by the following bivariate Gaussian which have been found to give an optimally smooth fit [Poggio and Girosi 1990].

$$G(x,y) = exp\left(-\frac{(x-x_c)^2}{2\sigma_x^2} - \frac{(y-y_c)^2}{2\sigma_y^2}\right) \tag{7.1}$$

The desired basis field is simply the gradient of the potential function.

$$\varphi(x,y) = \nabla G = \left(\frac{\partial G(x,y)}{\partial x}, \frac{\partial G(x,y)}{\partial y}\right) \tag{7.2}$$

The functions defined in equations 7.1 and 7.2 are plotted in Figure 7.1. These simple elements are used to construct the field by centering these fields at different positions (x_c,y_c) in the workspace of the sampled data. The problem now comes down to finding the set of coefficients c_i which multiply each basis field to construct the actual field F as shown in Equation 7.3.

$$F \sim \sum_{i=1}^{k} c_i \varphi^i \tag{7.3}$$

where k is the number of basis centers. This fit can be done using a least squares criterion.

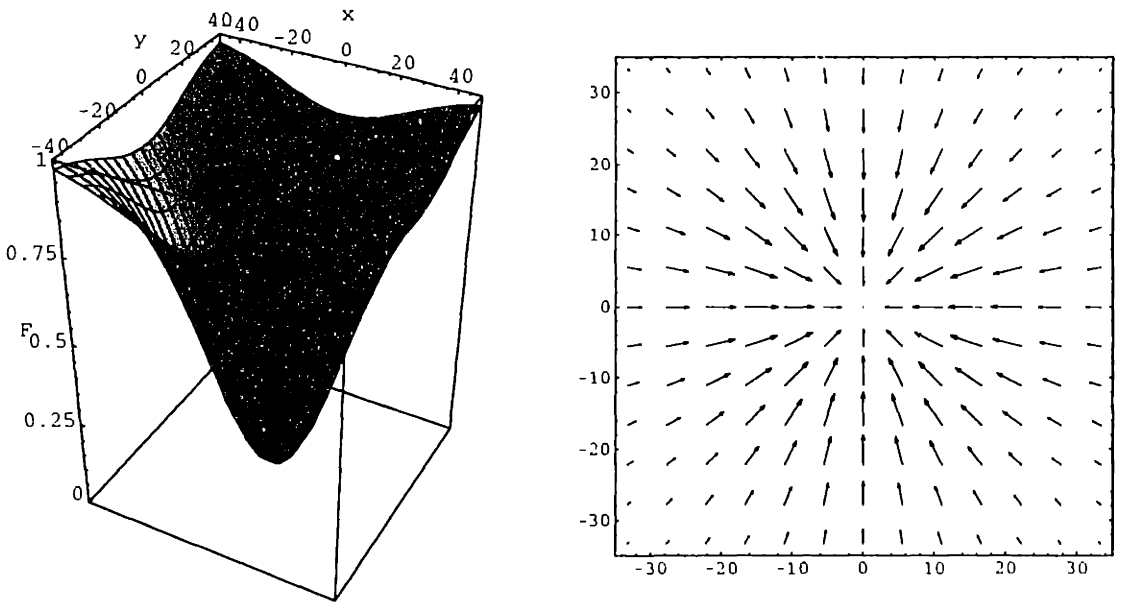

Figure 7.1: The Radial Basis Element - the potential function and its derivative vector field.

With the set of coefficients, a complete description of the measured forces about equilibrium has been found with no modelling assumptions besides an assumption of integrability. The joint space torque field can be found from the endpoint fit by simply transforming through the Jacobian which at a fixed location is a linear operator.

7.3.2 The velocity dependent impedance

A significant difficulty with working with a dynamic model of the human arm is that so little is known about the characteristics of the neuromuscular damping. Flash (1987) in her simulations also points out the need for "establishing experimentally what the actual values of the joint visco-elastic coefficients during different two-joint movements."

Studies have been performed on single joint movements where the damping torque were found to be proportional to the velocity of the joint to the power of one-sevenths [Wu et al. 1990]. However it is still unclear how this translate to a multi-joint case where a single muscle can effect the behavior of more than a single joint.

7.3.3 The inertia parameters

The inertia parameters used for the human arm were based on cadaver studies by Dempster and others. It is unclear whether these are sufficiently accurate representations of a living human for the purposes of this study. Changing the shape of the inertia tensor could have a marked effect on the simulations especially during the release movements. Therefore tuning the inertia parameters while staying in acceptable bounds could improve the quantitative agreement between the actual data and the simulations.

7.4 Final Remarks

This results of the experiments in this thesis have significant implications in the future of arm movement studies. The experiments were able to identify a consistent set of behavior for the human during movement. It can be said that the majority of the analyses being carried out on human movement today use kinematic objectives or cost function as a means of validating results. However in the opinion of this author, using such an objective to evaluate the model of a dynamic system such as the human arm creates an ill-constrained problem. Kinematic correspondence can be achieved with a set of parameters which will not guarantee similar behavior when looking at the dynamic response from a perturbation.

Bibliography

Abend W., Bizzi E., and Morasso P. (1982) Human Arm Trajectory Formation. *Brain* 105:331-348.

Asatryan D.G. and Feldman A.G. (1965) Functional Tuning of Nervous System with Control of Movement or Maintenance of a Steady Posture - I. Mechanographic Analysis of the Work of the Joint on Execution of a Postural Task. *Biophysics* 10(5):925-934.

Bennett D.J., Hollerbach J.M., Xu Y., and Hunter I.W. (1992) Time-Varying Stiffness of the Human Elbow Joint During Cyclic Voluntary Movement. *Exp. Brain Research.*

Bizzi E., Dev P., Morasso P., and Polit A. (1978) Effect of Load Disturbances During Centrally Initiated Movements. *J. Neurophysiology* 41:542-556.

Bizzi E., Chapple W., and Hogan N. (1982) Mechanical Properties of Muscles: Implications for Motor Control. *Trends in Neuroscience* 5:395-398.

Bizzi E., Accornero N., Chapple W., and Hogan N. (1984) Posture Control and Trajectory Formation During Movement. *J. Neuroscience* 4:2738-2745.

Busby H.R. and Trujillo D.M. (1985) Numerical Experiments with a New Differentiation Filter. *J. Biomechancial Engineering* 107:293-299.

Colgate J.E. and Hogan N. (1988) Robust Control of Dynamically Interacting Systems. *Int. J. Control* 48:65-88.

Cooke J.D. (1979) Dependence of Human Arm Movements on Limb Mechanical Properties. *Brain Research* 165:366-369.

Dohrmann C.R. (1986) A Dynamic Programming Approach to Smoothing and Differentiating Data with Splines. Master's Thesis, Ohio State University.

Dohrmann C.R., Busby H.R., and Trujillo D.M. (1988) Smoothing Noisy Data Using Dynamic Programming and Generalized Cross-Validation. *J. Biomechanical Engineering* 110:37-41.

Eppinger S.D. and Seering W.P. (1987) Understanding Bandwidth Limitations in Robot Force Control. *IEEE J. Robotics and Automation* pp. 904-909.

Fasse E.D. (1987) Stability Robustness of Impedance Controlled Manipulators Coupled to Passive Environments. S.M. Thesis, Department of Mechanical Engineering, M.I.T.

Fasse E.D. (1992) On the Use and Representation of Sensory Information of the Arm by Robots and Humans. Ph.D. Thesis, Department of Mechanical Engineering, M.I.T.

Faye I.C. (1986) An Impedance Controlled Manipulandum for Human Movement Studies. S.M. Thesis, Department of Mechanical Engineering, M.I.T.

Feldman A.G. (1966) Functional Tuning of Nervous System with Control of Movement or Maintenance of a Steady Posture - II. Controllable Parameters of the Muscles. *Biophysics* 11(3):565-578.

Feldman A.G. (1980) Superposition of Motor Programs - I. Rhythmic Forearm Movements in Man. *Neuroscience* 5:81-90.

Feldman A.G. (1986) Once More on the Equilibrium Point Hypothesis (λ Model) for Motor Control. *J. Motor Behavior* 18(1):17-54.

Flash T. and Hogan N. (1985) The Coordination of Arm Movements: An Experimentally Confirmed Mathematical Model. *J. Neuroscience* 5(7):1688-1703.

Flash T. (1987) The Control of Hand Equilibrium Trajectories in Multi-Joint Arm Movements. *Biological Cybernetics* 57:257-274.

Georgopoulos A.P., Kalaska J.F., Caminiti R., and Massey J.T. (1982) On the Relations Between the Direction of Two-Dimensional Arm Movements and Cell Discharge in Primate Motor Cortex. *J. Neuroscience* 2:1527-1537.

Georgopoulos A.P., Caminiti R., Kalaska J.F., and Massey J.T. (1983) Spatial Coding of Movement: A Hypothesis Concerning the Coding of Movement Direction by Motor Cortical Populations. *Exp. Brain Research (Supplement)* 7:327-336.

Gomi H., Koike Y., and Kawato M. (1992) Human Hand Stiffness During Discrete Point-to-Point Multi-Joint Movement. *International Conference of the IEEE Engineering in Medicine and Biology Society.*

Hasan Z. (1991) Moving a Human or Robot Arm with Many Degrees of Freedom: Issues and Ideas. In: *Lectures in the Sciences of Complexity III*, L. Nadel and D.L. Stein, Editors, Addison-Wesley.

Hogan N. (1984a) Adaptive Control of Mechanical Impedance by Coactivation of Antagonist Muscles. *IEEE Automatic Control* 29(8):681-690.

Hogan N. (1984b) An Organizing Principle for a Class of Voluntary Movements. *J. Neuroscience* 4(11): 2745-2754.

Hogan N. (1985) Impedance Control: An Approach to Manipulation: Part I - Theory. *Journal of Dynamic Systems, Measurement and Control* 107:1-7.

Hogan N., Bizzi E., Mussa-Ivaldi F.A., and Flash T. (1987) Controlling Multi-Joint Motor Behavior. *Exercise Sport Sciences Reviews* 15:153-190.

Hogan N. (1987) Planning and Execution of Multi-Joint Movements. *Canadian Journal of Physiol. Pharmacology* 66:508-517.

Hogan N. (1988) On the Stability of Manipulators Performing Contact Tasks. *IEEE J. Robotics and Automation* 4:677-686.

Hogan N. (1990) Mechanical Impedance of Single and Multi-Articular Systems. In: *Multiple Muscle Systems: Biomechanics and Movement Organization*, J.M. Winters and S.L.-Y. Woo, Editors, Springer-Verlag.

Hollerbach J.M. and Atkeson C.G. (1987) Deducing Planning Variables from Experimental Arm Trajectories: Pitfalls and Possibilities. *Biological Cybernetics* 56:279-292.

Jeannerod M. (1992) The Interaction of Visual and Proprioceptive Cues in Controlling Reaching Movements. In: *Motor Control: Concepts and Issues*, D.R. Humphreys and H.J. Freund, Editors. John Wiley and Sons, Ltd., pp. 277-291.

Kane T.R. (1983) Formulation of Dynamical Equations of Motion. *Am. J. Phys.* 51(11).

Kane T.R. and Levinson D.A. (1985) *Dynamics: Theory and Applications*. McGraw Hill Book Company.

Karnopp D.R. (1985) Computer Simulation of Stick-Slip Friction in Mechanical Dynamic Systems. *J. Dynamic Systems, Measurement, and Control* 107:100-103.

Jacobsen L.S. and Ayre R.S. (1958) *Engineering Vibrations with Applications to Structures and Machinery*. McGraw Hill Book Company.

Joyce G.C., Rack P.M.H., and Westbury D.R. (1969) The Mechanical Properties of Cat Soleus Muscle During Controlled Lengthening and Shortening Movements. *J. Physiology* 204:461-474.

Joyce G.C. and Rack P.M.H. (1969) Isotonic Lengthening and Shortening Movements of Cat Soleus Muscles. *J. Physiology* 204:475-491.

Katayama M. and Kawato M. (1992) Virtual Trajectory and Stiffness Ellipse During Multi-Joint Arm Movement Predicted by Neural Inverse Models. Paper in Progress.

Lacquaniti F., Licata F., and Soechting J.F. (1982) The Mechanical Behavior of the Human Forearm in Response to Transient Perturbations. *Biological Cybernetics* 44:35-46.

Lestienne F., Polit A., and Bizzi E. (1981) Functional Organization of the Motor Process Underlying the Transition from Movement to Posture. *Brain Research* 230:121-131.

Mansfield J.M. (1992) Functional Assessment of Amputee Performance. Ph.D. Thesis, Department of Mechanical Engineering, M.I.T.

McIntyre J. (1990) Utilizing Elastic System Properties for the Control of Posture and Movement. Ph.D. Thesis, Department of Brain and Cognitive Sciences, M.I.T.

McMahon T.A. (1984) *Muscles, Reflexes, and Locomotion*. Princeton University Press.

Miller and Nelson (1973) *Biomechanics of Sport*. Lea and Feiger, Editors.

Morasso P. (1981) Spatial Control of Arm Movements. *Exp. Brain Research* 42:223-227.

Murphy M.C. (1990) Geometry and the Kinematics of the Normal Human Knee. Ph.D. Thesis, Department of Mechanical Engineering, M.I.T.

Mussa-Ivaldi F.A., Hogan N., and Bizzi E. (1985) Neural, Mechanical, and Geometric Factors Subserving Arm Posture. *J. Neuroscience* 5:2732-2743.

Mussa-Ivaldi F.A., Morasso P., and Zaccaria R. (1988) Kinematic Networks: A distributed Model for Representing and Regularizing Motor Redundancy. *Biological Cybernetics* 60:1-16.

Mussa Ivaldi F.A., Bizzi E., Giszter S.F. (1991) Transforming Plans into Actions by Tuning Passive Behavior: A Field Approximation Approach. In: *Proceedings of the IEEE International Symposium on Intelligent Control* pp. 101-109.

Plagenhoef (1971) *Patterns of Human Motion*. Prentice-Hall, Inc.

Poggio T. and Girosi F. (1990) A Theory of Networks for Learning. *Science* 247:978-982.

Polit A. and Bizzi E. (1979) Characteristics of Motor Programs Underlying Arm Movements in Monkeys. *J. Neurophysiology* 42:183-194.

Rack P.M.H. and Westbury D.R. (1969) The Effects of Length and Stimulus Rate on Tension in the Isometric Cat Soleus Muscle. *J. Physiology* 204:443-460.

Sanes J.N. (1983) Inaccurate Limb Positioning after Unexpected Perturbations During Movement. *Soc. Neuroscience Abstract* 9:630.

Shadmehr R. (1991) A Computational Theory for Control of Posture and Movement in a Multi-Joint Limb. Ph.D. Thesis, U.S.C.

Shadmehr R. (1992) Postural Force Fields of the Human Arm and Their Role in Generating Multi-Joint Movements. Submitted to the *J. Neuroscience*.

Smith A.M. and Humphrey D.R. (1991) What Do Studies of Specific Motor Acts Such as Reaching and Grasping Tell us About the General Principles of Goal-Directed Motor Behavior? In: *Motor Control: Concepts and Issues*, D.R. Humphreys and H.J. Freund, Editors. John Wiley and Sons, Ltd., pp. 357-381.

Storch J. and Gates S. (1989) Motivating Kane's Method for Obtaining Equations of Motion for Dynamic Systems. *J. Guidance and Control* 12(4):593-595.

Valbo A.B. (1973) The Significance of Intramuscular Receptors in Load Compensation During Voluntary Contractions in Man. In: *Control of Posture and Locomotion*, R.B. Stein, K.G. Pearson, R.S. Smith, and J.B. Redford, Editors.

Whitney D. (1977) Force Feedback Control of Manipulator Fine Motions. *J. Dynamic Systems, Measurement, and Control* pp. 91-97.

Wolfram S. (1991) *Mathematica: A System for Doing Mathematics by Computer*. Addison-Wesley Publishing.

Wu C-h., Houk J.C., Young K-Y., and Miller L.E. (1990) Nonlinear Damping of Limb Motion. In: *Multiple Muscle Systems: Biomechanics and Movement Organization*, J.M. Winters and S.L.-Y. Woo, Editors, Springer-Verlag.

Appendix A

Robot System Identification

A simple procedure was used to estimate the inertia parameters of the smaller manipulandum used for the reaching movement experiments. In addition, estimates of the coulomb and viscous friction at each of the joint was also estimated. However, these friction values will not be considered as accurate measures since the bearings were not heavily loaded transversely during the testing. In the actual experiment, the hand of the subject resting on the handle of the robot causes a significant increase in friction within the bearings.

A.1 The Goal

The object of this set of experiments is to determine the three unknown entries of the manipulator's symmetric inertia tensor. Although the manipulator is a semi-direct mechanism with a drive shaft for the elbow joint parallel to the inner link, the model of the manipulator assumed a simple two-link configuration with the parallel drive link lumped with the inertia of the outer link as shown in Figure A.1. This simpler configuration gives us the following equations of motion for the system for a two link robot with absolute joint coordinates or with both joints measured with respect to the base frame.

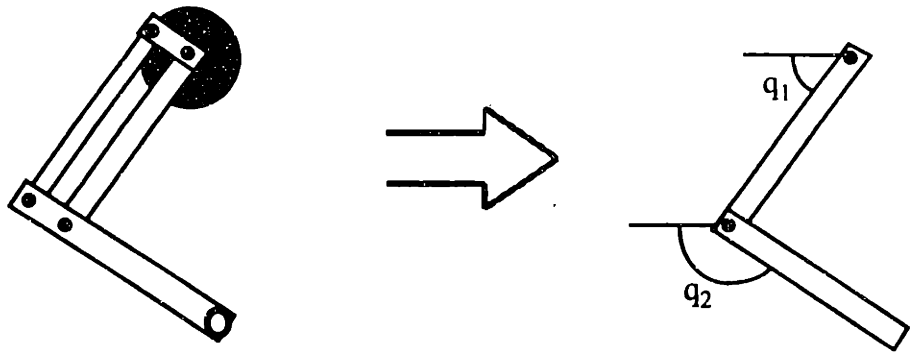

Figure A.1: Modelling assumption of the four-bar linkage configuration of the robot. The robot will be assumed to be a simple two-link mechanism.

$$\tau_1 = H_{11}\ddot{q}_1 + H_{12}\ddot{q}_2 + \frac{\partial H_{12}}{\partial q_2}\dot{q}_2^2 \tag{A.1}$$

$$\tau_2 = H_{12}\ddot{q}_1 + H_{22}\ddot{q}_2 + \frac{\partial H_{12}}{\partial q_1}\dot{q}_1^2 \tag{A.2}$$

where q_1 and q_2 are the shoulder and elbow angles of the robot and H_{ij} are the terms in the 2x2 symmetric positive definite manipulator inertia matrix given by the following.

$$H(\vec{q}) = \begin{bmatrix} H_{11} & H_{12} \\ H_{12} & H_{22} \end{bmatrix} = \begin{bmatrix} m_1 c_1^2 + I_1 + m_2 l_1^2 & m_2 l_1 c_2 \cos(q_2 - q_1) \\ m_2 l_1 c_2 \cos(q_2 - q_1) & m_2 c_2^2 + I_2 \end{bmatrix} \tag{A.3}$$

It is the goal of this appendix to find actual numerical values of the entries of this matrix for the manipulandum.

A.2 The Experiment

A.2.1 The Apparatus

In order to identify the inertia parameters, a simple apparatus was constructed which can convert the linkages of the robot into a simple harmonic oscillator. Essentially, it is a frame by which a set of springs in tensions can be attached to the manipulandum as shown in Figure A.2. This apparatus is used to oscillate a single degree of freedom of the robot. This is done by locking or constraining the other degree of freedom and by placing the line of action of the springs tangentially along the circular path created by the link moving about a single joint.

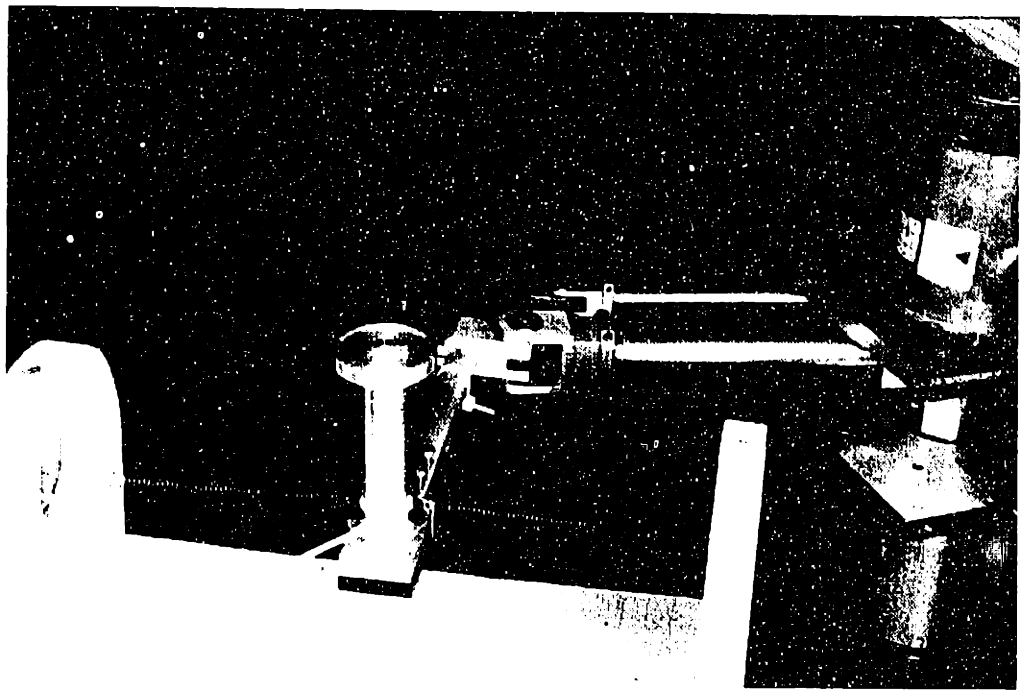

Figure A.2: The system identification hardware where springs are attached to the handle of the robot to provide oscillations about a single degree of freedom.

Figure A.3 shows the force-displacement curves for the springs used in the experiments. Over the displacements imposed within these experiments, the springs are essentially linear with a stiffness of 44 N/m. However, the assumption of a linear spring is not confined to the behavior of the spring itself. The apparatus attempts to use two translational springs in order to simulate a single torsional spring with twice the stiffness about the joint. Obviously large angular displacements will cause large transverse displacements at the handle as shown in Figure A.4 which would make the assumption of a linear torsional spring suspect. Therefore the amplitude of oscillations will be kept below 5 cm away from the equilibrium position.

A.2.2 The Data Collection

The diagonal entries of the inertia matrix are relatively trivial to find through simple oscillations. By locking one joint with the brakes, the oscillations about the free joint will provide enough information about the inertia of one of the diagonal terms. For example, locking the elbow joint reduces the equations of motion to the following.

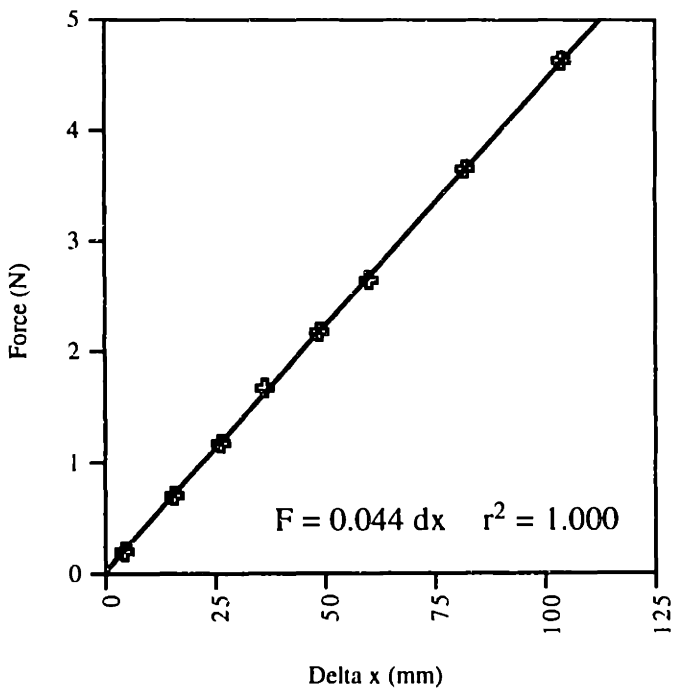

Figure A.3: Force-displacement curve for the spring used in the apparatus. A linear regression is performed to find the best fit stiffness to the data.

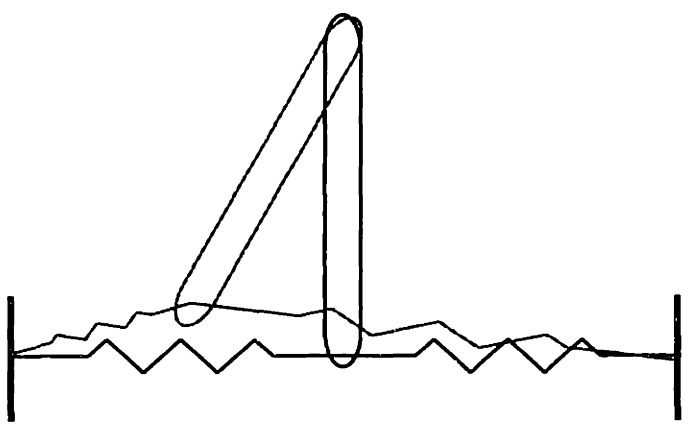

Figure A.4: Assumption of a linear spring. If the rotational displacement is too large, significant transverse displacements will undermine the assumption of a linear conservative stiffness element.

$$\tau_1 = H_{11}\ddot{q}_1 = (m_1 c_1^2 + I_1 + m_2 l_1^2)\,\ddot{q}_1 \tag{A.4}$$

Locking the shoulder joint results in an equation of motion with only the H_{22} inertia in motion.

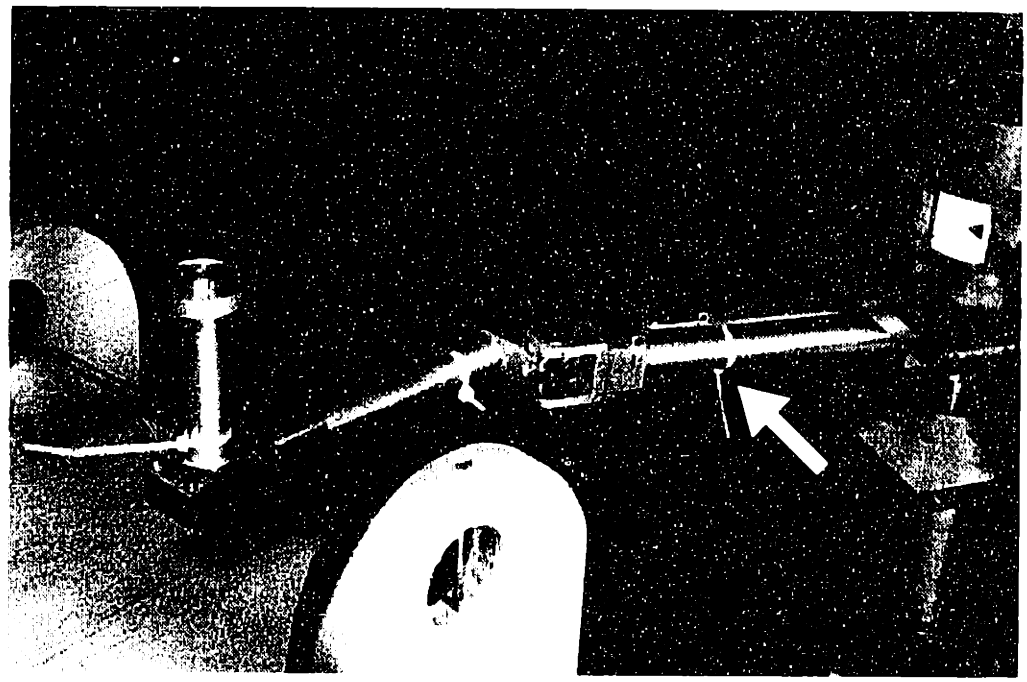

Figure A.5: Locking the outer link relative to the inner link. The plastic tie (indicated by arrow) will keep the relative angle between the inner and outer links at a constant.

$$\tau_2 = H_{22}\ddot{q}_2 = (m_2 c_2^2 + I_2)\ddot{q}_2 \tag{A.5}$$

Less trivial to find is the off-diagonal term of $H(\dot{q})$. This term was found by forcing the relative angle between the outer and inner link to be zero. In other words, the robot is constrained to maintain a zero difference in the elbow angle and the shoulder angle during the oscillations. This effect was attained by unlocking both brakes and by tying the outer link to the inner link as shown in Figure A.5.

The equations of motion can then be reformulated in terms of relative joint coordinates.

$$\tau_1 = H_{11}^{*}\ddot{q}_1 + H_{12}^{*}\ddot{q}_{2r} + h_1\dot{q}_{2r}^2 + h_3\dot{q}_1\dot{q}_{2r} \tag{A.6}$$

$$\tau_2 = H_{12}^{*}\ddot{q}_1 + H_{22}^{*}\ddot{q}_{2r} + h_2\dot{q}_1^2 \tag{A.7}$$

where q_1 is the same angle as before but q_{2r} is now the difference between q_2 and q_1. H_{ij}^{*} and h_k are inertia terms. The new inertia matrix now becomes

$$H^*(\ddot{q}^*) = \begin{bmatrix} H_{11}^* & H_{12}^* \\ H_{12}^* & H_{22}^* \end{bmatrix} = \begin{bmatrix} I_2 + m_1 c_1^2 + I_1 + m_2 (l_1^2 + c_2^2 + 2 l_1 c_2 \cos q_{2r}) & m_2 l_1 c_2 \cos q_{2r} + m_2 c_2^2 + I_2 \\ m_2 l_1 c_2 \cos q_{2r} + m_2 c_2^2 + I_2 & m_2 c_2^2 + I_2 \end{bmatrix} \tag{A.8}$$

In this frame, tying the links together results in setting the $\ddot{q}_{2r}$ and $\dot{q}_{2r}$ terms to zero in the equations of motion of A.6 and A.7. As a result, the equations of motion with the outer link locked in the relative frame reduce to the following.

$$\tau_1 = H_{11}^* \ddot{q}_1 = (m_1 c_1^2 + I_1 + m_2 l_1^2 + m_2 c_2^2 + I_2 + 2 m_2 l_1 c_2 \cos q_{2r}) \ddot{q}_1 \tag{A.9}$$

The inertia H_{11}^* in equation A.9 can be reformulated in terms of the inertia terms of the absolute joint angle system of equation A.3.

$$H_{11}^* = H_{11} + H_{22} + 2 m_2 l_1 c_2 \cos(q_2 - q_1) \tag{A.10}$$

Therefore the coefficient of the cosine term of H_{12} can be found by identifying H_{11}^*, H_{11}, and H_{22} experimentally and then solving the following equation.

$$m_2 l_1 c_2 = \frac{H_{11}^* - (H_{11} + H_{22})}{2 \cos(q_2 - q_1)} \tag{A.11}$$

All three of these trials were performed with the springs attached to handle. In all trials, the springs were situated so that the line of action of the springs were normal to the radius of the circular path. The handle was given an initial displacement and then released. Joint position data was recorded at a 100 Hz by a LSI 11/73 computer.

A.2.3 Data

The data for the three cases are shown in Figure A.6. As can be seen in the plots, the oscillations are essentially second order in nature although they do not show the exponential damping envelope inherent to a simple spring-mass-damper system. Instead, the decay envelope is almost linear which would imply a system dominated by coulomb friction which is not too surprising a finding. Therefore the system identification procedure will assume a simple linear spring, damper, and mass in conjunction with coulomb friction.

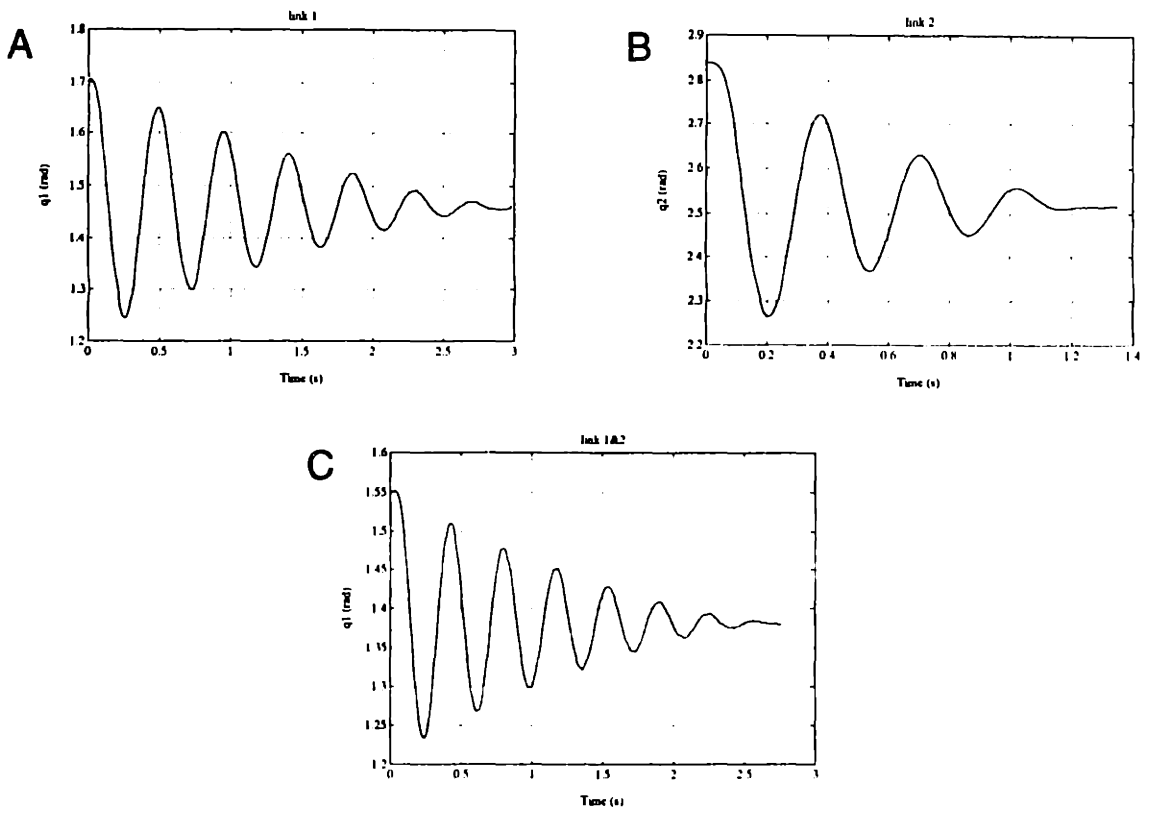

Figure A.6: Measured data for the three cases. (A) Link 1 (elbow joint locked in the absolute frame). (B) Link 2 (shoulder joint locked). (C) Link 1&2 (elbow joint locked in the relative frame).

A.3 A Simple Model

The model used for this analysis is a rotational second order system with coulomb and viscous damping as the resistive losses. The equation of motion for such a system is given as follows.

$$I\ddot{q} + b\dot{q} + kq + F_f \operatorname{sgn}\dot{q} = 0 \tag{A.12}$$

where I, b, and k are the inertia, damping, and stiffness of the system. F_f is the kinetic friction which will be assumed to be a non-zero constant during movement. The kinetic friction can be viewed as a constant bias on the spring force. Setting $\Delta = F_f/k$, the friction can be seen as a bias on the equilibrium length of the spring.

$$I\ddot{q} + b\dot{q} + k(q + \Delta \operatorname{sgn}\dot{q}) = 0 \tag{A.13}$$

or

$$\ddot{q} + 2\zeta\omega_n\dot{q} + \omega_n^2(q + \Delta \operatorname{sgn}\dot{q}) = 0 \tag{A.14}$$

The solution to this second order differential equation is simply the superposition of the viscous damping solution with the coulomb damping solution.

$$q + \Delta \operatorname{sgn}\dot{q} = e^{-\zeta\omega_n t}(A_1 \cos\omega_d t + A_2 \sin\omega_d t) \tag{A.15}$$

Assuming at $t = 0$, the system is at rest at $x = x_o$ and that $\operatorname{sgn}\dot{q} = -1$ since the system is on a downswing, the constants A_1 and A_2 can be solved for.

$$q + \Delta \operatorname{sgn}\dot{q} = e^{-\zeta\omega_n t}(x_o - \Delta)\left(\cos\omega_d t + \frac{\zeta}{\sqrt{1-\zeta^2}}\sin\omega_d t\right) \tag{A.16}$$

Knowing that a maxima or minima occurs at time t_n where

$$t_n = \frac{n\pi}{\omega_d} \tag{A.17}$$

and letting $\delta = e^{-\zeta\omega_n t}$, it is trivial to show that the maximum and minimum displacements can be found by the following series expansion [Jacobson and Ayre 1958].

$$x_n = \mp\delta^n(x_o - \Delta) \pm 2\Delta(\delta^{n-1} + \delta^{n-2} + \ldots + \delta) \pm \Delta \tag{A.18}$$

where the upper sign is taken if n is an odd integer and the lower sign if n is an even integer. Therefore when n is odd, the displacement will be a minima and vice-versa.

The viscous damping exponential δ and the friction length Δ can be found by measuring the values of x_o, x_1, and x_2 from the experimental data. Taking the two forms of equation A.18 which give the x_1 and x_2 values and solving simultaneously will numerical values for δ and Δ. A check can be performed by taking the values found, calculating the x_3 displacement, and comparing to the experimental data. From the damping ratio ζ, the natural frequency can be found from the measured ω_d. Coulomb friction does not affect frequency.

$$\omega_n = \frac{\omega_d}{\sqrt{1-\zeta^2}} \tag{A.19}$$

And finally from the natural frequency, the inertia can be calculated with knowledge of the system stiffness.

$$I = \frac{k}{\omega_n^2} \tag{A.20}$$

A.4 Simulations

The previous analysis supplies estimates of the coulomb friction, the damping ratio, and the inertia of the system from the measured data and from the stiffnesses of the attached springs. In order to verify and to further tune these values, a simulation of the one degree of freedom system was created in Matlab. The values of Δ and ζ were adjusted from the predicted values to improve the correspondence between the simulation result and the experimental results.

A.4.1 Simulation Results

The final results of the system identification are presented in this final subsection. As it turns out, the best method of finding parameters is through the simulations. The analysis of Section A.3 provides only a gross approximation of the parameters. The estimates from the model can be as much as 50 to 75% off of the values found from the simulations. Therefore, further tuning through simulations was always required.

The damped natural frequency is measured from the actual data. The object of the simulations is then to tune the values the resistive parameters, Δ and ζ, in order to match the simulations in both the number of swings as well as the amount of attenuation in amplitude at each swing.

Link1 (H11)

Link 1 is the inertia of the manipulandum when the elbow joint has been locked in the absolute frame. The experimental data showed a damped natural frequency of 13.7 rad/sec. The best fit set of parameters were as follows.

$$\Delta = 0.005 \text{ rad} \tag{A.21}$$

$$\zeta = 0.03 \tag{A.22}$$

Figure A.7 displays the results of the simulation superimposed over the experimental results. Note that at the beginning of the oscillations the correspondence is excellent between the simulation and the actual. However further along in time, the simulation begins to disagree in frequency and slightly in amplitude. This phenomenon is definitely due to the nonlinear affects such as stiction or coulomb friction on the system. However, the overall corre-

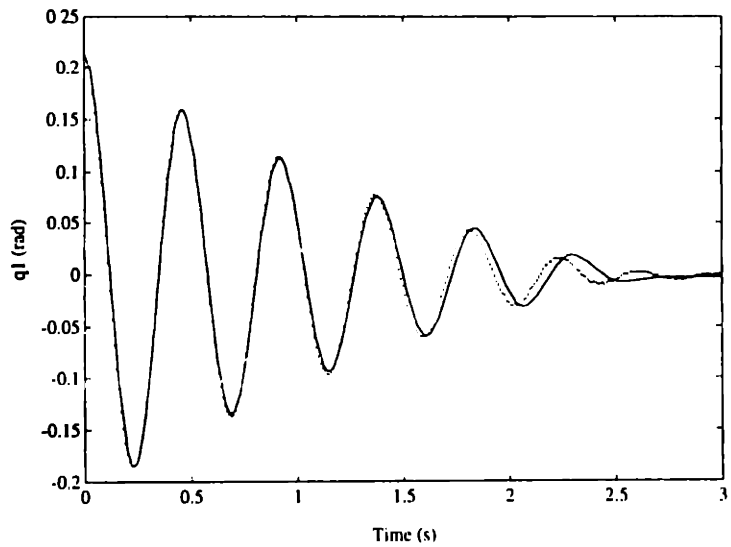

Figure A.7: Simulated versus actual data for link1. Dotted line is the actual data. Solid line is the simulation result.

spondence is satisfactory to predict the inertia within an acceptable degree of error. Since the damping was small, the natural frequency ω_n was about 13.7 rad/sec. The predicted inertia is then

$$H_{11} = 0.026 \text{ kg m}^2 \tag{A.23}$$

Link 2 (H22)

Link 2 is the inertia of just the outer link when the shoulder joint is locked. The measured data showed a damped natural frequency of 18.9 rad/sec. The best fit set of parameters were as follows.

$$\Delta = 0.014 \text{ rad} \tag{A.24}$$

$$\zeta = 0.036 \tag{A.25}$$

Figure A.8 shows the results of this simulation. In this case, the correspondence between simulated and actual is excellent throughout the swings. Small discrepancies do exist near the end of the oscillations, but overall the fit is more than satisfactory. The predicted inertia from the estimated natural frequency of 18.85 rad/sec is shown below.

$$H_{22} = 0.0094 \text{ kg m}^2 \tag{A.26}$$

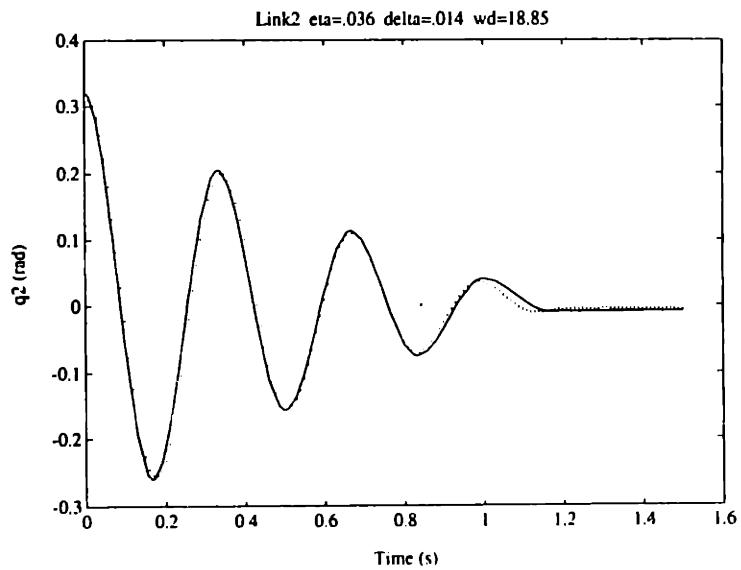

Figure A.8: Simulation versus actual data for link 2. The dotted line is the measured data while the solid line represents the simulation.

Link 1 and 2 (H12)

The inner and outer links were tied together so that they a constant relative angle of 0.362 rad exists between the two links. The measured damped natural frequency of this oscillation was approximately 16.9 rad/sec. The best fit resistive values were as follows.

$$\Delta = 0.003 \text{ rad} \tag{A.27}$$

$$\zeta = 0.03 \tag{A.28}$$

Figure A.9 shows the result of the simulation with these parameters. Overall correspondence is excellent with some discrepancies at the termination of the oscillations. The inertia of this system is the first entry of the inertia matrix in equation A.8.

$$H_{11}^{*} = H_{11} + H_{22} + 2m_2 l_1 c_2 \cos(q_2 - q_1) = 0.054 \text{ kg m}^2 \tag{A.29}$$

Knowing the difference in q_1 and q_2 to be 0.362 rad to solve for the configuration independent term of H_{12} $(m_2 l_1 c_2)$, we find

$$m_2 l_1 c_2 = 0.01 \text{ kg m}^2 \tag{A.30}$$

A.4.2 Summary

Therefore the estimated inertia matrix $H(\hat{q})$ is

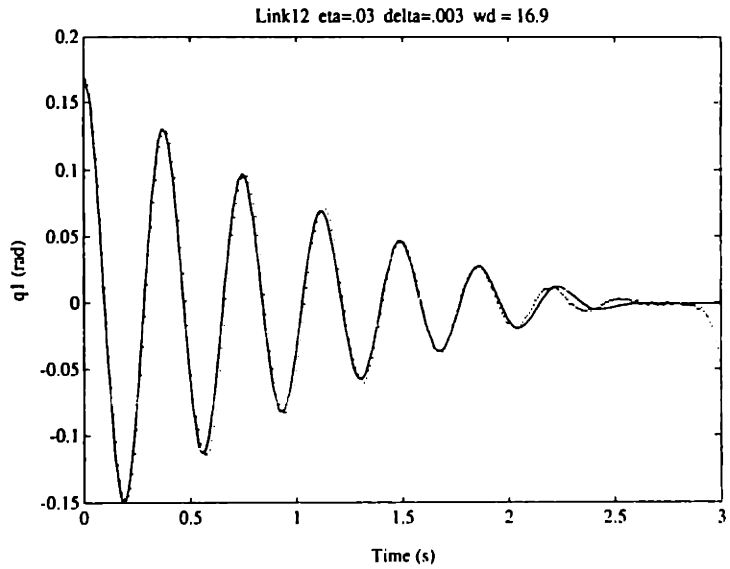

Figure A.9: Simulated versus actual for links 1 and 2 tied relative to one another. The dotted line is the measured data. The solid line is the result of the simulation.

$$H(\dot{\hat{q}}) = \begin{bmatrix} 0.026 & 0.01\cos(q_2 - q_1) \\ 0.01\cos(q_2 - q_1) & 0.0094 \end{bmatrix} \tag{A.31}$$

Appendix B

Movement Data

This appendix presents the hand paths and evoked force vectors for all of the subjects in all of the recorded trials.

B.1 Subject A

Right Handed Male

Forearm length = 32 cm.

Upper Arm length = 30 cm.

Weight = 145 lbs

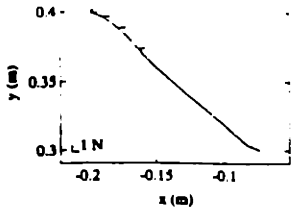
1 N
y (m)
x (m)

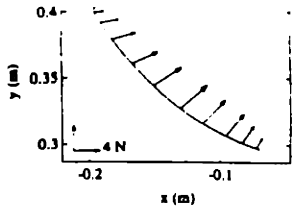
4 N
y (m)
x (m)

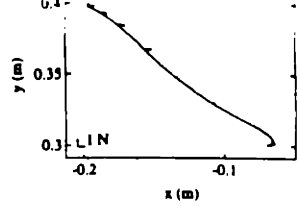
1 N
y (m)
x (m)

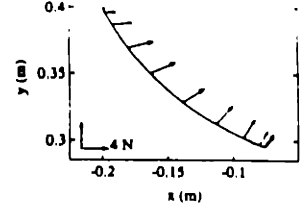
4 N
y (m)
x (m)

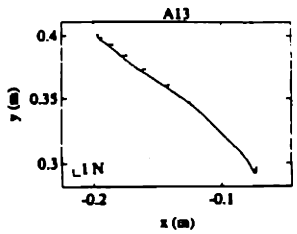
A13
1 N
y (m)
x (m)

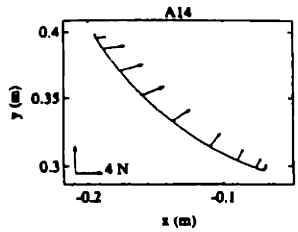
A14
4 N
y (m)
x (m)

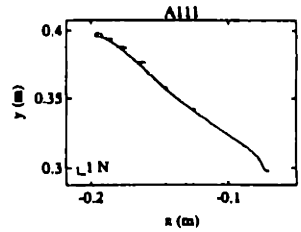
A111
1 N
y (m)
x (m)

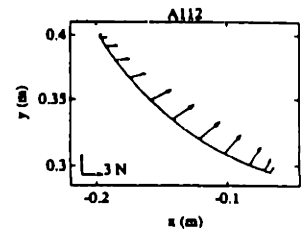
A112
3 N
y (m)
x (m)

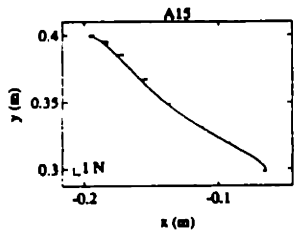
A15
1 N
y (m)
x (m)

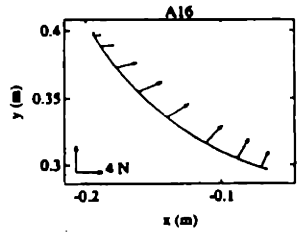
A16
4 N
y (m)
x (m)

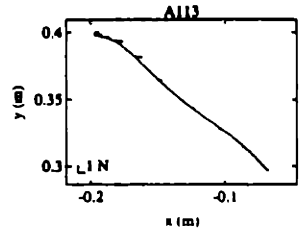
A113
1 N
y (m)
x (m)

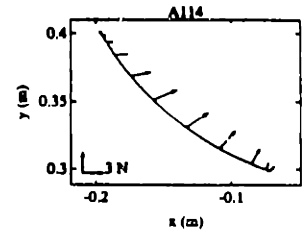
A114
3 N
y (m)
x (m)

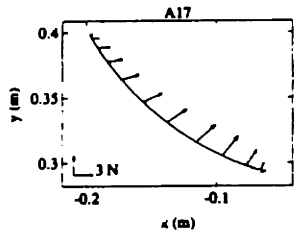
A17
3 N
y (m)
x (m)

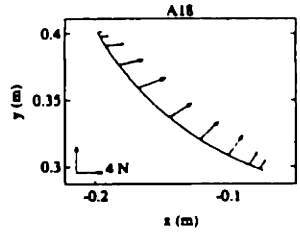
A18
4 N
y (m)
x (m)

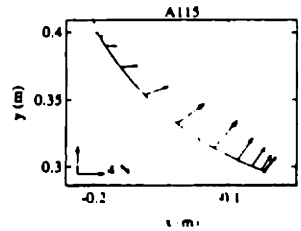
A115
y (m)

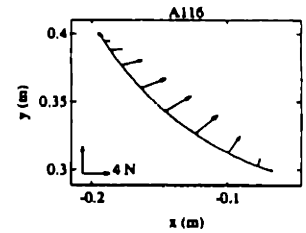
A116
4 N
y (m)
x (m)

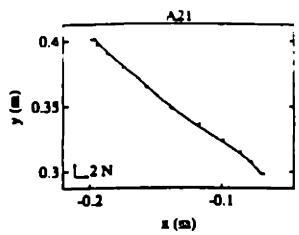
A21
2 N
y (m)
x (m)

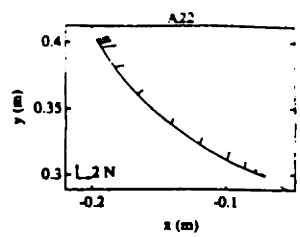
A22
2 N
y (m)
x (m)

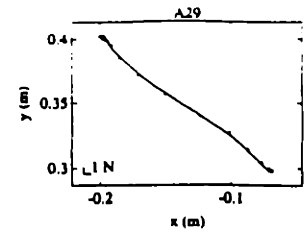
A29
1 N
y (m)
x (m)

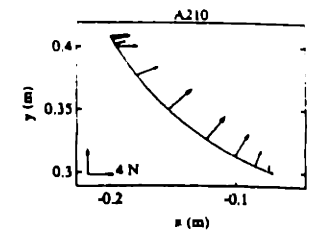
A210
4 N
y (m)
x (m)

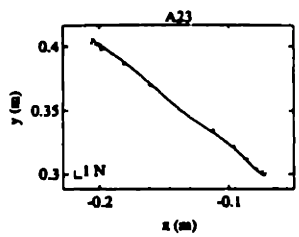
A23
1 N
y (m)
x (m)

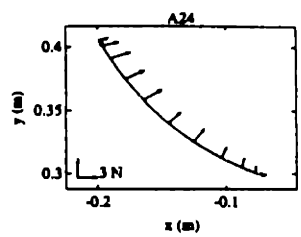
A24
3 N
y (m)
x (m)

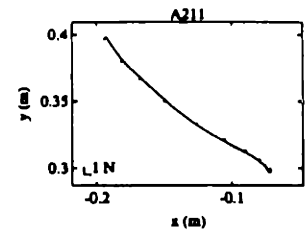
A211
1 N
y (m)
x (m)

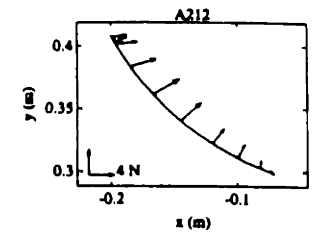
A212
4 N
y (m)
x (m)

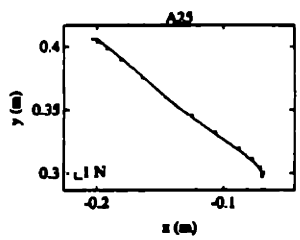
A25
1 N
y (m)
x (m)

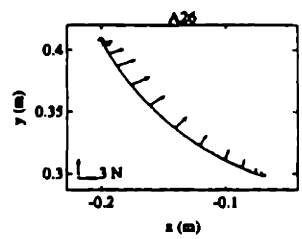
A26
3 N
y (m)
x (m)

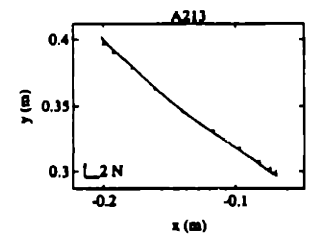
A213
2 N
y (m)
x (m)

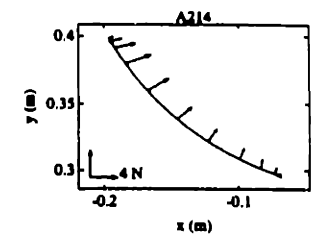
A214
4 N
y (m)
x (m)

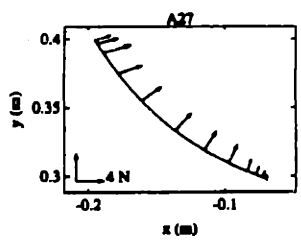
A27
4 N
y (m)
x (m)

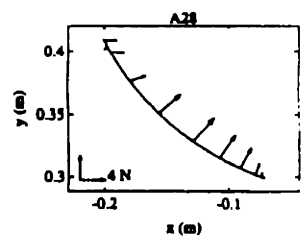
A28
4 N
y (m)
x (m)

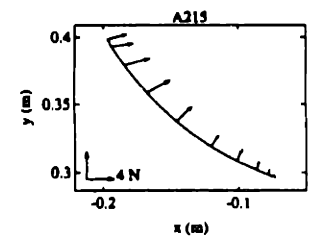
A215
4 N
y (m)
x (m)

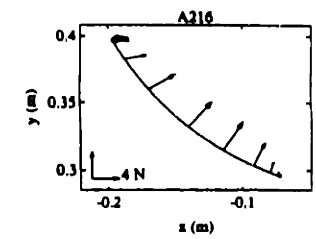
A216
4 N
y (m)
x (m)

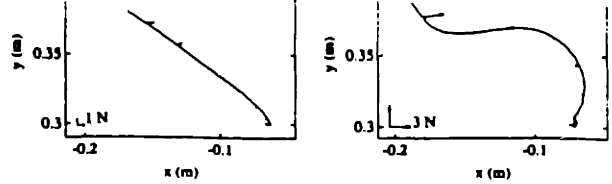
y (m)
0.35
0.3
1 N
-0.2
-0.1
x (m)
3 N

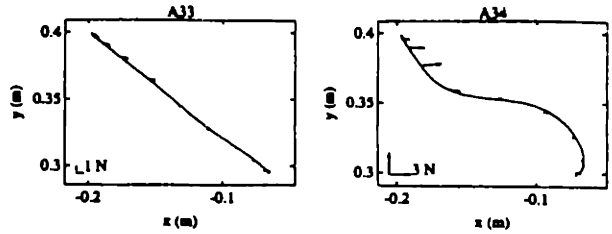
A33
A34
0.4
0.35
0.3
y (m)
1 N
3 N
-0.2
-0.1
x (m)

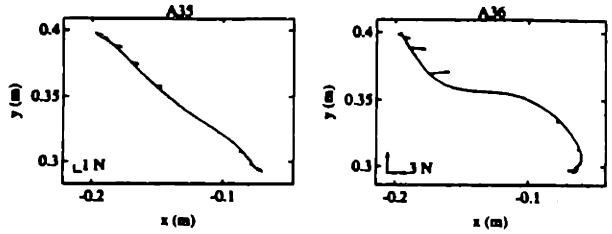
A35
A36
0.4
0.35
0.3
y (m)
1 N
3 N
-0.2
-0.1
x (m)

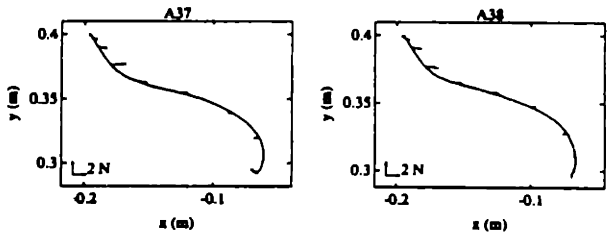
A37
A38
0.4
0.35
0.3
y (m)
2 N
2 N
-0.2
-0.1
x (m)

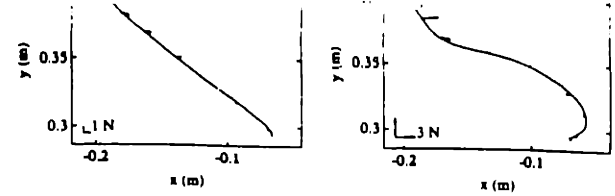
0.35
0.3
y (m)
1 N
3 N
-0.2
-0.1
x (m)

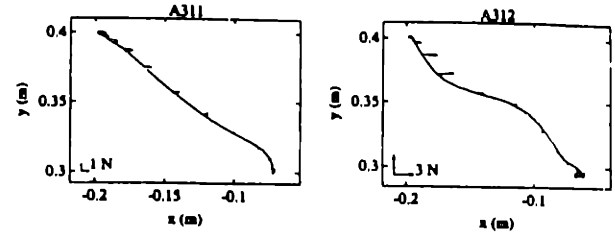
A311
A312
0.4
0.35
0.3
y (m)
1 N
3 N
-0.2
-0.15
-0.1
x (m)

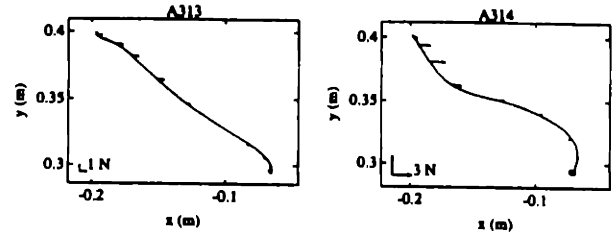
A313
A314
0.4
0.35
0.3
y (m)
1 N
3 N
-0.2
-0.1
x (m)

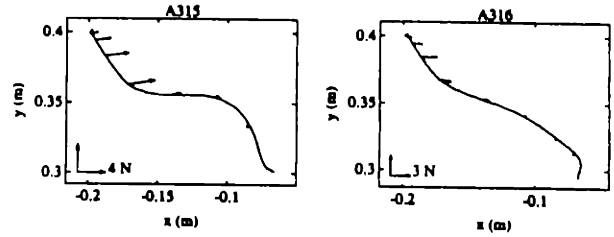
A315
A316
0.4
0.35
0.3
y (m)
4 N
3 N
-0.2
-0.15
-0.1
x (m)

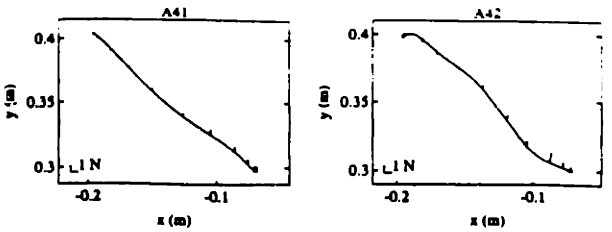
A41
A42
0.4
0.35
0.3
y (m)
1 N
1 N
-0.2
-0.1
x (m)

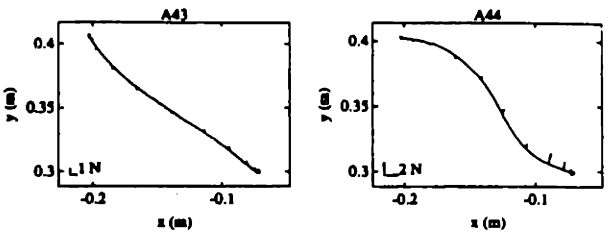
A43
A44
0.4
0.35
0.3
y (m)
1 N
2 N
-0.2
-0.1
x (m)

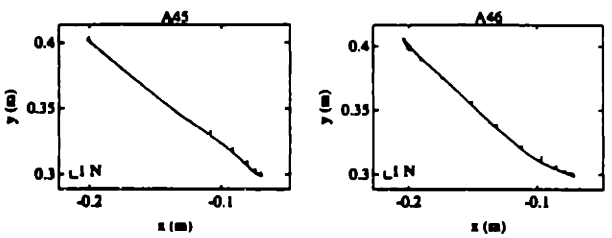
A45
A46
0.4
0.35
0.3
y (m)
1 N
1 N
-0.2
-0.1
x (m)

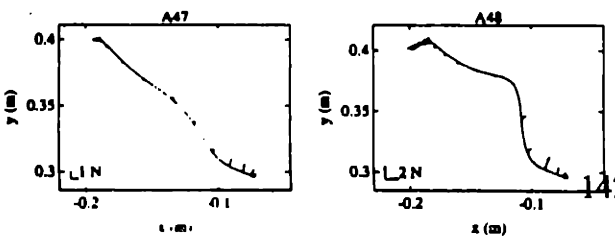
A47
A48
0.4
0.35
0.3
y (m)
1 N
2 N
-0.2
-0.1
x (m)

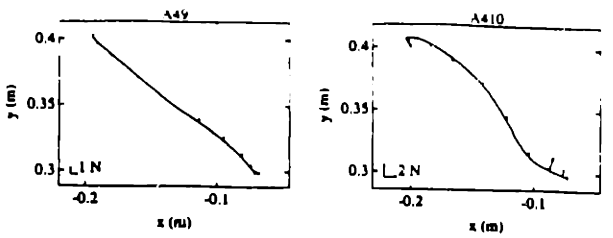
A49
A410
0.4
0.35
0.3
y (m)
1 N
2 N
-0.2
-0.1
x (m)

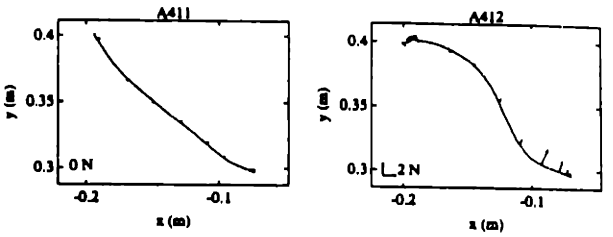
A411
A412
0.4
0.35
0.3
y (m)
0 N
2 N
-0.2
-0.1
x (m)

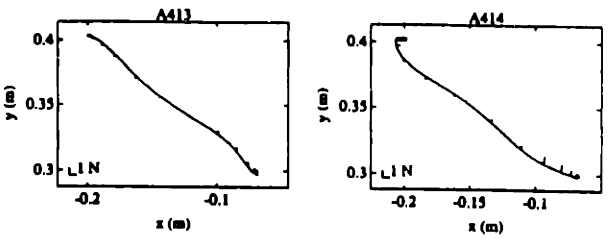
A413
A414
0.4
0.35
0.3
y (m)
1 N
1 N
-0.2
-0.15
-0.1
x (m)

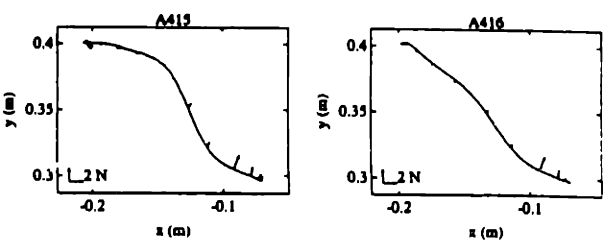
A415
A416
0.4
0.35
0.3
y (m)
2 N
2 N
-0.2
-0.1
x (m)

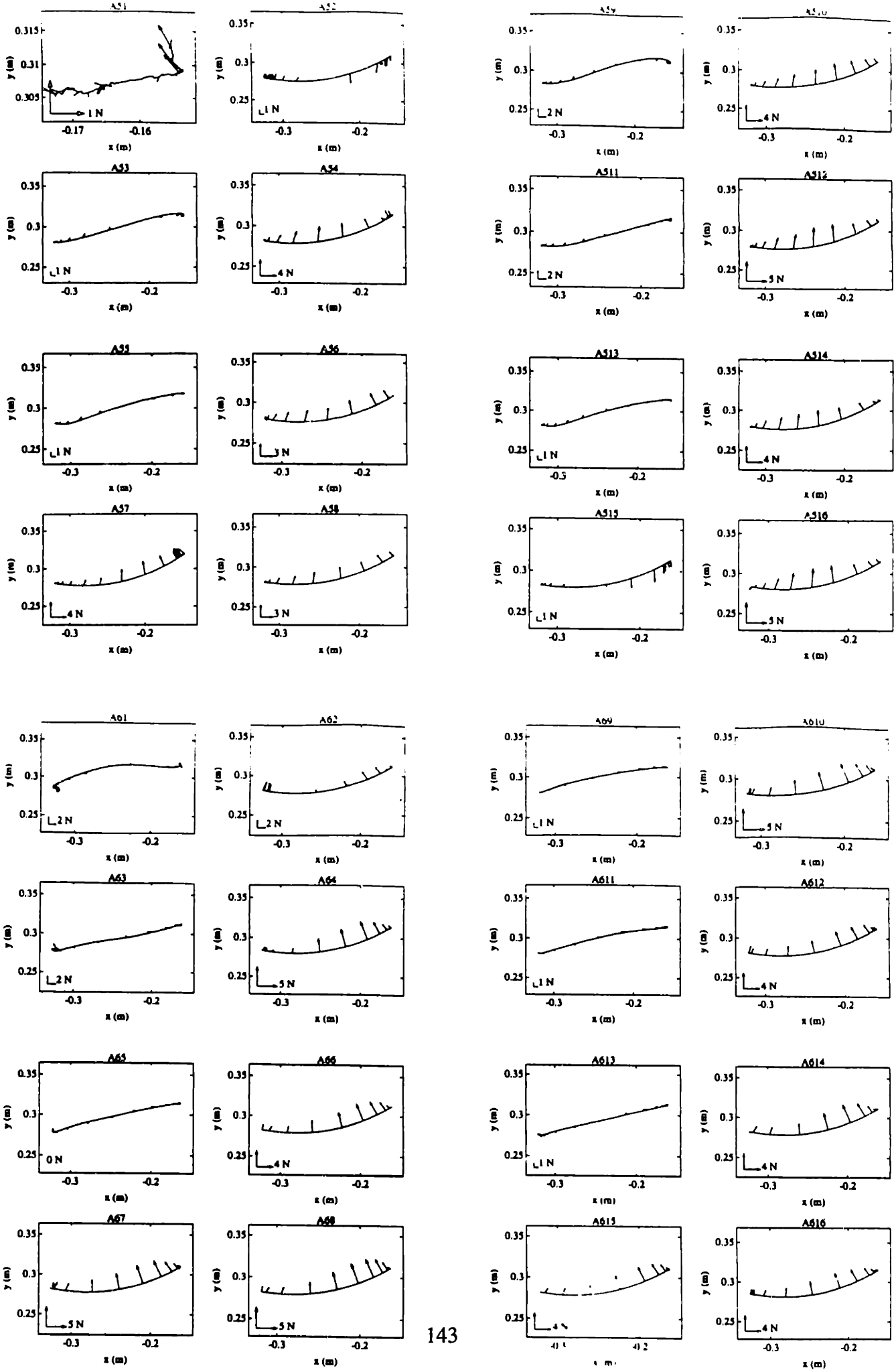
A51
A52
A59
A510
A53
A54
A511
A512
A55
A56
A513
A514
A57
A58
A515
A516
A61
A62
A69
A610
A63
A64
A611
A612
A65
A66
A613
A614
A67
A68
A615
A616
y (m)
x (m)
1 N
2 N
3 N
4 N
5 N
0 N

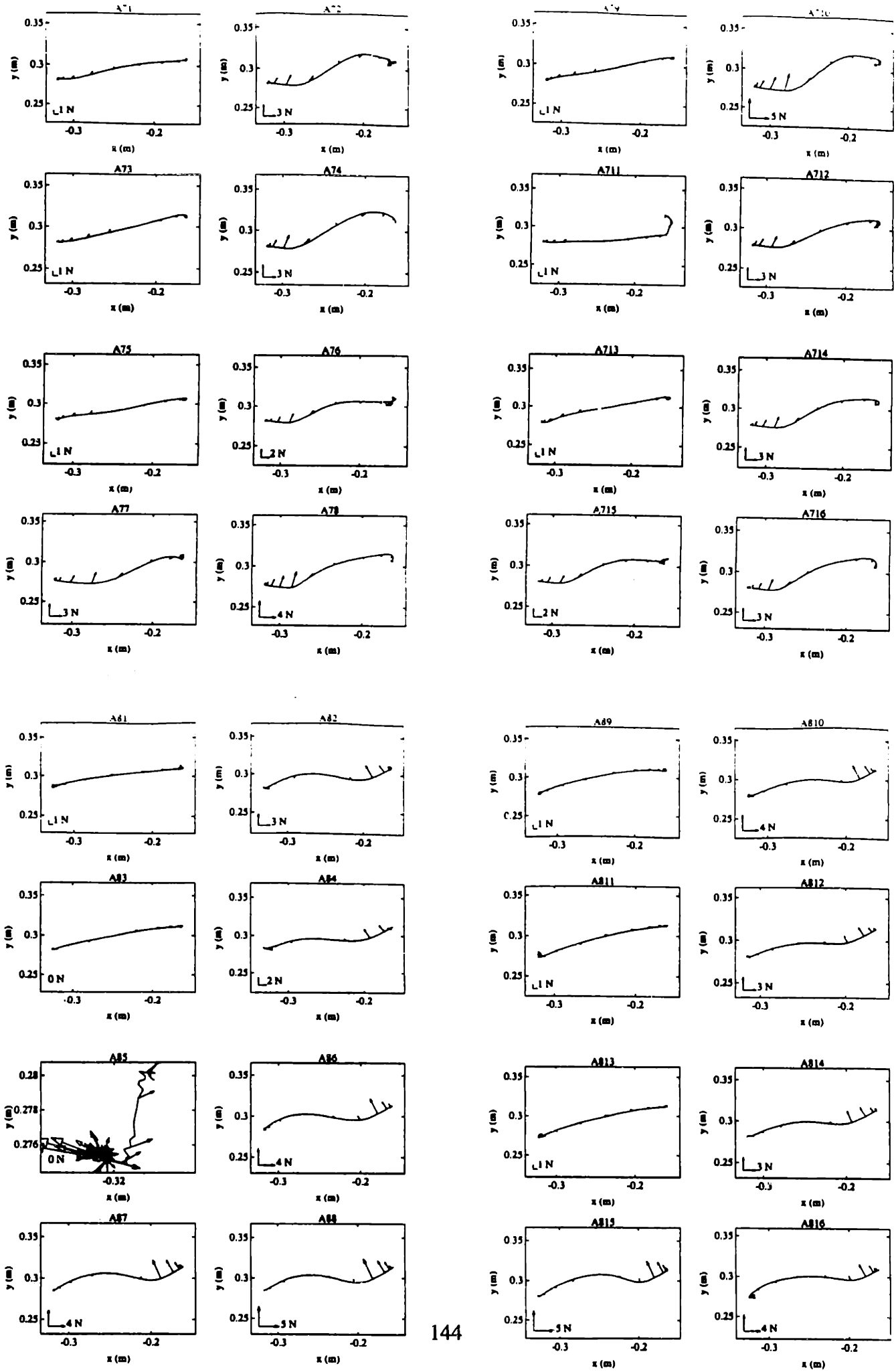
A71
A72
A79
A710
A73
A74
A711
A712
A75
A76
A713
A714
A77
A78
A715
A716
A81
A82
A89
A810
A83
A84
A811
A812
A85
A86
A813
A814
A87
A88
A815
A816
y (m)
x (m)
1 N
3 N
5 N
2 N
4 N
0 N

No Dam

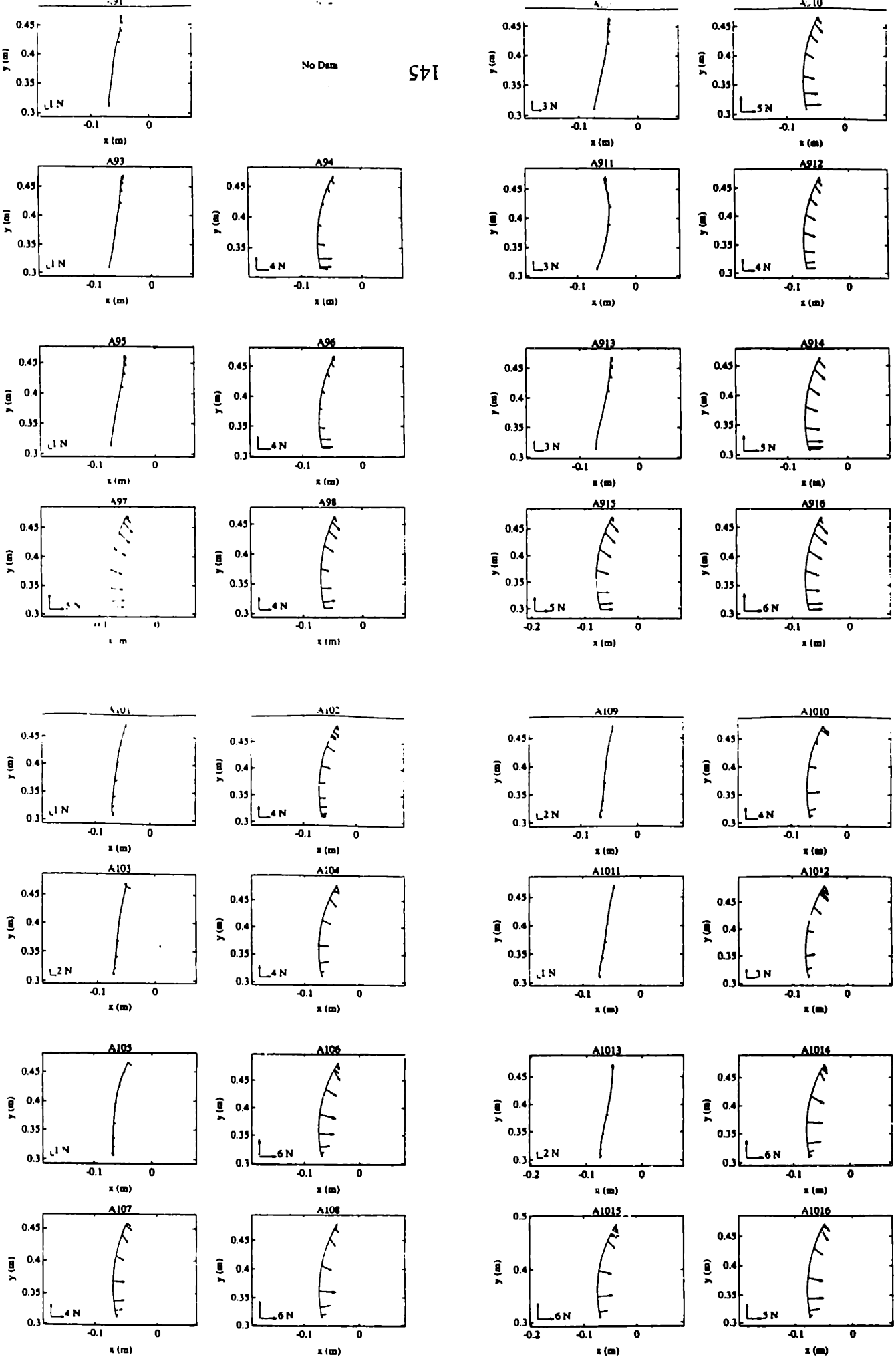
A91
A92
A93
A94
A95
A96
A97
A98
A101
A102
A103
A104
A105
A106
A107
A108
A910
A911
A912
A913
A914
A915
A916
A109
A1010
A1011
A1012
A1013
A1014
A1015
A1016
y (m)
x (m)
1 N
2 N
3 N
4 N
5 N
6 N

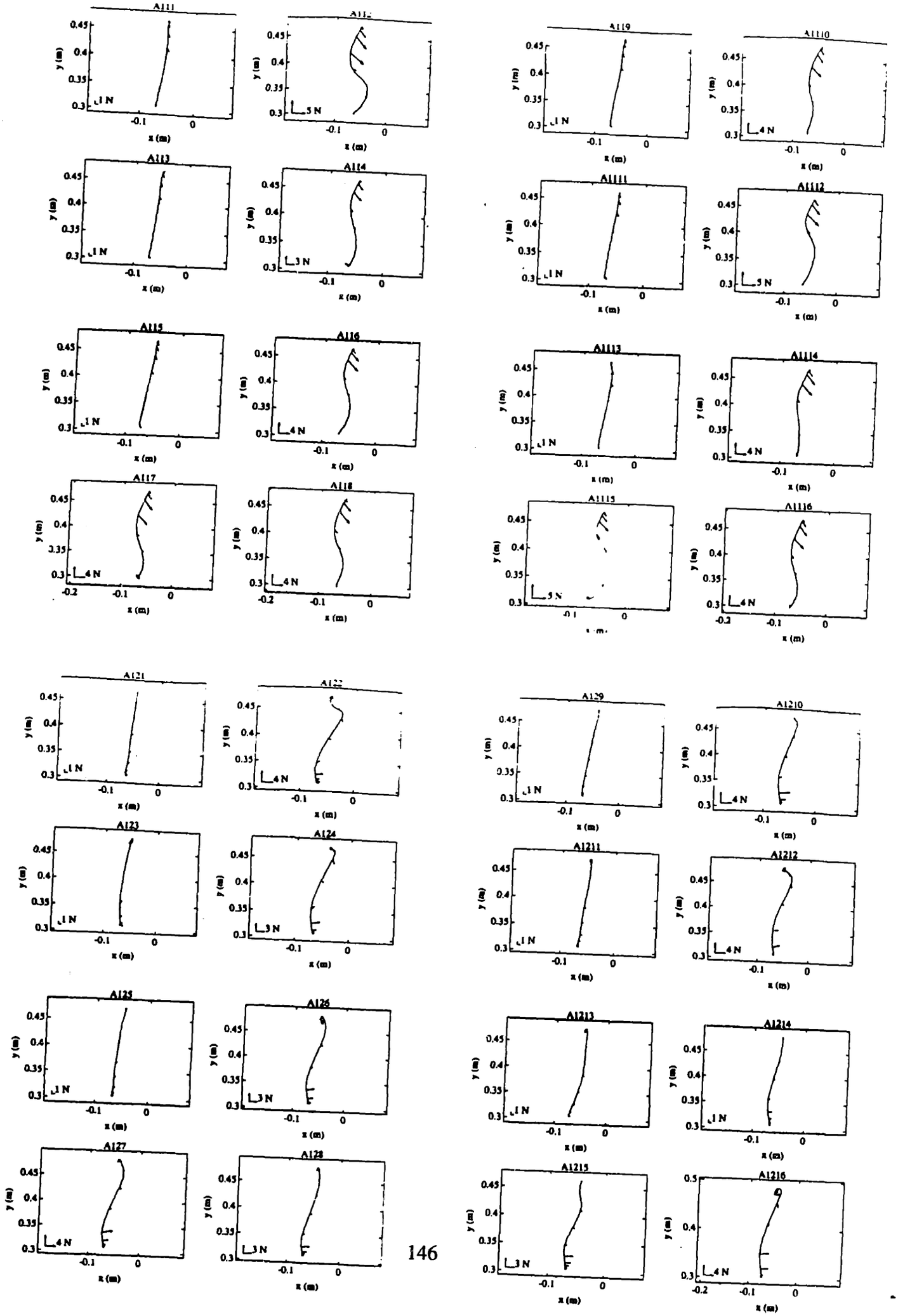
A111
A112
A113
A114
A115
A116
A117
A118
A119
A1110
A1111
A1112
A1113
A1114
A1115
A1116
A121
A122
A123
A124
A125
A126
A127
A128
A129
A1210
A1211
A1212
A1213
A1214
A1215
A1216
y (m)
x (m)
1 N
5 N
4 N
3 N

B.2 Subject B

Right Handed Male

Forearm length = 32.5 cm

Upper Arm length = 31 cm

Weight = 180 lbs

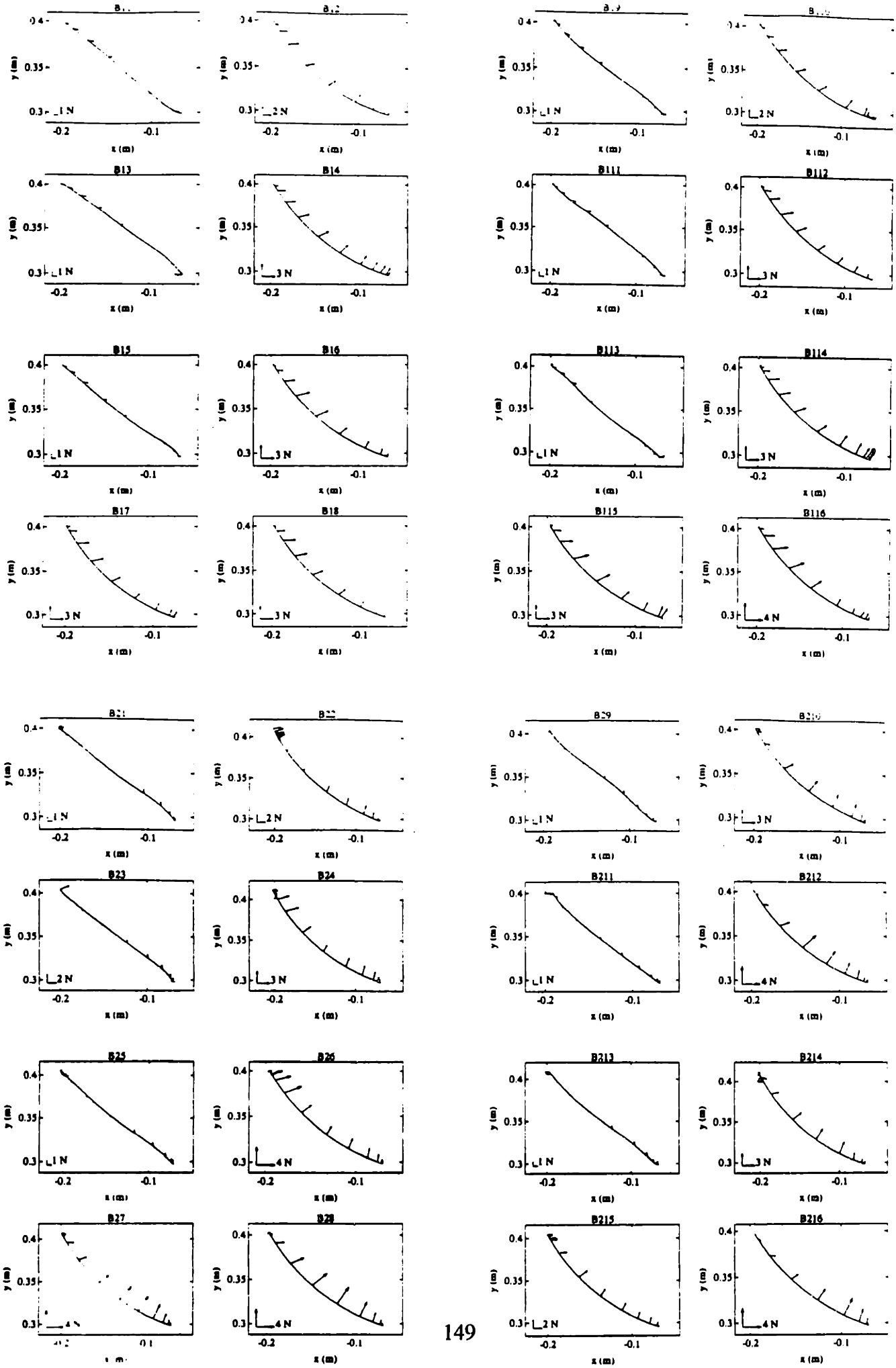
B13
B14
B111
B112
B15
B16
B113
B114
B17
B18
B115
B116
B23
B24
B211
B212
B25
B26
B213
B214
B27
B28
B215
B216
y (m)
x (m)
0.4
0.35
0.3
-0.2
-0.1
1 N
2 N
3 N
4 N

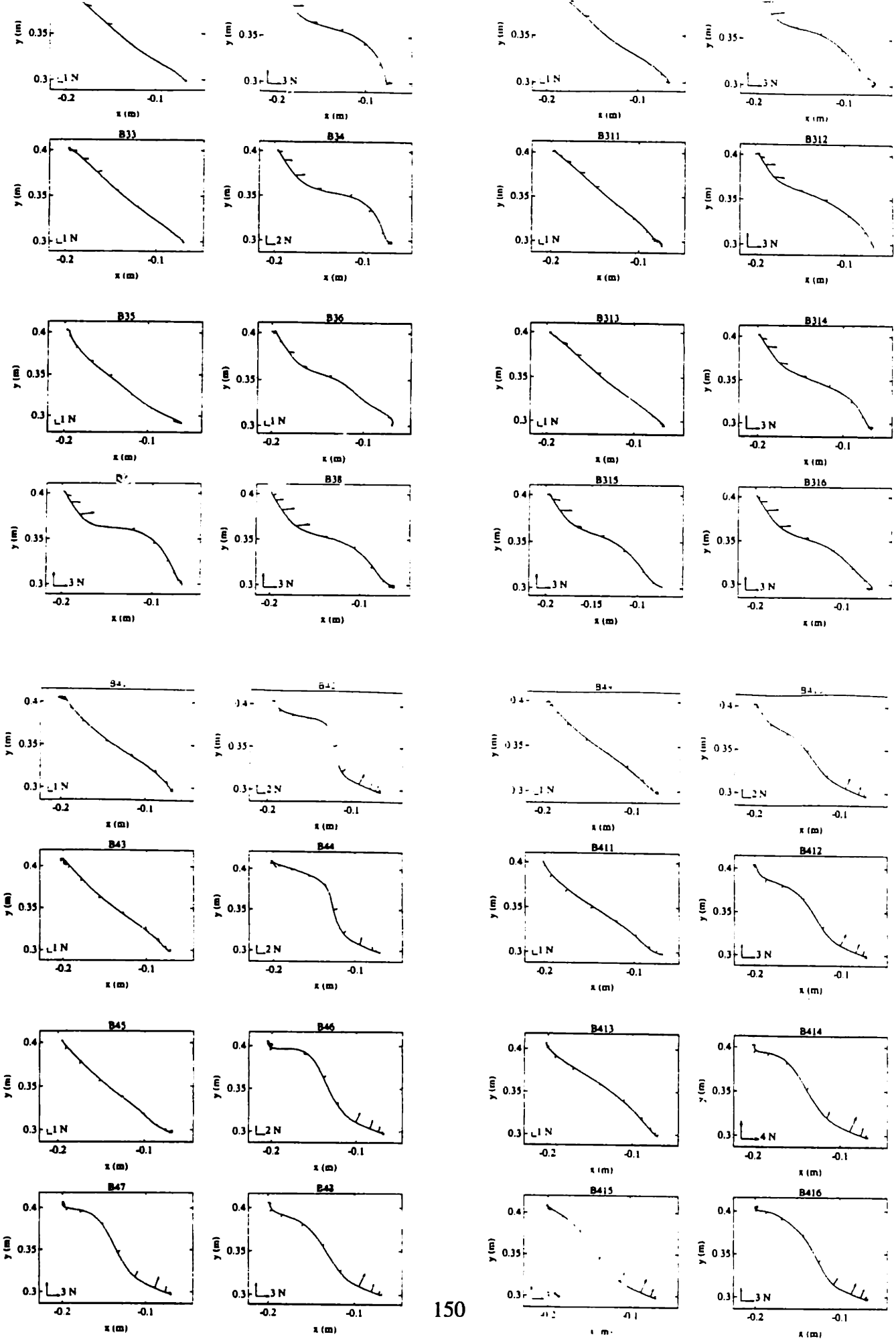
B33
B34
B311
B312
B35
B36
B313
B314
B38
B315
B316
B43
B44
B411
B412
B45
B46
B413
B414
B47
B48
B415
B416
y (m)
x (m)
1 N
2 N
3 N
4 N

No Data

No Data

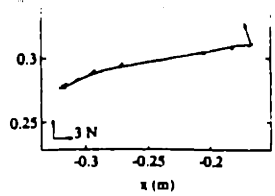

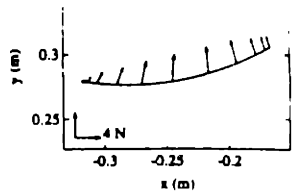

No Data

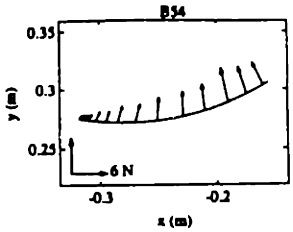

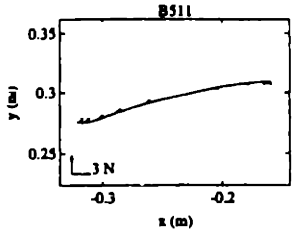

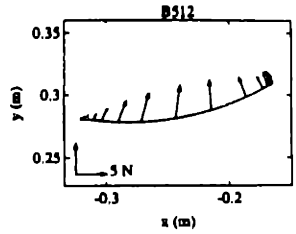

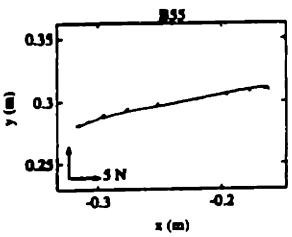

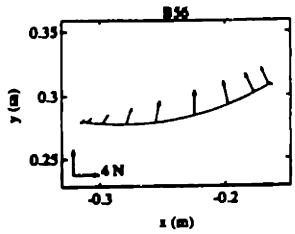

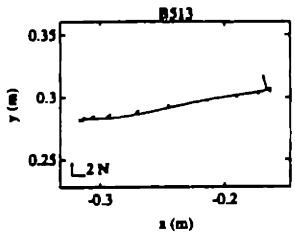

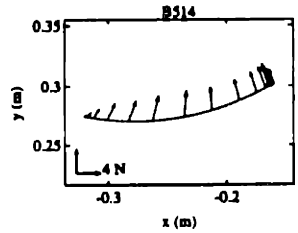

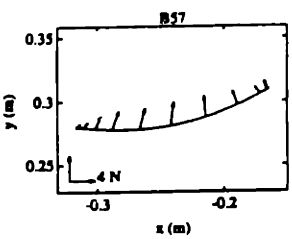

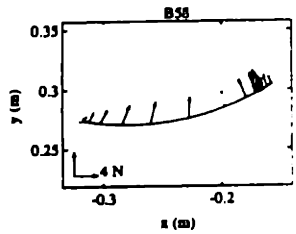

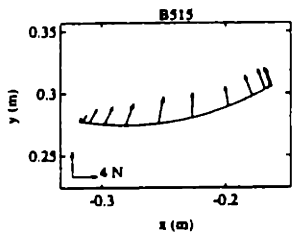

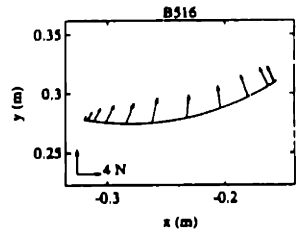

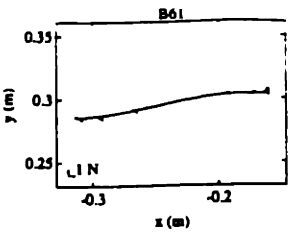

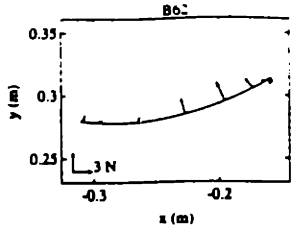

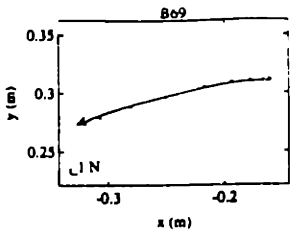

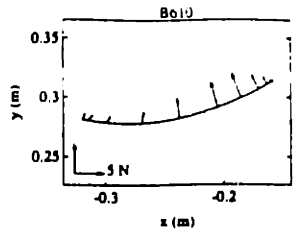

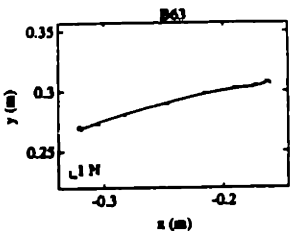

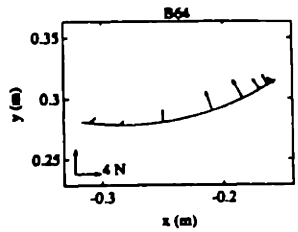

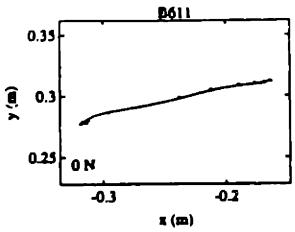

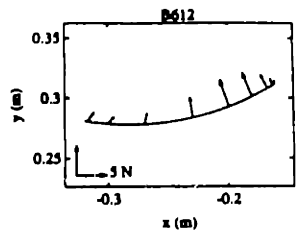

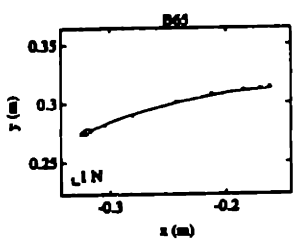

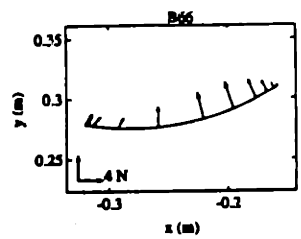

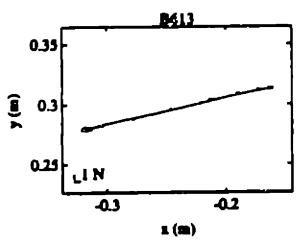

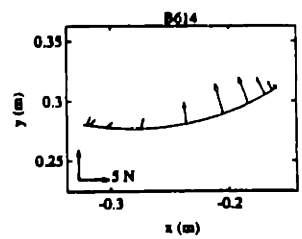

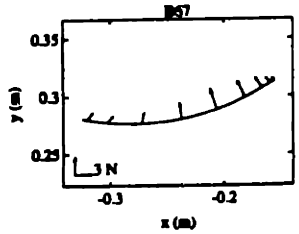

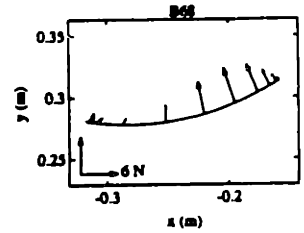

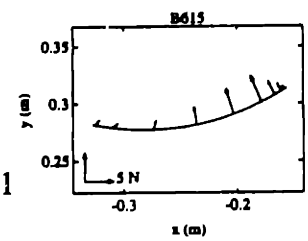

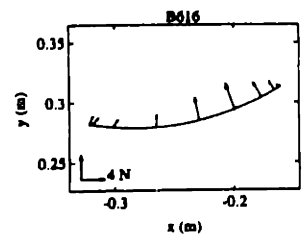

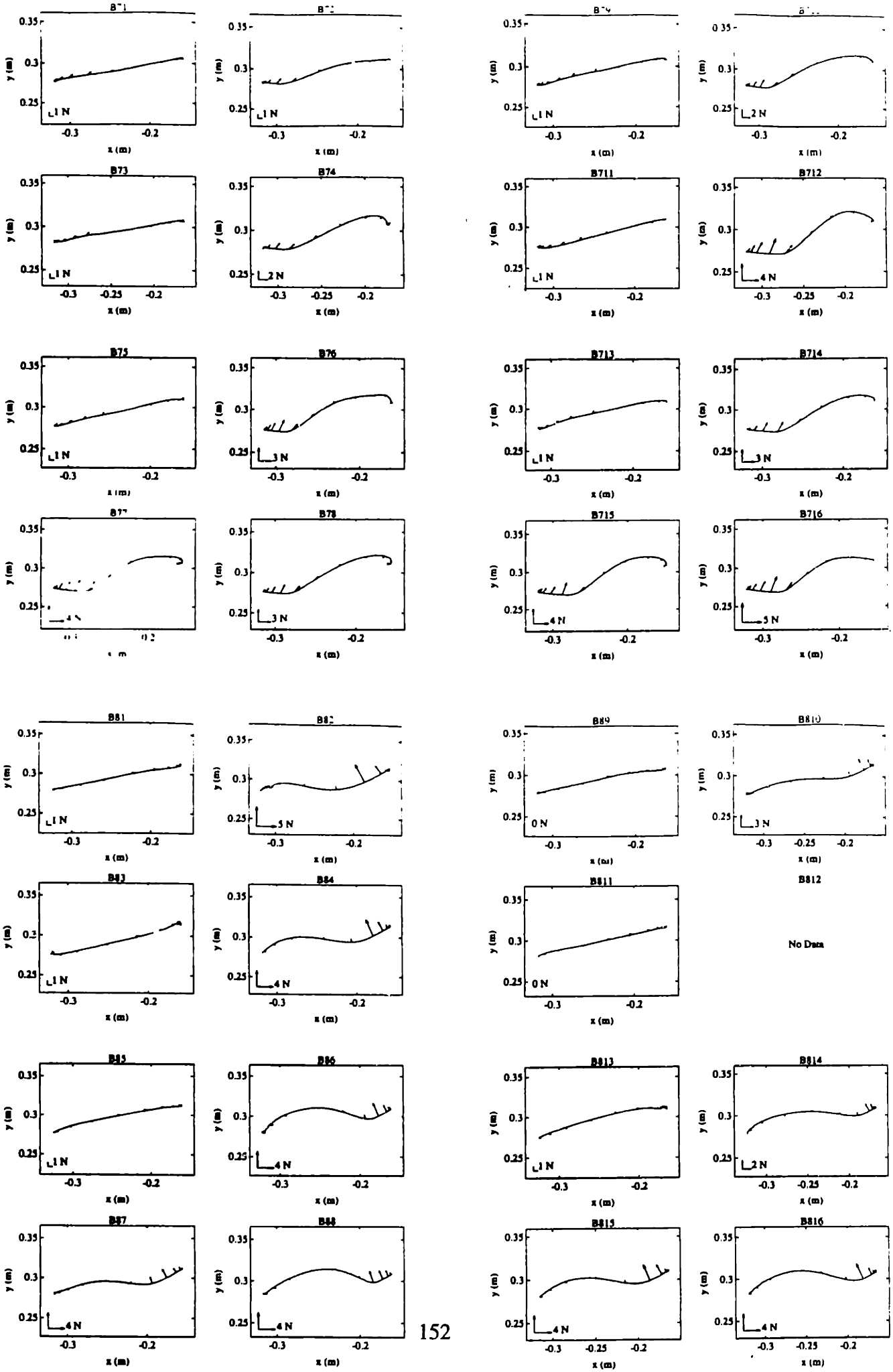
B73
B74
B711
B712
B75
B76
B713
B714
B78
B715
B716
B81
B82
B89
B810
B83
B84
B811
B812
No Data
B85
B86
B813
B814
B87
B88
B815
B816
y (m)
x (m)
1 N
2 N
3 N
4 N
5 N
0 N

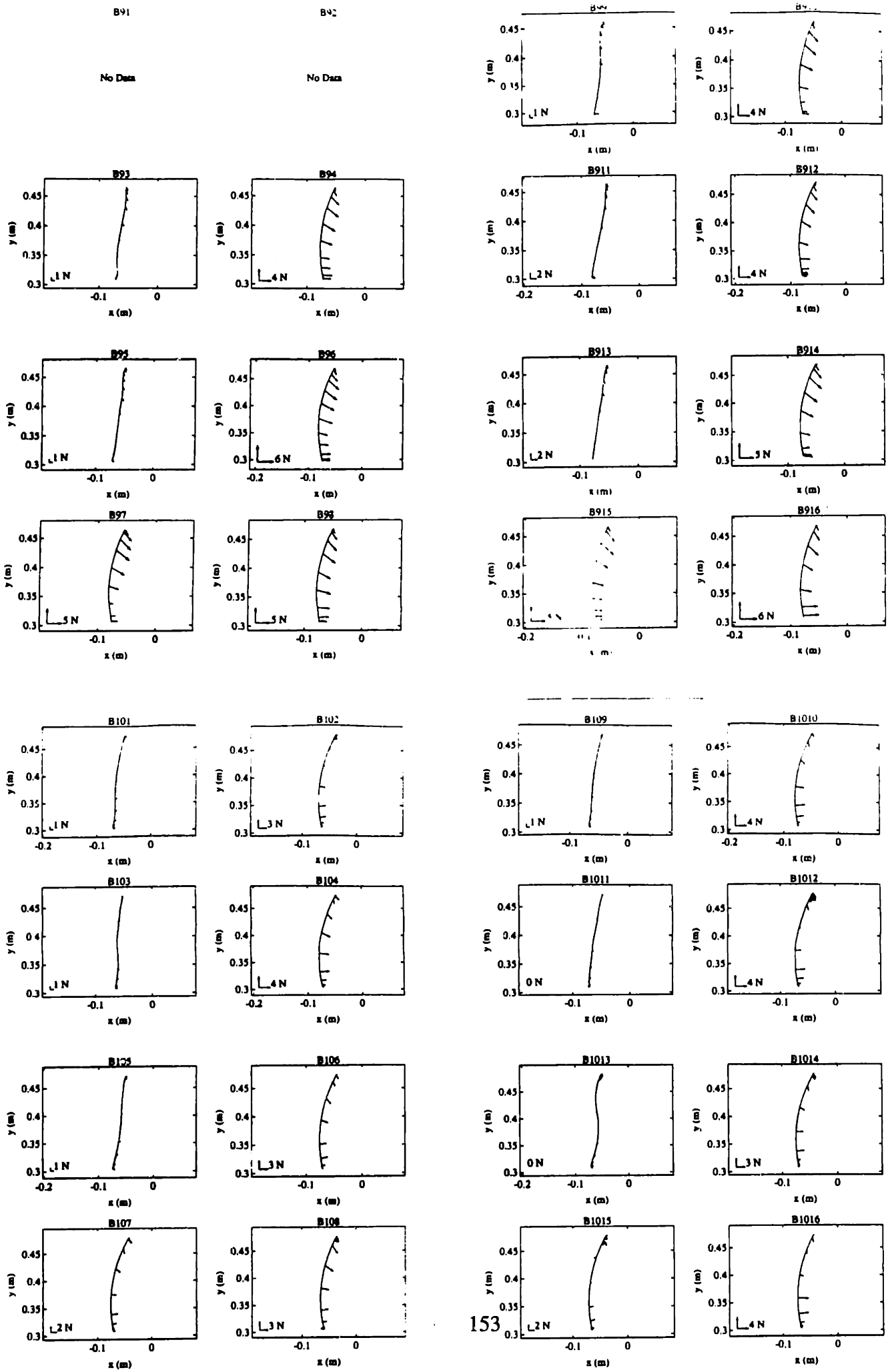
B91
No Data
B92
No Data
B93
1 N
B94
4 N
B95
1 N
B96
6 N
B97
5 N
B98
5 N
B101
1 N
B102
3 N
B103
1 N
B104
4 N
B105
1 N
B106
3 N
B107
2 N
B108
3 N
B911
2 N
B912
4 N
B913
2 N
B914
5 N
B915
B916
6 N
B109
1 N
B1010
4 N
B1011
0 N
B1012
4 N
B1013
0 N
B1014
3 N
B1015
2 N
B1016
4 N
y (m)
x (m)

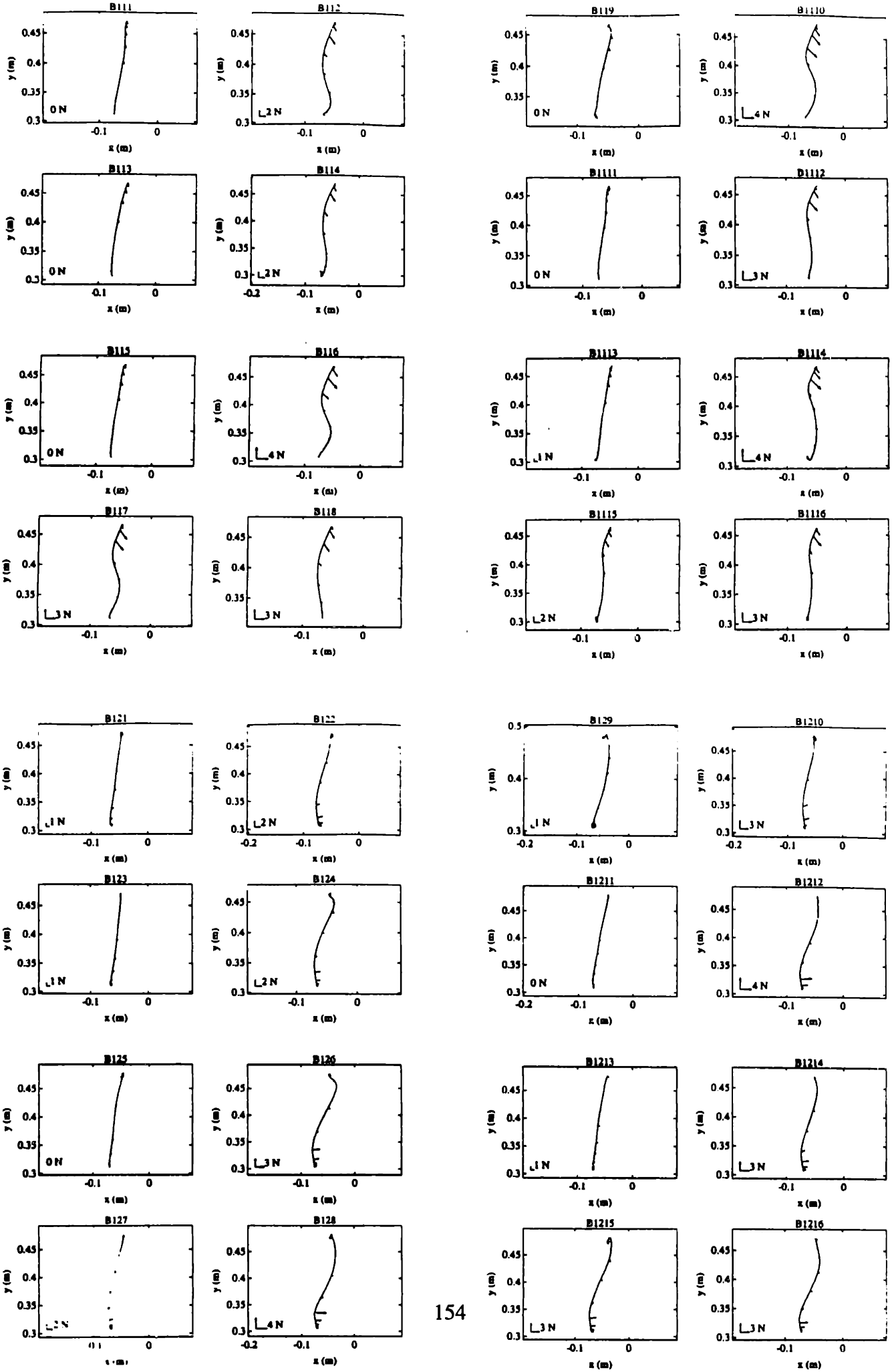
B111
B112
B119
B1110
B113
B114
B1111
B1112
B115
B116
B1113
B1114
B117
B118
B1115
B1116
B121
B122
B129
B1210
B123
B124
B1211
B1212
B125
B126
B1213
B1214
B127
B128
B1215
B1216
y (m)
x (m)
0 N
2 N
4 N
3 N
1 N

B.3 Subject C

Right Handed Male

Forearm length = 31 cm

Upper arm length = 30 cm

Weight = 140 lbs

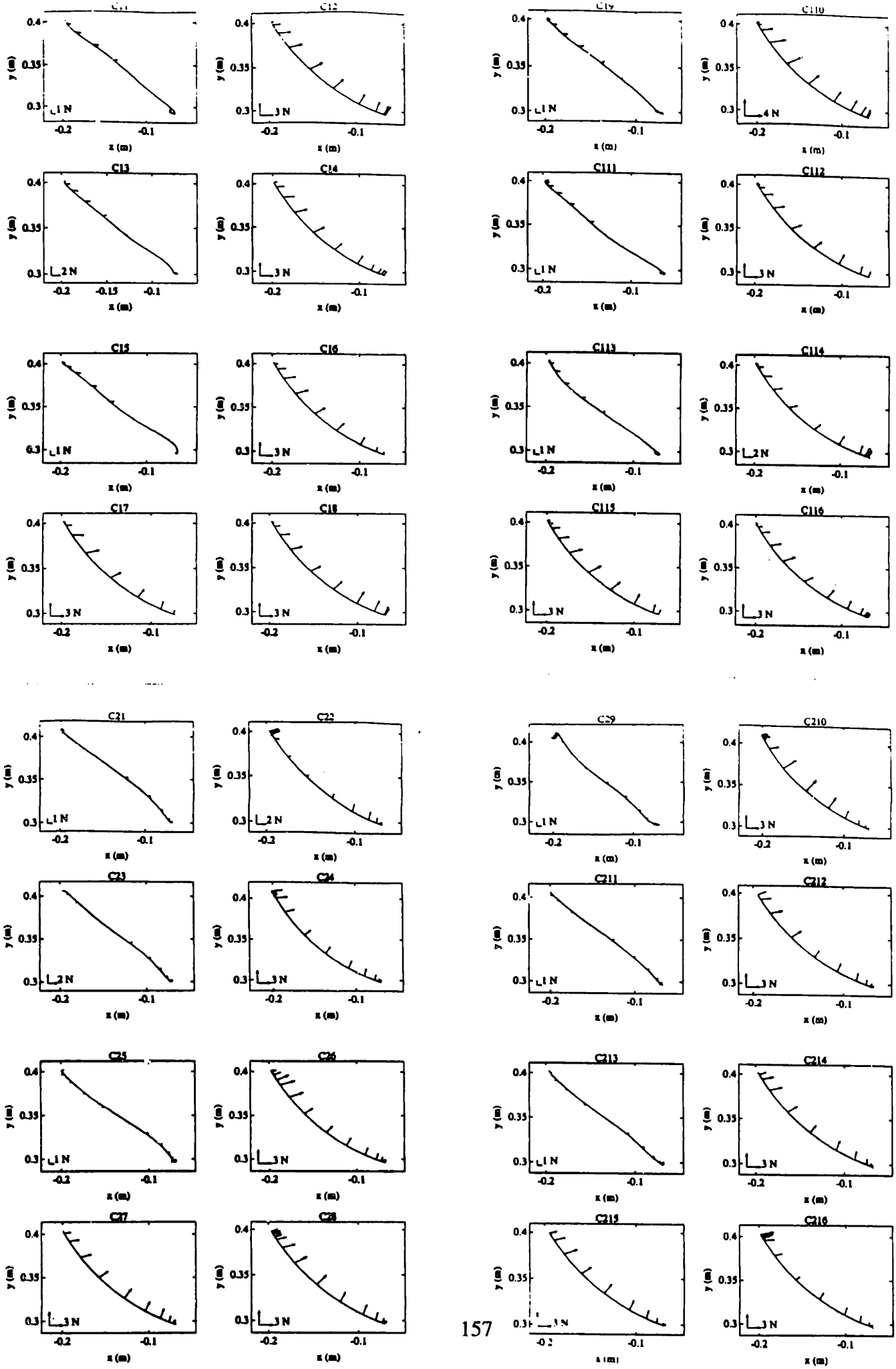
C11
C12
C19
C110
C13
C14
C111
C112
C15
C16
C113
C114
C17
C18
C115
C116
C21
C22
C29
C210
C23
C24
C211
C212
C25
C26
C213
C214
C27
C28
C215
C216
y (m)
x (m)
1 N
2 N
3 N
4 N

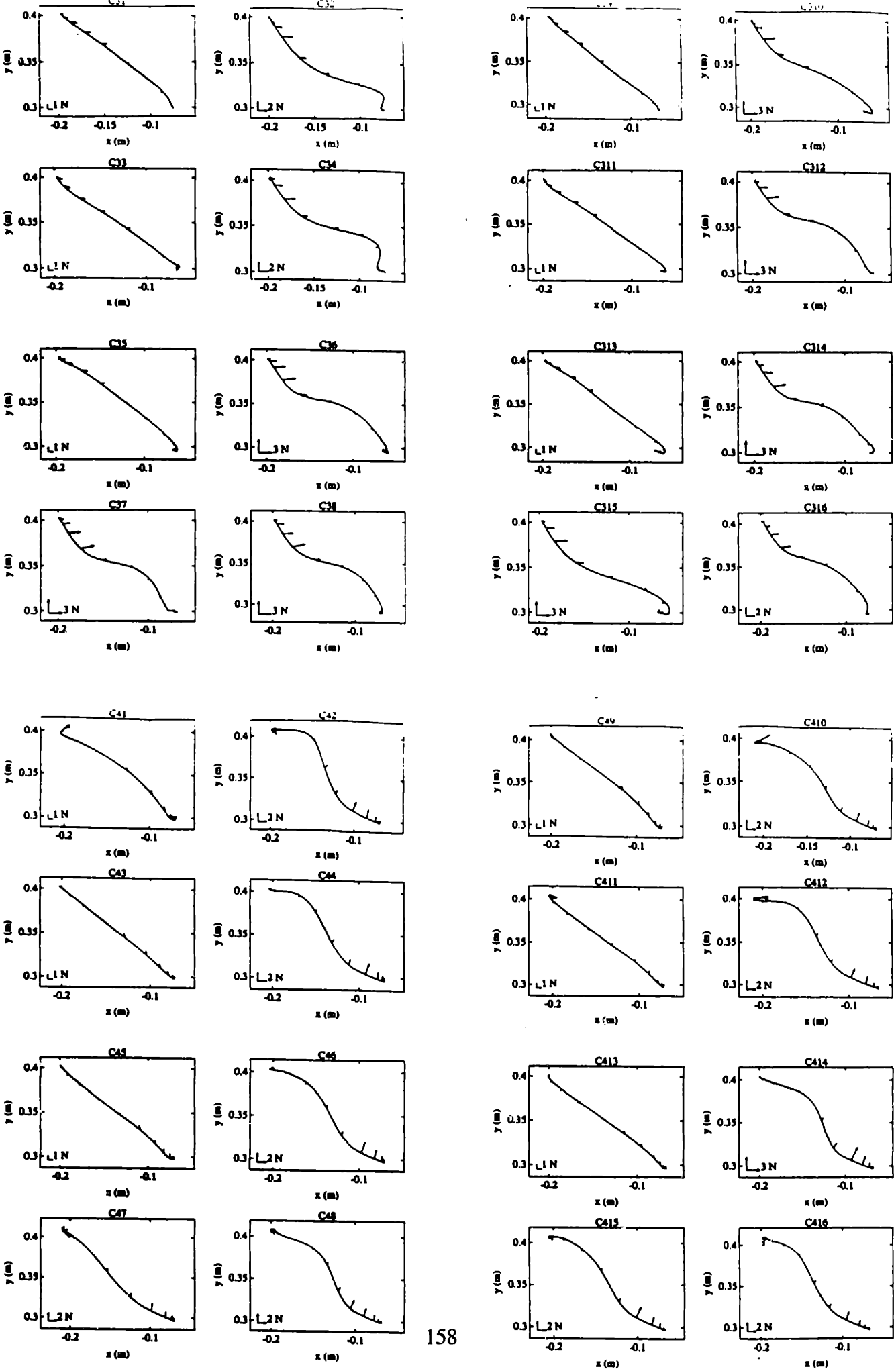
C33
C34
C35
C36
C37
C38
C41
C42
C43
C44
C45
C46
C47
C48
C49
C410
C411
C412
C413
C414
C415
C416
C311
C312
C313
C314
C315
C316
y (m)
x (m)
L1 N
L2 N
L3 N

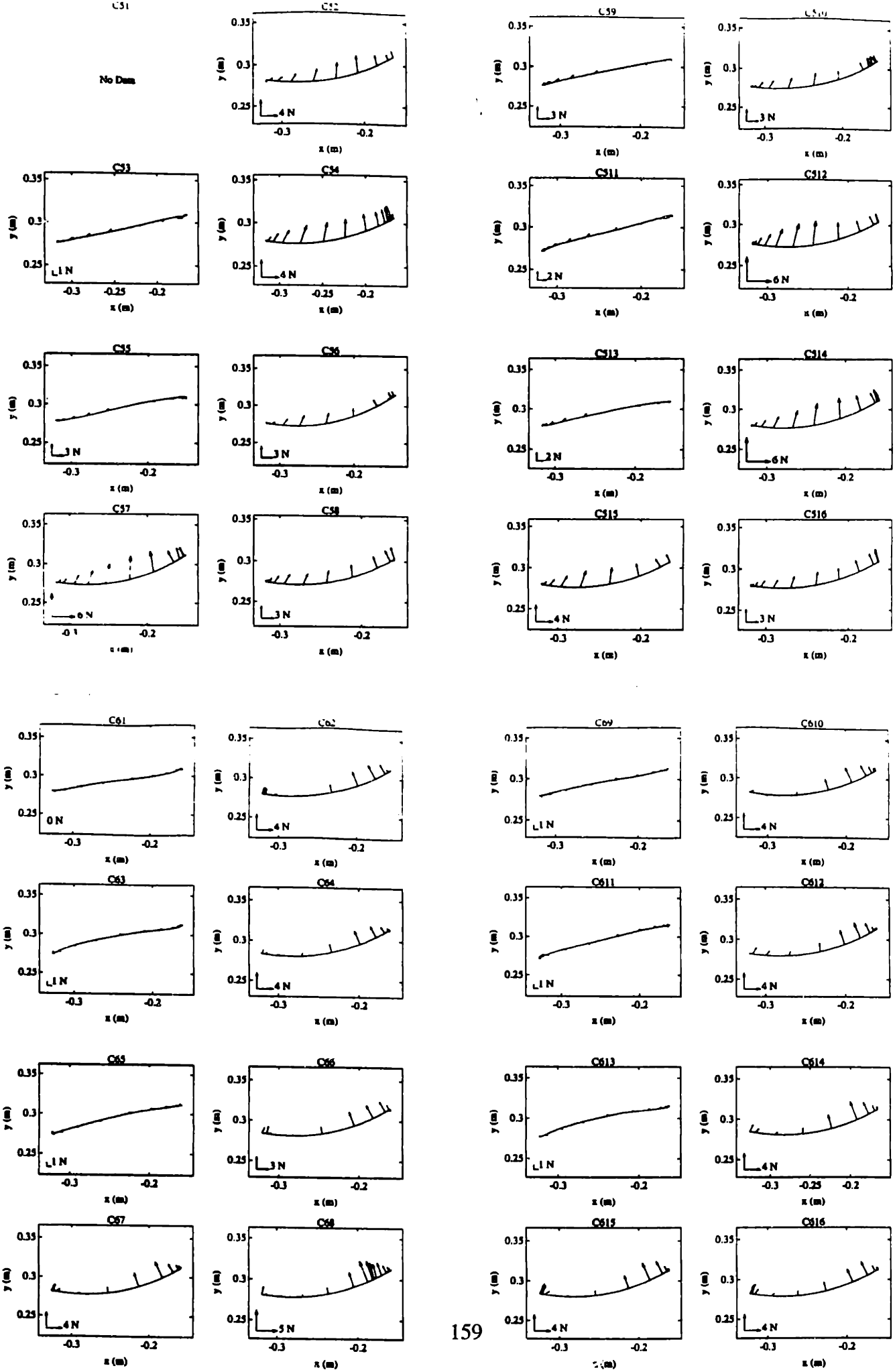
C51
No Dam
C52
4 N
C59
3 N
C510
3 N
C53
1 N
C54
4 N
C511
2 N
C512
6 N
C55
3 N
C56
3 N
C513
2 N
C514
6 N
C57
6 N
C58
3 N
C515
4 N
C516
3 N
C61
0 N
C62
4 N
C69
1 N
C610
4 N
C63
1 N
C64
4 N
C611
1 N
C612
4 N
C65
1 N
C66
3 N
C613
1 N
C614
4 N
C67
4 N
C68
5 N
C615
4 N
C616
4 N
y (m)
x (m)

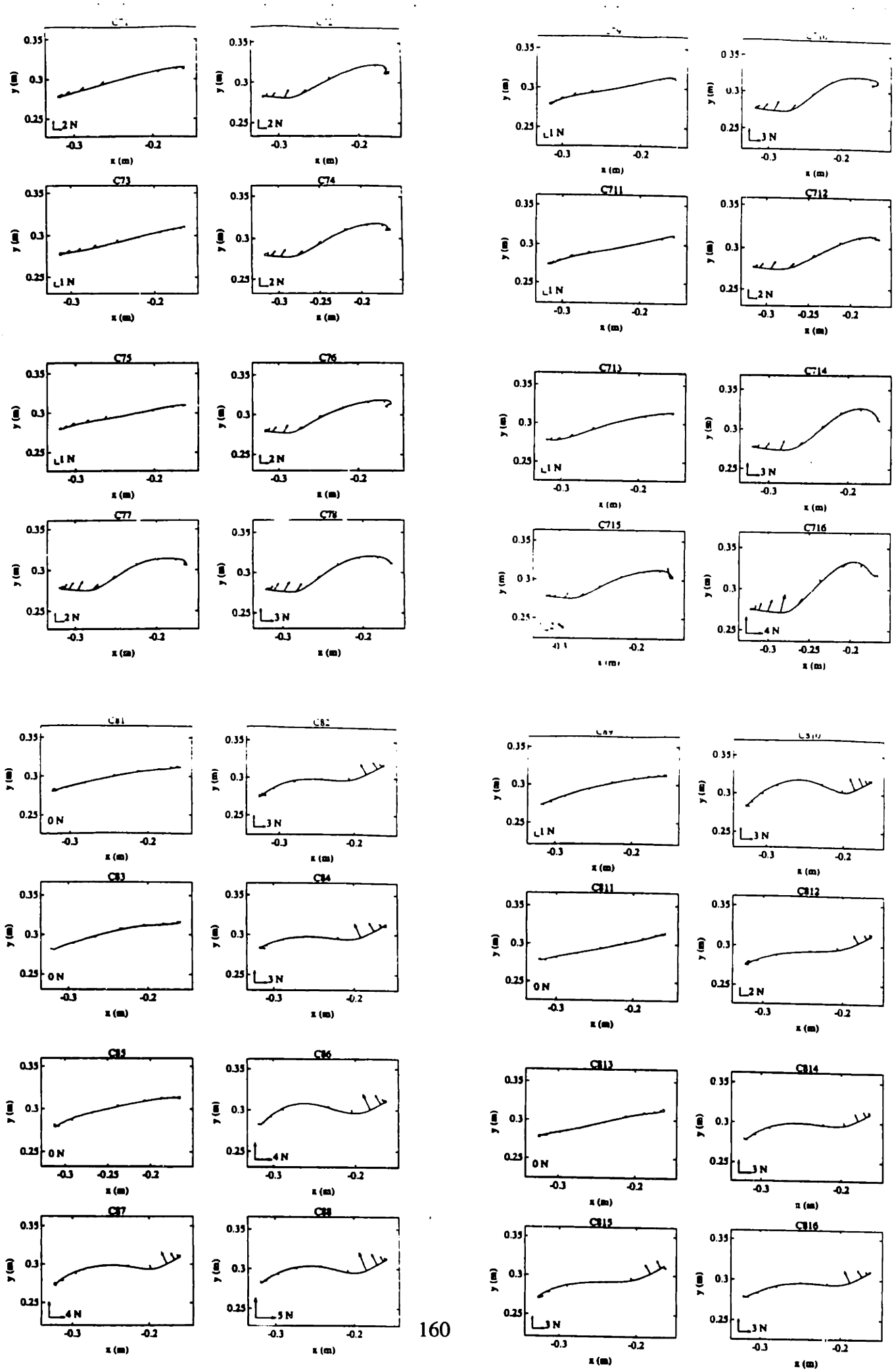
C73
C74
C75
C76
C77
C78
C711
C712
C713
C714
C715
C716
C83
C84
C85
C86
C87
C88
C811
C812
C813
C814
C815
C816
y (m)
x (m)
0.35
0.3
0.25
-0.3
-0.25
-0.2
0 N
1 N
2 N
3 N
4 N
5 N

C91

No Data

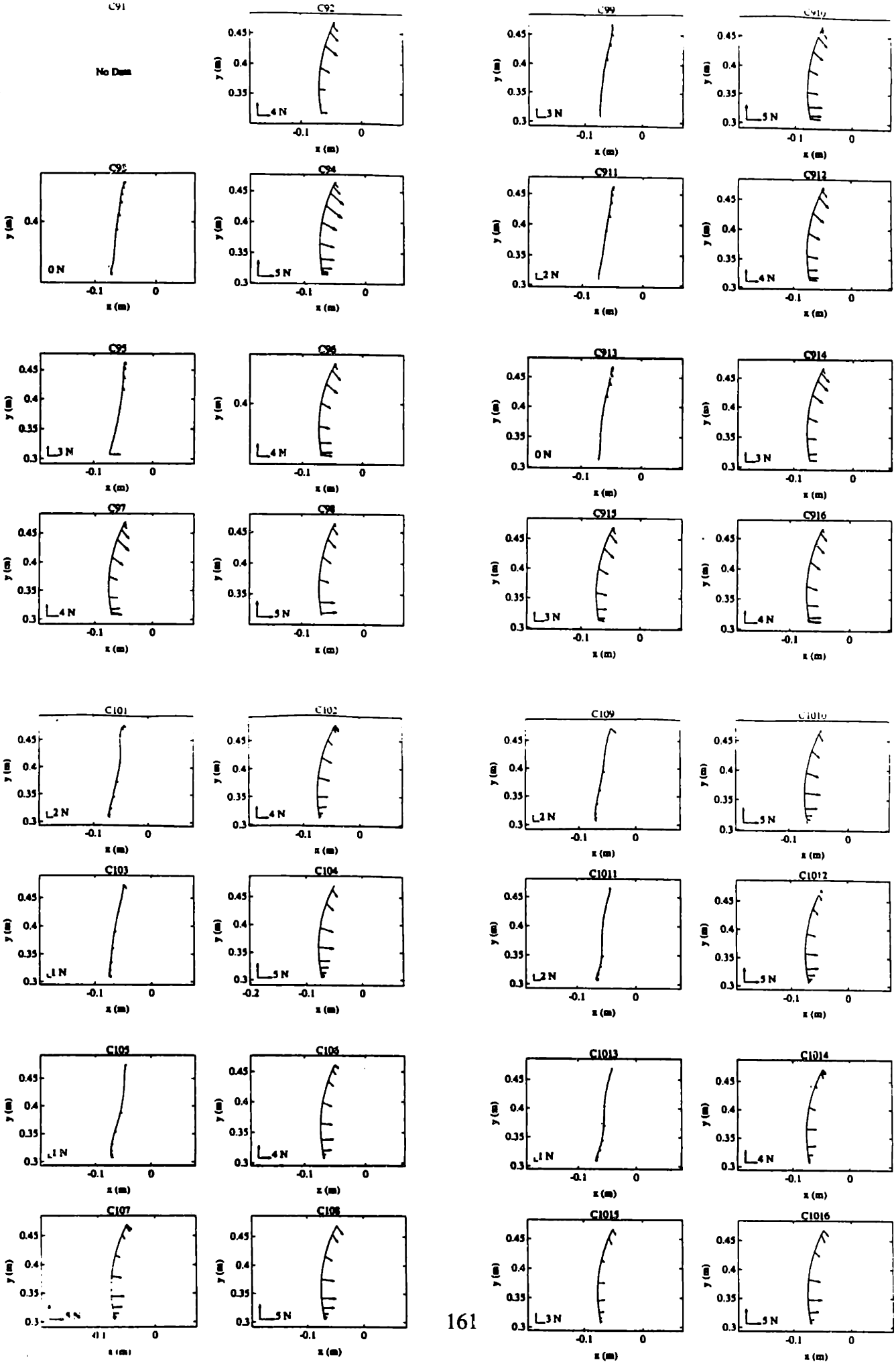
C92
4 N
C99
3 N
C910
5 N
C93
0 N
C94
5 N
C911
2 N
C912
4 N
C95
3 N
C96
4 N
C913
0 N
C914
3 N
C97
4 N
C98
5 N
C915
3 N
C916
4 N
C101
2 N
C102
4 N
C109
2 N
C1010
5 N
C103
1 N
C104
5 N
C1011
2 N
C1012
5 N
C105
1 N
C106
4 N
C1013
1 N
C1014
4 N
C107
C108
5 N
C1015
3 N
C1016
5 N
y (m)
x (m)

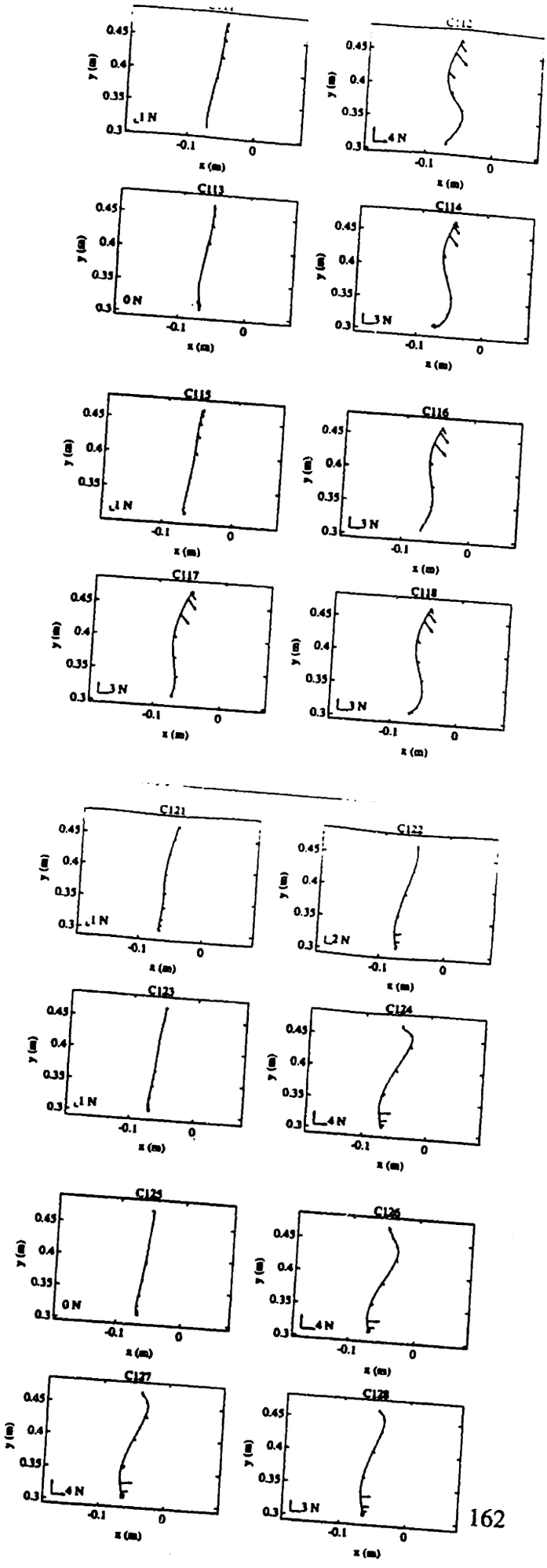
C112
C113
C114
C115
C116
C117
C118
C121
C122
C123
C124
C125
C126
C127
C128
y (m)
x (m)
1 N
4 N
0 N
3 N
2 N

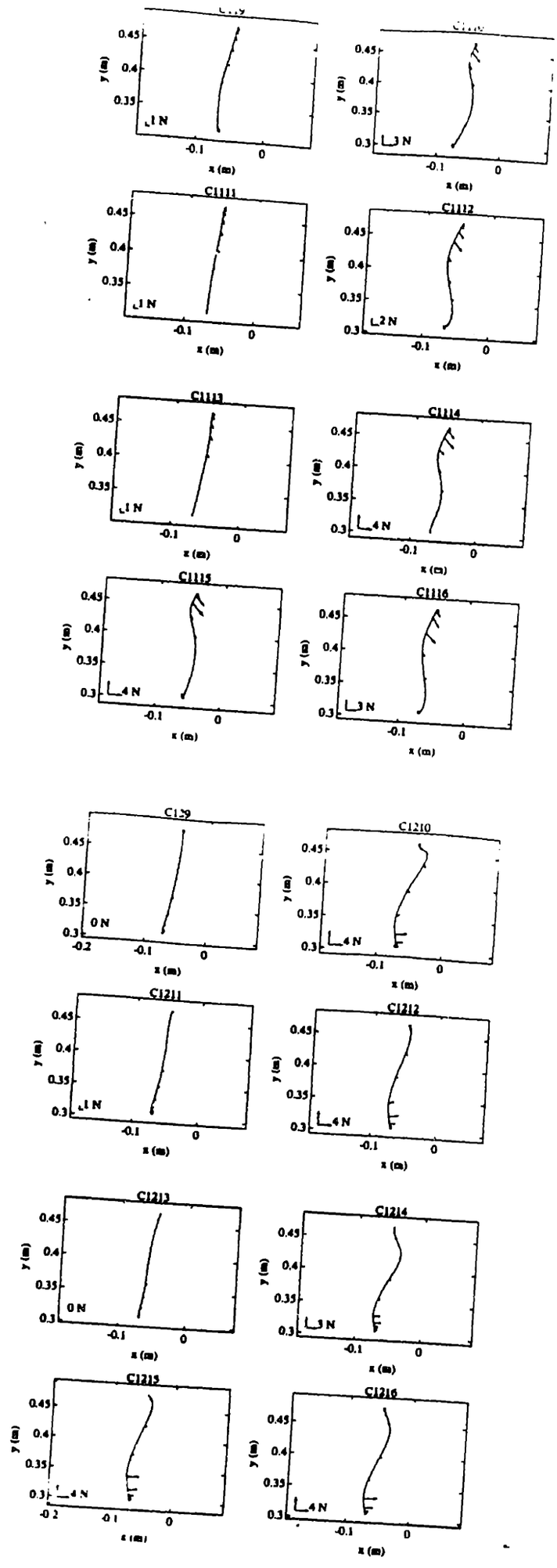
C1111
C1112
C1113
C1114
C1115
C1116
C129
C1210
C1211
C1212
C1213
C1214
C1215
C1216
y (m)
x (m)
1 N
3 N
2 N
4 N
0 N

B.4 Subject D

Right Handed Male

Forearm length = 31 cm

Upper Arm length = 29.5 cm

Weight = 135 lbs

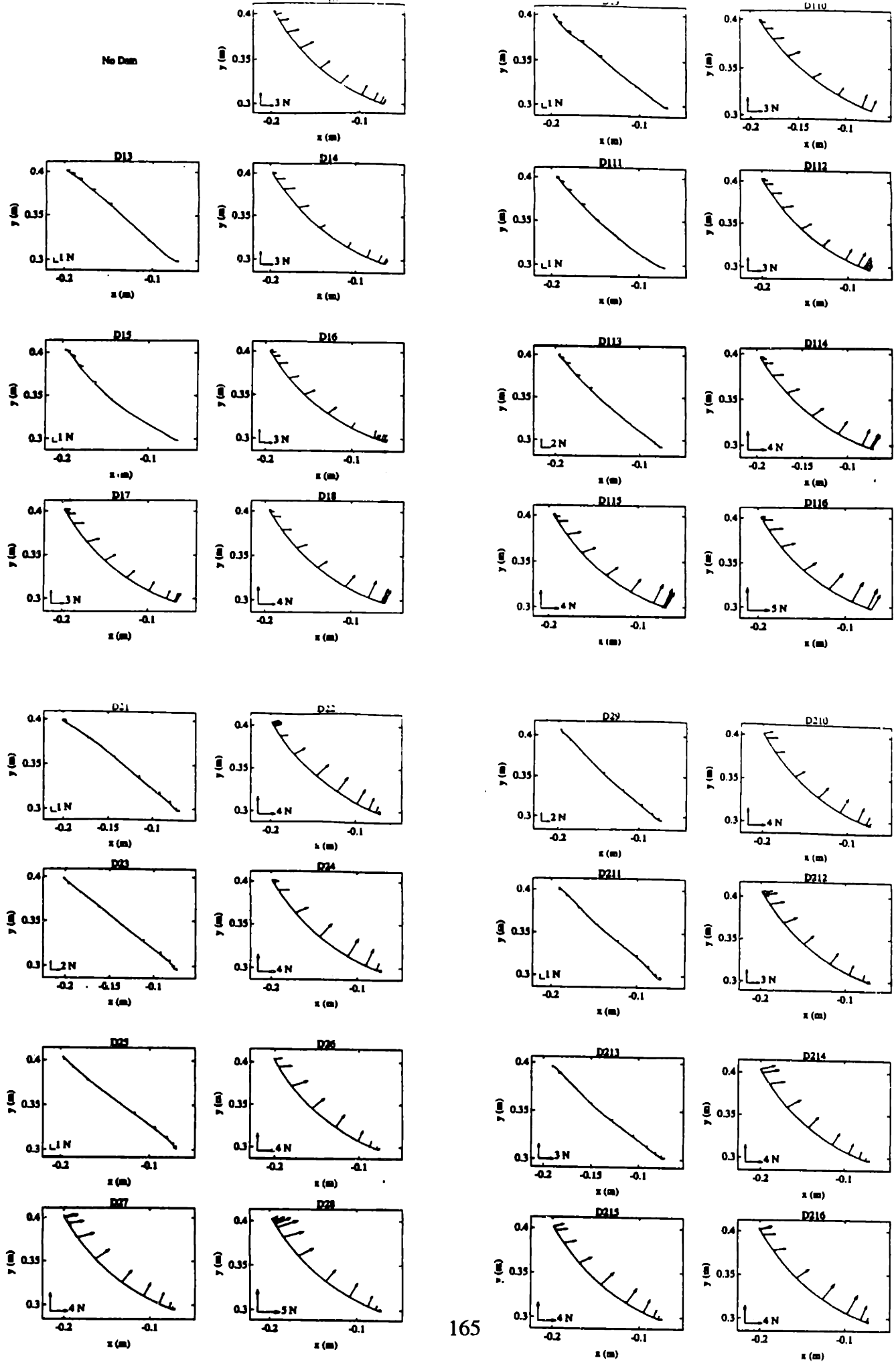
No Dam
D13
D14
D15
D16
D17
D18
D21
D22
D23
D24
D25
D26
D27
D28
D29
D210
D211
D212
D213
D214
D215
D216
D110
D111
D112
D113
D114
D115
D116
y (m)
x (m)
0.4
0.35
0.3
-0.2
-0.15
-0.1
1 N
2 N
3 N
4 N
5 N

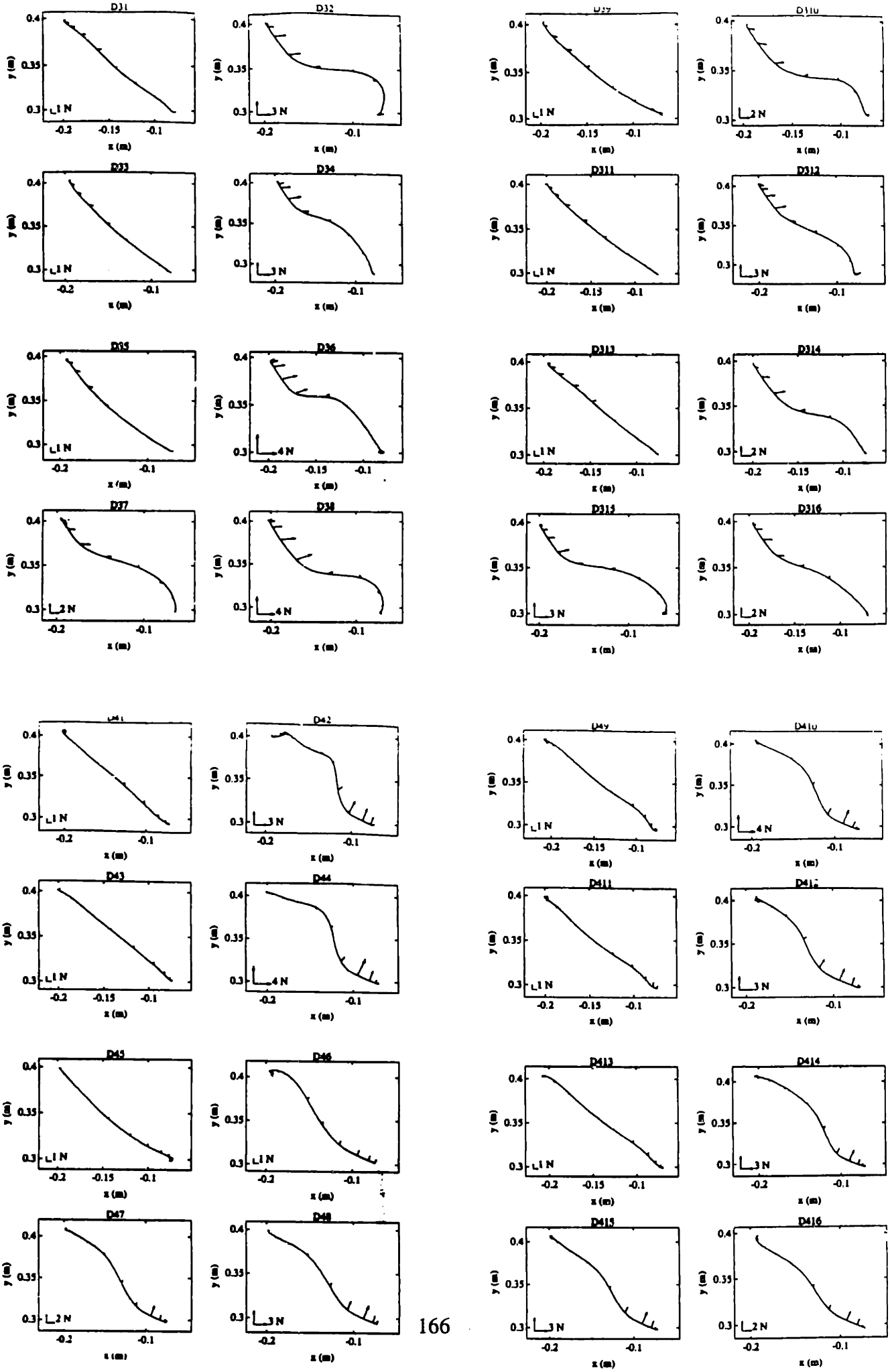
D31
D32
D39
D310
D33
D34
D311
D312
D35
D36
D313
D314
D37
D38
D315
D316
D41
D42
D49
D410
D43
D44
D411
D412
D45
D46
D413
D414
D47
D48
D415
D416
y (m)
x (m)
1 N
2 N
3 N
4 N

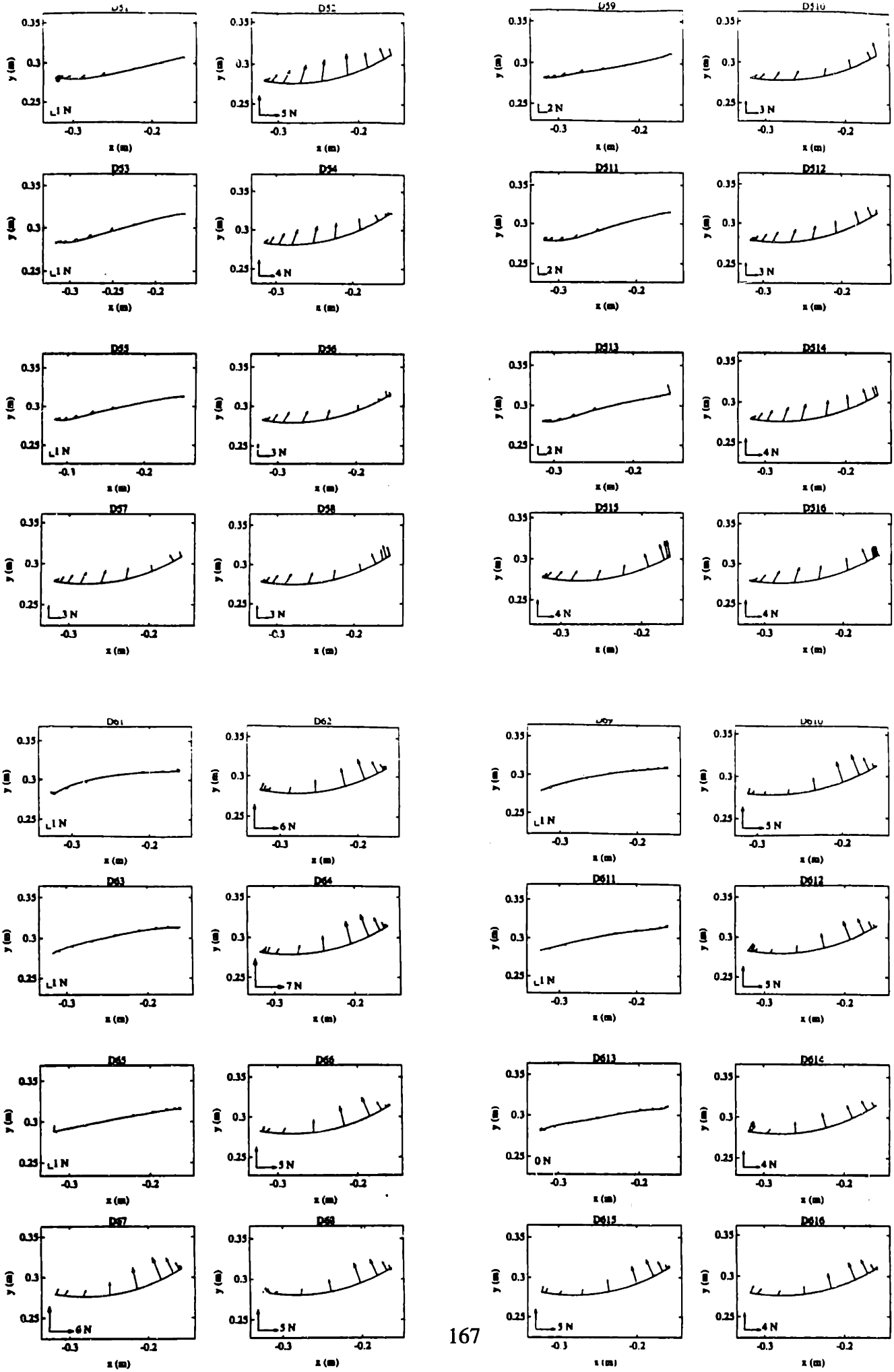
D51
D52
D59
D510
D53
D54
D511
D512
D55
D56
D513
D514
D57
D58
D515
D516
D61
D62
D67
D610
D63
D64
D611
D612
D65
D66
D613
D614
D67
D68
D615
D616
y (m)
x (m)
1 N
5 N
2 N
3 N
4 N
6 N
7 N
0 N

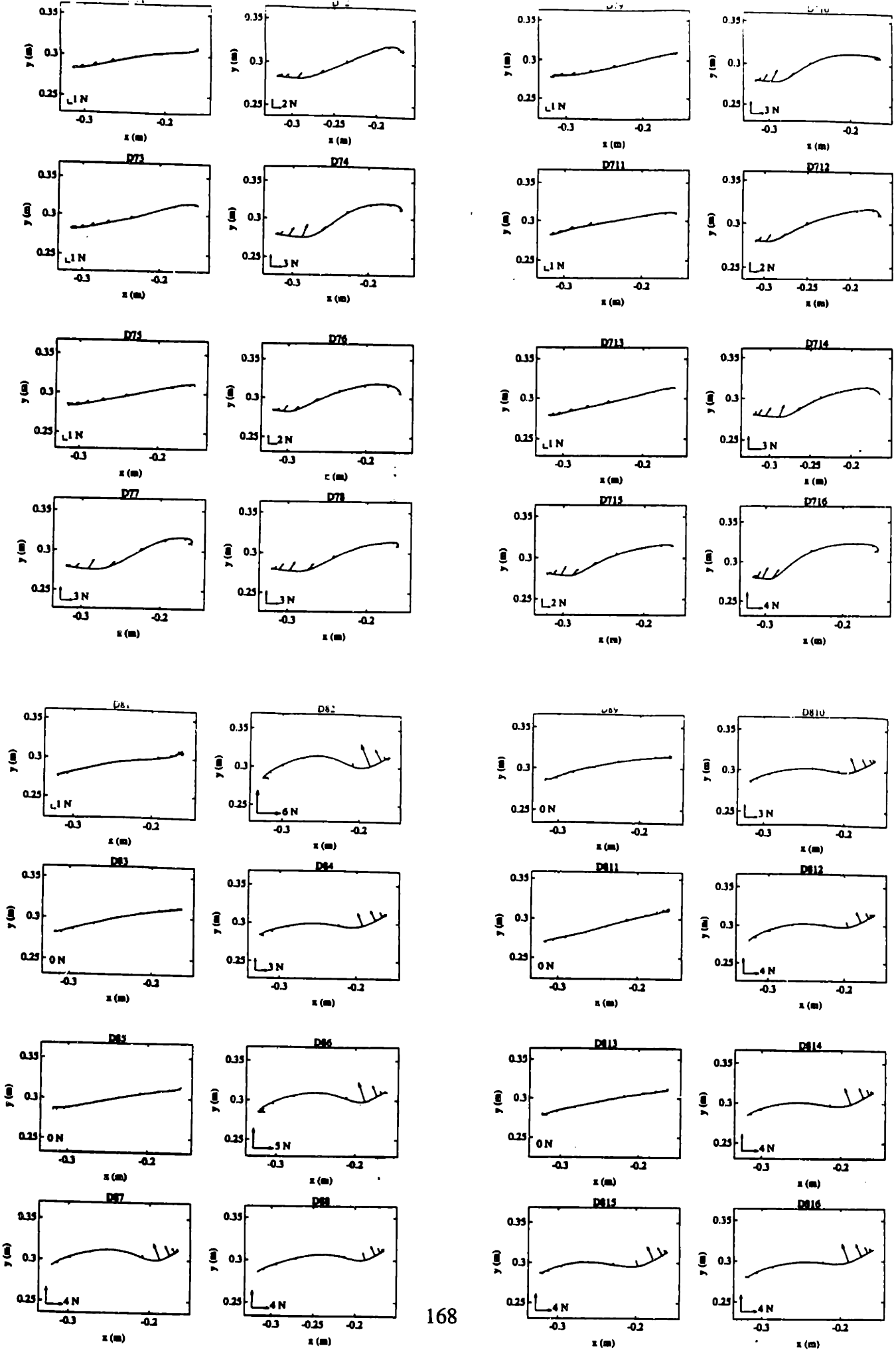
D73
D74
D75
D76
D77
D78
D711
D712
D713
D714
D715
D716
D83
D84
D85
D86
D87
D88
D811
D812
D813
D814
D815
D816
y (m)
x (m)
1 N
2 N
3 N
4 N
5 N
6 N
0 N

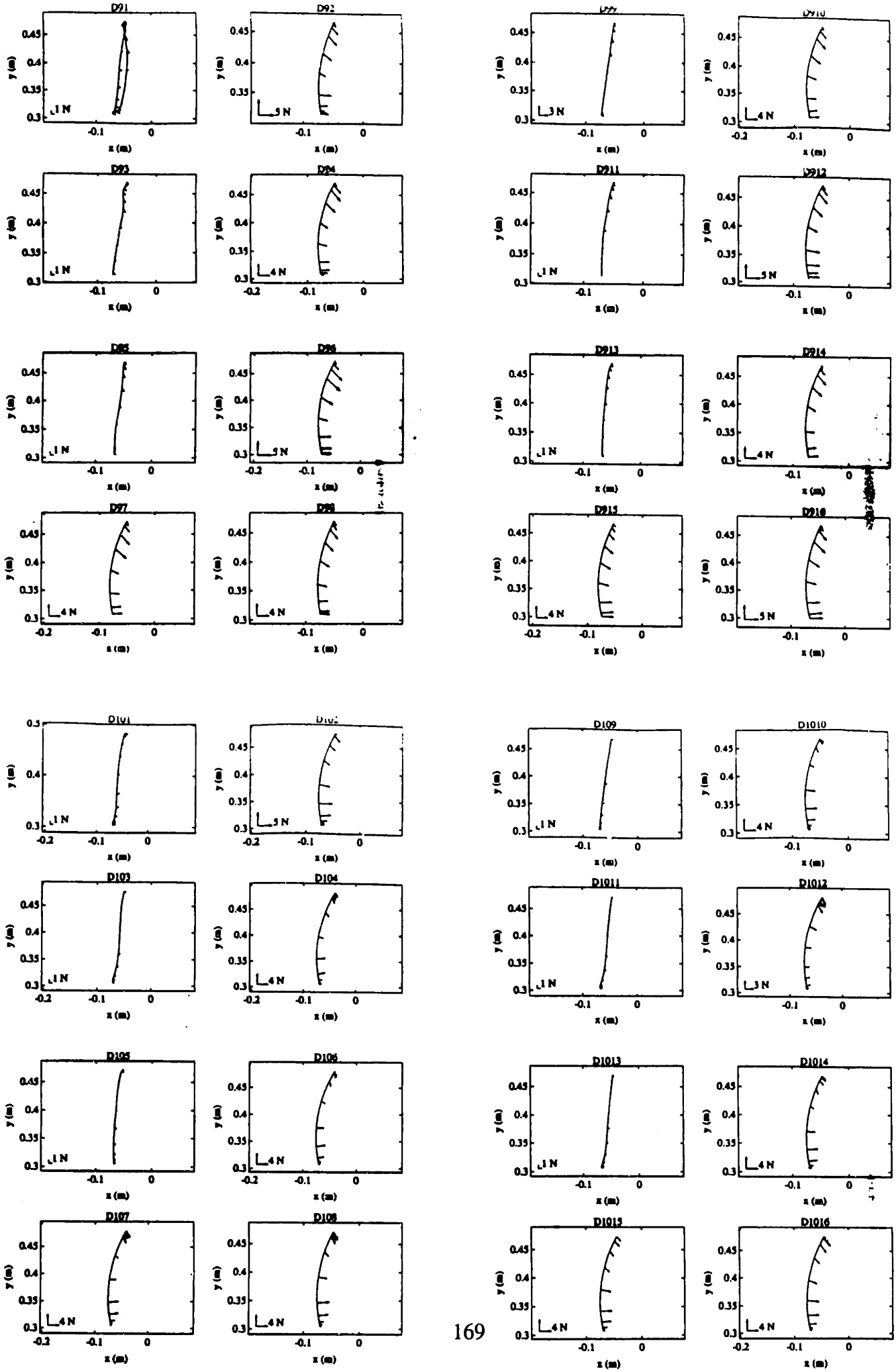
D91
D92
D93
D94
D95
D96
D97
D98
D101
D102
D103
D104
D105
D106
D107
D108
D109
D1010
D1011
D1012
D1013
D1014
D1015
D1016
y (m)
x (m)
1 N
5 N
3 N
4 N

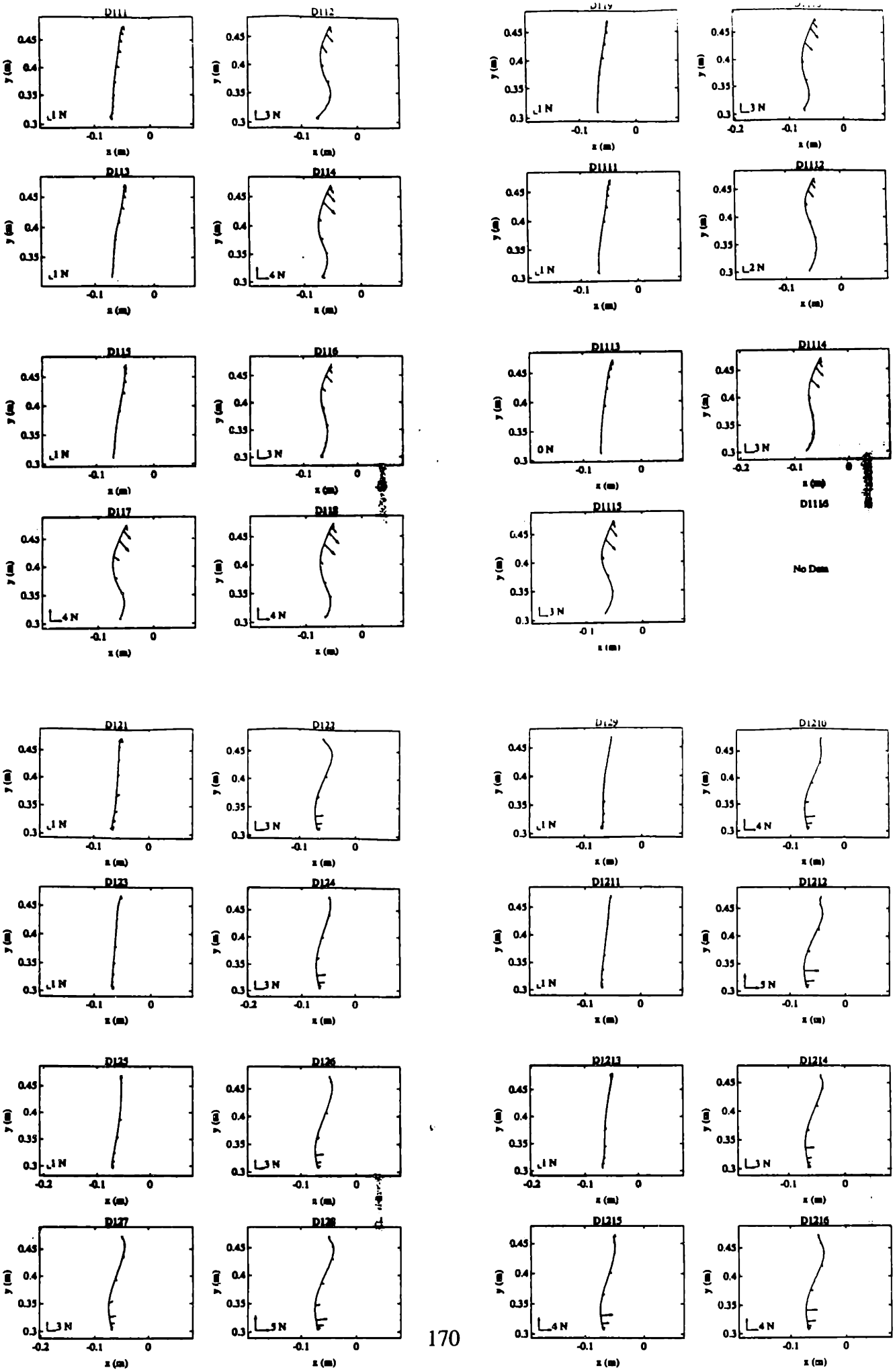
D111
D112
D113
D114
D115
D116
D117
D118
D119
D1110
D1111
D1112
D1113
D1114
D1115
D1116
No Data
D121
D122
D123
D124
D125
D126
D127
D128
D129
D1210
D1211
D1212
D1213
D1214
D1215
D1216
y (m)
x (m)
1 N
2 N
3 N
4 N
0 N

B.5 Subject E

Right handed Male

Forearm length = 32.4 cm

Upper arm length = 31 cm

Weight = 160 lbs

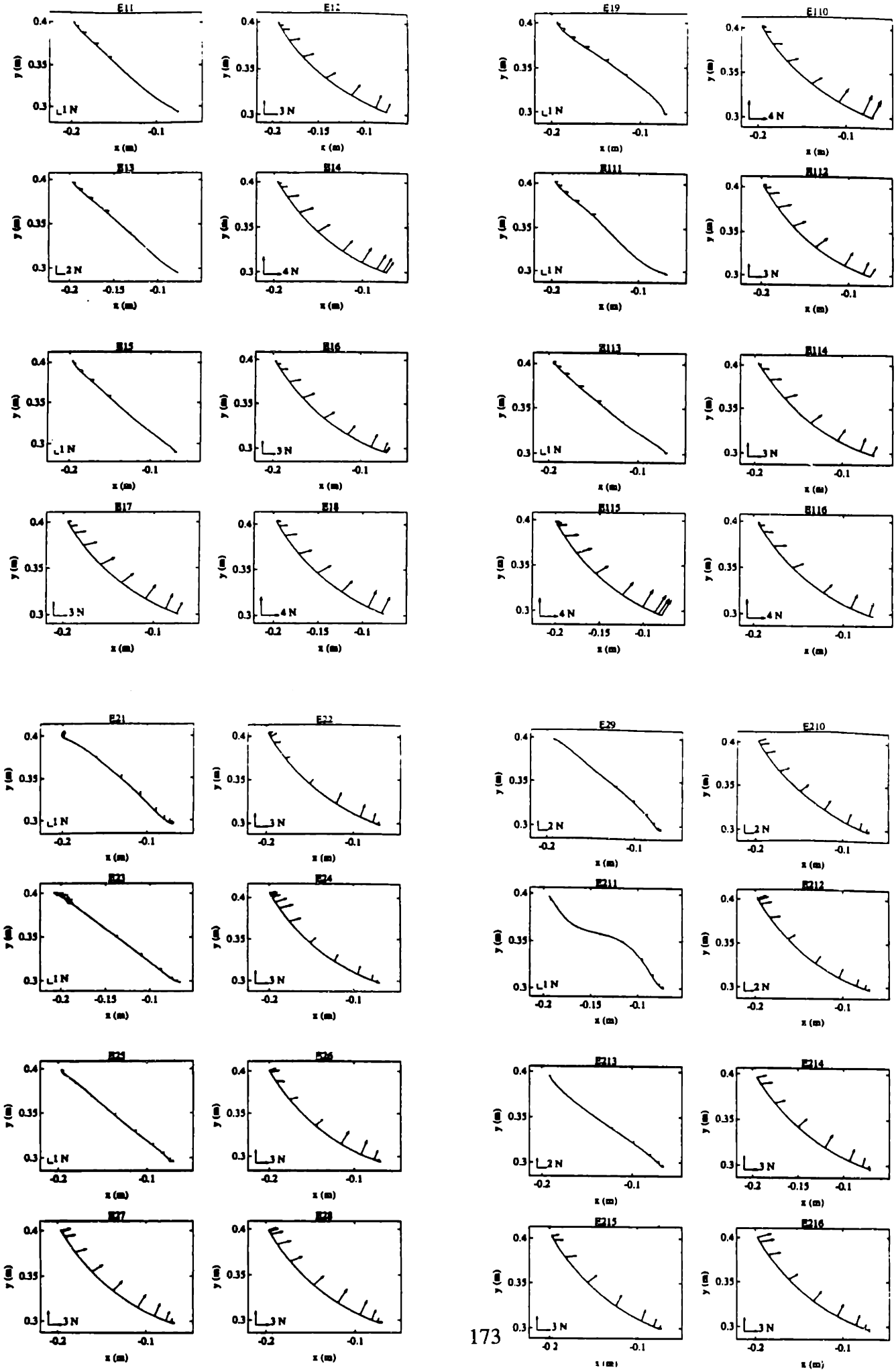
E11
E12
E19
E110
E13
E14
E111
E112
E15
E16
E113
E114
E17
E18
E115
E116
E21
E22
E29
E210
E23
E24
E211
E212
E25
E26
E213
E214
E27
E28
E215
E216
y (m)
x (m)
1 N
2 N
3 N
4 N

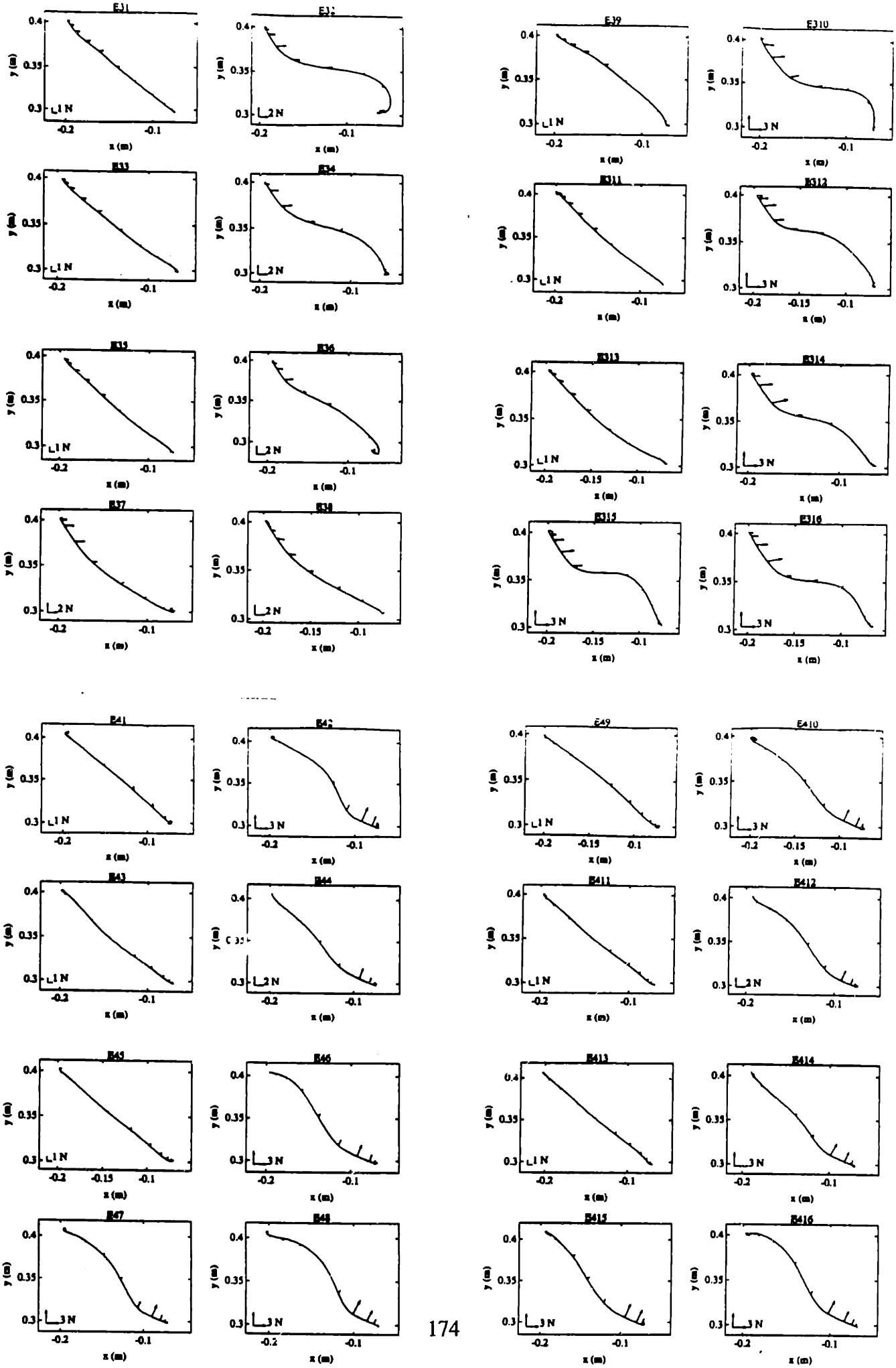
E31
E32
E33
E34
E35
E36
E37
E38
E39
E310
E311
E312
E313
E314
E315
E316
E41
E42
E43
E44
E45
E46
E47
E48
E49
E410
E411
E412
E413
E414
E415
E416
y (m)
x (m)
1 N
2 N
3 N

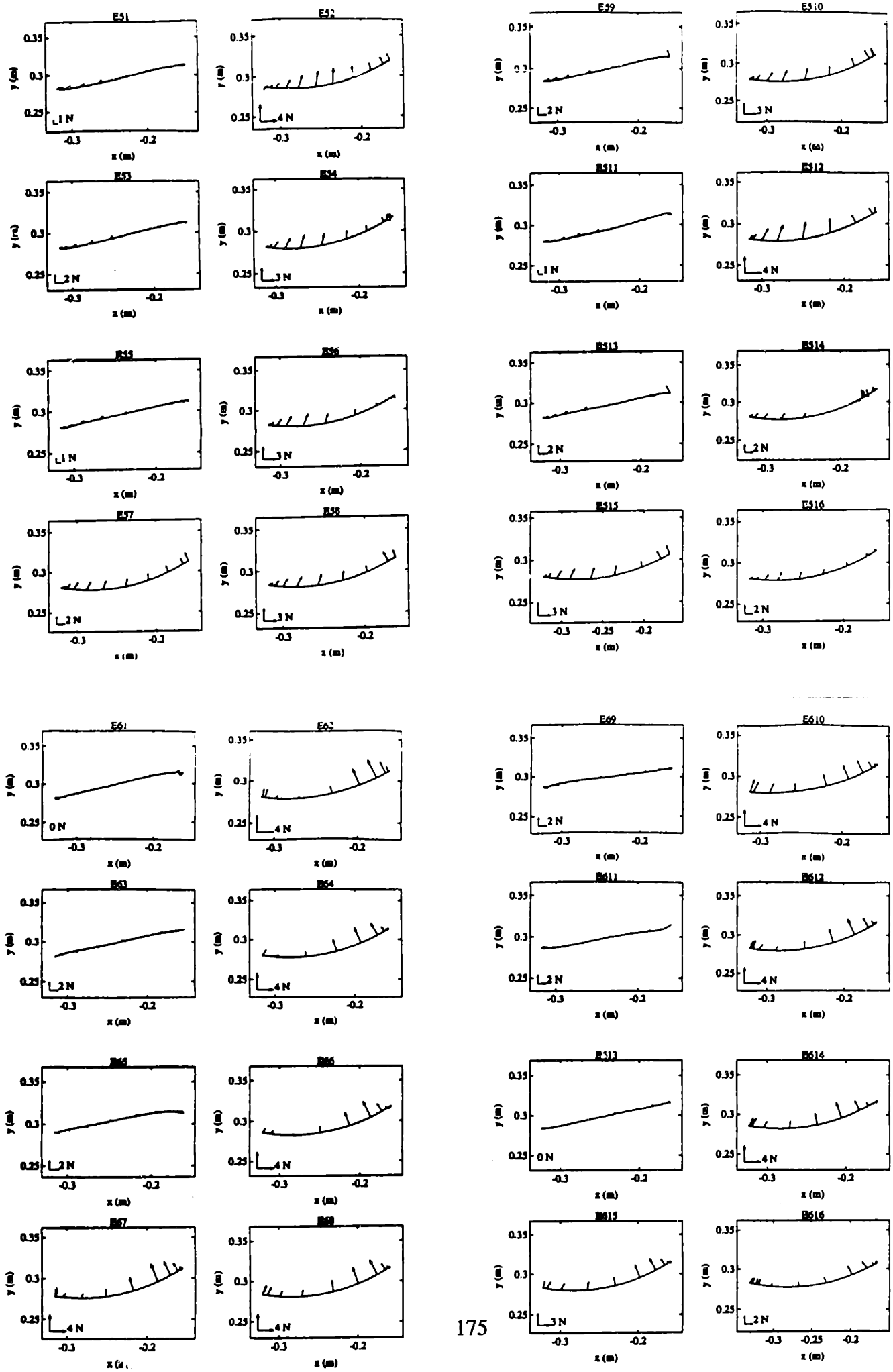
E51
E52
E53
E54
E55
E56
E57
E58
E59
E510
E511
E512
E513
E514
E515
E516
E61
E62
E63
E64
E65
E66
E67
E68
E69
E610
E611
E612
E613
E614
E615
E616
y (m)
x (m)
0.35
0.3
0.25
-0.3
-0.25
-0.2
1 N
2 N
3 N
4 N
0 N

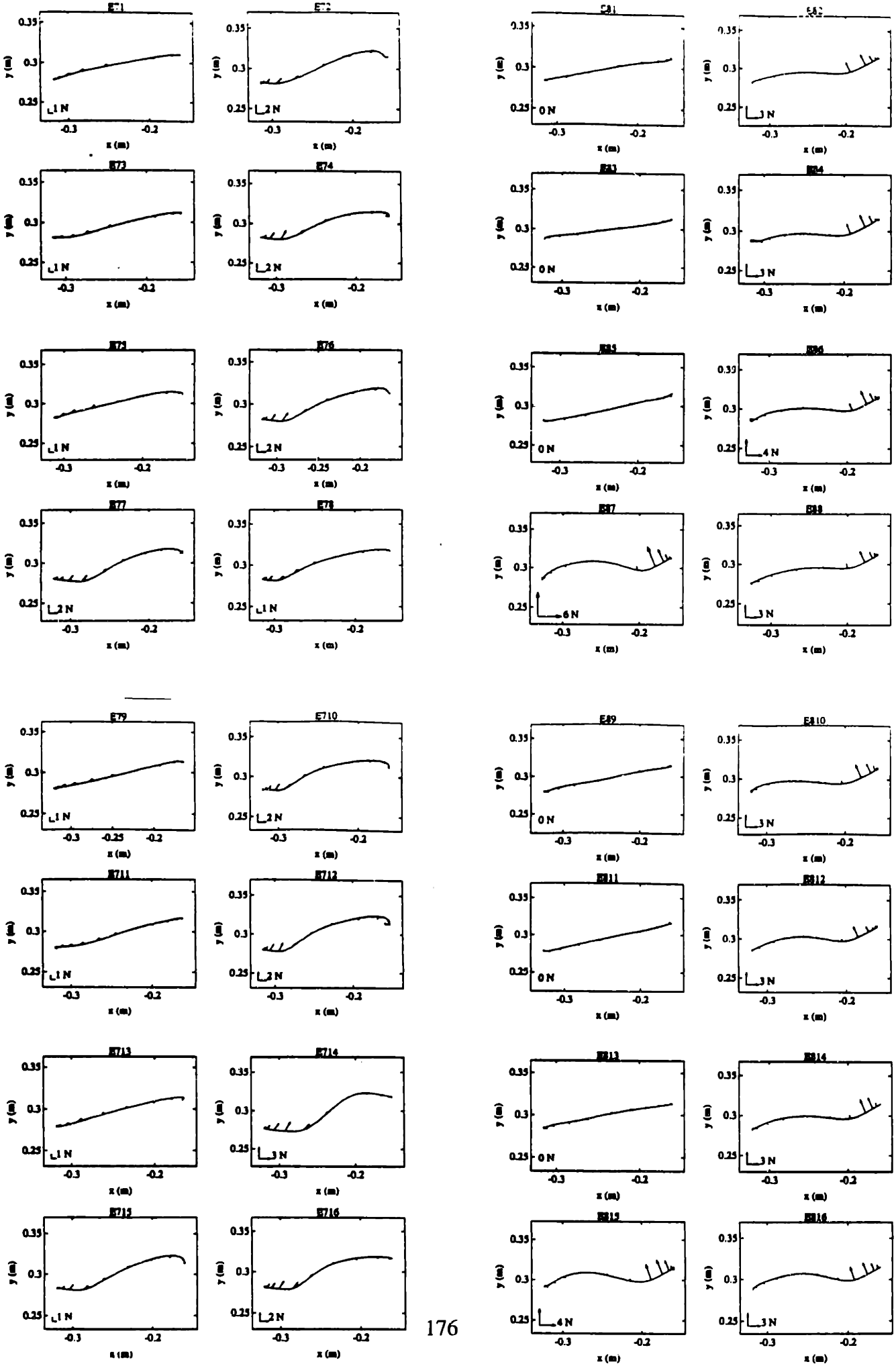
E71
E72
E81
E82
E73
E74
E83
E84
E75
E76
E85
E86
E77
E78
E87
E88
E79
E710
E89
E810
E711
E712
E811
E812
E713
E714
E813
E814
E715
E716
E815
E816
y (m)
x (m)
0.35
0.3
0.25
-0.3
-0.25
-0.2
1 N
2 N
0 N
3 N
4 N
6 N

Appendix C

Informed Consent Document

The document which follows is the "Informed Consent Document" which all subjects read and signed as required by the M.I.T. Committee on the Use of Humans as Experimental Subjects.

Informed Consent Document

Title of Study: **Control of Partially Constrained Hand Movements by Humans**

Principal Investigator: **Professor Neville Hogan**

Associated Investigator: **Justin Won**

Purpose of Study

Even with today's technology, robots still have great difficulty in completing tasks involving dynamic interaction with constrained environments. Humans, however, perform these everyday manipulatory tasks with ease and dexterity. The purpose of this experiment is to study the methods which humans use in controlling hand movements for partially constrained tasks. Through a better understanding of the strategies underlying human movement, it may be possible to apply some of these concepts to the fields of robotics and prosthetics.

Experimental Protocol

Subjects will be asked to hold and move the handle of the two-link manipulator shown in figure 1. A video screen will be used to display the desired starting and ending targets as well as the current position of the manipulator's handle. This system is completely passive except for two electromagnetic brakes which can lock the rotation of either the inner or outer link.

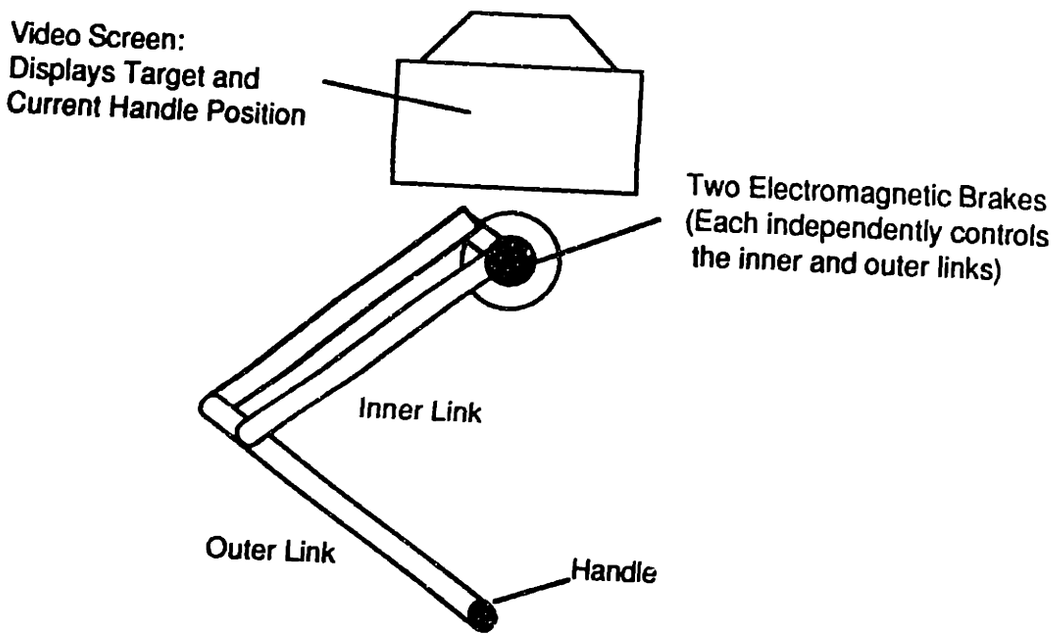

Figure 1: Top View of Apparatus

The subject will begin at a starting handle position designated by a target on the video screen. Once at that position, the subject will wait until the original target is erased and a new target is illuminated. When the new target is visible, the subject will move the handle to the position designated by the new target. Subjects will be asked to move the handle as if they were reaching for an object at the target position. Once at the new target, the subject will again wait until this target is erased and the original starting point is illuminated. The subject will then move back to the starting position. This back and forth trajectory will be repeated several times. For some of the movements, one of the electromagnetic brakes will be engaged so that the subject's motion will be constrained to a rotation about the unlocked link. This constraint will be applied in such a way so that the subject will still be able to reach the desired target. This procedure will be repeated for several different combinations of starting and ending points.

Since we wish to study the control of the arm by the shoulder and elbow joints only, a brace will be placed on the subject to immobilize the wrist. In order to further simplify the study, all motions will be performed in the horizontal plane. The subject will be placed in an elbow sling to support the weight of the arm and constrain it to the horizontal plane.

Risks and Benefits

The apparatus used in this experiment is completely passive. No actively controlled forces will be applied to the subject except for the use of a brake to immobilize one of the joints on the apparatus. As a result, there is little risk for the subject in moving the apparatus through the various trajectories. However in the case of an emergency, the subject can let go of the handle at anytime during the experiment without risk. The manipulator arm cannot move under its own power once the subject has released the handle.

There is a possibility of discomfort in wearing the wrist brace. It is a nylon shell molded into the shape of the lower palm and wrist. The brace will be placed on the subject and tightened with conventional medical tape. Any discomfort will be slight, and the brace can be adjusted to provide a more comfortable fit.

There are no known benefits from this experiment for the subjects.

The subject agrees to the following:

I am free at any time to seek further information regarding the experiment. In addition, I am also free to withdraw consent and discontinue participation at any time.

The subject will remain anonymous in all publications of the results of this experiment.

In the unlikely even of physical injury resulting from participation in this research, I understand that medical treatment will be available from the M.I.T. Medical Department, including first aid emergency treatment and follow-up care as needed, and that my insurance carrier may be billed for the cost of such treatment. However, no compensation can be provided for medical care apart from the foregoing. I further understand that making such medical treatment available, or providing it, does not imply that such injury is the investigator's fault. I also understand that by my participation in this study I am not waiving any of my legal rights. Further information may be obtained by calling the Institute's Insurance and Legal Affairs Office at 253-2822.

I understand that I may also contact the Chairman of the Committee on the Use of Humans as Experimental Subjects, M.I.T. 253-1772, if I feel I have been treated unfairly as a subject.

I have read the above consent document and understand the experiments described in the document. I agree to participate in the experiments as a subject.

The project investigators retain the right to cancel or postpone the experimental procedures at any time they see fit.

Date: _____

Subject's Name: _____

Subject's Signature: _____

Witness Name: _____

Witness Signature: _____